BONDING MECHANISM IN A NEW REFRACTORY CASTABLE

MOHAMMED AKRAM

A Thesis Submitted for the Degree of Doctor of Philosophy

The University of Aston in Birmingham

December 1996

The University of Aston in Birmingham

BONDING MECHANISM IN A NEW REFRACTORY CASTABLE

by

MOHAMMED AKRAM

A thesis submitted for the degree of Doctor of Philosophy, 1996

A Study of the individual components of the new refractory castable was carried out. The initial study was of the kaolin clay component, where it was shown that the source of the clay had an important bearing on the purity of the clay, which in turn affected the changes taking place on thermal treatment.

Two component mixes of the calcined kaolin (metakaolin) and potassium silicate were studied. The particular silicate used in the mix had a strong influence on the reactions taking place and as a result on the product formed. A third component of the refractory was introduced to the two component systems, this was alumina or silica. Silica had a mainly diluant effect on the metakaolin-silicate interactions but there is evidence that alumina is taking part in reactions.

An attempt was made to synthesise the kaolinite clay by employing microwave techniques. A number of different methods of kaolin synthesis were followed but at the point of hydrothermal treatment microwave treatment was carried out. Microwaves were found to be unsuccessful for kaolin synthesis.

Calcined montmorillonite was substituted for the metakaolin to assess its suitability as a component for the new refractory. Subsequently the parent montmorillonites were modified by exchanging with different iron complexes. These modified clays were then tested for their suitability as adsorbents for phenol, 2- chlorophenol and 2,4,6-trichlorophenol.

Key words: Refractory, Castable, Kaolinite, Metakaolin, Montmorillonite, Microwave, Phenols

To My Parents,
Zaman Ali and Sarwar Jan
and
in memory of my Grandmother

ACKNOWLEDGEMENTS

I am greatly indebted to Professor W. R. McWhinnie for his support, guidance and patience for the duration of my PhD and would like to express my sincere gratitude and thanks.

I would like to express my gratitude to Dr A. Wynn, Morgan Materials Technology Limited, for always being available to offer help and advice.

Many thanks to Dr Mike Perry for providing NMR data .

I would also like to offer thanks to the technical staff for their assistance.

Finally I am grateful to EPSRC and Morgan Materials Technology Limited for funding this research.

CONTENTS

Chapter 5

CALCINED CLAY MINERAL AND SILICATE INTERACTIONS

Chapter 6

THREE COMPONENT MIXES

List of Tables

List of Figures

Chapter One

INTRODUCTION

1.1 Introduction

A new refractory castable has been developed by Morgan Materials Technology Limited which is an improvement over conventional refractories. Applications of this refractory have been studied in a variety of environments, but each time the refractory bond formulation has to be altered considerably in order to optimise properties. A knowledge of the bonding mechanism and the factors that affect it is required so that a more exact approach to tailoring the bond to each new application can be developed. This attempt at identifying the bonding mechanism is made by firstly characterising the individual starting materials. The component clay minerals were deemed to be the active ingredients therefore an initial and more thorough characterisation study was carried out on these minerals before and after calcining at various temperatures up to 1200°C. The other components of the refractory were potassium silicates (X, Y and Z), alumina and silica. These were individually studied before different combinations of two component and then three component mixtures were prepared. These mixtures were then studied using various spectroscopic techniques before and after calcining, in order to identify the interactions taking place and the differences between the different component mixtures.

An effort was made to synthesise the clay mineral using microwave methods rather than published high temperature and pressure methods[1,2,3,4]. This was attempted in order to reduce the time required for the synthesis as conventional methods take several days, and also to give access to a pure clay mineral.

Another semi-project involved modifying montmorillonites by exchanging transition metal complexes synthesised in the laboratory. Tests were carried out on these modified montmorillonites to study their capability to adsorb chlorinated phenols.

1.2 Origin of Refractories

It is believed that man first baked earth in Western Asia some time around 6000 BC. People in this region realised that after keeping a fire burning for many hours the underlying earthen floor became impermeable to water. They also discovered that of all types of earthy materials, clay with its relatively higher viscosity can be used to make any shape of this hard, impermeable material. This knowledge led to the developement of the water jug which is baked in fire to give it the final form. Other utensils were also made in neighbouring countries. Baked in the open, these were referred to as "keramos" in Greece. The word ceramic is derived from this.

Man progressed from using heat from a fire kindled in a simple earth cavity to stoves. Archaeological finds in New Mexico include stoves made of three large stones secured with clay. This invention allowed for the more efficient use of heat produced from a fire.

Around 3500 BC people in Western Asia began melting copper to make sharp edged tools. Simple holes dug in the earth smeared with clay, to make the earth fire resistant, were used as hearths to deoxidise the oxide ore. However, ordinary clay contained impurities which caused it to crack. The clay was purified by adding water to it to form a slush and allowing to stand in the holes of a colander. This allowed the light impurities to rise to the top and the heavy impurities to settle to the bottom, the intermediate layer being purified clay. This method is not disimilar to the method used to purify clays nowadays. Thus the earliest refractory used by man was clay. As this clay was also formed into definite shapes (bricks), clay was also the original castable refractory.

I.2.1 Brick Built Furnaces

Improvements in thermal efficiency were made over the furnaces dug in the earth by using closed vessels. Furnace capacity was increased to provide a larger heating volume. These furnaces were erected by piling up blocks that gave them the required mechanical strength. One of the first places where these blocks or baked bricks were used was in the basin of the Indus river in Pakistan. Smelting of minerals to extract glass, copper, iron etc. was carried out in these furnaces. Bricks have been used for the construction of furnaces from the Bronze to the iron age. Brick lined furnaces were used for an uninterrupted span of 2000 or more years, beginning with their application for iron making to the age of the alchemists in Europe. The temperature in these furnaces, up to the 16th century, was not very high. This meant high quality refractories were not required. However, from the beginning of the 18th century this was no longer true. Smelting techniques were improved in the iron and steel industry, leading to the development of furnaces that were required to withstand high temperatures. As a result, many new types of refractory raw materials appeared. The techniques of manufacturing refractories also improved ultimately leading to the development of a variety of furnaces.

1.2.2 Development of Castable Refractories

The shape of firebricks is the most important factor bearing on the deveolpment of the modern furnace. The fact that firebricks of different shapes could be utilised in various combinations has gone a long way in moulding the shape of furnaces. However, use of firebricks imposed certain restrictions on furnace construction:

a) The combination of mortar and bricks tends to make the joints throughout the furnace susceptible to thermal shock. In places, the bricks may bulge and fall out.

b) More sophisticated furnaces often involve more complex shapes. This involves cutting the bricks during furnace construction by a specially trained worker resulting in an increase in expenses incurred in wages.

c) Local repair in a furnace calls for removing the area where the damage has occurred. This tends to loosen and break the bricks in areas unaffected by the damage, unnecessarily increasing the time and costs required for repair and affecting the furnace operation cycle.

These problems continued for many years in furnace operations. When walls were erected by laying bricks which were expected to serve the role of todays furnace shells as well, the shape of the bricks and their mechanical strength were indispensable factors for the desired qualities of a furnace. However , when steel plate started use as the material for furnace shells, bricks no longer fulfilled this past role.

When the shape of furnaces no longer depended on that of the bricks, designers began thinking how defects with bricks after prolonged use could be eliminated. Refractory bricks are made by adding water to refractory raw materials and moulding the resulting material into the brick shape. These bricks are fired in a calcining furnace to develop the ceramic properties. W. A. L Schaefer of the U. S. A. believed it possible to transfer the raw material to site, build the furnace with it, and then calcine it. After many attempts he identified the importance of setting material in determining refractory strength. In addition to this he welded supporting elements (mainly metallic) on to the shell of the furnace. In this way he was able to erect a self-supporting wall. This pliable material was initially used to repair brick walls in boilers and as the superior merits of the material were recognised it was used to build a monolithic lining structure. The manufacture of castable refractories, a powdery cement like product, on an industrial scale started in 1932.

1.2.3 Castable Refractories

Refractories are primarily heat resistant materials. Their mechanical strength and chemical properties being unaffected by repeated and prolonged exposure to high temperatures. In an application environment, refractories not only have to withstand heat but also extreme fluctuations in temperatures. This is known as thermal shock and can lead to cracks appearing[5]. Another property that a good refractory must have is the ability to withstand the abrasive nature of the material being cast, slag attack (in the steel industry this is generally iron oxide, in the glass industry it may be alkalis) and the cutting action of flue gases.

Till the advent of castable refractories in the beginning of the 20th century, firebricks were the main refractories in use. Castable or monolithic refractories are so called to distinguish them from conventional firebrick. Castable refractories differ from firebrick in two ways:

a) The absence of shape in castables

b) The method of preparation

Castable refractories are referred to using various names as follows:

Unshaped refractories	Mouldable refractories
Specialities	Pliable refractories
Speciality refractories	Refractory concrete
Jointless firebrick	Monolithic refractories

Each of these terms of reference takes into account some characteristic of these refractories. Raw materials used in the preparation of both firebrick and castable refractories are similar but the method of preparation is different. Castable refractories do not require forming and firing, hence, preparation is simpler compared with firebrick. Advantages to this method of preparation include energy savings, faster delivery and higher labour productivity.

1.2.4 Comparing Castable and Firebrick Refractories[6]

Castable refractories are an improvement over firebrick in a number of ways:

1) They require a shorter manufacturing process as they do not need forming and firing. This makes prompt delivery of the product possible and reduces the need for storage space.

2) Absence of firing means energy savings as well as eliminating the need for air pollution equipment for exhaust gases.

3) Nowadays , for better thermal and operating efficiency, furnaces often must be built in larger sizes and complicated shapes. Linings in these furnaces as a result are also complex in shape and therefore require highly skilled bricklayers to build these linings with firebrick. Castable refractories, however, allow the construction of complicated linings with ease. The time required for completion is also reduced. This is because castable refractories can be poured, gunned, rammed, and trowelled in accordance with particular furnace structure.

4) Castable refractories allow the building of a stronger and larger lining structure by using a variety of rigidly held supports.

5) In general castable refractory linings are quite durable even when they are thinner then firebrick linings. Firebrick linings are self supporting and are generally built by bonding bricks of regular size with mortar. As a result, the taller lining must be built thicker in order to prevent it from collapsing. Furnace roofs especially must be made thicker to form an arch. In fact the thickness of the firebrick lining is often determined more by structural considerations than by the need for heat insulation.

Castable refractories are sustained by supports rigidly fixed to the shell and beams. These linings, therefore, need not be made self supporting or arched and can be built to the thickness required to suspend them from supporting fixtures. Thickness of these linings does not determine the strength of the lining structure. Thus thickness of the castable refractory can be determined by heat insulation requirements solely.

6) Firebrick linings are installed by bonding with mortar which deteriorates over time resulting in break up of the joints due to thermal stress. Castable refractory linings are of solid and jointless construction, avoiding this problem.

7) Firebrick linings show greater thermal expansion. Changes in temperature can cause deformation and spalling (fracture due to thermal stress) of brick linings. Castable refractories do not suffer from this because of the firm support given by the supporting fixtures preventing movement due to thermal expansion and contraction. Hence, the lifetime of castable refractories is prolonged.

8) Castable refractories are classified into several types according to their installation technique or physical properties. In addition, they are available in various consistencies and grain sizing powder, paste, clay etc. Methods have been developed for construction to suit the respective materials/installation procedure. Thus castable refractories may be poured, trowelled, gunned, rammed, patched or injected.

The castable material can be pumped over a large distance and in large quantities and poured into position. Depending on the castable chosen, the right method can be selected for transferring and application. This saves on labour costs.

9) Castable refractory structures can be repaired locally. Areas can be repaired without affecting the surrounding area as the castable refractory in a furnace is sustained by a large number of supports. The local repair can be restored by a castable refractory which adheres very well to the surrounding area.

10) Castable refractories are suitable for the installation of gas tight walls. The furnace load is sustained by supports that help the castable materials adhere to the shell and prevent leakage of gases. Castable refractories have a lower thermal expansion than firebricks, and this expansion is checked by supports. Therefore castable refractory walls do not require clearances for thermal expansion that often allow passage for the gases to leak. These clearances are important for firebrick walls because of their thermal expansion. This sealing ability of castable refractories makes them suitable for pressure vessels operating at high temperature and pressure.

1.2.5 Affect of Monolithic Refractories on the Refractories Industry

As users have become aware of the advantages of monolithic refractories, market share of monolithic refractories has steadily increased. Infact, in the late eighties monolithic refractories accounted for nearly 50% of total refractory consumption in the U.S.A. Figure 1.2.1 shows the increase in monolithic refractory consumption since the sixties.

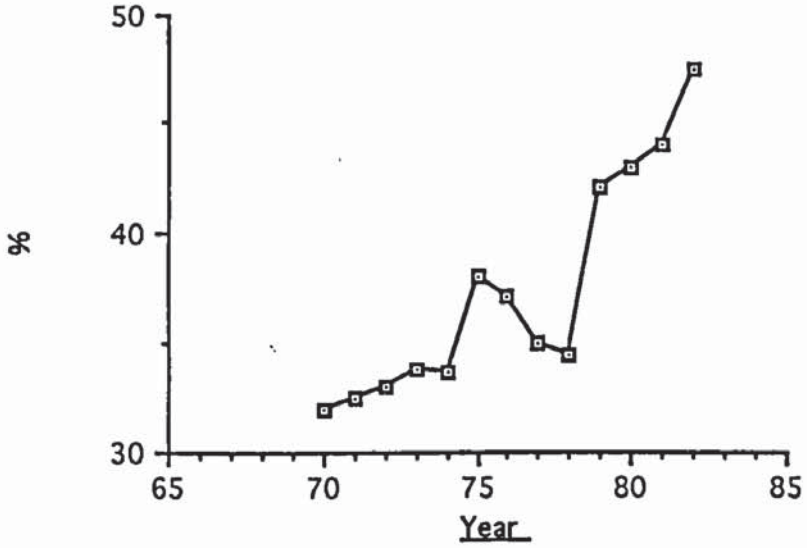

Fig 1.2.1 Change in the ratio of monolithic refractories to total refractories production in the U.S.A (unit:ton)

With castable refractories another important development is the decrease in refractory consumption per ton of steel produced. The steel industry accounts for 72% of total refractory production. Figure 1.2.2 demonstrates the decrease in refractory consumption per ton of steel.

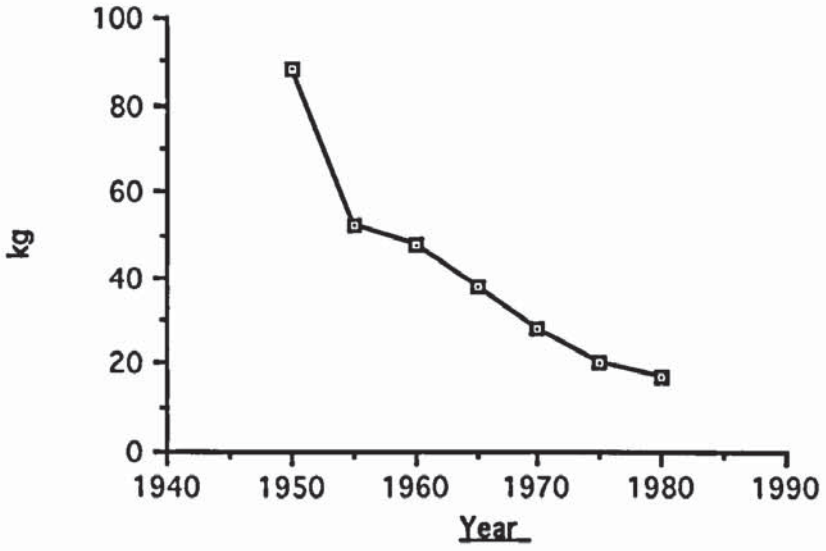

Fig 1.2.2 Decreasing ratio between refractory consumption (kg)/steel production (ton)

1.2.6 The Different Types of Monolithic Refractories and their Classification

Table 1.2.1 The variety and features of principal monolithic refractories.

Materials	Features
Castable refractories	Refractory materials consisting of coarse and fine refractory grains and suitable bonding cement which are installed by pouring after mixing with water.
Trowellable refractories	A sort of castable refractory installed by trowelling.
Plastic refractories	Refractory materials tempered with water and/or added with a binder which have suitable plasticity to be pounded or rammed into place.
Ramming refractories	Similar materials to plastic refractories but more stiffer.
Patching refractories	Refractory materials tempered with water and/or with a binder which have soft plasticity to be patched into place.
Gunning refractories	Refractory materials consisting of coarse and fine refractory grains and suitable bonding agent, and installed with a gunning machine.
Injection refractories	Refractory materials that can be injected into a furnace in the slurry state.
Vibratable refractories	Refractory materials which are exclusively installed by a vibrating cast.
Slinging refractories	Refractory materials which are installed with a slinging machine.
Coating refractories	Refractories which are used for coating on the working surface of the lining having a thin thickness.
Refractory mortars	Finely ground refractory materials which are trowellable when tempered with water, and are used for laying and bonding refractory shapes.

As can be seen from table 1.2.1 the name of the refractory product quite often suggests the method of application or in some cases the physical state of the refractory.

Classification of refractories is carried out using a number of methods. For example refractories are grouped according to their physical state, they are classified according to whether they are in the powder, mud or paste state. Another method of classification is the way in which the refractory is applied, i. e. whether they are poured, trowelled, gunned, injected etc. Other methods of classification are based on setting characteristics, chemical composition and performance. Different methods of setting are hydraulic , heat , air and chemical setting. Various raw materials are used for monolithic refractories, leading to varying chemical composition of the final product. For example refractories produced from quartz or silica sand are termed as silicious refractories, whereas when alumina or bauxite are used as the raw materials the refractories are called alumina refractories. Pyrophyllite, fireclay, sillimanite, and synthetic mullite based products are called silica-alumina refractories.

In terms of classification according to performance, refractories are grouped depending on the temperature they can be used at. Materials are tested for modulus of rupture or cold crushing strength to determine their grouping. Alumina refractories differing only in the amounts of alumina in them, can be placed in different groups using this method of classification depending on their service temperatures.

1.3 Development of a Refractory

Nowadays the attainment of high temperatures has become a relatively simple task. Many engineering processes have made use of this fact. Consequently there is a demand for refractories that can withstand increasingly higher temperatures and broader applications.

The development of a good refractory is dependant on the awareness of a number of important points. Refractories at high temperatures consist of a heat resisting substance and a fusible substance. If the proportion of fusible material becomes too great on prolonged exposure to high temperatures, the refractory will cease to resist the action of heat, becoming soft and distorted hence collapsing under any load. Therefore, on heating, the refractory must have a slow rate of formation of fused material (vitrification rate). Material being processed must not dissolve in the fusible material as this will increase the proportion of fusible material, again leading to collapse of the refractory when a load is applied. Slags (oxides produced when metals are melted) and certain other substances (fluxes) react chemically with refractory materials which they come in contact with, thereby again increasing the proportion of fused material and leading to collapse of the refractory. Refractories must have a minimum surface area to reduce contact with fluxes and abrasives. This is achieved by having refractory materials of low porosity. Shape of the material is also important, one with minimum joints is required. In this respect monolithic refractories have an advantage as they can be cast into various shapes without the need for joints.

1.3.1 A New Refractory Castable

A new bonding technology has been developed for refractory castables by Morgan Materials Technology Limited. Tests have shown this new material to be an improvement over coventional refractory castables in a number of ways[7]. Firstly it is inert to slag attack, low alkali content of the material aids inertness. Figures 1.3.1a and 1.3.1b demonstrate the greater hot strength of the new refractory compared with conventional refractories (HMOR represents hot modulus of rupture). At the temperatures at which conventional refractories show a dip in hot strength, not only is there no such dip in hot strength for the new refractory but there is an increase in hot strength. Furthermore, at temperatures above 1370°C conventional castable refractories show very little hot strength but the new refractory still has residual hot strength. This is because the rapid decline in hot Strength seen in conventional castables at temperatures beyond 1300°C is much more gradual in the new castable refractory.

1.3.2 The Components of the Refractory

The chief constituents of this refractory are bauxite, fumed silica, calcined alumina, clay mineral, potassium silicate and water. Using the method of classification of refractories based on chemical components, the new material is a silica-alumina monolithic refractory.

1.3.2.1 Potassium Silicates

Potassium silicates are poor refractories, forming glasses at high temperatures. However they have ideal adhesive, acid resistance and sintering (binding of a granular or powdered substance by a solid state reaction by heating) properties at low temperatures. These properties account for their use in castable refractories.

Figure 1.3.1a Hot strength of new refractory

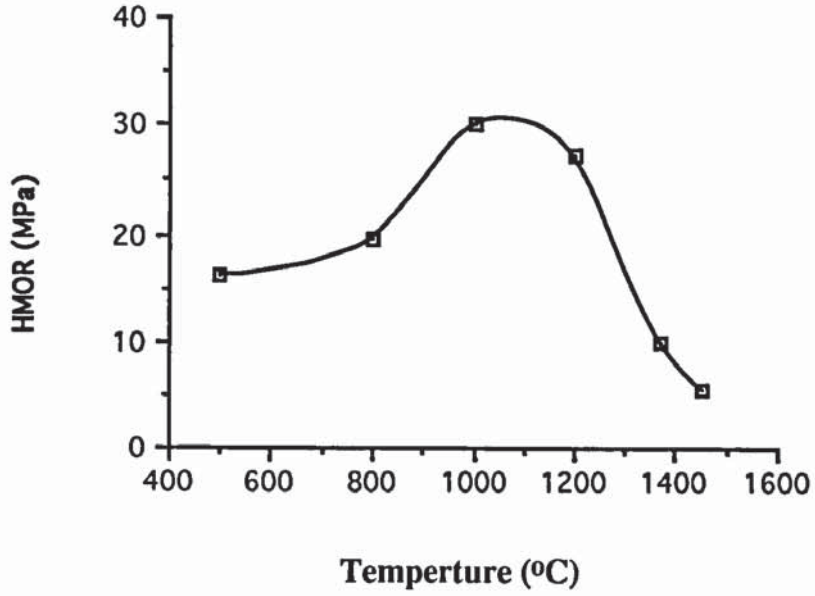

Figure 1.3.1b Hot strength of a conventional refractory

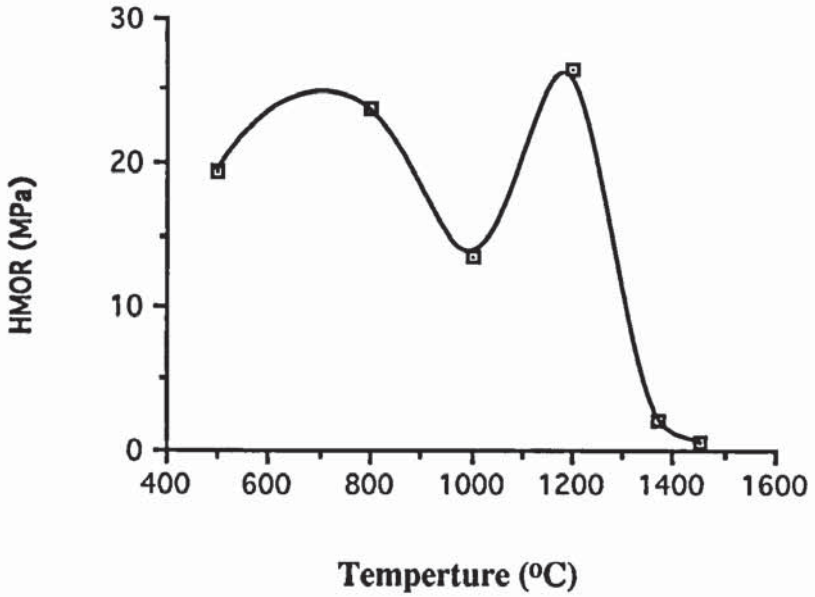

1.3.2.2 Alumina

Alumina is the oxide of the metal aluminium. It occurs in nature in a crystalline form known as corundum and as emery. Emery being more impure and useless as a refractory. Hydrated alumina occurs in such forms as bauxite, laterite, diaspore, boehmite, bayerite and gibbsite. Bayerite and Gibbsite are polymorphs of alumina trihydrate ($Al_2O_3.3H_2O$ or $Al(OH)_3$). Boehmite and diaspore are polymorphs of the monohydrate alumina ($Al_2O_3.H_2O$ or $AlO(OH)$).

Bauxite is the most typical natural raw material based on hydrated alumina, it has a variable composition. The best specimens of bauxite contain only 90% alumina. The hydrated alumina content is mainly as the monohydrate boehmite and the trihydrate gibbsite. Major impurities include silica, iron oxide, water and other minor impurities such as titanium oxide and manganese oxide. The greater the impurity content, particularly if it is iron oxide, the less useful the bauxite is as a refractory. Bauxite may be purified and pure alumina obtained by roasting the crude material to oxidise the iron. The roasted material is then fused with sodium carbonate and the cold mass is treated with water. The alumina is then precipitated by agitation with a small quantity of aluminium hydrate or by passing carbon dioxide through the solution. Another source of alumina is calcined, artificially synthesised alumina hydrate.

The pure alumina melts at 2000-2050°C. It is an important raw material for refractories. When alumina is mixed with clay, it produces a refractory which is an improvement over the bauxite-clay refractory but the disadvantage is the expense of the former.

Alumina exists in a number of forms. α-alumina is the most common form of alumina. This is the form which is produced at temperatures above 1000°C. It is formed when a hydrated alumina is calcined to high temperatures to remove the

combined water, a process often carried out in the preparation of raw aluminous materials for refractory use. The naturally occurring mineral corundum has the α-alumina form. β-alumina is formed by the crystallisation from molten aluminosilicates and by heating alumina with an alkali metal such as Na_2O, K_2O or Li_2O. As such it is not a true allotrope of alpha alumina. γ-alumina is stable below 900°C. It is often amorphous.

1.3.2.2.1 High Alumina Refractories

High alumina refractories are those containing more than 45% alumina, i.e. more than the amount of alumina present in calcined kaolinite. For the production of these refractories use is made of both natural and artificial high alumina materials. Minerals of the sillimanite ($Al_2O_3.SiO_2$) group (cyanite, andalusite, and sillimanite) natural hydrated aluminas contained in bauxite, artificially calcined hydrated alumina and natural corundum can all be used to produce high alumina refractories.

Refractory bricks made from sillimanite minerals have approximately 50% content of alumina. These bricks can withstand acid slags and glasses. Refractory bricks containing 70-73% alumina are known as mullite bricks. Bauxite is used as the raw material to achieve the higher alumina content. These refractories can even withstand iron oxide and lime.

The stable phases formed at high temperatures are dependant on the percentage content of alumina. Refractories with less than 72% alumina have mullite ($3Al_2O_3.2SiO_2$) as the stable phase. When alumina content is greater than 72% corundum or α-alumina as well as mullite are formed as the solid phases. The amount of mullite decreases as the proportion of alumina is increased and the amount of corundum increases. In refractories where alumina content is as high as 95% only corundum is present as the stable phase.

1.3.2.3 Silica

Silica (SiO_2) is a most abundant material. However, only a small proportion is useful for refractory purposes. Silica has a melting point of 1713°C. Refractory silica bricks must contain more than 95% silica to be effective. There are many forms of both crystalline and amorphous silica:

allotrope	stability range
α-quartz	below 573°C
β-quartz	573-870°C
α-cristobalite	below 270°C
β-cristobalite	1470-1713°C
α-tridymite	below 117°C
ß-tridymite	117-163°C
γ-tridymite	870-1470°C
fused silica (amorphous)	below 1713°C
diatomite	below 870°C

The naturally occurring form of silica is α-quartz, this transforms rapidly and reversibly to β-quartz at 573°C. The volume change during this process is great enough to cause shattering of an unfired refractory brick if calcining is not slow enough. β-quartz is stable to 867°C but may persist to higher temperatures. The conversion of β-quartz to tridymite is slow unless catalysed by a mineraliser such as calcium tungstate. Above 1470°C β-cristobalite is the stable allotrope and again the transformation either from tridymite or quartz is slow without the use of mineralisers.

Fused silica, also called fused quartz, consists of amorphous silica glass. It is manufactured by the fusion of high purity silica. Fused silica has a low thermal coefficient (this is important to prevent cracking) and excellent resistance to corrosion.

Diatomite originates from siliceous skeletons of diatoms and consists of amorphous and hydrous silica.

1.3.2.3.1 Silica brick refractories

Refractories of silica brick can be used at temperatures of 1710-1730°C. Under load however initial softening occurs at 1670-1700°C. The thermal expansion of silica between the allotropic change points is very low, therefore spalling (fracture of the refractory unit by thermal, structural or mechanical fracture) resistance is good at high temperatures. Resistance to slag is impressive, even basic slags have much less effect than one would expect considering the acidic nature of the silica refractory brick. Permeability and porosity are also low in silica brick refractories. Another property of silica brick refractories which can be an advantage in some applications is their low density. The most common uses of silica bricks have been as roofs for open hearth steel making furnaces and walls of coke ovens. Silica brick refractories are being replaced and have been replaced by better performing alternatives such as mullite.

1.3.2.4 Clay minerals

Clay minerals are discussed in section 1.4

1.4 Clay Minerals

Clays are hydrous silicates or alumino-silicates and may be broadly defined as those minerals which predominately make up the colloidal fraction of soils, sediments, rocks and waters. The majority of the clay minerals belong to the class of layer silicates or phyllosilicates because their structural framework is basically composed of layers comprising of silica and alumina sheets, joined together in varying proportions and stacked on top of each other. The sheets consist of tetrahedrally coordinated cations of composition X_2O_5 (X = cation) and cations octahedrally coordinated to oxygens and hydroxyls. These sheets are linked to each other by shared oxygens. When one octahedral sheet is linked to one tetrahedral sheet a 1:1 layer is formed as in kaolinite, when one octahedral sheet is shared with two tetrahedral sheets a 2:1 layer is formed as in talc or pyrophyllite.

Since the type of cation occupying tetrahedral and octahedral sites is determined by ionic size and coordination rather than by valency, there is considerable scope for isomorphic substitution in these structures. The site and extent of this substitution form the basis of classifying the clay minerals. For example, in minerals where Al^{3+} occupies the octahedral positions, only 2 out of every 3 of the available octahedral sites are filled to achieve the required charge balance, these are referred to as dioctahedral minerals. Kaolinite is an example of a dioctahedral clay mineral, comprising of an aluminium substituted octahedral sheet and silicon substituted tetrahedral sheet. Minerals where the octahedral sites are occupied by divalently charged cations such as Mg^{2+}, to achieve charge balance every 2 Al^{3+} cations have to be replaced by $3Mg^{2+}$. These are called trioctahedral minerals.

The more commmon situation is the partial substitution of Si^{4+} and Al^{3+} in tetrahedral and octahedral sites respectively, for cations of similar size and coordination but of different (usually lower valency). Such a process gives rise to structures with a

permanent net negative charge. The positive charge deficiency is balanced by sorption of extraneous cations which may or may not be exchangeable. The charge per formula unit is important in classifying the minerals, as is the relative order or disorder of layer stacking.

1.4.1 Kaolin group

The kaolin group also known as the kandite group comprises of clay minerals with 1:1 type layer structure. The name kaolin is a corruption of the Chinese kauling meaning high ridge, a name of a hill were this material is found[6]. The best known mineral of this group is kaolinite, other stuctural varieties include nacrite, dickite and halloysite (kaolinite layers separated by water).

The kaolin minerals consist of a gibbsite sheet ($Al(OH)_3$) and a silica sheet condensed together to form a 1:1 layer structure, one tetrahedral layer of silica and one octahedral layer of alumina. The structure can be represented by $Al_2O_3.2SiO_2.2H_2O$. The structure is capable of indefinite extension in two directions along the a and b crystallographic axis. In clay mineralogy the c distance is known as the basal spacing or d_{001}, in kaolinite the basal spacing is approximately 7Å. The basal spacing is 10Å in halloysite where the layers are separated by water molecules.

As figure 1.4.1a shows two aluminium atoms lie directly above each ring of silicon atoms, however there are three possible cation positions over each ring where an octahedrally coordinated cation could fit. If each of these positions was to be filled by a trivalent cation then the structure would not be electronically neutral. Alumininm ions only fill two thirds of these sites in kaolinite, as shown in figure 1.4.1b, therefore kaolinite is referred to as a dioctahedral mineral.

Figure 1.4.1a Schematic representation of kaolinite

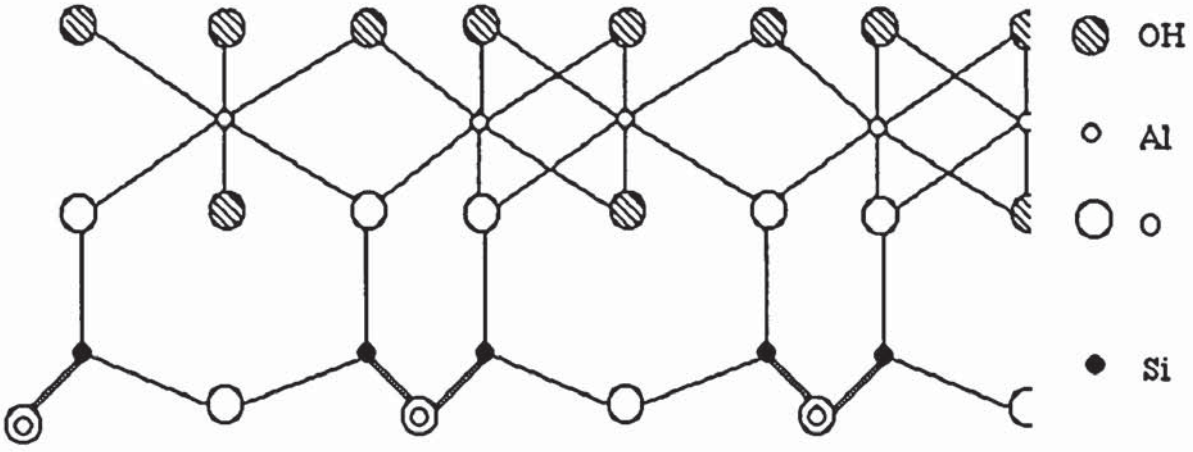

The double lines and double circles in the tetrahedra indicate bonds to two oxygen atoms, one in front and one behind.

Figure 1.4.1b The structure of a formula unit of kaolinite

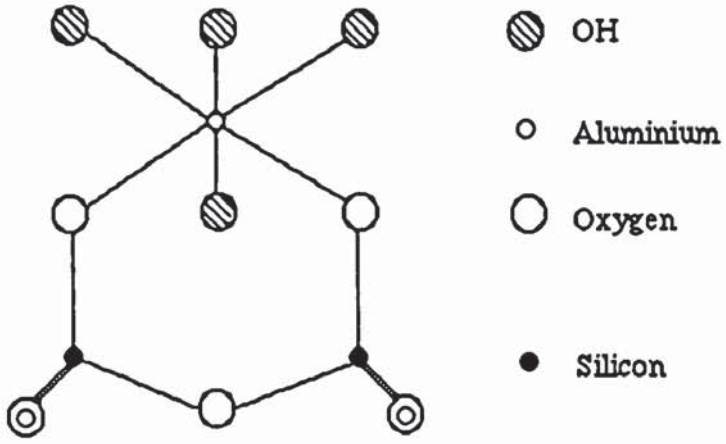

The diagrams show each silicon sharing three oxygens with three silicon tetrahedra and one oxygen with two octahedral aluminiums. Each aluminium shares two oxygens with two silicons from the tetrahedral sheet and is also coordinated to four hydroxyl groups. Two aluminiums in the octahedral sheet share two hydroxyl groups, or one oxygen and one hydroxyl group.

There is very little isomorphic substitution in kaolinite by Mg^{2+}, Fe^{2+}, or Fe^{3+} for Al^{3+}. This is reflected in the low cation exchange capacity (C.E.C) of kaolinite, which

ranges from 3-15m.eq./100g of clay[9]. In kaolinite the C.E.C. is mainly caused by broken bonds around the edge of the crystal, giving rise to unsatisfied charges which must be balanced by exchangeable cations. Kaolinite edge surfaces occupy 10-20% of the total crystal area (15 -40m^2g^{-1}). This is large compared to other minerals, for example in montmorillonite edge surfaces rarely occupy more than 5% of the total area.

Kaolinite is formed from the action of water and carbon dioxide (weathering agents) on feldspar[10].

$$2KAlSi_3O_8 + 2H_2O + CO_2 \rightarrow Al_2O_3.2SiO_2.2H_2O + 4SiO_2 + K_2CO_3$$

Feldspar Kaolinite Quartz

The ideal composition of kaolinites is: 46.54% SiO_2, 39.5% Al_2O_3, 13.96% H_2O. However, in natural kaolinite this composition is rarely seen. Impurities such as iron oxide, titanium oxide, magnesium oxide and copper oxide are commonly found in kaolinites. This ensures that despite there being little isomorphic substitution, kaolinites from different sources are rarely identical.

1.4.1.1 Use of Kaolinite as a Refractory

Refractories produced in greatest volume are made from fireclay[11], the main constituent of which is the silicate mineral kaolinite. Kaolinite is used as a refractory chiefly because of its ability to form crystalline phases (mullite and crystobalite) at high temperatures[12]. Formation of these heat resisting crystalline phases prevents the collapse of the material when a load is applied.

Before the crystalline phases are formed, dehydroxylation of the kaolinite takes place between temperatures of 300°C to 600°C[13]. This dehydroxylation process is seen as a broad endotherm peak centred around 550°C in differential thermal analysis[14]. The dehydroxylation of kaolinite produces amorphous metakaolin ($Al_2Si_2O_7$)[15].

$$\underset{\text{kaolinite}}{Al_2Si_2O_5(OH)_2} \longrightarrow \underset{\text{metakaolin}}{Al_2Si_2O_7} + 2H_2O$$

The hydroxyls are removed from the kaolinite octahedral layer by a layer by layer sequence until metakaolin is formed[16]. The structure of metakaolin consists of anhydrous regions of distorted Al-O tetrahedra containing randomly distributed isolated residual hydroxyls associated with Al-O configurations of regular octahedral and tetrahedral symmetry[17].

At calcination temperatures of 980°C metakaolin decomposes to form spinel phase, amorphous silica and poorly crystalline mullite. This transformation is exothermic[18]. The composition of this spinel phase has been widely debated. Chakraborty and Gosh[18] proposed a $2SiO_2.3Al_2O_3$ chemical composition, while Brindley and Nakahira proposed the composition to be $3SiO_2.2Al_2O_3$[19]. More recently Okada and Otsuka[20] found results from various methods showed the spinel to be γ-alumina. However, even they reported presence of 8wt% SiO_2 in the spinel phase on chemical

analysis. The problem seems to have been resolved by Mazumdar and Mukherjee[21]. They have used lattice energies to characterise the spinel phase. Good agreement has been found on comparing theoretical values with experimental values for the enthalpy of reaction to form γ-alumina from metakaolin. This suggests the spinel is indeed γ-alumina.

As calcination temperatures are increased beyond 980°C the spinel phase is replaced by mullite and cristobalite. At 1200°C a second exothermic reaction takes place in which the spinel phase disappears and mullite and cristobalite are more readily detectable[22]. Mullite exists as needle like crystals at this temperature with no preferred orientation. However morphology and size can be affected by impurities already present or artificially added to the original kaolin mineral[23,24]. Flash calcination, the process by which kaolinite particles are heated at such speeds that steam released within them is generated faster than it can escape by diffusion[25], can yield different products yet again[26,27]. For example, metakaolin generated by flash calcination is predominately pentacoordinate as opposed to tetracoordinate[28].

The major techniques used to study clays and the reactions they undergo on calcining to temperatures up to and above 1000°C are XRD, NMR, infrared and thermogravimetric analysis. As metakaolin is amorphous, it is not amenable to XRD study. However, infrared and nmr studies of the formation of metakaolin and the phases formed at higher temperatures when kaolinite is heated are extensive.

1.4.1.2 ^{27}Al and ^{29}Si NMR Studies of Thermal Reactions of Kaolins

1.4.1.2.1 ^{29}Si NMR studies

Lippmaa and co-workers identified the potential usefulness of ^{27}Al and ^{29}Si NMR in the study of aluminosilicates.[29,30] Since then considerable improvements have been made in the technology. The usefulness of the technique lies in the appearance of well separated peaks depending on the local environment of the Al or Si atoms. For example, an isolated silicate tetrahedron (monosilicate (Q^o)) will show different chemical shift ranges to a silicate tetrahedron which shares one of its oxygen atoms with another Si atom (disilicate (Q^1)); this in turn has different ranges to silicate sharing 2,3 or all 4 of its vertices. These different types of silicates are represented by Q^2, Q^3 and Q^4 respectively. In terms of silicate structures, Q^2 represents Si Sharing two of its vertices, Q^3 represents chain branching sites, Q^4 represents three dimensional crosslinked framework. Furthermore ^{29}Si chemical shifts were correlated with the degree of aluminium substitution for silicon.[31] The greater the aluminium substitution the greater the downfield shift (i.e. less negative numbers). Table 1.4.1 demonstrates the relationship between ^{29}Si chemical shift and silicate structure. Table 1.4.2 demonstrates the relationship between ^{29}Si chemical shift for Q4 resonances and aluminium substitution for silicon.

Table 1.4.1 Ranges of ^{29}Si chemical shift of different structural units of silicate anions in solid silicates.[29](w.r.t tetramethylsilane)

Type of Silicon-oxygen tetrahedra	^{29}Si Chemical Shift Range (ppm)
single tetrahedra (Q^0)	-66 to -76
end group (Q^1)	-78 to -83
middle group (Q^2)	-86 to -89
branching site (Q^3)	-96 to -99
cross-linked group (Q^4)	--107 to -111

Table 1.4.2 ^{29}Si chemical shift ranges for aluminosilicates[32].

Degree of Al Substitution	29Si Chemical Shift Range (ppm)
Si(0Al)	-103 to -114
Si(1Al)	-97 to -105
Si(2Al)	-92 to -99
Si(3Al)	-83 to -94
Si(4Al)	-83 to -87

Si(nAl) designates the SiO_4 tetrahedron connected through shared oxygen atoms with $nAlO_4$ tetrahedra in the aluminosilicate framework.

1.4.1.2.2^{29}Si NMR studies of kaolins

^{29}Si NMR study of kaolinite yields a single resonance at -91.5ppm (with respect to tetramethyl silane (TMS)) which is consistent with a single $Q^3(OAl)$ silicon environment[33]. Impurities such as α-quartz and α-crystobalite appear as signals at -107.6ppm and -109.3ppm respectively. When kaolinite is heated above 450°C the ^{29}Si NMR signal becomes broader and shifts to -98ppm, the wide breadth of the peak is consistent with a large variety of 4-coordinate Si site geometries[15]. On heating to higher temperatures there is a shift in peak position to more negative values (upfield) reflecting a decrease in the number of aluminium groups bonded to the SiO_4. This is because silica is separating from the aluminosilicate phase[34]. At 800°C a broad peak appears at -102ppm characteristic of metakaolinite[35]. Around 900°C the position of the line is -110ppm. This value is the same as the Q^4 signal seen for Si in silica (Si surrounded by four other Si). Spectra of samples heated above 1050°C have two components, the first at -110ppm is attributed to amorphous silica and the second at -88ppm is due to the appearance of poorly crystalline mullite[36]. The mullite and cristobalite resonance has also been reported to appear as a shoulder at -90ppm on the free silica resonace[35]. This resonance at -90ppm corresponds to the main silicate resonance in mullite.

1.4.1.2.3 ^{27}Al NMR studies

High resolution ^{27}Al solid state NMR has proved useful for determining the coordination number in various aluminium containing compounds. ^{27}Al NMR yields distinctive shifts depending on the coordination environment of the aluminium. Octahedrally coordinated Al resonates at 0 +/- 10ppm relative to $[Al(H_2O)_6]^{3+}$. Tetrahedrally coordinated Al resonates at 50-80ppm. For example, tetrahedral aluminium peak shift value in aluminosilicates is 55ppm and in aluminates it is 80ppm[37]. Despite the quadrupolar interactions resulting in a broadening of the resonance for atoms with a nuclear spin quantum number (I) of greater than 1/2 (I=5/2 for ^{27}Al), substantial information can be gained from solid state Al NMR studies. It has been shown that shift values are dependant on the number of silicons attached to the Al via Oxygen[38]. Table 1.4.3 demonstrates the relationship between Si substitution and the ^{27}Al nmr shift values.

Table 1.4.3 ^{27}Al shift values relative to structure.

^{27}Al Shift w.r.t $(Al(H_2O)_6)^{3+}$.	Structural Unit
79.5ppm	AlO_4 (Q^0)
74.3ppm	AlO_3OSi (Q^1)
69.5ppm	$AlO_2(OSi)_2$ (Q^2)
64.2ppm	$AlO(OSi)_3$ (Q^3)

Chemical shifts between 30 and 40ppm are rare and have been ascribed to the five coordinated AlO_5 units[39]. Dehydroxylated form of pyrophyllite contains mainly five coordinated aluminium, this is seen as a signal at around 40 ppm in ^{27}Al NMR[40].

1.4.1.2.4 ^{27}Al NMR studies of kaolins

^{27}Al NMR spectrum of uncalcined kaolinite consists of a single sharp peak at -3ppm due to the octahedral aluminium layer[38]. Heating the kaolinite to 490°C (just before dehydroxylation) produces no change in the ^{27}Al NMR spectra. At temperatures at which dehydroxylation has occurred the signal intensity is reduced to 8% of the original intensity and a tetrahedral signal appears at 65-70 ppm as well as the octahedral signal[34]. The loss in signal intensity on dehydroxylation is due to the aluminium being present in distorted sites which are neither tetrahedral nor octahedral. The ratio of the tetrahedral and octahedral aluminiums is 1:1 according to measurements of peak areas. However there have been reports that tetrahedral Al absorptions are more intense even when the the ratio of occupancies for the different geometries are the same[41], therefore this has to be taken in to consideration before quantification is attempted by ^{27}Al NMR[41]. At calcination temperatures of 700°C to 800°C a second peak appears at 35-38 ppm, it has been shown this signal is consistent with penta-coordinated aluminium. This is formed after the removal of two hydroxyl groups to form the common bond between the two neighbouring AlO_6 octahedra[42], hence the appearance of this peak only after dehydroxylation or metakaolin formation. ^{27}Al NMR of metakaolinite yields a spectrum of a strong signal at 58ppm and two weaker signals at 28 ppm and 2 ppm representing tetrahedral, penta-coordinate and octahedral aluminium respectively[43]. At temperatures above 1000°C, mullite and γ-alumina are formed. The chemical shift for tetrahedral Al in crystalline mullite is 46-48 ppm[15], whereas for γ-alumina it is 62 ppm[44].

1.4.1.3 Infrared studies of kaolinite and it's thermal reactions

Chemical bonds and hence clay mineral structure can be identified using infrared analysis. A thorough study has been carried out of all layer silicates by V. C. Farmer and J. D. Russell[45]. The OH vibrations of clay minerals have been even more closely scrutinized by the replacement of OH for OD[46,47]. Not only can infrared spectroscopy identify mineral group types, it can also identify the extent and type of isomorphic substitution[48]. V. Stubican and R. Roy were able to assign infrared absorption bands to the particular cations (Al^{3+}, Mg^{2+}, Fe^{3+} Fe^{2+}) in the octahedral sites[49]. Infrared spectroscopy has also been used to distinguish between octahedral and tetrahedral substitutions in illite and smectite clay minerals[50].

Infrared analysis can not only identify kaolinite from other mineral groups but also from halloysite and dickite[51]. Infact infrared analysis can be used to make semi-quantitative estimations of the kaolin minerals. Since infrared spectra of kaolinite are clearly defined as are those of halloysite and dickite, the content of these three mineral mixtures can be determined by a ratio between the depths of their hydoxyl absorptions[52]. Modern innovations such as Diffuse Reflectance and Photoacoustic Spectroscopy have also been used to study kaolin and other clay minerals[53]. The study of cation exchanged minerals by photoacoustic spectroscopy has been shown to be an improvment over conventional KBr pellet infrared analysis as absorptions appear which are not seen using the KBr pellet method of analysis[54]. Table 1.4.4 gives assignments of absorption maxima in infrared spectra of kaolinites.

Table 1.4.4 Assignments of absorption maxima in infrared spectra of kaolinites

Band position wavenumbers (cm^{-1})	Peak Assignments
3696	OH stretching of gibbsite sheet[48]
3669	OH in plane vibrations[48]
3652	"
3620	OH stretching on tetrahedral sheet[48]
1109	In plane stretching vibration of SiO[49]
1032	"
1008	"
937	Al-OH in plane vibration rocking vibration[46]
914	"
798	Si-OAl vibrations[48]
758	"
670	OH bending of gibbsite layer in a direction perpendicular to the layers[55]

The presence of a number of hydroxyl absorptions in the 3600-3700 cm^{-1} region reflects the different hydroxyl environments. Hydroxyl groups in the basal plane are known as interlamellar hydroxyls and absorb at the higher wavenumbers of 3700 cm^{-1} the other type are intralamellar hydroxyl groups found in the lattices[56]. Quartz, indicated by a characteristic doublet at 800 cm^{-1} and 780 cm^{-1} and absorption at 700 cm^{-1} is a common impurity in most clay minerals[57].

1.4.1.3 Infrared analysis to study dehydroxylation in kaolin

Infrared analysis can be used to study the extent of dehydroxylation of kaolinite on heating. The hydroxyl peaks in the 3600-3700 cm^{-1} region and peaks representing AlOH vibrations at lower wavenumbers, decrease in intensity as dehydroxylation proceeds. The Si-O stretching maxima is also sensitive to heating, studies have shown there is almost a direct relationship between the temperature at which a silicate is calcined and the shift in wavenumber[58]. The higher the temperature of calcination the greater the shift Of the Si-O maxima to higher wavenumbers. Metakaolinite is characterised by the appearance of a broad band centered around 810 cm^{-1}[56] and a reduction in the band at 538 cm^{-1}, this is due to a shift from octahedral coordination of aluminium in kaolinite to tetrahedral coordination in metakaolinite. The assignments of metakaolinite band wavenumbers are given in table 1.4.5.

Tabel 1.4.5 Assignment of metakaolinite band wavenumbers(cm^{-1})[59]

Si-O bond from SiO_4	Al^{IV}-O bond from AlO_4
1260 w,sh	807 m,br
1203 s,sh	
1152 s,sh	
1071 s,br	
665 w,sh	
479 m	
456 m,br	
428 m,sh	

s=strong, m=medium, w=weak, br=broad, sh=shoulder

Mullite formation which occurs at temperatures above 1000°C can also be identified using infrared spectroscopy. The assignments of mullite band wavenumbers are given in table 1.4.6.

Tabel 1.4.6 Assignment of mullite band wavenumbers(cm^{-1})[59]

Si-O bond from SiO_4	Al^{IV}-O bond from AlO_4	Al^{VI}-O bond from AlO_6	unassigned
1171 s	832 s,br	613 m,sh	1081 w
1120 ms,sh	740 m,sh	567 s	1000 m,sh
960 ms,sh			725 w,sh
927 s,sh			640 w,sh
901 s,br			420 w,sh
542 s,sh			344 w,sh
500 m,sh			306 w,sh
445 m,sh			
362 w,sh			

1.4.2 Pyrophyllite and Talc

Pyrophyllite has a dioctahedral structure, as shown in figure 1.4.2a, with the chemical composition of $Al_2Si_4O_{10}(OH)_2$, the basal spacing is 9.3Å. Talc is a trioctahedral mineral . The octahedral layer consists of Mg rather than Al (see figure 1.4.2b). The mineral can be characterised as $Mg_3Si_4O_{10}(OH)_2$.

There is very little substitution in the tetrahedral or octaheral layers, therefore the sheets are electronically neutral and there are no cations in the interlayer region. The layers are only held together by Van Der Waal's forces.

1.4.3 True micas

When a second tetrahedral silicate condenses onto the octahedral layer sandwiching it, a 2:1 layer structure is formed. Illites are characterised by this 2:1 type layer structure. The mica group can be divided into many sub-groups but for the purposes of our study we need mention only a few.

1.4.3.1 The Micas and illites

The illites are also part of the mica group. Micas differ from talc and pyrophyllite in that the layers in the micas are not electrically balanced. This results in the presence of cations in the interlayer region to achieve charge balance resulting in a fundamental change in properties. The layers have a large charge deficiency, approximately one per unit, corresponding to the substitution of approximately one in every four silicons by an Al^{3+} ion. The cation introduced into the interlayer to achieve charge balance is held very strongly as the bonding is similar to ionic bonding. This introduces a link between successive sheets through these cations. These cations cannot be exchanged or removed without the decomposition of the mineral. The introduction of water into

the interlayer does not swell the mineral as the layers are held together. The octahedral layer can contain many different cations, this diversity accounts for the many types of mica:

Muscovite mica which can be represented by $KAl_2(AlSi_3)O_{10}(OH)_2$.

The biotite micas such as phlogopite ($KMg_3(AlSi_3)O_{10}(OH)_2$) and biotite ($KMgFe_3(AlSi_3)O_{10}(OH)_2$). Brittle micas such as margarite($CaAl_2(Al_2Si_2)O_{10}(OH)_2$).

Illites are similar to micas but the amount of substitution of aluminium for silicon in the tetrahedral layer is much less, only one in eight silicons are substituted. As a consequence there are fewer cations in the interlayer region. Isomorphic substitution of the octahedral aluminium by Mg^{2+}, Fe^{2+} and Fe^{3+} is possible. Na^+ and Ca^{2+} can appear in the interlayer as well as H_3O^+ ion which can lead to more water in the interlayer than in the micas. Glaucite is a member of the illite group. The basic structural formula for the illites is $K_xAl_2(Si_{4-x}Al_x)O_{10}(OH)_2$, where $0.5 < X < 0.75$.

1.4.4 The smectite group`

Clay minerals in this group have a 2:1 layer structure and can be dioctahedral or trioctahedral. The chemical composition is similar to the mica group, but the bonds between the layers are weaker because of internal chemical substitutions. Due to these weak interlayer bonds smectites have the unique ability to exchange interlayer cations and swell by absorption of water onto the interlayer surface or cation. Smectite structures are based on those of pyrophyllite and talc, deviations occur by the Isomorphic substitution which occurs both in the octahedral and tetrahedral layers. The substituting cations are usually of a lower valency which results in a layer charge of 0.2 - 0.6 per sructural unit. Sodium and calcium are normally the cations seen in the interlayer to achieve charge balance. These interlayer cations, unlike in other minerals, are easily exchanged. Hence, smectites have a large cation exchange capacity range of 80 -150 meq per 100g of clay. The general formula for this clay group is $Al_2Si_4O_{10}(OH)_2.nH_2O$.

Hectorite has the formula $Na_{0.33}(Mg_{2.67}Li_{0.33}OSi_4O_{10}(OH)_2$ and saponite with the formula $Na_{0.5}(Mg_3)Si_{3.5}Al_{0.5}O_{10}(OH)_2$ are examples of trioctahedral smectites. Montmorillonite $(Na_{0.33}(Al_{1.67}Mg_{0.33})Si_4O_{10}(OH)_2)$ is an example of a dioctahedral smectite, other dioctahedral smectites include biedellite and nontronite.

The extent of swelling of the smectites caused by the hydration of the interlayer cation is dependant on two factors:

a) Relative humidity

b) Nature of the interlayer cation

When sodium is the interlayer cation, hydrates with upto 3 layers of water molecules between the layers are seen and at greater humidities the 2:1 layers may disperse. When Calcium is the interlayer cation this swelling is limited to the three water layers, where the 2:1 layers are separated by 9 Å[60].

1.4.4.1 Cation Exchange Capacity

For montmorillonite to have a high exchange capacity (80-150meq/100g of clay) and peculiar hydration properties that it has, requires a relatively low amount of isomorphous substitution (0.25-0.6 per unit formula) in the basic pyrophyllite structure on which it is based. 80% of the cation exchange capacity of smectite clays is due to this isomorphous or structural substitution, while 20% is due to charges from broken bonds at the edge of crystals[61]. Mg^{2+}, Fe^{2+} and Fe^{3+} are the common substituents in the octahedral layer. Al^{3+} can be found substituted for the Si^{4+} in the tetrahedral layer but this is to a lesser extent. The average value of cation content, deduced from a large number of montmorillonites-beidellites are 1.49 and 0.19 for octahedral aluminium and iron, respectively, and 0.16 for tetrahedral aluminium expressed on a per formula unit basis.

Cations such as Ca^{2+}, Mg^{2+}, Na^{+} and H^{+} are present on smectites to achieve charge balance after the imbalance caused due to isomorphic substitution. In the 2:1 type phyllosilicates such as montmorillonite only a relatively small proportion of the extraneous cations balancing the negative charge layer is located at external crystal surfaces, the majority being present in the interlayer space. In montmorillonites and vermiculites, all of these cations are normally exchangeable for other species in solution allowing adsorption of foreign ions/molecules on to montmorillonite. In fact the presence of exchangeable cations plays a dominant role in the commercial use of smectite clays.

1.4.4.2 Smectites as Absorbants for Organics

In addition to their ability to absorb water and inorganic cations, smectites are capable of taking up organic molecules in the interlamellar regions. The organic molecules can bind to the interlamellar surface by physical adsorption to the silicate structure or in some cases bond to the metal ions present at the ion exchange sites. For example, benzene, toluene and xylene form highly coloured complexes with copper (II) ions on montmorillonite[62]. This is achieved by π-complex formation between the aromatic molecules and the metal ion . The dioctahedral montmorillonite of the smectite group is the most important and widely used adsorbent for organic compounds. The capability of montmorillonite to accommodate guest molecules is due to its ability to show extensive interlayer expansion or swelling which allows exposure to a large active surface area (700 - 800m^2g^{-1})[63].

Besides the charge balancing cations, water is normally present in the interlayer space where it tends to associate with cations, forming hydration shells around them. Water coordinated to the exchangeable cations plays an important part in the interaction of montmorillonite with small, uncharged organic compounds. This is so because the polar groups of such compounds compete with water for the same ligand sites around the cation. A simple example of a smectite clay-organic reaction is one involving glycerol or ethylene glycol. These organic compounds replace water layers on the interlamellar surfaces and so become attached to the clay. The replacement of the water by the larger organic molecule results in an increase in the interlayer distance.

Organic acid anions such as oxalic acid, polyacrylate, polyacrylamide and sulphonated polyacrylamide can also be adsorbed by smectite clays despite the high negative charge of the layers. The chief mechanism of binding these organic anions is the formation of chelate complexes between the Al-ions and the carboxylate group of

the anions. Divalent ions can also bind to the anions via cation bridges. The sites for anion adsorption are primarily on the surface of crystal edges[64].

Because of the ability of smectites to adsorb various organics and inorganics, increasing use is being made of them to absorb organic and inorganic contaminants from industrial waste water. In these processes a small amount of clay is added to the water to adsorb the contaminants, then other chemicals are added to flocculate the clay for easy removal.

1.4.4.3 Smectites Modified by Ion Exchange

Quarternary ammonium ions can replace the exchangeable cations on the montmorillonites resulting in a modification of the properties of the clays. Addition of a quarternary ammonium salt to montmorillonite leads to the rapid and essentially complete removal of the exchangeable ions[65]. The ammonium salt exchanged clay is very stable, solvents do not significantly dissolve the amine from the clay and high concentrations of the exchanged cations also cannot replace the ammonium compound. If the quarternary ammonium has a long organic chain (the affinity of organic ions for the clay increases with chain length[66]), an organophilic clay is produced. Such clays have a variety of applications including paints, oil-well drilling fluids, plastics and greases. Trimethylphenylammonium (TMPA) cations when exchanged onto montmorillonite or other smectites aid the sorption of aromatic compounds. It is thought the perpendicular orientation of TMPA on montmorillonite allows other aromatic compounds to sorb in the clay interlayer with their aromatic ring perpendicular to the surface. This allows aromatics to interact with TMPA via π-π interactions, therefore enhancing sorption[67]. Another example of this type of modification of smectite clays is Fe (II) and Cu (II)-1,10-phenanthroline chelate complexes with hectorite. Again the presence of the complex in the interlayer region

improves the adsorption of molecules. This is achieved by increasing the interlayer space. The magnitude of the interlayer space in this modified smectite is 8 Å[68].

Metal complexes of the ligand 2,2-bipyridyl and tripyridylamine which is synthesised from 2,2-bipyridyl, have been exchanged onto clays and their behaviour studied[69,70]. These metal complexes when bound to the interlayer surfaces of smectite again expand the interlayer distance, thus exposing the surface regions between the exchange ions for adsorption or surface catalysed reactions.

Since many catalysts tend to have a similar structure to these metal complexes that can be so easily exchanged onto montmorillonites, montmorillonites can be used as supports for these catalysts. Clay supported catalysts for organic reactions have advantages such as greater ease of phase separation and occasionally shorter reaction times[71].

Smectites are also modified by the intercalation of hydroxy-metal polycations. This involves introduction of large metal polycations into the interlayer spaces of the clays using ion exchange from aqueous solutions. The polycations act as "pillars" supporting the layers. After calcination the "pillars" are converted to oxide "pillars" and the structure becomes more rigid[72]. These modified smectites have a large surface area, porous structure and high surface acidity.

1.5 Microwave Technology

Microwave ovens have been added to the chemist's repertoire of methods of accelerating chemical reactions. Closed teflon vessels in microwaves have been employed to improve the speed of many reactions.

The microwave region of the electromagnetic spectrum lies between infrared radiation and radio frequencies and corresponds to wavelengths of 1 cm to 1 m (frequencies of 30 GHz to 300 MHz respectively). The wavelengths between 1 cm and 25 cm are extensively used for RADAR transmissions and telecommunications make use of the remaining wavelength range. To avoid interfering with these uses, domestic and industrial microwave heaters are required to operate either at 12.2 cm (2.45 GHz) or 33.3 cm (900 MHz) unless the apparatus is shielded in such a way that no radiation losses occur. Domestic microwave ovens normally operate at 2.45 GHz. The microwaves are generated by a device called a magnetron[73].

Microwave heating in synthesis reactions can only be applied if at least one of the components is able to absorb microwave radiation. Only molecules with a charge or dipolar molecules such as water are able to absorb microwaves. However reactions of reactants not receptive to microwaves can be carried out by using solvents that are receptive to microwaves.

Microwaves can heat liquids and solids in two ways. If there are charged particles present in the reaction mixture that can move then these will move under the influence of the alternating electric field, producing an oscillating electric current. Resistance to their movement causes energy to be transferred to the surroundings as heat. This is known as conduction heating. If there are no particles which can move freely but there are molecules such as water which have dipole moments, then the electric field acts to align the dipole moments. This produces an effect known as dielectric heating. It is

this effect acting on water molecules that is resposible for the heating of food. The electric field of microwave radiation, like that of all electromagnetic radiation, is oscillating at the frequecy of the radiation. The electric dipoles in the solid do not change their alignment instantaneously but with a characteristic time, τ. If the oscillating electric field changes its direction slowly so that the time between changes is much greater than τ then the dipoles can follow the changes. A small amount of energy is transferred to the surroundings as heat each time the dipole aligns but this is only a small heating effect. If the electric field of the radiation oscillates very rapidly then the dipoles cannot respond fast enough and do not realign. If the frequency of the microwave radiation is such that the electric field changes sign at a speed that is the same order of magnitude as τ, then under these conditions the dipole realignment lags slightly behind the change of electric field and the solid absorbs microwave radiation. This absorbed energy is converted to heat. The quantities governing this process are the dielectric constant, which determines the extent of dipole alignment and dielectric loss, which governs how efficiently the absorbed radiation is converted to heat.

1.5.1 Microwave Assisted Synthesis

Microwave heating has been used to improve rates of reaction in both the organic and inorganic chemistry fields. Certain organic reactions have been reported to be up to 1240 times faster when carried out using closed teflon vessels in a microwave oven compared with conventional reflux techniques[74]. The reaction times of well known organic reactions such as Diels-Alder and Claisen reactions have been dramatically reduced using microwaves as the method of heating[75].

Microwave technology has been just as impressive in the inorganic chemistry field. For example, a number of ternary inorganic oxides have been synthesised in high yield and in a fraction of the time required for conventional heating methods[76]. The synthesis time of the catalyst magnesium aluminophosphate-5 has been reduced from 24 hours using conventional hydrothermal conditions to 20 minutes using microwave heating. A further advantage using microwaves for this synthesis is the increased surface area of the product, this is useful in the compounds capacity as catalyst[77]. An even more impressive reduction in time for synthesis has been in the clay chemistry field. Lithium-exchanged laponite can be produced in 5 minutes in the microwave oven compared with several weeks using traditional methods[78]. Other uses of microwaves in the clay chemistry field include drying of intercalated smectites without affecting any other properties[79].

Chapter Two

ANALYTICAL TECHNIQUES

2.1 Atomic Absorption Spectroscopy

Atomic absorption measurements were carried out on a Perkin Elmer 360 instrument. Standard sodium nitrate solution was used as the reference material for sodium analysis.

2.2 Fourier Transform Infrared Spectroscopy (FT-IR)

Infrared spectra were obtained using the Bio-rad FTS-40A spectrometer incorporating a 600 microwatt 632.8 nm CW class II laser. Spectra were gained in the frequency range 5000cm^{-1} to 4000cm^{-1} (near-IR region) and 4000cm^{-1} to 500cm^{-1} (middle IR region) using compressed KBr discs. Spectra in the frequency range 500cm^{-1} to150cm^{-1} (far-infrared region) were obtained using polyethylene discs.

Diffuse reflectance IR spectra were obtained using a powdered mull of sample and KBr.

2.3 Magic Angle Spinning Nuclear Magnetic Resonance Spectroscopy (MASNMR)

^{29}Si and ^{27}Al MASNMR spectra were obtained using the Brucker AC300 instument at Aston univeristy. Tetramethylsilane and aluminium sulphate were used as standards respectively. Samples were analysed using rotor spinning speeds of 5 MHz.

^{29}Si and ^{27}Al MASNMR analysis was also obtained from Germany using rotor spinning speeds of 14 MHz. The reference material used was octahedral Yttrium aluminium garnet.

2.4 Melting Points

A Gallenkamp electrically heated melting point apparatus with a mercury thermommeter was used to determine melting points.

2.5 pH Measurements

pH measurements were made using a Hanna Piccolo 1 pH meter with a range of 1-13pH.

2.6 Raman Spectroscopy

Spectra were gained using facilities at Brunel University. A Perkin Elmer 1710 FT Raman accessory was used.

2.7 Scanning Electron Microscopy

Information using scanning electron microscopy was obtained from the analytical department at Morgan Materials Technology Limited.

2.8 Thermogravimetric and Differential Thermal Analysis

Thermogravimetric and Differential Thermal Analysis data were obtained using a Linseis L81 instrument (version: V4.30 from PL Thermal Sciences) with a maximum temperature range of 1200°C.

2.9 Ultraviolet/visible Spectrophotometer (UV)

Ultraviolet/visible solution spectra were obtained from a Pye Unicam SP1800 spectrometer using 1 cm quartz cells.

2.10 X-Ray Diffraction

X-ray diffraction studies of the different types of kaolinites and their thermally treated versions were obtained using facilities at Aston University (Phases were identified using reference data) and at the analytical department of Morgan Materials Technology Limited.

3.11 X-Ray Photoelectron Spectroscopy (XPS)

XPS analysis was obtained using a VG-Scientific ESCALAB 200-D instrument using MgK (1254eV) radiation. The reference used was the C(15) photo peak.

Chapter Three

EXPERIMENTAL

3.1 Treatment of the Clay Minerals

Kaolin minerals A, B, and C were provided in the calcined and uncalcined forms. The uncalcined minerals were treated in an electric muffle furnace at various temperatures for 2 hours. The minerals were then labelled according to the temperatures at which they were calcined, for example mineral A calcined at 200°C was labelled A200, mineral C calcined at 400°C was called C400 and so on. Mineral B was provided in the calcined form only, so this heat treatment could not be carried out. These heat treated samples were then analysed using IR, MASNMR, XRD, XPS, and Raman spectroscopy. Comparisons were made on the effects of each calcination temperature on individual minerals and the differences between corresponding minerals.

3.2 Preparation of refractory component mixtures

3.2.1 Apparatus and Materials Used

Apparatus used for the preparation of refractory component mixtures were: furnace, oven, electric stirrer, beaker, brickette moulder and an air-tight bag.

Components of the refractory supplied by Morgan Materials Technology Limited included calcined and uncalcined clay minerals (A, B, and C), potasium silicates (X, Y, and Z), alumina and silica.

3.2.2 Preparation of two component mixes

Calcined kaolin clay mineral and potassium silicate were mixed in a 1:1 weight ratio, water was added while the mix was manually stirred until a flowing but viscous mix was produced. The mixture was left stirring using an electric stirrer for 2 h. The mixture was then poured into the brickette moulder, placed in an air-tight bag and left to set overnight. After setting, the brickette of the mix was oven dried for 24 h at 80°C. The brickette was then divided in half, one half was calcined at desired temperatures (normally 1000° C) for 2 hrs while the other half was not treated further. Both halves were studied using a variety of analytical techniques. A variety of mixes were prepared by this method by using different combinations of calcined clay mineral and potassium silicate.

3.2.3 Preparation of three component mixes

Clay mineral, potassium silicate and alumina or silica were mixed in 1:1:1 weight ratio and treated as for the two component mixtures. Several of these three component mixes were prepared by using various combinations of the materials.

3.3 Preparation of Samples for Infrared Analysis

3.3.1 Middle IR Region ($4000cm^{-1}$ - $400cm^{-1}$)

Accurate weighings of mineral samples and oven dried potassium bromide were carried out in order to obtain a mixture of 2% concentration. Thorough mixing was carried out to ensure a homogeneous mixture was produced. The mixture was ground into fine particles and 0.05g of the mixture was used to prepare the disc for IR analysis. Standard procedure of using a vacuum pump was followed to prepare the potassium bromide disc. This procedure was accurately repeated for each sample to ensure the infrared results could be used semi-quantitatively.

3.3.2 Near IR region ($5000cm^{-1}$ - $4000cm^{-1}$)

Samples were prepared using a similar method as for the middle IR region but discs of 3% concentration were prepared in this case.

3.3.3 Far IR region ($400cm^{-1}$- $150cm^{-1}$).

Polyethylene was used as the matrix material. Discs were again prepared using a similar method as for the middle IR region. Due to the difficulty in handling polyethylene, no attempt was made to obtain quantitative measurements.

3.3 4 Diffuse Reflectance FTIR measurements

Samples of minerals and potassium bromide were ground together to a fine powder. Standardised samples of 2% concentration by weight were prepared again ensuring thorough mixing of the sample and KBr was achieved. The mixture was then packed in a column before analysis.

3.4 Microwave Synthesis of Kaolinite

Microwave synthesis was attempted using an industrial microwave of the MES 1000 range built by the CEM corporation.

3.4.1 Microwave kaolin synthesis based on the method applied by C. DeKimpe and M. C. Gastuche[1]

0.2 cm^3 of ethyl silicate was added to 16 cm^3 of 0.1 M HCl in a teflon vessel, this was followed by 0.1 g of aluminium hydroxide (gibbsite). The mixture was thoroughly mixed before microwave treatment. The experiment was repeated many times using various combinations of microwave power output, maximum temperature and pressure settings and time lengths of treatment were applied. After microwave treatment the teflon vessel was left in an oven at 70°C overnight. The powdery remains were analysed using infrared analysis.

3.4.2 Microwave kaolin synthesis based on the method applied by A. Leonard *et. al*[2].

2.9 cm^3 (2.7g) of tetraethylsilicate (TEOS) was added to 20 cm^3 of deionised water in a teflon vessel. 2.65 g of aluminium isopropoxide dissolved in 50 cm^3 of isopropanol was slowly added over a period of 20 min. The mixture was continuously stirred during the addition. 15 cm^3 aliquots of the mixture were microwave treated. Again the experiment was repeated many times using various combinations of microwave power output, maximum temperature and pressure settings and time lengths of treatment before infrared analysis.

3.4.3 Microwave kaolin synthesis based on the method applied by S. Satokawa *et. al*[3].

1M Sodium silicate (Na_2SiO_3) aqueous solution was prepared from a mixture of water glass (supplied by Morgan Materials) and NaOH. A 0.5 M aqueous solution of aluminium sulphate was also prepared. Both solutions were added dropwise constantly (100 cm^3/min) at the same time and stirred in a teflon reaction vessel at 40°C. The Si/Al ratio was adjusted to 1.0, which is equal to that of kaolinite. pH was adjusted to pH 4.2 by using NaOH. Na ion impurities were removed by using a cation exchange resin and sulfate ions were removed by boiling. The purified gels were treated in the microwave oven using various combinations of microwave power output, temperature and pressure settings and time lengths of treatment.

3.5 Intercalation of Metal Complexes onto Montmorillonite

3.5.1 Purification of Montmorillonite

Wyoming bentonite was supplied by Steetley Minerals Ltd. 6 g of wyoming bentonite were placed in a conical flask containing 175 cm^3 of distilled water. The flask was sealed and left shaking on a mechanical shaker at 300 rpm overnight. After shaking, the flask was left to stand for approximately 2 h to allow heavy impurities to settle out. The purified montmorillonite was decanted. The impurities were dried and weighed to allow the calculation of montmorillonite in suspension. The suspended montmorillonite was stored ready for use.

3.5.2 Preparation of metal complexes

3.5.2.1 Synthesis of the tri-(2-pyridyl)amine ligand

Tri-(2-pyridyl)amine was synthesised by using a literature method[80].

5.5 g of di-(2-pyridyl)amine was introduced to a three neck round bottom flask followed by 2g of copper bronze (catalyst), trace of potassium iodide, 6g of anhydrous potassium carbonate, 50 cm^3 of xylene and 5.2 g of 2-bromopyridine. This mixture was left stirring and refluxing for 16 h. Steam distillation was used to remove the excess solvent and 2-bromopyridine. The liquid product (quickly solidifies on cooling) was collected by hot filtration.

3.5.2.2 Synthesis of Tris-2,2-bipyridyl iron(II) perchlorate, $[Fe(bipy)_3](ClO_4)_2$

2,2-Bipyridyl transition metal complex of Fe(II),$Fe(bipy)_3](ClO_4)_2$ was synthesised using a literature method[81].

0.2 g of 2,2-bipyridyl was dissolved in 300 cm^3 of hot water. This solution was then treated with an excess of iron(II) sulphate and sodium perchlorate solution. The resulting red solution was treated on a hot plate for one hour and then left to cool. The red crystalline perchlorate which separated was filtered, washed with distilled water and dried under vacuum.

3.5.2.3 Synthesis of bis-tri-(2-pyridyl)amineiron(II) perchlorate or :

Fe(II), $[Fe(tripyam)_2](ClO_4)_2$

Tri-(2-pyridyl)amine metal complex of Fe(II), $[Fe(tripyam)_3](ClO_4)_2$ was synthesised using literature methods[82,83].

0.19 g of iron perchlorate hexahydrate dissolved in 10 cm^3 of ethanol were mixed with 0.24 g tri-(2-pyridyl)amine dissolved in 10 cm^3 of acetone. The orange brown solution which deposited during 2 h was collected by filtration and recrystallised from a 1:1 acetone/water solution before being air dried.

3.5.2.4 Synthesis of bis-(hydrotris-(1-pyrazolyl)borato)iron(II), $Fe[HB(pz)_3]_2$

Bis-[hydrotris-(pyrazolyl)borato]iron complex was synthesised using literature methods[84,85].

Aqueous solution of iron (II) perchlorate (0.45 g) was added to an aqueous solution of sodium hydrotris-(1-pyrazolyl)borate (0.9 g). A purple precipitate immediately appeared, the mixture was left stirring for 0.5 h. The precipitate was collected by filtration and recrystallised from xylene.

3.5.3 Preparation of metal complex-exchanged montmorillonite

The amount of complex required to exchange onto a given amount of montmorillonite was calculated using the equation:

$$\text{g of complex needed} = \frac{\text{meq of clay} * \text{kg of clay used} * \text{RMM of the complex}}{\text{purity of the complex} * \text{valency of complex}}$$

where:

Purity of complex is expressed as a percentage

valency of the complex = charge on the salt

meq of montmorillonite = 90

The calculated mass of complex was added to the purified montmorillonite in a conical flask and sealed. The sealed vessel was placed on a rotary mechanical shaker at 300 rpm and left shaking for one week. After shaking, the exchanged clay was centrifuged, washed with deionised water, air dried and ground to a fine powder.

3.5.3.1 Intercalation of Bis[hydridotris-(1-pyrazolyl)borato]Fe (II)

When the complex Bis[hydridotris-(1-pyrazolyl)borato]Fe (II) was intercalated, a 1:1 mixture of ethanol and water were used as the suspending solvents during the week long shaking period.

100 mg of montmorillonite exchanged with one of the synthesised complexes was added to a variety of concentrations of trichlorophenol (1.0, 0.8, 0.6, 0.5, 0.4, 0.2, 0.1 mmole/g) in distilled water. The total volume of the solution was 100 cm^3 in each case. The flasks were shaken over two nights in a temperature controlled water bath at 20°C, filtered, and the solution analysis carried out by UV. This was repeated using chlorophenol and phenol. Adsorption isotherms were plotted using absorptions at 293 nm for trichlorophenol and at 274 nm for the chlorophenol and phenol in the UV spectrum. These particular wavelengths were used as it was found that Beer-Lambert law is obeyed at these wavelengths in the concentration ranges used[86].

Chapter Four

KAOLIN CLAY MINERALS

4.0 Introduction

The initial study has been mainly concerned with characterising the clay minerals. The three clay minerals provided by Morgan Materials: A, B and C are all of the same kaolin mineral group but are from different natural sources. They are chemically similar but their effect on the performance of the novel bond suggests minor differences between them. These minor differences between the clay minerals are to be expected because of their natural origins, clay minerals from different natural deposits being rarely identical. It is important to identify these minor differences and relate them to performance so Morgan Materials can make suitable moulds for different applications without the need to go through laborious trial and error procedures. The clay minerals have also been compared after thermal treatment at various temperatures as it was anticipated that these minor differences may be more apparent after calcining.

4.1 XRD

The clay minerals were analysed by X-ray diffraction, key reflections were observed to identify differences and presence of impurities in the minerals. On comparing minerals A and C (uncalcined minerals), A is found to have kaolinite as the major component, whereas a number of other phases are present in mineral C. Table 4.1 and table 4.2 show the phases present in minerals A and C respectively. Catalogue reference numbers are also given in the tables for the phases identified.

Table 4.1 Phases identified in mineral A

Phase	Formula	Reference Number
Kaolinite	$Al_2Si_2O_5(OH)_4$	14-164
Kaolinite-1A	$Al_2Si_2O_5(OH)_4$	29-1488

Table 4.2 Phases identified in mineral C

Name	Formula	Reference Number
Kaolinite	$Al_2Si_2O_5(OH)_4$	14-164
Muscovite	$KAl_3Si_3O_{10}(OH)_2$	19-814
Halloysite	$Al_2Si_2O_5(OH)_4.2H_2O$	29-1489
Quartz (possibly)	SiO_2	33-1161
Rutile (possibly)	TiO_2	34-180

Tables 4.1 and 4.2 clearly demonstrate the differences between the clay minerals A and C. Material C contains two minerals from the kaolin group (kaolinite and halloysite) as well as a mineral from the mica group namely muscovite. Polestar was not available in the uncalcined state so was not included in this study. Figures A1 and A2 in the appendix show XRD traces of these kaolins.

XRD spectra of calcined minerals A, B and C showed fewer peaks present and a broadening of the peaks that were present. In fact minerals calcined to 600°C and above gave very poor spectra, phases seen in the uncalcined materials could not be identified in these materials. The poor spectral quality is probably due to the loss in crystallinity during calcination. This is consistent with literature which states that at 550°C dehydroxylation of the mineral occurs, resulting in an intimate amorphous mixture of alumina (Al_2O_3) and silica (SiO_2).

4.2 XPS

Essentially preparation of the new refractory involves reactions at the surface of the components used. Surface differences as opposed to bulk differences between the clay minerals could be important in affecting the performance of the moulds. Hence XPS analysis has been undertaken to investigate these possible differences. Figure 4.1 is an XPS spectrum obtained from the analysis of mineral C. Table 4.3 exhibits results obtained on XPS analysis of minerals A, B and C.

Table 4.3-Results from XPS studies of minerals A, B and C

Elemental Identity	Atomic (%)		
	Mineral A	Mineral B	Mineral C
Al	17.5	15.6	16.2
Si	19.1	20.3	21.6
C	14.7	17.2	15.1
K	-	0.3	0.7
O	48.6	45.9	46.3
F	-	0.5	0.9

XPS analysis has identified major surface differences between the minerals. Table 4.3 shows mineral A to contain no elements in the surface other than the ones expected

for this type of mineral. Minerals B and C contain potassium and fluorine in varying proportions demonstrating the differences between the minerals. Presence of potassium in mineral C is further evidence for the presence of muscovite in this material.

Another difference of potential importance is the ratio of Al:Si. A high ratio is desirable because the crystalline mullite ($3Al_2O_3.2SiO_2$) which forms at high temperatures and is important for refractory strength contains a high proportion of alumina. The Al:Si ratios for the three minerals are:

Mineral A	0.92
Mineral B	0.76
Mineral C	0.75

XPS analysis reveals that mineral A contains a higher Al:Si ratio compared with minerals B and C, bulk chemical analysis data obtained from manufacturers also identified mineral A to contain a higher proportion of alumina when comparing with minerals B and C.

4.3 Raman Spectroscopy

Theoretical considerations of lattice vibrations of layer silicates by V.C. Farmer and J.D. Russell[45] have suggested some of the vibrations in these minerals to be Raman active. With this knowledge the Raman spectroscopy facility at Brunel University was accessed. However this technique proved to be of no value, since no peaks could be obtained. A possible explanation for these poor results is the poor polarisability of the 'hard' Si, Al, and O atoms and it was later learnt a much longer time period is required for Raman spectroscopic analysis of clay minerals than was applied at the time.

Figure 4.1 XPS spectrum of C800

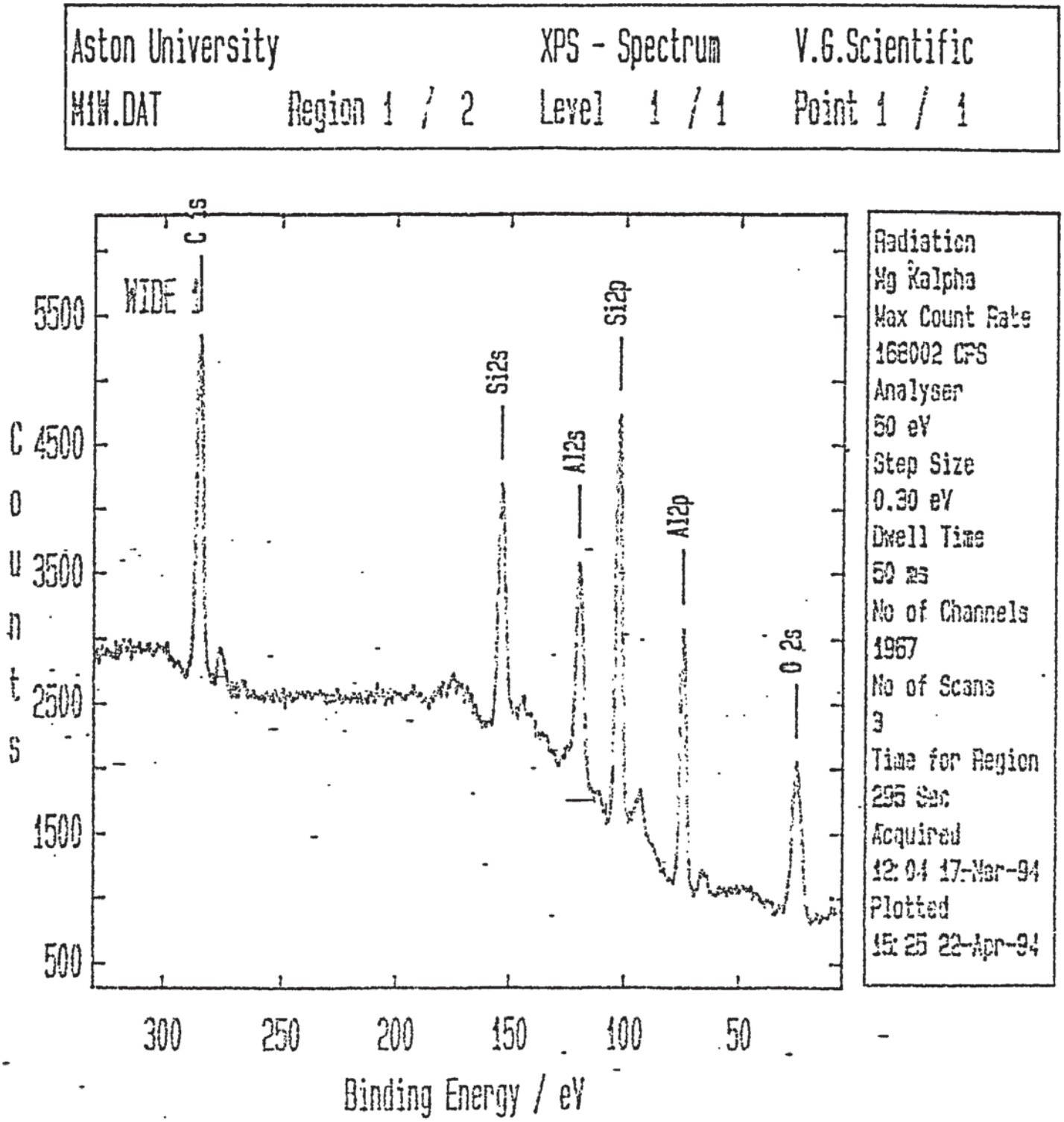

4.4 FT-IR

A comprehensive study was undertaken using FT-IR spectroscopy. The near, middle and far infrared regions were all inspected. Considerable effort was required to achieve optimum sampling conditions and to ensure results were reproducible.

4.4.1 Near IR Region

On reading work carried out by J.L. Post and P.N. Noble[87], where the near IR region is used to identify micas, the same paper also mentions the presence of peaks for other mineral groups in this region. It was realised that this region could also be useful in characterising the minerals in our study. As a result, a study of the minerals A, B and C as well as the thermally treated versions was carried out.

Only weak peaks were observed in the near infrared region, the intensity of which is comparable to the peaks present due to noise in this region. This meant it was difficult to identify which peaks are due to noise and which are due to vibrations in the minerals. Thus this technique was deemed inadequate for our purposes.

4.4.2 Middle IR Region

Many papers have been published on the study of clay minerals in the middle IR region demonstrating usefulness of infrared analysis as a technique for characterising clay minerals, for example kaolinite has bands at 1020 cm^{-1}, 934 cm^{-1}, 787 cm^{-1} and 690 cm^{-1} that do not appear in other clay minerals[88], therefore allowing identification of kaolinite from other minerals. An attempt is made to exploit this technique further by investigating if clay minerals from the same mineral group but different natural origins can be distinguished from each other using infrared analysis. This technique has also shown to be useful in following chemical changes on thermal treatment[56,59]. It is reasonable to expect differences in infrared spectra of the same mineral but from a different natural source because infrared spectroscopy in this region is very sensitive. Variability in infrared spectra of the similar minerals are seen if there are:

a) impurities present

b) differences in crystal orientation

c) polymorphism, different crystalline forms of the same compound are capable of exhibiting slightly different IR spectra [88]

The possibility of obtaining different spectra on repeat analysis of a material due to crystal orientation is dealt with by grinding samples in to very fine particles, thus ensuring complete random orientation of crystals. Small particle sizes of the sample also minimise loss of energy due to reflectance[46]. Table 4.4 compares infrared spectra of mineral A and mineral c and assigns peaks to particular modes of vibration.

Table 4.4-Infrared absorptions for minerals A and C

A (cm^{-1})	C (cm^{-1})	Peak Assignments
3696	3697	OH stretching of gibbsite sheet[48].
3669	3669	OH in plane vibrations[48].
3652	3652	"
3620	3621	OH stretching on tetrahedral sheet[48].
-	2925	
1109	1113	In plane stretching vibration of SiO[49].
1032	1032	"
1008	1009	"
937	936	Al^{IV}-OH in plane rocking vibration[46]
914	913	"
849	-	-
798	795	Si-OAl vibrations[48]
758	757	"
670	698	OH bending of gibbsite layer in a direction perpendicular to the layers[55].
650	651	-

Table 4.4 shows uncalcined minerals A and C to be generally similar, major peaks differing only by 1 cm^{-1}. Such differences can be ignored since repeat spectra of the same mineral can give this much error. However, minor differences are present. Mineral C contains a peak at 2925 cm^{-1} but there is no corresponding peak in mineral A. Mineral A contains a weak peak at 849 cm^{-1} but a corresponding peak is absent in

mineral C. Table 4.4 identifies presence or absence of particular vibrations in the minerals but there are other differences such as relative peak intensity. Figure 4.2 and figure 4.3 are infrared spectra of minerals A and C respectively. The spectra exhibit differences in peak intensity in the Si-O-Al vibration region (750-800 cm^{-1}), in mineral A both Si-O-Al vibrations are of equal intensity but this is not the case for mineral C.

4.4.2.1 Infrared analysis of calcined minerals

A200 and C200

On comparing spectra for A200 (mineral A calcined at 200°C) and C200 (mineral C calcined at 200°C) we see subtle differences. Spectra for A200 reveal the appearance of weak shoulders on the peaks at 913 cm^{-1} and 791 cm^{-1}. A200 spectra exhibit a sharp peak at 650 cm^{-1} but this peak is absent in C200. This shows even at relatively low temperatures of calcination the subtle thermal changes taking place are not of the same nature in mineral A and mineral C.

On comparing individual minerals before and after calcination, we see in general a shift of peaks to slightly higher wavenumbers consistent with a decrease in order in the material. When comparing mineral C with C200 we see an alternation of relative peak intensity for the peaks at 757 cm^{-1} and 794 cm^{-1} (Si-OAl vibration). This change is also seen when comparing mineral A with A200. A diagrammatic representation of this change in relative peak intensities is given in figure 4.4. Careful observation and comparison of spectra for mineral A and A200 reveals appearance of a new weak peak at 820 cm^{-1} and an increase in resolution and intensity of the weak peak at 650 cm^{-1}.

Figure 4.2 Infrared spectrum of mineral A

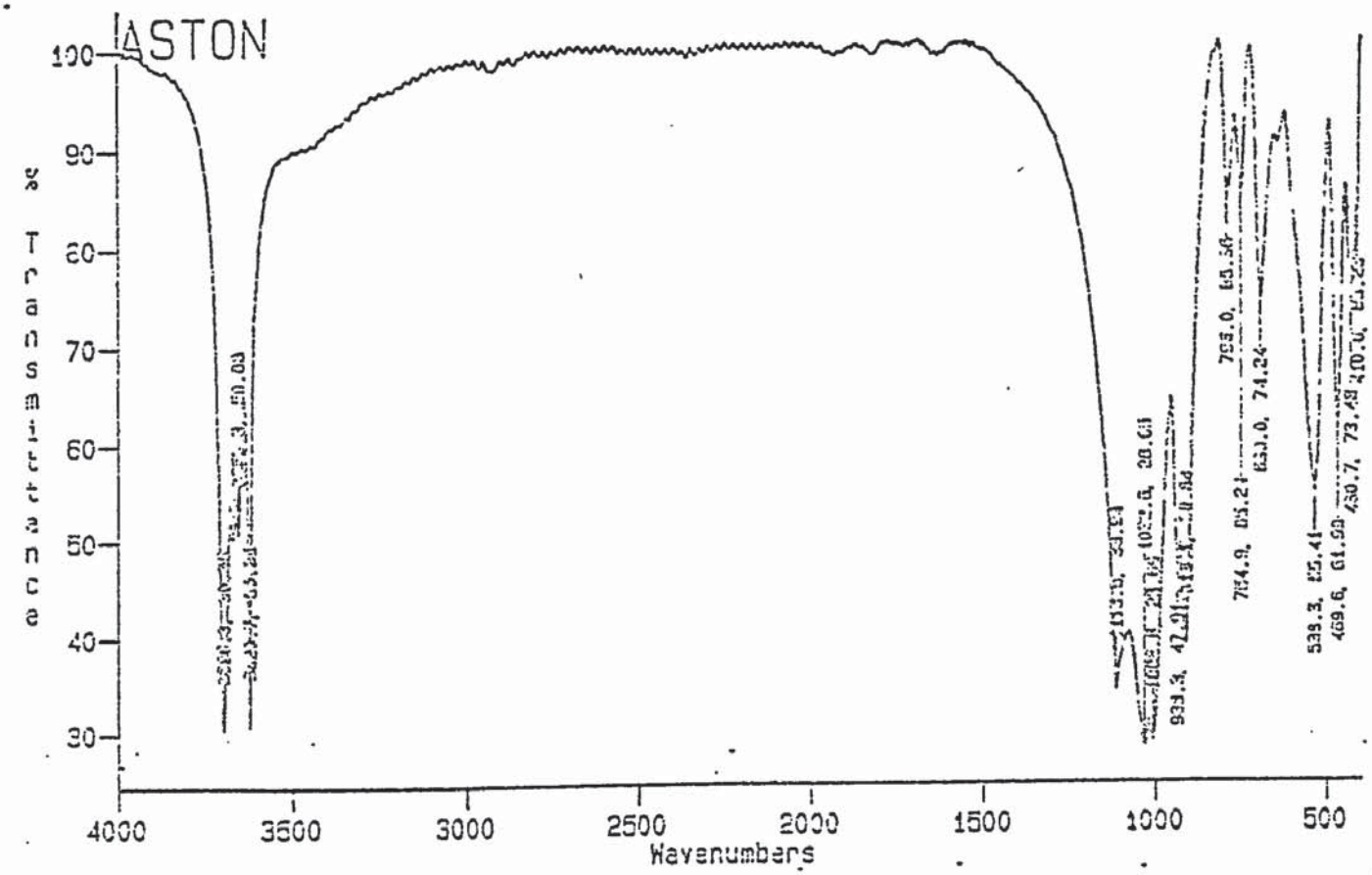

Figure 4.3 Infrared spectrum of mineral C

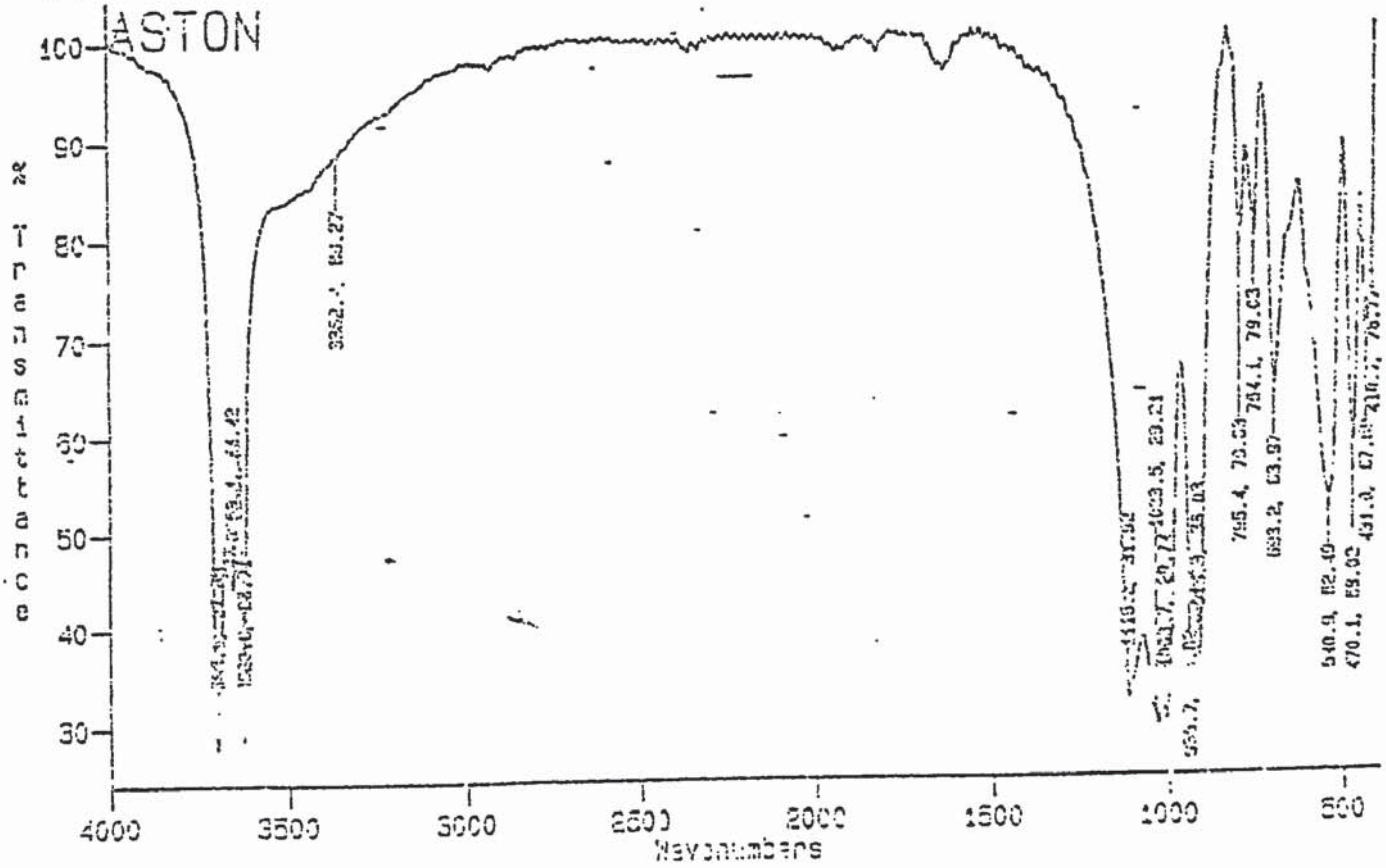

Figure 4.4 Diagrammatic representation of the change in peak intensity on calcination

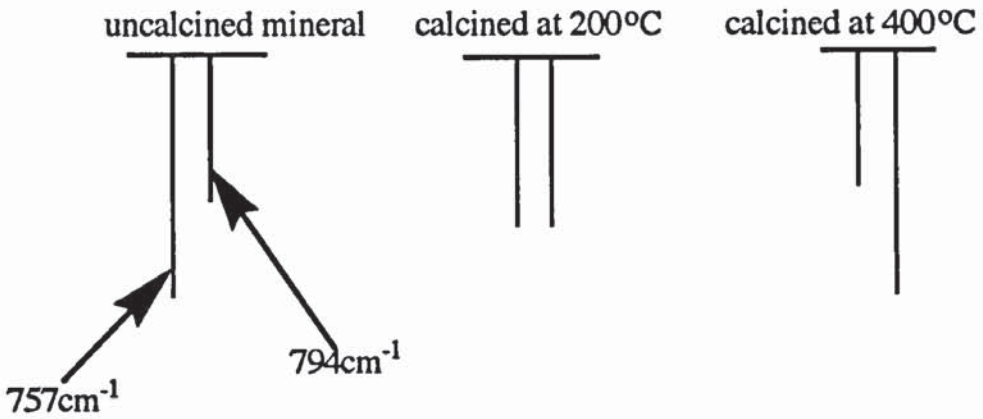

A400 and C400

Weak peaks seen in A200 at wavenumbers: 850 cm^{-1}, 820 cm^{-1} and 650 cm^{-1} are not seen in A400 (mineral A calcined to 400°C). Peaks in the region 600 cm^{-1} to 900 cm^{-1} have shifted to higher wavenumbers. The peak at 2924 cm^{-1} has become more intense in C400 compared to C200 and shifted to higher wavenumbers. The change in relative intensities with heating of the peaks initially at 757 cm^{-1} and 794 cm^{-1} has continued, the peak at 794-780 cm^{-1} becoming more intense as demonstrated in figure 4.4. This is probably due to formation of some Al^{IV}-O , this bond vibrates in the 800 cm^{-1} region.

A600 and C600

Comparing infrared spectra of A600 with spectra of C600 differences are apparent. C600 still has residual intralamellar hydroxyls, A600 has no residual intralamellar hydroxyls suggesting the breakdown in structure is greater in mineral A. Another difference is the intensity of Al^{IV}-O absorption is greater in A600 then in C600, this is consistent with XPS and XRD data which indicated greater alumina in mineral A. The shift in Si-O peak position to higher wavenumbers is greater in A600 than in C600, this suggests greater disorder in A600.

Significant changes are seen when comparing spectra of minerals calcined at 600°C compared to spectra calcined at lower temperatures. Firstly there is a loss in resolution of peaks, most of the sharp peaks seen in minerals calcined at lower temperatures

have been replaced by two broad peaks. Al^{VI}-OH peaks at 936 cm^{-1} and 913 cm^{-1} have disappeared suggesting complete dehydroxylation of aluminum. Spectra for A600 show the hydroxyl peaks in the region 3600-3700 cm^{-1} have all disappeared, again demonstrating complete dehydroxylation of the material has occurred, although C600 spectra shows some residual intrallamellar hydroxyls. Si-O peak has shifted to higher wavenumbers and become broader. There is a broad peak centred approximately at 800 cm^{-1} due to Al^{IV}-O vibrations in both minerals, this peak is characteristic of the dehydroxylated form of the mineral.

A800, B800 and C800

Peaks for A800 and B800 have again shifted to higher wavenumbers. C800 shows Si-O peak to be at the greatest wavenumber and to be the broadest compared with A800 and B800, suggesting greater disorder in C800.

A1000 and B1000.

Spectra of these kaolinites again show a general shift of peaks to higher wavenumbers and a further broadening of the peaks. A1000 reveals a shoulder to the Si-O peak in the 1200 cm^{-1} position indicative of the presence of amorphous Si-O absorptions[59].

4.4.2.2 Rates of Dehydroxylation

On observation of infrared spectra of the minerals after calcining at 400°C and 600°C it is obvious that dramatic changes are taking place between this temperature range. These changes are due to the dehydroxylation of the mineral to produce an amorphous dehydrated phase. Samples were calcined at various temperatures in the temperature range of 400°C to 600°C and infrared analysis carried out to compare the extent of dehydroxylation in the minerals at particular temperatures.

This study revealed dehydroxylation has begun to occur at calcination temperatures of 500°C, this is seen as a decrease in the Al-OH peak intensity in both minerals A and B. A decrease in intensity is seen in the intralamellar hydroxyl absorptions at calcination temperature of 510°C. At 530°C mineral C still shows a weak peak due to

an Al-OH vibration, there is no such peak in mineral A. At this same temperature all the absorptions due to hydroxyls are absent in mineral A but in mineral C there is still a residual intralamellar peak as shown in figure A3 in the appendix.

4.4.3 Infrared Analysis using Diffuse Reflectance

Diffuse reflectance was used to observe samples by infrared analysis to see if there would be an improvement in the spectral quality compared to the KBr disc method. The most obvious difference between the two methods is the appearance of peaks in the 1300-2000cm^{-1} region when using the diffuse reflectance method of observation. These additional peaks are due to hydrogen bonding. These peaks are not seen in the KBr method of observation because the sample is exposed to high pressures and vacuums which removes most of the H-bonded water. In diffuse reflectance there is no such exposure to high pressures and vacuums (sample is simply manually packed in the observation column) therefore H-bonded water is present and is seen in the infrared spectra. All the peaks due to other groups in the sample that are seen in the spectra obtained using KBr disc are also observed using the diffuse relectance method of analysis. However relative peak intensities are different for the two methods. Figures 4.5 and 4.6 show IR spectra of C600 obtained using KBr and diffuse relectance method of sample preparation. Apart from the broad peaks seen using the latter method in the 1300-2000 cm^{-1} region, a distinct peak is observed at 1167 cm^{-1} (due to Si-O in silica). This peak appears as a shoulder when KBr disc is used as a method of preparation. The alternation in peak intensities in the 750-800 cm^{-1} region are seen using the diffuse reflectance method as well as the residual intralamellar hydroxyl peaks suggesting the method's potential usefulness.

4.4.4 Far infrared region.

There are advantages in working in this region. The particle size of many naturally occurring specimens such as the minerals being studied is such that while they scatter shorter wavelength radiation they will act as simple absorbers for longer

wavelengths[55]. Additionally work done by E. E. Angino[52] reported characteristic absorptions of kaolinite, montmorillonite and illite in this region of the infrared spectrum. As a result of this knowledge spectra were gained for the series of calcined mineral A samples and uncalcined mineral C. The spectra were used to identify differences between minerals A and C and to identify changes occurring on calcining the mineral.

Table 4.5-Comparison of kaolins A and C peaks in the far IR region

A (cm^{-1})	C (cm^{-1})	Peak Assignments
469	469	Si-O bending vibration [57]
429	429	"
367	366	Si-O of silica[59]
345	345	Al-O vibration of Al-O(OH)
278	274	-

Table 4.5 demonstrates there is little difference between uncalcined minerals A and C. Even on comparing peak intensities or peak resolution we see no apparent difference between the minerals.

A200

Comparison of spectra for A200 and unalcined mineral A show shoulder at 295 cm^{-1} becomes a distinct peak in A200.

A400

We see appearance of two new peaks at wavenumbers 418 cm^{-1} and 337 cm^{-1}, this suggests chemical change has occurred after calcining at 400°C.

A800

Spectra of poor quality were obtained, however the peak at 229 cm^{-1} has increased in intensity (this peak was very weak in the uncalcined sample) while all other peaks have decreased in intensity. In fact observation of the spectra show this is the major peak, all other peaks barely being distinguishable. This peak is associated with Al-O vibrations suggesting significant changes occurring centred on the Al atom.

Figure 4.2 Infrared spectrum of mineral A

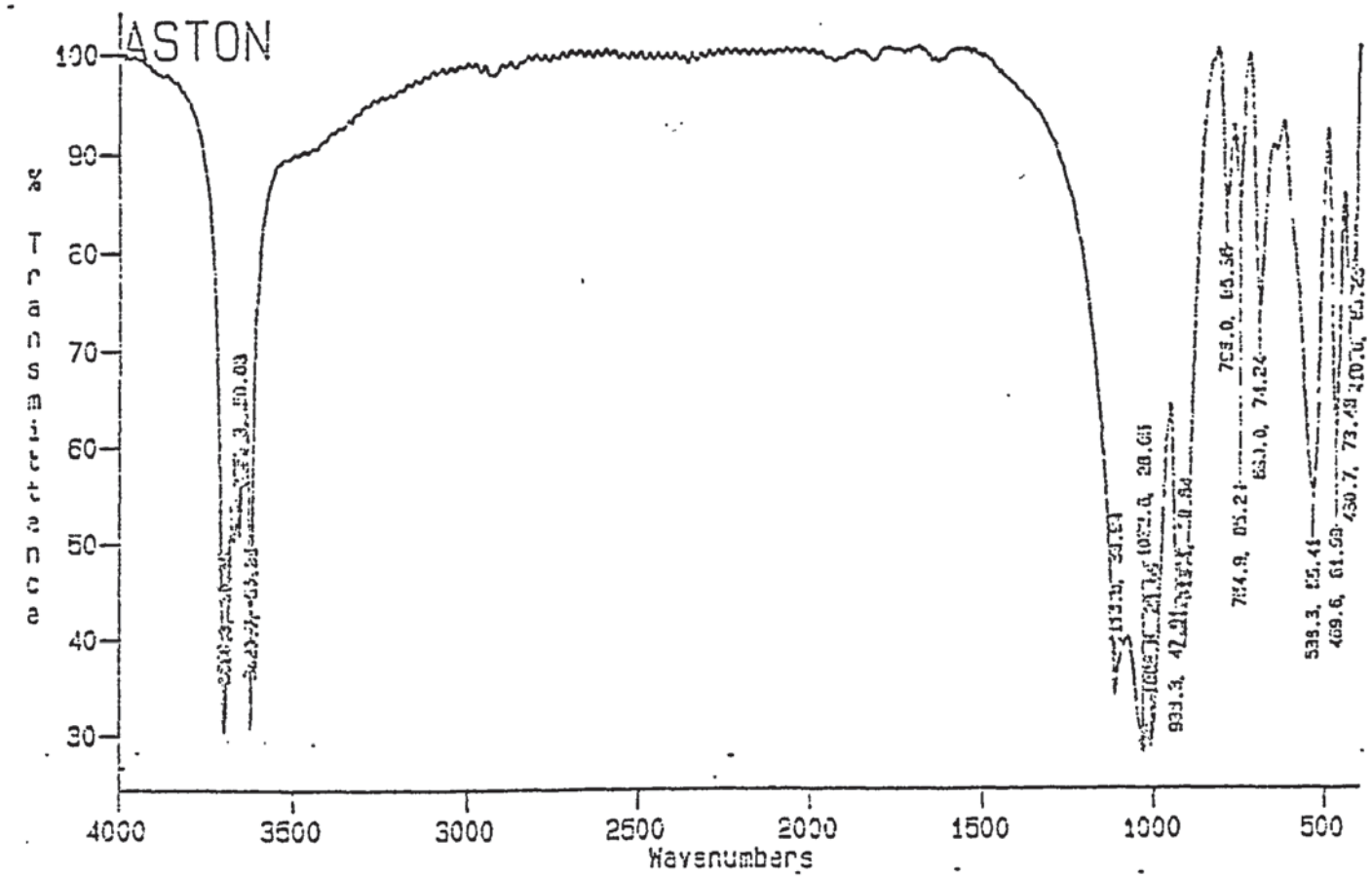

Figure 4.3 Infrared spectrum of mineral C

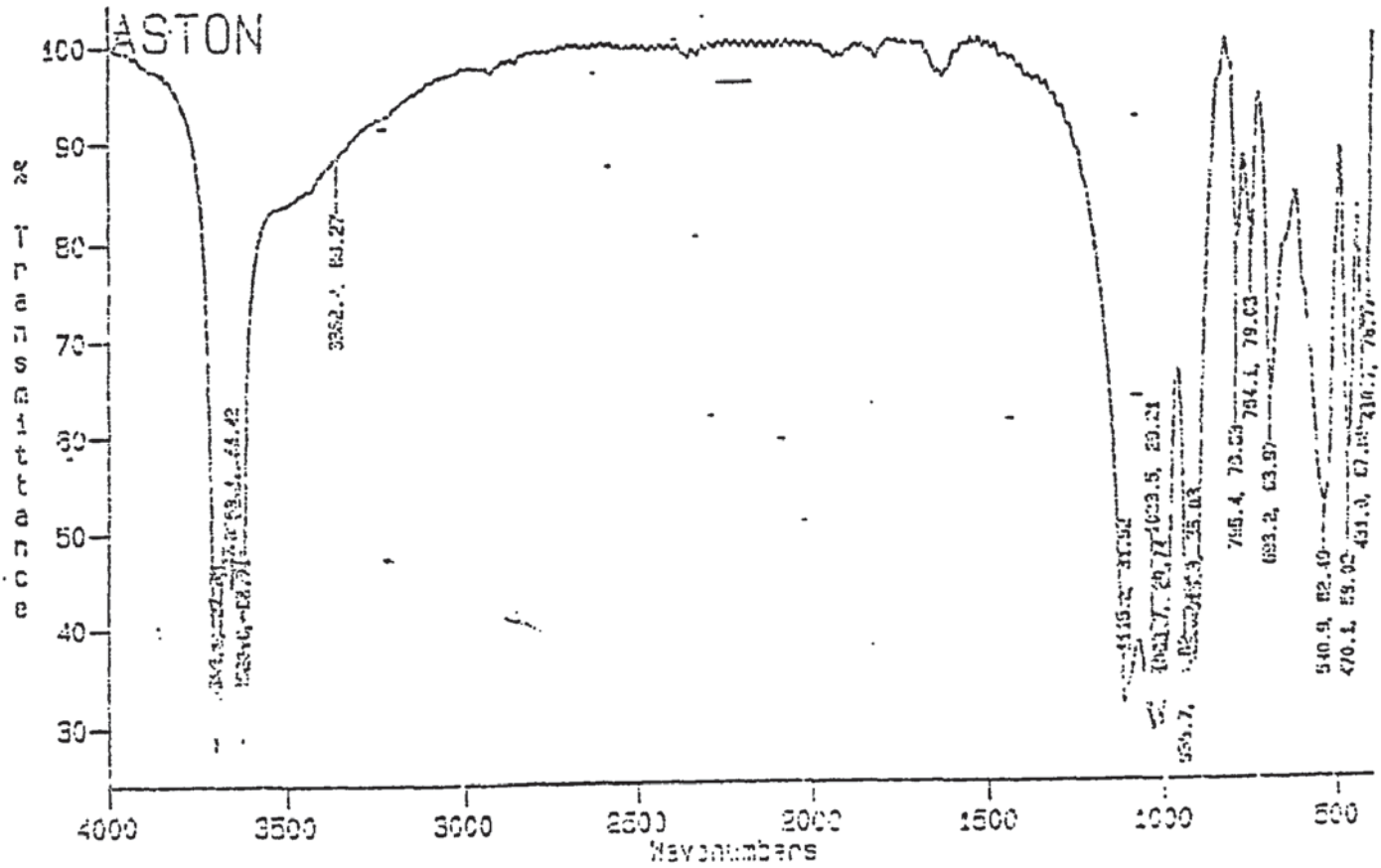

4.5 MASNMR

4.5.1 ^{27}Al MASNMR

Uncalcined mineral C gives a sharp peak centred at -3.7 ppm relative to aluminium sulphate, this shows all aluminium atoms are in octahedral coordination[37]. Spectra of C800 (C calcined to 800°C) shows 3 peaks at -0.1 ppm, 28 ppm and 51.7 ppm, thus aluminium is now in 3 different environments, octahedral, pentacoordinate, and tetracoordinate respectively[39]. Calcination of mineral C induces a change to lower coordination numbers for aluminium.

Uncalcined mineral A again gives a single sharp peak consistent with octahedral coordination. On observation of spectra for A800 we again see appearance of 3 distinct peaks, suggesting 3 different aluminium environments present. On comparison with spectra for C800 we see relative intensities of the peaks are different, peak intensities for the different coordination numbers in spectra of C800 are similar, whereas in A800, the peak representing tetra-coordinated aluminium is barely visible and the peak representing octahedral coordinated aluminium has the greatest intensity of the 3 peaks.

The spectrum of mineral B calcined at 800°C shows 3 peaks but relative intensities of the peaks are different compared with A800 and C800. The peak consistent with aluminium in a tetrahedral environment has the greatest intensity and the peak assigned to aluminium in an octahedral environment is weakest. Figures 4.7, 4.8 and 4.9 are ^{27}Al NMR spectrum of A800, C800 and B800 respectively.

^{27}Al MASNMR analysis reveals considerable changes occuring centred around the aluminium atoms on calcining these minerals. The changes occurring differ from mineral to mineral at particular temperatures of calcination.

Figures 4.7 and 4.8 ^{27}Al MASNMR spectrum of metakaolin A800 and C800 respectively

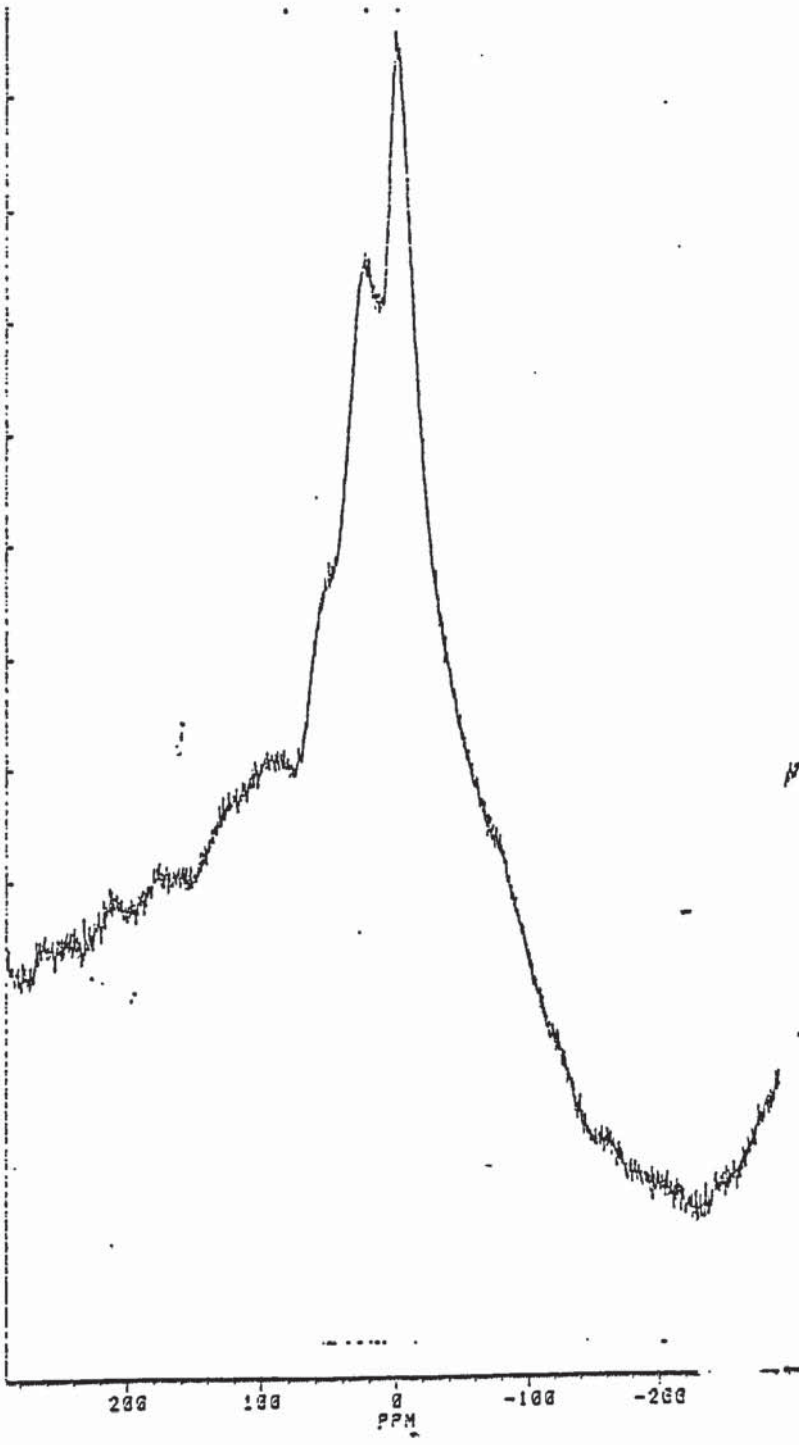

Figure 4.7

Figure 4.8

Figure 4.9 ^{27}Al MASNMR spectrum of metakaolin B800

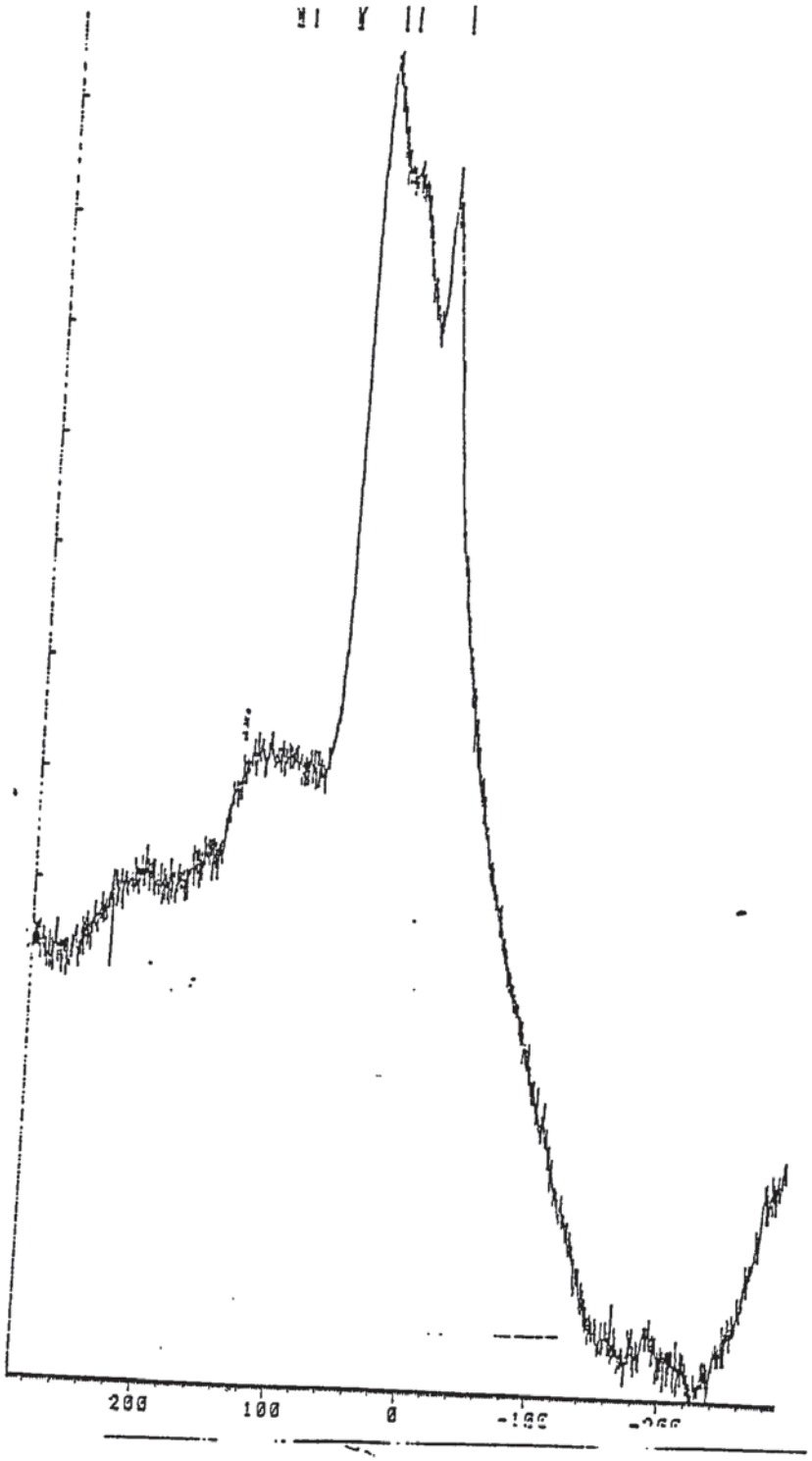

Table 4.6-Comparison of peak widths and shifts for calcined and uncalcined minerals

Mineral type	Peak width at half height (cm)	Peak width at half height (Hz)	Shifts (ppm)
A800	1.1	$1.66*10^3$	-101.7
B800	1.1	$1.26*10^3$	-107.1
C800	1.1	$1.66*10^3$	-98.6
A	0.1	$1.15*10^2$	-90.9
C	0.1	$1.15*10^2$	-91.1

Table 4.6 shows on calcination of the minerals , generally there is a shift to lower field and peaks become broader.

Mineral A and C yield peaks at -91.1 ppm and -90.9 ppm respectively, this is indicative of silicon sharing three of its tetrahedral vertices with three other silicons (Q^3)[33]. The peaks for the uncalcined minerals can be considered to be identical as errors of up to 1 ppm can be expected using the Brucker instrument. On calcining samples to 800°C we see a shift in the ^{29}Si NMR signal to more negative values and peak widths become broader. Mineral B800 has the most negative value with a signal centred at -107.1 ppm (indicative of a Q^4 environment[32]). This sample has been provided in the calcined form and there is no uncalcined version of it available, therefore comparisons with the other minerals have to be made with these facts in mind. Comparing shift values for A800 and C800 we see differing shift values although the general trend seems to be a move towards Q^4 shift values.

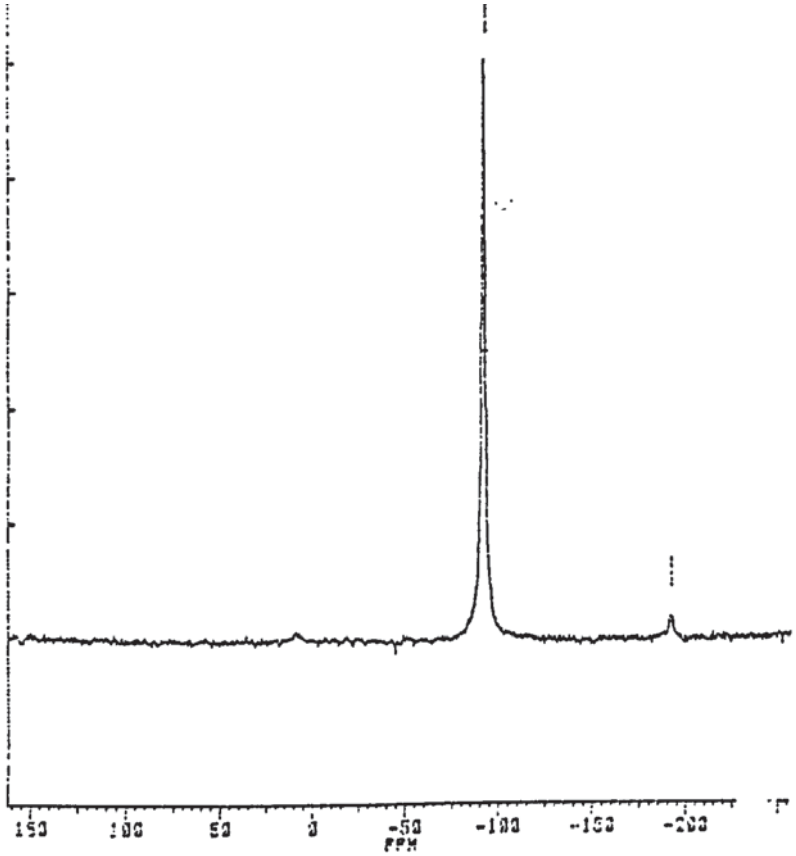

Figure 4.11 ^{29}Si MASNMR spectrum of kaolin C after calcining

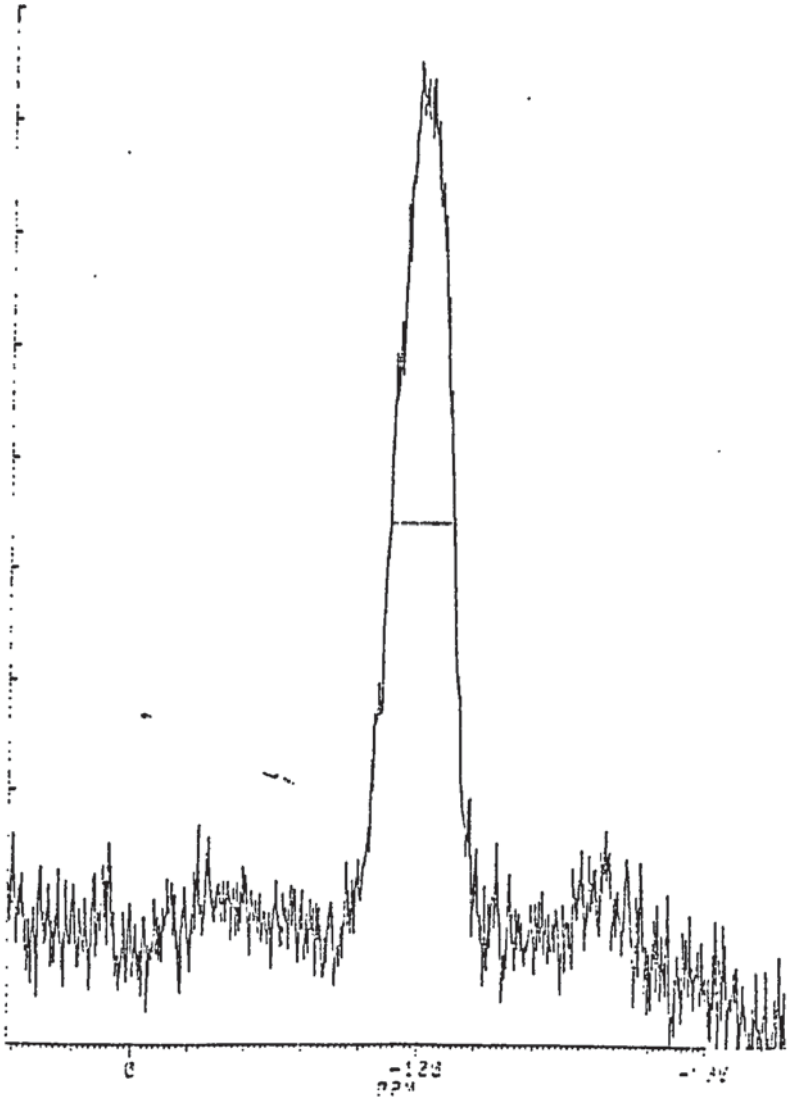

4.6 Thermogravimetric and Differential Thermal Analysis

Thermogravimetric analysis reveals a consistently greater percentage mass loss in mineral A compared with mineral B at a given temperature. There is also a faster rate of mass loss in mineral A, the slope for mass loss in themogravimetric analysis being steeper in this mineral. These results are consistent with infrared studies on dehydroxylation rate.

Differential thermal analysis (DTA) of this mineral is characterised by an endothermic (loss of water) and an exothermic peak at 1000°C (crystallisation of the mineral). The exothermic peak is more intense in mineral A implying crystallisation occurs to a greater extent in this mineral and hence gives increased strength at high temperatures. Figure 4.12 is a thermogravimetric and DT analysis plot of kaolin A

Figure 4.12 Thermogravimetric and Differential Thermal Analysis of kaolin A

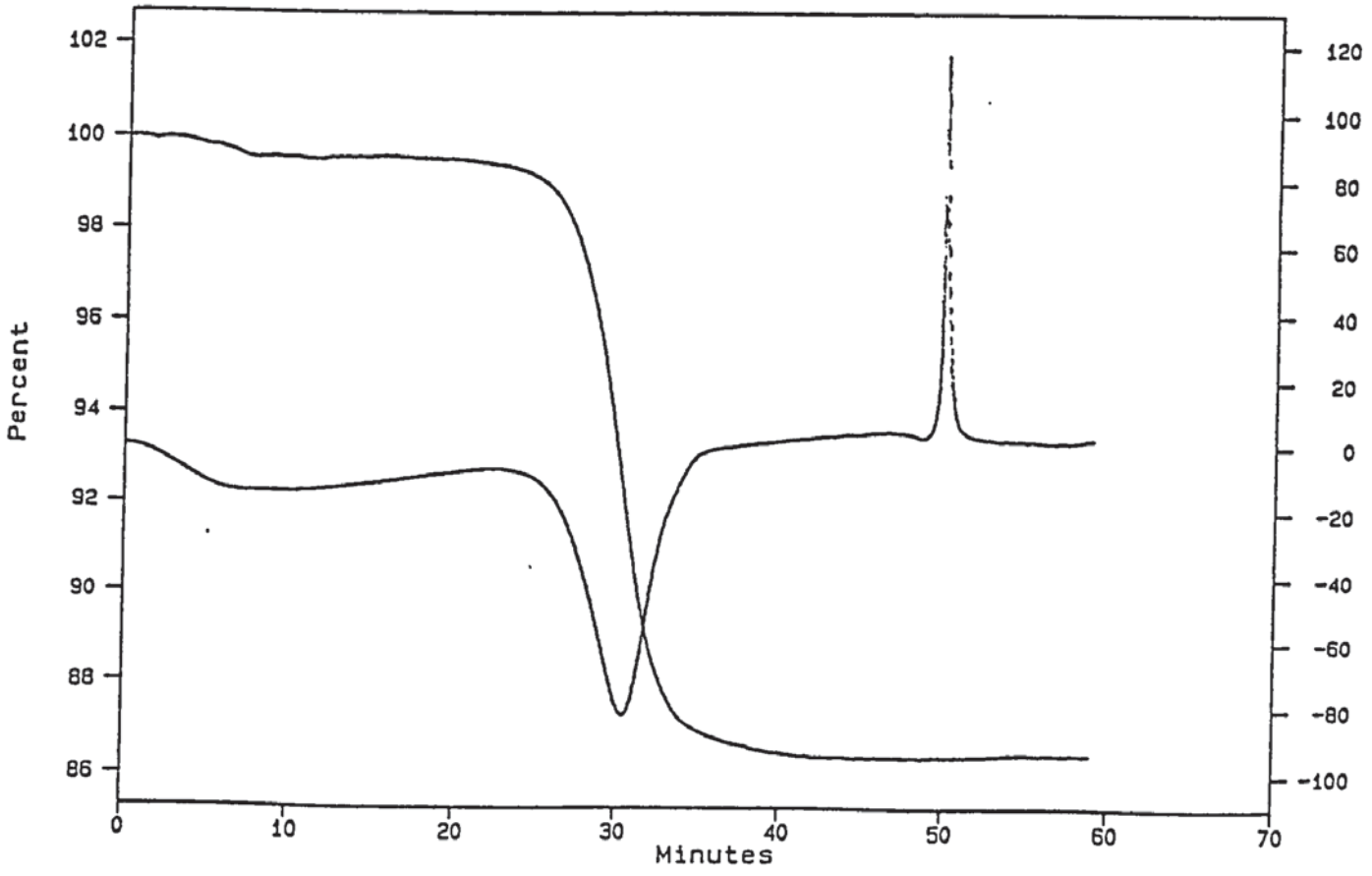

4.7 Microwave Synthesis of Kaolinite

A Method of synthesising kaolinite was established as early as 1935[4]. Since then many other methods have been developed[1,2,3] but most of these involve working at high temperatures and pressures as well as long time periods in order to replicate the conditions in which kaolinite is made in nature.

Kaolinite synthesis has been attempted in order to make available a relatively pure kaolinite and to see if microwave methods can reduce the time required for synthesis. This pure kaolinite would then be used to prepare the refractory to see if there is an improvement in the refractoriness of the material, hence establishing the importance of purity of the kaolin to the quality of refractory.

Kaolinite syntheses were attempted using various upper limits for pressure and temperatures and time periods for microwave treatment. We were able to program the microwave to work at the required conditions. Table 4.7 shows an example of the program variables.

Table 4.7. An example of the program variables

Stage	1	2	3	4	5
Power	70%	60%	60%	60%	60%
Pressure	150 psi	150 psi	150 psi	150 psi	150 psi
Temperature	150°C	150°C	150°C	150°C	150°C
Run time	6 min.	6 min.	6 min.	6 min.	6 min.

In the microwave treatments upper limits of temperature and pressure are set, when one of the upper limits is reached the microwave is automatically switched off and the reaction vessel is allowed to cool before further microwave heating until one of the upper limits is reached again, continuing the cyclical process until the end of the set

time for the run. In all cases the upper limit of temperature rather than pressure was reached first. The products were analysed using infrared analysis.

Infrared spectra obtained of samples using the method described in section 3.4.1 show interactions taking place between the reacting tetraethylsilicate and aluminium hydroxide. Infrared spectra of these gave Broad peaks typical of aluminium hydroxide at 600 cm^{-1}, 1000 cm^{-1} and 1500 cm^{-1}. Infrared spectra obtained of samples prepared using the same program variables but with time period of 0.5 h and 3 h respectively are similar. This indicates 0.5 h is a sufficient time period for the microwave induced reactions to take place. However when changing the microwave power output infrared spectra indicated appearance of new peaks including a peak in the 960 cm^{-1} region, generally associated with Al^{VI} -OH in clay minerals. Changes in the upper pressure and temperature limits from 100 psi to 150 psi and 100°C to 150°C showed very little change in the infrared spectra.

When synthesis was attempted using the method described in 3.4.2 again infrared spectra indicated reactions had taken place. However when microwave power output was set at 20%-30% there was no appearance of a peak in the Al^{VI} -OH region despite increasing the upper temperature and pressure limits from 100°C to 150°C and 100 psi to 150 psi respectively. This was not the case when power output was increased to 70%-80%, as can be seen from figure 4.13 a peak appears at 940 cm^{-1} indicative of an octahedral aluminium environment.

Comparing calcined kaolinites with calcined microwave materials we see there are similarities in their infrared spectra and hence their structure.

Kaolinite synthesis attempted using the method described in section 3.4.3 yielded no peak in the aluminium octahedral region on infrared analysis as can be seen from figure 4.14.

Figure 4.13 Infrared spectrum of the product obtained from kaolin synthesis using A. Leonard method.

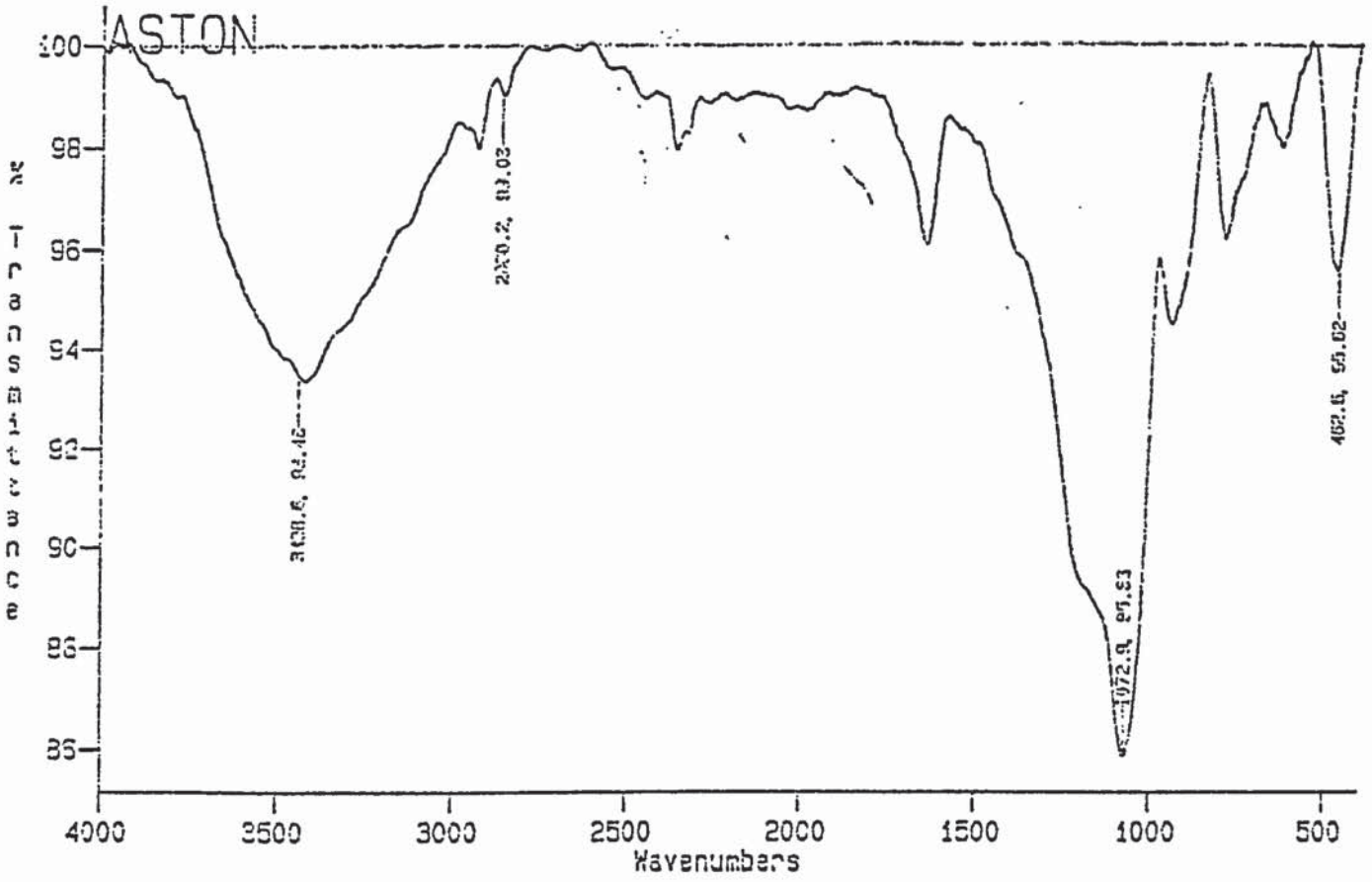

Figure 4.14 Infrared spectrum of the product obtained from kaolin synthesis using S. Satokawa method

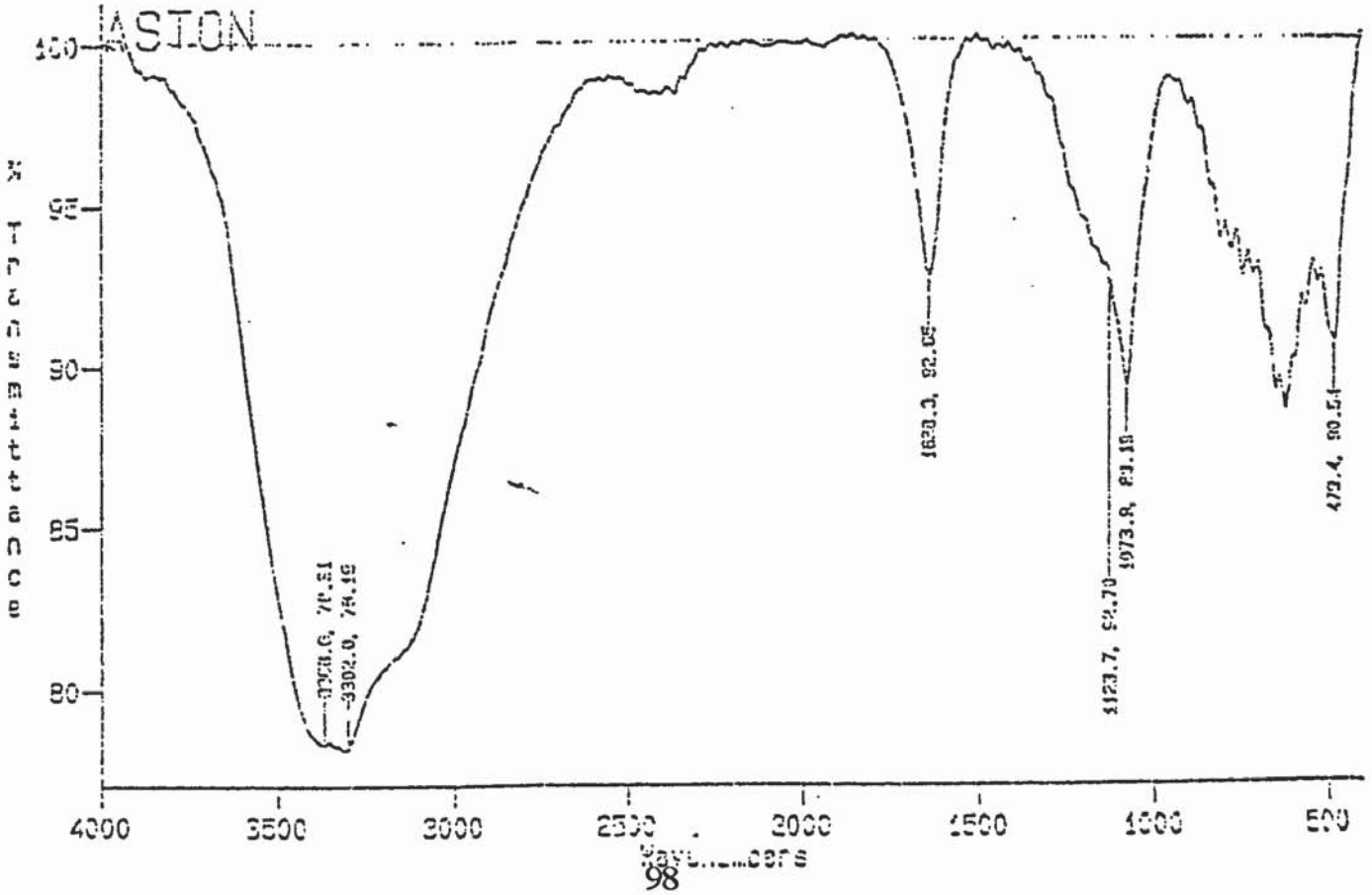

4.8 Conclusions

Results show the greatest change in structure occurs at temperatures in between 400°C and 600°C. This is because when we calcine a kaolinite to such high temperatures, we dehydoxylate the kaolinite to give metakaolinite[89].

$Al_2Si_2O_5(OH)_4$ dehydroxylate to give $Al_2Si_2O_7 + 2H_2O$

kaolinite metakaolinite

At other calcination temperatures there is a gradual increase in disorder with no major chemical changes visible with infrared analysis. At higher temperatures we lose the spectral resolution seen with uncalcined samples because of the calcination process breaking the regular structures of the kaolinites.

Analysis of XRD data led us to believe rutile(TiO_2) and quartz(SiO_2) could be present in mineral C but XPS and ^{29}Si MASNMR have proved rutile and silica to be absent from the kaolinite, since no titanium is seen on XPS analysis and no Q^4 peaks are seen on NMR analysis.

XPS and XRD data has shown there are varying purity levels amongst the minerals. Kaolin A was discovered to be the most pure mineral. XPS also revealed differences in surface Al:Si ratio. This ratio was much greater in kaolin A800 relative to the other kaolins.

Both infrared and ^{27}Al MASNMR show there are significant changes occurring centred on the aluminium atom. ^{27}Al MASNMR has shown there is a shift to lower coordination numbers after calcining the kaolinites, low frequency infrared analysis shows Al-O peak previously absent appears on calcining and in A800 is the major peak. Middle infrared region also shows changes in intensity and position of the peaks associated with aluminium, this may be explained by the change in aluminium coordination numbers.

Changes centred on the aluminium seen by NMR seem to correlate with changes seen using infrared analysis. These changes are centred around the aluminium atom particularly, the shift to lower coordination numbers are to be expected since progressive dehydroxylation reduces the number of anions bonded to the aluminium ions. If the ^{27}Al MASNMR technique can be assumed to be semi-quantitative then relative intensities of the peaks for the calcined kaolinites show there are varying amounts of tetra, penta and hexacoordinate aluminium. This again illustrates the three kaolinites to be slightly different.

^{29}Si MASNMR has revealed there is a general breakdown in structure on calcining the kaolinites. This breakdown seems to have progressed furthest in metakaolin B but as this material is only available in the calcined form, we cannot be sure that the thermal history is identical with the other kaolinites, therefore we cannot say whether the difference in ^{29}Si NMR signal is due to differences between the kaolinites or differences in thermal treatment. Thermal treatments of A800 and C800 were identical. Hence differences in shift values for these materials can be said to be due to subtle differences in structure. Comparing shift values, more negative values are seen for A800 (-101.7 ppm) than for C800 (-98.6 ppm) suggesting greater breakdown in structure in the former. Given that both these kaolinites were exposed to identical thermal environments we can conclude that there are differences between these kaolinites which are manifesting themselves on heating the samples.

Other differences include rate of dehydroxylation. Dehydroxylation has occurred to a greater extent in kaolin A, suggesting breakdown of the mineral is pogressing faster in mineral A. Differential thermal analysis shows a more intense exothermic peak for kaolin A than for other minerals suggesting greater extent of crystallisation in this mineral, hence greater strength at high temperatures.

Studies of the kaolin minerals have established the most valuable techniques to study our materials to be ^{29}Si MASNMR, ^{27}Al MASNMR and infrared spectroscopy with X-ray diffraction also giving good support.

Both XPS and XRD analysis have shown the differences between the kaolin minerals from different sources, MASNMR and infrared analysis has shown differences are even more apparent after calcining the minerals. Hence we can expect these minerals to interact differently with other components of the refractory.

Synthesis of the kaolin minerals could not be achieved using the microwave. This was probably due to the fact that we are limited to the temperatures (200°C) and pressures (150 psi) that can be applied or it may be the case that microwave technology cannot speed up these particular reactions.

4.8.1 Comparison of data with relevant literature

On study of the infrared spectra of kaolin A and kaolin B differences between the spectra were identified. However, when comparing these spectra with infrared spectra of kaolinites obtained by other workers, larger differences are observed. For example Angino[57] reported the three in-plane Si-O stretching vibrations to be at 1014 cm^{-1}, and 1042 cm^{-1}, 1080cm^{-1} whereas in this work the first two vibrations are found at 1008cm^{-1} and 1032 cm^{-1} in both kaolins and the third one to be at 1109 cm^{-1} for kaolin A and 1113 cm^{-1} for kaolin C. Russell and Farmer[45] reported the importance of the physical state of the material in determining the position and sharpness of these resonances, the third vibration band has been shown to appear as a broad shoulder near 1080 cm^{-1} when the crystal size is large (equivalent spherical diameter greater than 2μ). Whereas when the crystals are very fine the band is sharp and at 1109 cm^{-1}. From this evidence it is reasonable to suggest the difference between kaolin infrared spectra obtained in this study and by Angino could be due to sample particle size. This could explain the differences observed between the infrared spectra of kaolin A and kaolin C. This could in turn explain the observed differences in rate of dehydroxylation between A and C. Larger crystal size means a smaller surface area, therefore rate of dehydroxylation would be slower in such a sample of kaolinite. It has been reported that 60-70% of the dehydroxylation is diffusion controlled[27], this means differences in compaction and particle size could result in differences in rate of dehydroxylation.

A literature search revealed a number of factors, as well as the ones mentioned above, that have been identified by researchers as causes for fluctuations in rate of dehydroxylation; they are specimen size, shape, particle size distribution, crystallinity, sample volume and chemical composition[27,28,32]. Another explanation could be the residual hydroxyl peaks seen on calcination of kaolin C maybe due to muscovite which is an impurity in this kaolin.

The observation made by Miller[56] that interlamellar hydroxyl groups are lost at a faster rate than intralamellar hydroxyl groups on dehydration is also borne out in our studies. On calcination, both kaolins A and C showed residual peaks corresponding to intralamellar hydroxyls after the disappearance of bands from interlamellar hydroxyl on infrared analysis.

Evidence for the alternation in intensity of the peaks at 757 cm^{-1} and 794 cm^{-1} when calcining at temperature of 400°C was difficult to find because no work has been done on studying the changes in kaolins after calcining at such low temperatures. However infrared spectra shown by Percival et al.[59] of uncalcined kaolin and kaolin calcined at 470°C for 1.5h lend support to these findings. These spectra show the uncalcined kaolin to display a relatively intense peak at 755 cm^{-1} and a weak band at 792 cm^{-1}; infrared spectra of the calcined sample revealed a weak band at 795 cm-1 and no band at 755 cm^{-1}.

^{29}SiNMR analysis of kaolins A and B gave single sharp resonances at -90.9ppm and -91.1ppm. This correlates well with work done by Slade and Davies[15]; in that study a resonance at -91.5ppm for kaolinite was obtained. After calcining their kaolin at 800°C these workers obtained a broad resonance centred at -100ppm. This compares well with our study for metakaolins A and C but not for metakaolin B, where the broad peak was centred at -107ppm. The thermal history of metakaolin B is not known but the shift upfield relative to the other metakaolins could be due to a number

of reasons. The calcination temperature or time period could have been greater for this metakaolin. Migration of Al into the silicate layer would reduce the upfield shift, therefore this migration maybe greater in samples A and B. Considering the products formed after calcination of the kaolins (see page), this is a very plausible explanation. It has also been shown by slade et al.[15] that flash calcines prepared in atmospheres progressively higher in H_2O give resonances further upfield on ^{29}Si NMR analysis. Since the exact thermal history is not known for kaolin B, this is another reasonable explanation for the observed differences in resonance positions on ^{29}Si NMR analysis between the metakaolins.

^{27}Al NMR analysis of kaolins A and C produces a single resonance in the octahedral position. This correlates with previous studies[34,35,39] Metakaolins A, B and C all yielded resonances in octahedral, pentacoordinate and tetrahedral positions but the relative intensities of these bands varied with the metakaolin. Meinhold[36] reported an octahedral:tetrahedral resonance ratio of 1:1 for a kaolin calcined at 650°C, this is the same as the ratio seen for metakaolin C, but this has been calcined at 800°C. A reduction in signal intensity on calcining the kaolins was observed in this work and was also noted by Meinhold who explained the phenomena to be due to the occurrence of aluminium in distorted geometries which are neither octahedral nor tetrahedral.

Differential thermal analysis for metakaolins A and B produced a broad endothermic peak centred at 200°C and a sharp exothermic peak at 1000°C, this is generally comparable with previous literature. However, Chakraborty[12] observed the exothermic peak at 980°C and also a small exothermic peak prior to the large 980°C exotherm in some clays. Chakraborty identified the origin of this small exothermic peak to be due to development of orthorhombic mullite. The large exotherm arises on the crystallisation of cubic mullite.

Chapter Five

CALCINED CLAY MINERAL AND SILICATE INTERACTIONS

5.1 Introduction

The investigation of the uncalcined and calcined kaolin minerals from different sources identified a number of differences between the materials. A second component of the new refractory formulation was introduced to the study. The second component was a potassium silicate, and again different types of these silicates (chemically similar) were available. The three silicates used were Henkel, K120 and Portil K, for the purposes of this study they are referred to as silicates X, Y and Z respectively. As with the kaolinites a study of the different potassium silicates was carried out.

5.1.1 Potassium Silicates

A number of analytical techniques were employed to elucidate the differences between the silicates. ^{29}Si MASNMR revealed very little difference in the Si environment between the silicates. The shift postions generally being in the -104 to -105 ppm region as shown in table 5.1.1. These peak positions are indicative of a Q^4 environment[30].

Table 5.1.1 ^{29}Si MASNMR data for the potassium silicates

Silicate Type	Peak Position (ppm)
Henkel (Silicate X)	-105.1
K120 (Silicate Y)	-104.3
Portil K (silicate Z)	-105.6

^{29}Si MASNMR data reveal the silicates to be very similar but chemical composition studies suggest major differences between the silicates. Table 5.1.2 exhibits the chemical composition of the potassium silicate and SiO_2:K_2O ratio.

Table 5.1.2 Chemical composition of the potassium silicates and SiO_2:K_2O ratio (%)

	Silicate X	Silicate Y	silicate Z
K_2O %	27.6	41.2	28
SiO_2 %	72.4	58.8	56
H_2O %	-	-	17
$SiO_2 : K_2O$	2.65	1.43	2

Table 5.1.1 illustates the differences between the silicates, in particular we see a large difference in the proportion of K_2O present in each silicate. Infrared and thermogravimetric studies of the silicates X, Y and Z yielded distinctive traces. Significant differences were seen on comparing spectra for the different silicates, hence there are significant differences in structure. Figures 5.1.1, 5.1.2 and 5.1.3 are thermogravimetric traces for the three silicates and illustrate their difference in structure. The trace for silicate Y is composed of mostly exothermic peaks, whereas traces for both silicate X and Z contain no exothermic peaks. On comparing thermogravimetric traces of silicate X and Z again differences are seen in terms of the temperature at which the endotherms appear and the broadness or sharpness of the peaks. For example, the initial endotherm seen in traces of silicate Z appears at 141.6°C and is broad, whereas the initial endothermic peak for silicate X appears at 81.2°C and is relatively sharp but weak in intensity. Comparing weight loss data reveals differences between the silicates, silicate X experiences a percentage weight loss of approximately half the weight loss seen in the other silicates on calcining to 1000°C.

5.1.2 Treatment of Silicate-Metakaolin Minerals

Silicate-calcined clay mineral mixtures were prepared using a 1:1 weight (g) ratio of the component calcined kaolin mineral, known as metakaolin, and silicate. Mixes were prepared as described in section 3.2.2. This new material was then named according to the component silicates and calcined clay present. For example, a mixture prepared using metakaolin A800 (kaolinite A calcined to 800°C for 2h) and silicate X was named A800-X, a mixture composed of B800 and silicate Y was named B800-Y and so on. These mixtures were then analysed using the following techniques: ^{29}Si MASNMR, ^{29}Si CPMASNMR, ^{27}Al MASNMR, XRD, Thermogravimetry, Scanning electron microscopy and Infrared spectroscopy. A portion of each metakaolin-silicate mixture was calcined at 1000°C for two hours and repeat analyses of this sample were carried out using the techniques mentioned above except ^{29}Si CPMASNMR. ^{29}Si CPMASNMR analysis relies on the presence of protons attached to the silicon , the lack of protons in the calcined sample would render this technique to be inappropriate.

Some of the ^{29}Si CPMASNMR and ^{29}Si MASNMR spectra produced such broad peaks that it was obvious more than one silicon environment existed in these materials but due to the lack of resolution it was difficult to identify the particular silicon environment. In these cases a deconvolution technique was applied in an attempt to resolve the broad peak into whatever component peaks it was composed of.

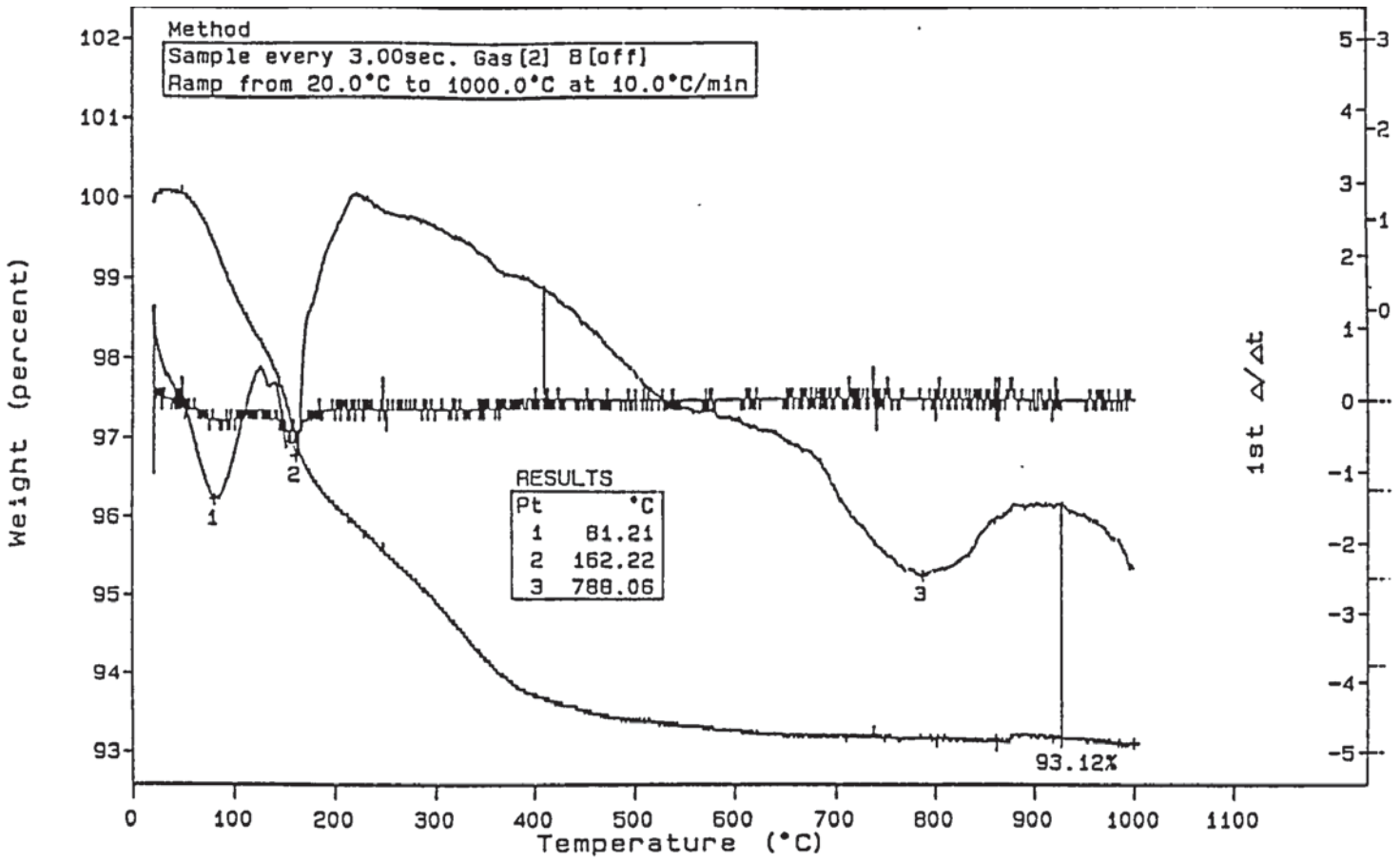

Figure 5.1.2 Thermogravimetric and DT analysis of potassium silicate Y

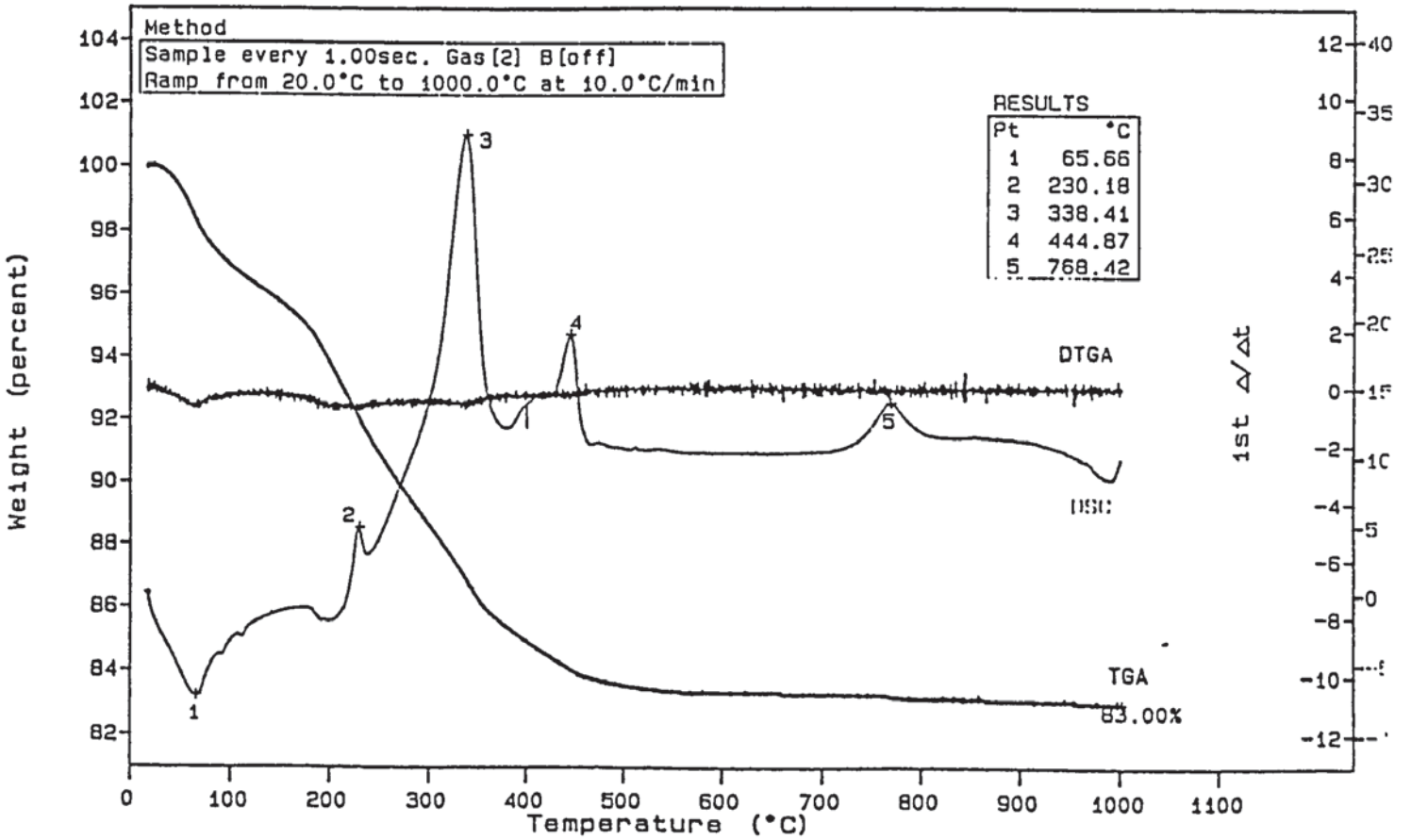

Figure 5.1.3 Thermogravimetric and DT analysis of potassium silicate Z

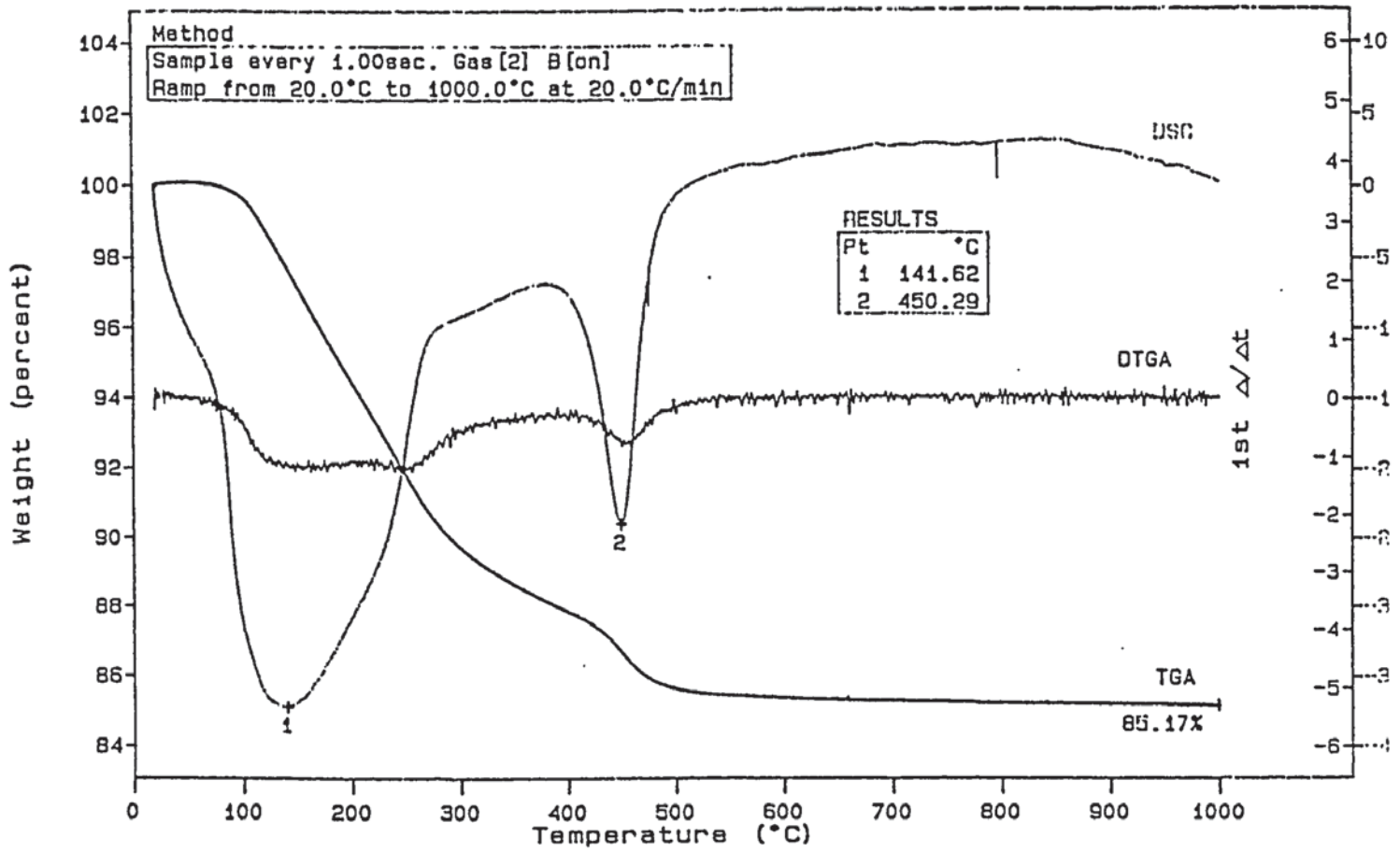

VERSION: V7.12

5.2 ^{29}Si MASNMR and ^{29}Si CPMASNMR

Tables 5.2.1, 5.2.2, 5.2.3, and 5.2.4 show peak positions with respect to TMS and peak widths at half height for the various calcined clay mineral and silicate mixtures and the calcined kaolinites before mixing.

Table 5.2.1 ^{29}Si MASNMR and CPMASNMR of mixtures of calcined kaolin A (labelled as A800) and silicates X, Y and Z

Sample Name	A800-X	A800-Y	A800-Z
MASNMR	-99.3 (1339)	-95.8 (892)	-97.5 (1413)
CPMASNMR	-94 (818)	-90.(1818)	-91.5 (818)

key:

Peak postions are expressed in ppm

Values in brackets are peak widths at half height and are expressed in Hz.

Table 5.2.2 ^{29}Si MASNMR data for the calcined kaolinites

Metakaolin type	Peak width at half height (Hz)	Shifts (ppm)
A800	1660	-101.7
B800	1260	-107.1
C800	1660	-98.6

Data in table 5.2.1 illustrate the differences in peak position and peak width at half height between mixtures of the same metakaolin but different silicate. Tables 5.1.1 and 5.2.2 identify the ^{29}Si NMR shift values for the silicates and mineral A800 pre-mixing to be -105 ppm and -101.7 ppm respectively, therefore we can comment on the changes that have occurred on mixing. A peak position of -101 ppm is indicative of a Q^4 environment, all 4 Si-O vertices of the $Si-O_4$ tetrahedra are shared. On mixing A800 with the silicates we generally see a shift to less negative values . The peak

widths as can be seen from table 5.2.1 and figure 5.2.1 are very broad, this is indicative of a variety of silicon environments.

^{29}Si CPMASNMR analysis allows the increase in intensity of resonances where the Si-O tetrahedra are in close proximity to protons. In other words, if silicons are present in a Q^3, Q^2 or Q^1 environment and are in close proximity to protons they should be seen more clearly under CPMASNMR analysis. Observation of CPMASNMR data in table 5.2.1 indicates presence of Si in a Q^3 environment. Figure 5.2.2 shows the resonance in the Q^3 region for the sample A800-silicate X.

Table 5.2.3 Peak shifts (ppm) with respect to TMS and peak widths at half height (Hz) for calcined kaolin B (B800) and silicates X, Y and Z

Sample Name	B800-X	B800-Y	B800-Z
MASNMR	-101 (1339)	-95.3 (1042)	-96.2 (1339)
CPMASNMR	-96.4 (818)	-90.9 (891)	-91.3 (558)

Table 5.2.4 Peak shifts (ppm) with respect to TMS and peak widths at half height (Hz) for calcined kaolin C800 and silicates X, Y and Z

Sample Name	C800-X	C800-Y	C800-Z
MASNMR	-98.7 (1233)	-93.7 (967)	-96.3 (1116)
CPMASNMR	-96.7 (818)	-90 (892)	-91.2 (372)

On comparing ^{29}Si MASNMR peak positions of the samples with data for the metakaolins: A800 -101 ppm, B800 -107 ppm, C800 -98.6 ppm and silicates: X and Z -105 ppm, Y -104 ppm we see a trend. Generally there is a shift in peak position for the mixtures towards less negative numbers relative to the position in the silicate or metakaolin. There is also a trend in that mixtures containing silicate X show little or no shift in peak position relative to the metakaolin peak position and are broader compared with other samples. This suggests a lack of reaction in the samples

Figure 5.2.1 ^{29}Si MASNMR Spectrum of sample A800-X

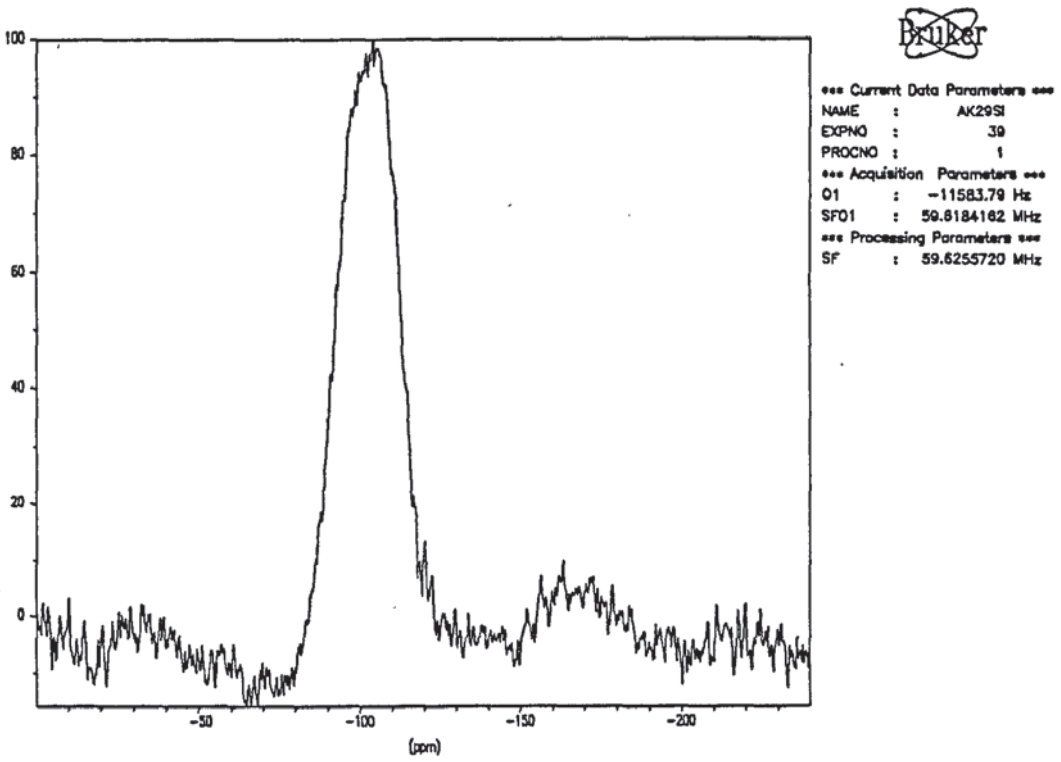

Figure 5.2.2 ^{29}Si CPMASNMR Spectrum of sample A800-X

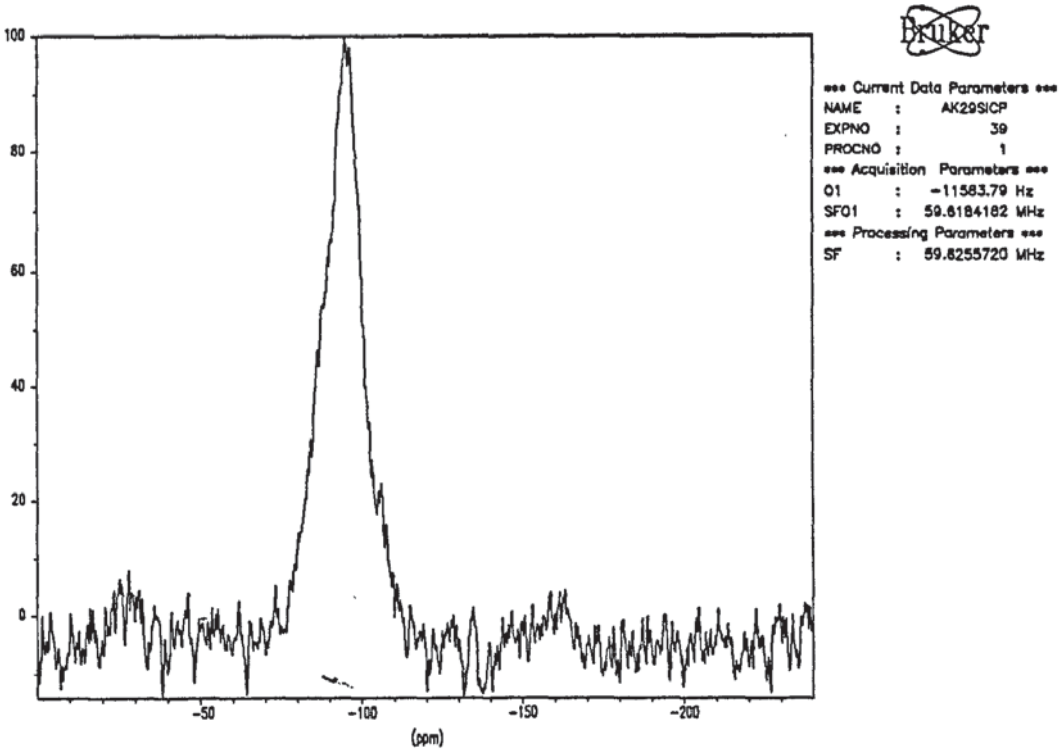

containing silicate X. CPMASNMR data in tables 5.2.3 and 5.2.4 reveal an absence of Q^3 resonances, this is to be expected if no reaction is occurring because both the component silicates and metakaolins of the sample yield Q^4 resonances only. Figures 5.2.3 and 5.2.4 compare the MASNMR and CPMASNMR spectra of sample B800-silicate X. As there are Q^3 resonaces in samples containing silicates Y and Z, this suggests a depolymerisation reaction is taking place in these materials.

The broadness of the peaks on ^{29}Si CPMASNMR analysis but more particularly on ^{29}Si MASNMR analysis and their positions indicate these peaks could be a simple sum of the metakaolin and potassium silicate peaks, although as identified by CPMASNMR, samples containing silicates Y and Z generate at least one peak other than a metakaolin or silicate peak. A deconvolution technique was applied to see if the broad peaks produced on MASNMR analysis could be resolved into component peaks.

5.2.1 Deconvoluted ^{29}Si MASNMR

Deconvoluted spectra of samples containing silicate X reveal the broad peaks to be composed of two peaks whose positions are similar to the positions of the component metakaolin and silicate. This point is demonstrated by figure 5.2.5 which shows the deconvoluted spectrum of sample B800-silicate X . This is further evidence of the lack of reactivity in mixtures containing silicate X. Deconvolution of spectra for the other mixtures either reveals the broad peak cannot be resolved as shown in figure 5.2.6 which is a spectrum of B800-Y, or if component peaks are observed their positions are removed from the positions expected for the component metakaolin and silicate as displayed in figure 5.2.7 which is a deconvoluted ^{29}Si MASNMR spectrum of sample C800-silicate Z. One of the component peaks is clearly in the Q^3 position providing further evidence for depolymeristion reactions occurring in these samples. Table 5.2.5 displays the results obtained on deconvoluting the ^{29}Si NMR spectra.

Figure 5.2.3 ^{29}Si MASNMR Spectrum of sample B800-X

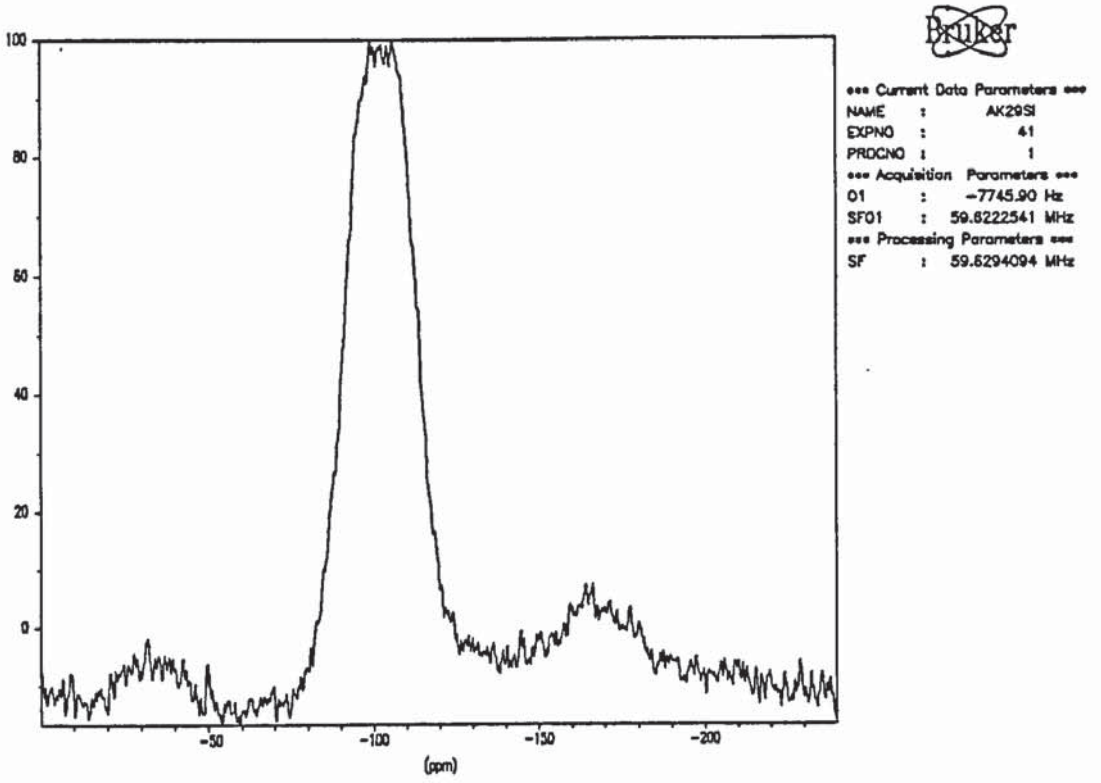

Figure 5.2.4 ^{29}Si CPMASNMR Spectrum of sample B800-X

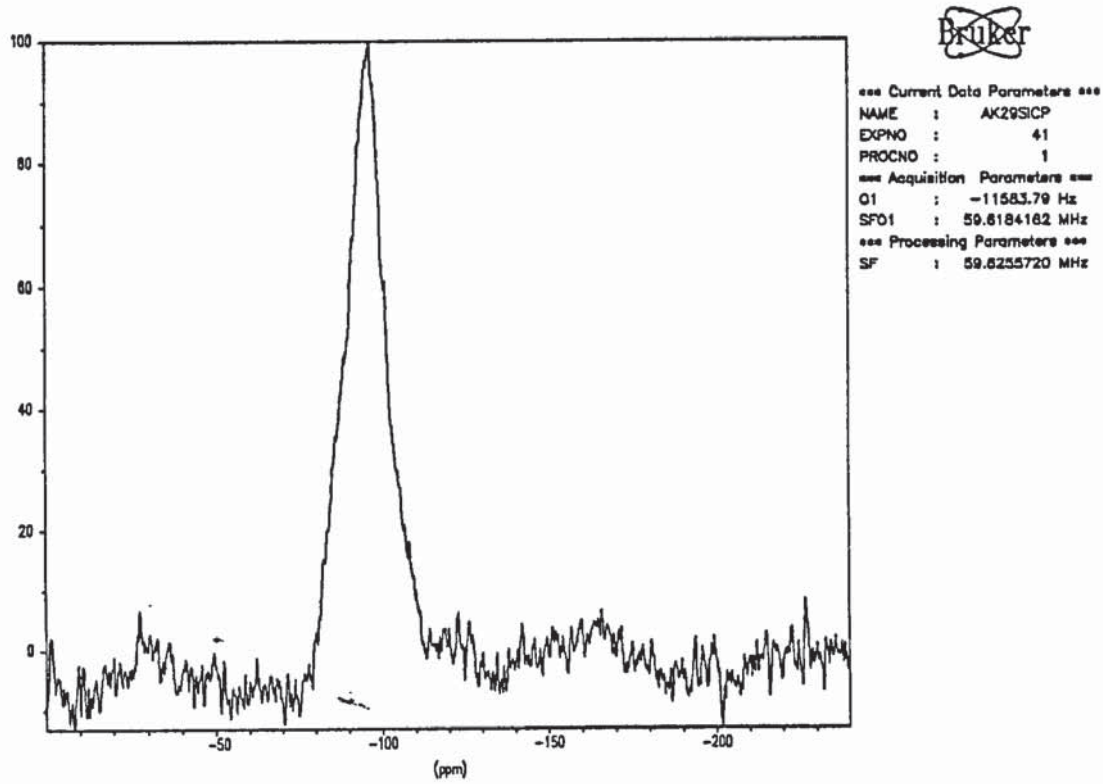

Figure 5.2.5 Deconvoluted ^{29}Si MASNMR Spectrum of sample B800-X

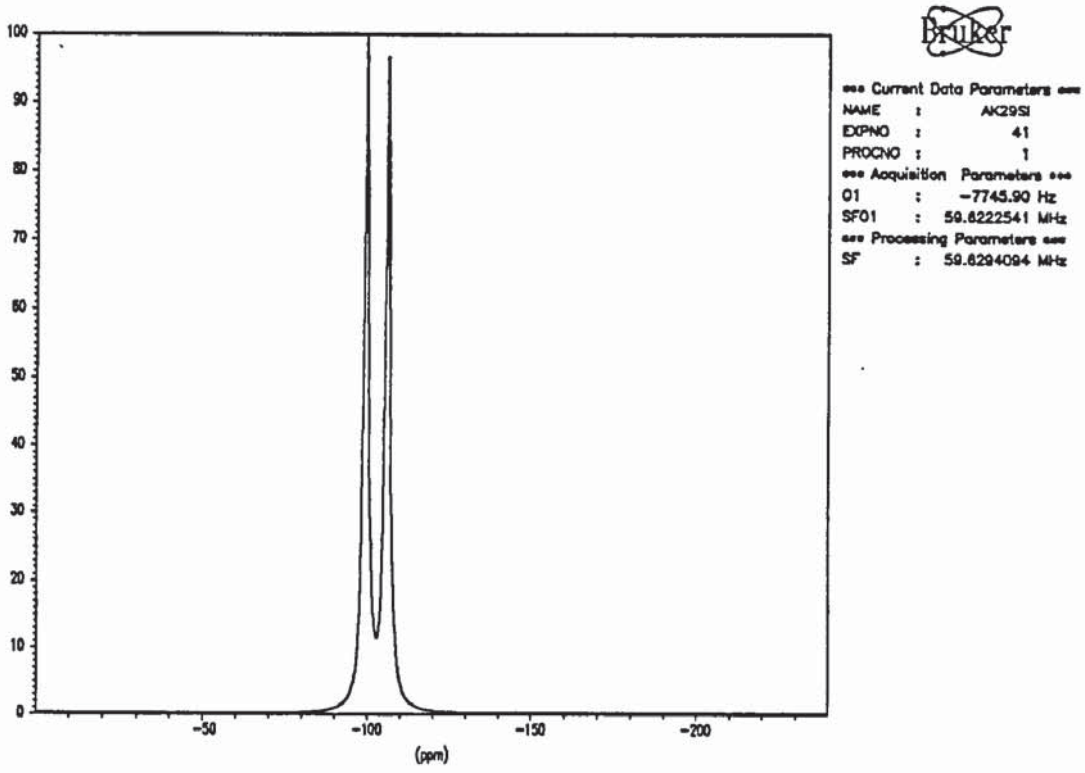

Figure 5.2.6 Deconvoluted ^{29}Si MASNMR Spectrum of sample B800-Y

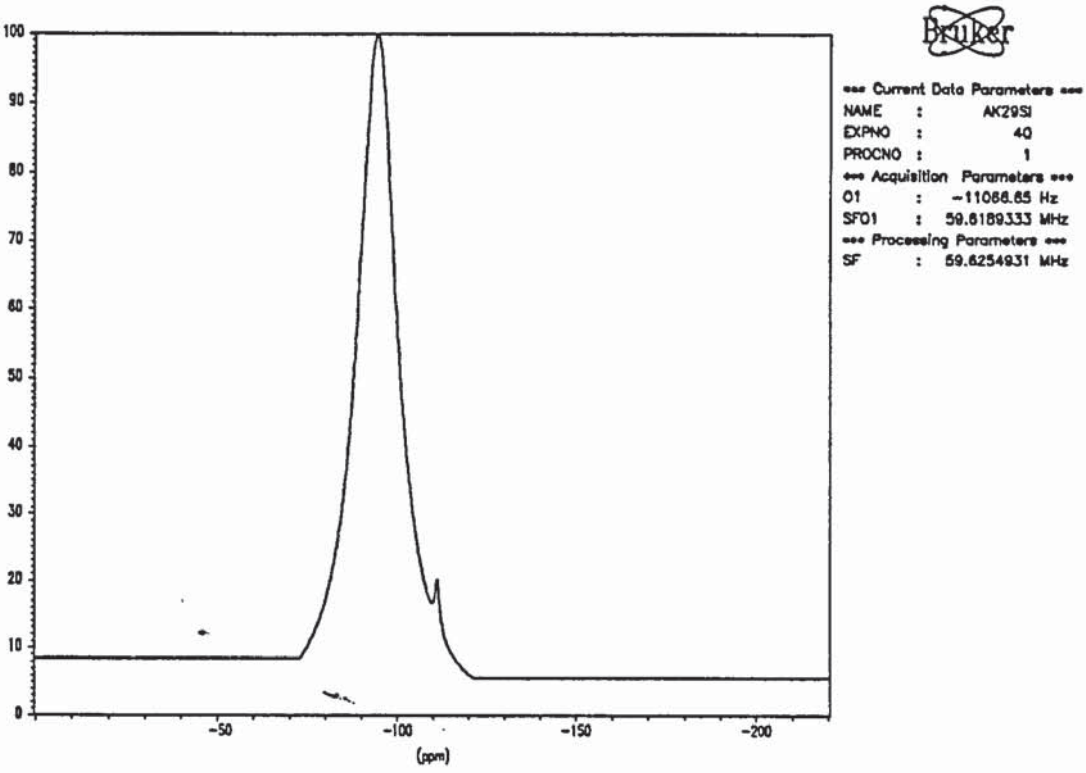

Figure 5.2.7 Deconvoluted ^{29}Si MASNMR Spectrum of sample C800-Z

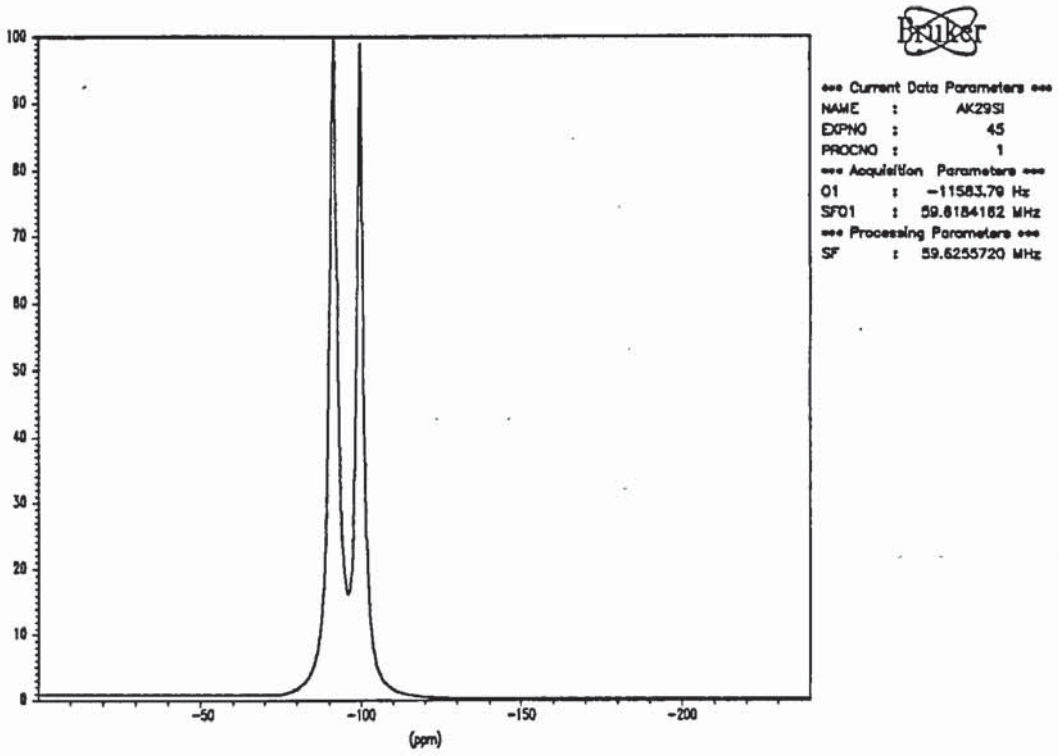

Table 5.2.5 Peak positions after deconvoluting ^{29}Si MASNMR and ^{29}Si CPMASNMR spectra.

Sample Name	^{29}Si MASNMR (ppm)	^{29}Si CPMASNMR (ppm)
A800-X	-99, -104, -108	-95, -106
A800-Y	-95	-90, -95
A800-Z	-93, -98, -105	-92
B800-X	-99, -105	-96
B800-Y	-95	-91, -105
B800-Z	-96	-91
C800-X	-99, -104	-96
C800-Y	-95	-88, -93
C800-Z	-92, -98	-91

On comparing data obtained from deconvoluted spectra after ^{29}Si MASNMR and ^{29}Si CPMASNMR analysis we see two obvious differences.

a) In CPMASNMR analysis there is a shift to low field in peak position compared with MASNMR.

b) Inspection of the individual spectra show peak widths are narrower in spectra obtained by ^{29}Si CPMASNMR analysis in corresponding samples.

Inspection of the data in table 5.2.5, to establish if there are patterns in the results obtained, indicates a trend concerning silicate X. The shift to low field in peak position on going from ^{29}Si MASNMR to ^{29}Si CPMASNMR analysis is least in samples containing silicate X.

In terms of peak narrowing, samples containing silicate Z gave the sharpest peaks. The position of these peaks centred around -91 ppm represents Q^3 resonance or a Q^4 resonance, where there is a high degree of substitution of Al for Si. This resonance is similar to the position of the Q^3 peaks seen in the uncalcined kaolinites, uncalcined

kaolins A and C have shift values of -90.9 ppm and -91.1 ppm respectively. However ^{27}Al MAS NMR analysis shows no kaolinite to be present in these samples. Therefore this resonance is due to a product of the silicate-metakaolin reaction.

On comparing peak widths at half height we ascertain samples containing silicate Z contain the least broad peaks, hence the most uniform silicon environment. CP MAS NMR spectra of samples containing silicate Z reveals a sharp peak in the Q^3 position and weaker shoulder in the Q^4 position, this does not necessarily mean a greater proportion of the silicon is in the Q^3 arrangement because CP MAS NMR has the effect of increasing the intensity of Q^3 peaks but not Q^4 peaks. This is because CP NMR relies on transferring polarisation from the protons to the silicons, resulting in a significant enhancement in silicon magnetization over the normal value. Moreover, CP allows successive free-induction decays to be obtained on the the time scale of the proton spin-lattice relaxation time rather than on the longer time scale of the silicon spin-lattice relaxation time, resulting in more rapid acquisition of the silicon spectrum. obviously this technique would be useless in enhancing Q^4 resonances since no protons are attached directly or via oxygen bridges to the silicon in such structures. This enhancement in spectra also overcomes the problem of low abundance of the magnetic isotope of silicon.

As is evident from table 5.2.5, deconvoluted ^{29}Si MASNMR spectra of samples containing silicate X reveal peaks in the -99 ppm+/-2 and -105 ppm region, these shift values are indicative of metakaolin and potassium silicate respectively and confirm the lack of reactivity of silicate X. The only other samples to yield a metakaolin peak are A800-Z and C800-Z but these also exhibit Q^3 peaks. Samples containing silicate Y show presence of no such metakaolin peak and therefore can be deemed the most reactive silicates.

Deconvoluted ^{29}Si CPMASNMR spectra of samples containing silicates X and Z generally yield a single peak, the position of which is determined by the silicate used. Silicate X generates peaks in the -95ppm region and silicate Z generating peaks in the -91 ppm region. samples containing silicate Y produce two peaks one of which is at the position seen for silicate Y, while the other varies depending on the metakaolin used.

5.2.2 ^{29}Si MASNMR analysis after calcining

The previous ^{29}Si MASNMR and ^{29}Si CPMASNMR studies were carried out on samples prepared by simple mixing, setting and then oven drying. These silicate-metakaolin samples were then calcined at 1000°C for 2 h and ^{29}Si MASNMR analysis repeated. The Spectra obtained revealed broad peaks in most cases so a deconvolution technique was applied in order to identify any component peaks. Table 5.2.6 exhibits the results obtained on ^{29}Si MASNMR analysis after calcining the materials.

Table 5.2.6 ^{29}Si MASNMR results (w.r.t TMS) of metakaolin-silicate mixtures after calcining at 1000°C for 2 h.

Sample Name	Peak Shifts (ppm)	Peak Shifts after deconvoluting spectra (ppm)
A800-X	-102.8	-102.8
A800-Y	-93.7,-97.2	-91, -97
A800-Z	-100.4	-100
B800-X	-91.6-109.3(broad)	-92, -99, -109
B800-Y	-92.2,97	-90.8, -97
B800-Z	-99.9	-99.5
C800-X	-96.5	-95.7, 103.6
C800-Y	-92.4,97.5	-90.8, -97.1
C800-Z	-100.2	-100

Figure 5.2.8 ^{29}Si MASNMR Spectrum of B800-X after calcining the sample

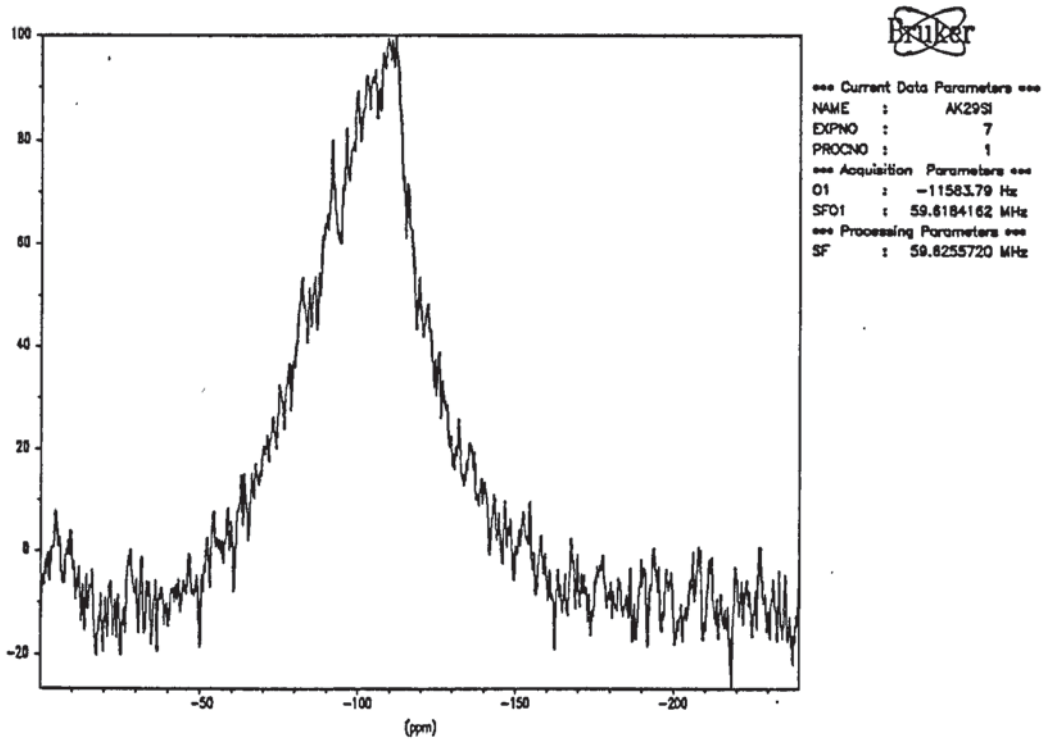

Figure 5.2.9 Deconvoluted ^{29}Si MASNMR Spectrum of B800-X after calcining the sample

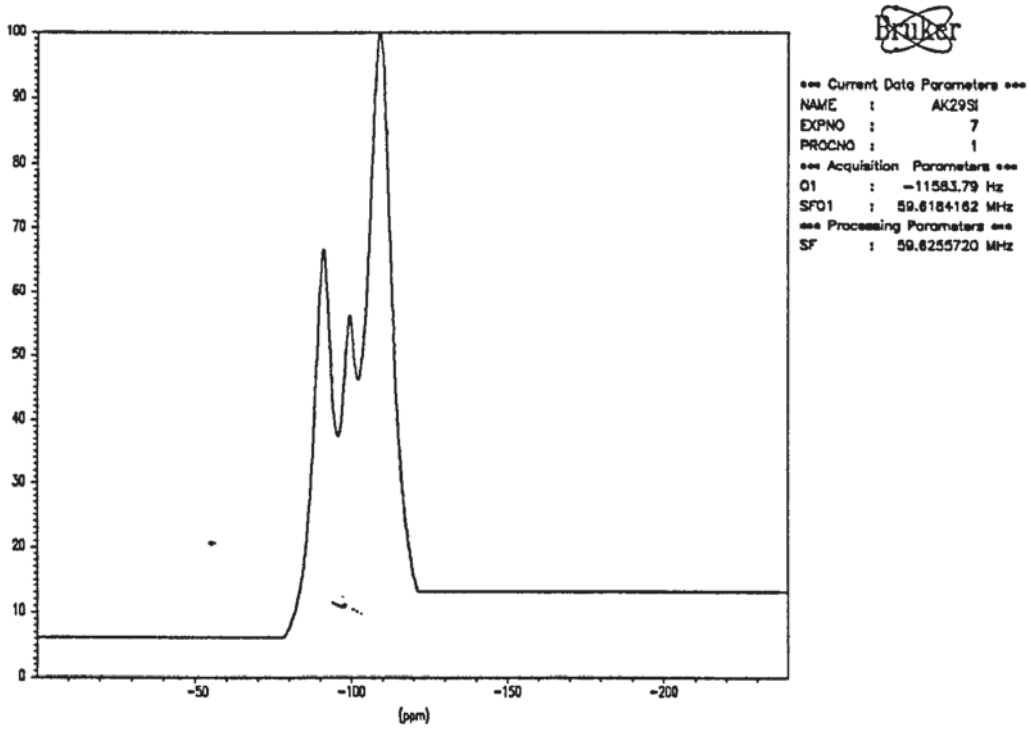

The ^{29}Si MASNMR spectra show that generally calcining has the effect of broadening the resonances. Materials containing silicate X generally show the broadest of peaks. In the case of sample B800-X, the broad peak stretching in to the region of -109 ppm is indicative of the presence of free silica (see figure 5.2.8). On deconvolution of the spectra, the broad peak is resolved into three peaks, the position of one of which is in a part of the Q^4 region associated with free silica. Figure 5.2.9 shows the deconvoluted ^{29}Si MASNMR spectrum of sample B800-X. Infact inspection of the deconvoluted ^{29}Si MASNMR data in table 5.2.6 reveals that only the samples produced from silicate X yield a Q^4 resonance associated with silica.

Samples containing silicate Y give two distinctive peaks after calcining: -92/93 ppm and -97 ppm, thus suggesting the presence of two silicon environments, the former is not seen in either of the components pre-mixing whereas the latter is not far removed from the position seen for the metakaolin peak . The position of -92 ppm corresponds to $Q^4(2Al)$. Work carried out by R. T. Slade[14] on calcining kaolinites at 1050°C also revealed the appearance of a second peak in the 80-90 ppm region which was assigned to mullite[14]. Figure 5.2.10 is typical of ^{29}Si NMR spectra obtained after calcining materials containing silicate Y.

Samples prepared using silicate Z were the only materials to have only one silicon environment. This is despite pre-calcining, there being at least two silicon environments in silicate Z containing materials as shown in table 5.2.5. This is a reversal of the process seen in samples concerning silicate Y. In these samples only one silicon environment was apparent before calcining but calcining produces two silicon environments. These results clearly show that the silicates are determining the products formed on calcination of the materials.

Figure 5.2.10 ^{29}Si MASNMR Spectrum of A800-Y after calcining the sample

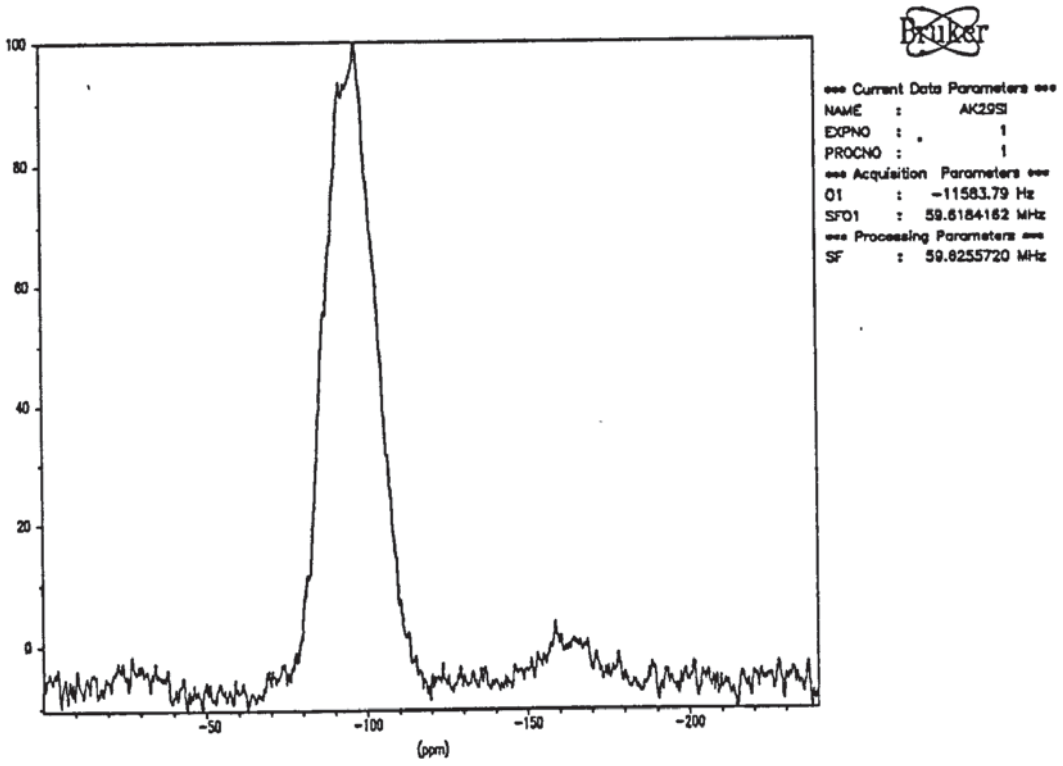

5.3 ^{27}Al MASNMR

Table 5.3.1 ^{27}Al MASNMR data for metakaolin-silicate mixtures before calcining, (values are expressed in ppm w.r.t. $[Al(H_2O)_6]^{3+}$).

	A800	B800	C800
Silicate X	57.2,40.8,3	57,4.6	55.6,27,4.7
Silicate Y	57.7	57.1	58.2
Silicate Z	56.5	56.2	56.9,5.5

Samples containing silicate X show a clear lack of reactivity as resonances in the octahedral and pentacoordinate regions seen in the metakaolins pre-mixing are retained in these mixtures. ^{27}Al NMR results confirm what was already suspected after ^{29}Si MASNMR analysis (table 5.2.5). Since metakaolin peaks are seen in silicate X containing samples on ^{27}Al NMR analysis and both silicate and metakaolin peaks are seen on ^{29}Si MASNMR analysis, it is obvious no reaction is occurring. Figure 5.3.1 is an example of ^{27}Al NMR spectra of samples containing silicate X.

Inspection of the data for the metakaolin-silicate Y series shows we have a single peak in the 57 - 58.2 ppm region for all of these mixtures. Figure 5.3.2 is a typical example of ^{27}Al NMR spectra of mixtures containing silicate Y. This shows all the aluminium atoms are in a tetrahedral environment whereas pre-mixing, the Al atoms were in pentacoordinate and octahedral environments as well. This shows dramatic changes have occurred centred on the Al atom on simple mixing of the metakaolins and silicate Y. The reduction in Al coordination number is consistent with the results obtained from ^{29}Si CPMASNMR analysis that depolymerisation reactions were occurring. Metakaolin-silicate Z mixtures again reveal most Al atoms to be in a tetrahedral environment apart from C800-Silicate Z mixture where there is still some residual Al in an octahedral environment. As resonances in the Q^3 position were seen on ^{29}Si MASNMR analysis it is obvious depolymeristion reactions have occurred in

samples containing silicate Z as well as samples containing silicate Y. Residual octahedral Al is seen in the sample C800-silicate Z which shows the reaction has not proceeded to completion in this sample. This validates the observation made after ^{29}Si MASNMR and ^{29}Si CPMASNMR study on the order of reactivity , namely silicate Y being most reactive, silicate Z intermediate and silicate X being the least reactive.

These results show a dramatic change in Al coordination numbers on addition of the silicates. Simple mixing of the metakaolin and silicates appears to play an important role in altering the structure of metakaolins probably because a depolymerisation reaction is occurring. If formation of tetrahedral Al at an early stage of the preparation of the refractory material is important in determining the strength of the refractory then one can predict silicate X will be the worst performer of the silicates.

Disappearance of octahedral and pentacoordinate Al on addition of the silicates shows the silicates are reacting with the Al of the metakaolin and in particular with the 5 and 6 coordinated aluminiums. Furthermore the appearance of residual octahedral peaks in some of the samples but no pentacoordinate peaks suggests pentacoordinate is the more reactive site of the two. This point is further emphasised when samples prepared using the relatively inert silicate X reveal on ^{27}Al NMR analysis, pentacoordinate Al is no longer present whereas octahedral aluminium is still observed, this is seen in sample B800-silicate X as shown in table 5.3.1.

The ^{27}Al NMR and ^{29}Si NMR studies have shown the importance of choice of silicate in refractory material preparation, the particular silicate chosen determining whether reactions occur or not. However, silicates are not solely responsible for reactivity. The choice of metakaolin is also important. Metakaolin-silicate Z materials yield single peaks representing tetrahedral aluminium but not when the metakaolin used is C800, in this case another peak is seen indicating the presence of octahedral aluminium. Figure 5.3.3 shows ^{27}Al NMR spectrum of sample C800-silicate Z.

Figure 5.3.1 ^{27}Al MASNMR spectrum of sample A800-silicate X

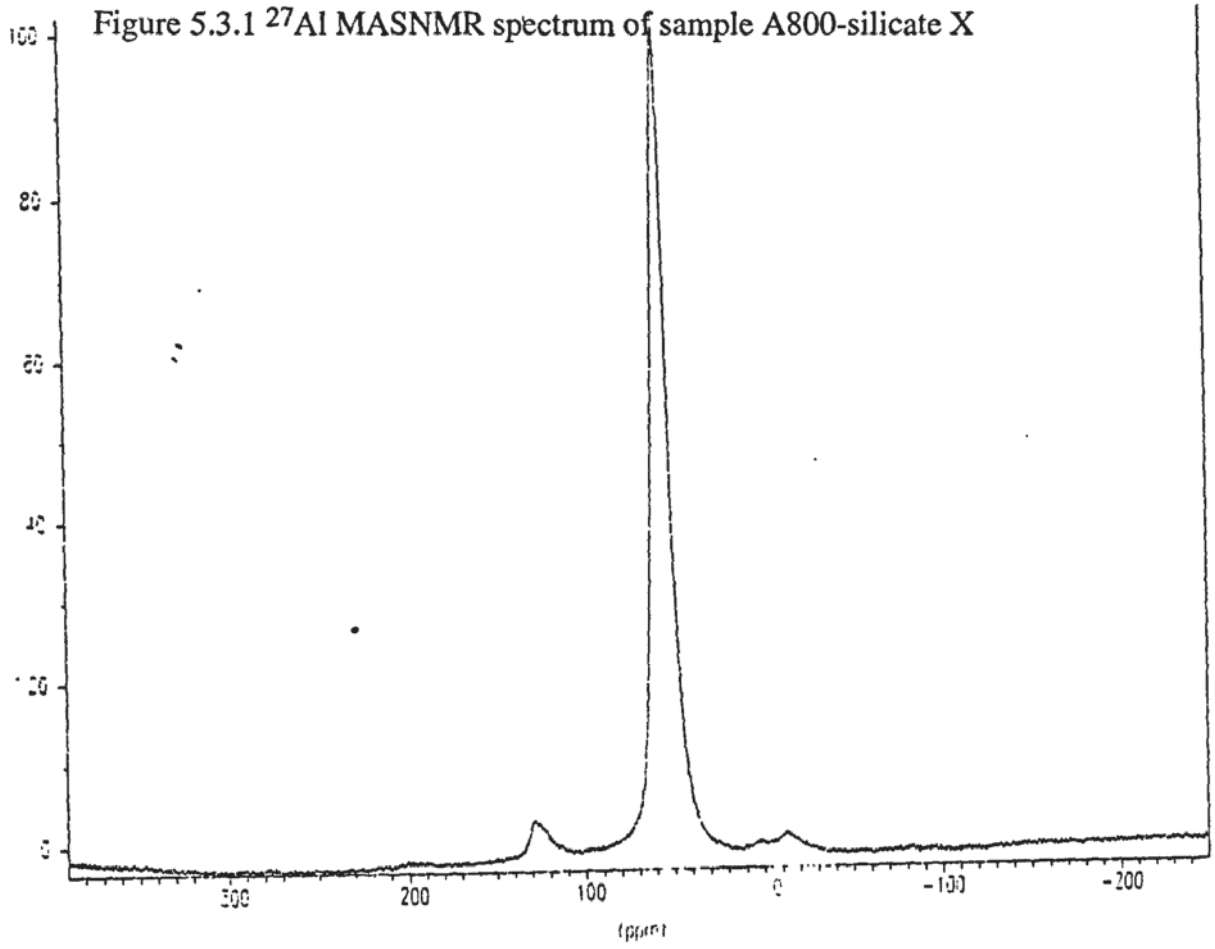

Figure 5.3.2 ^{27}Al MASNMR spectrum of sample A800-silicate Y

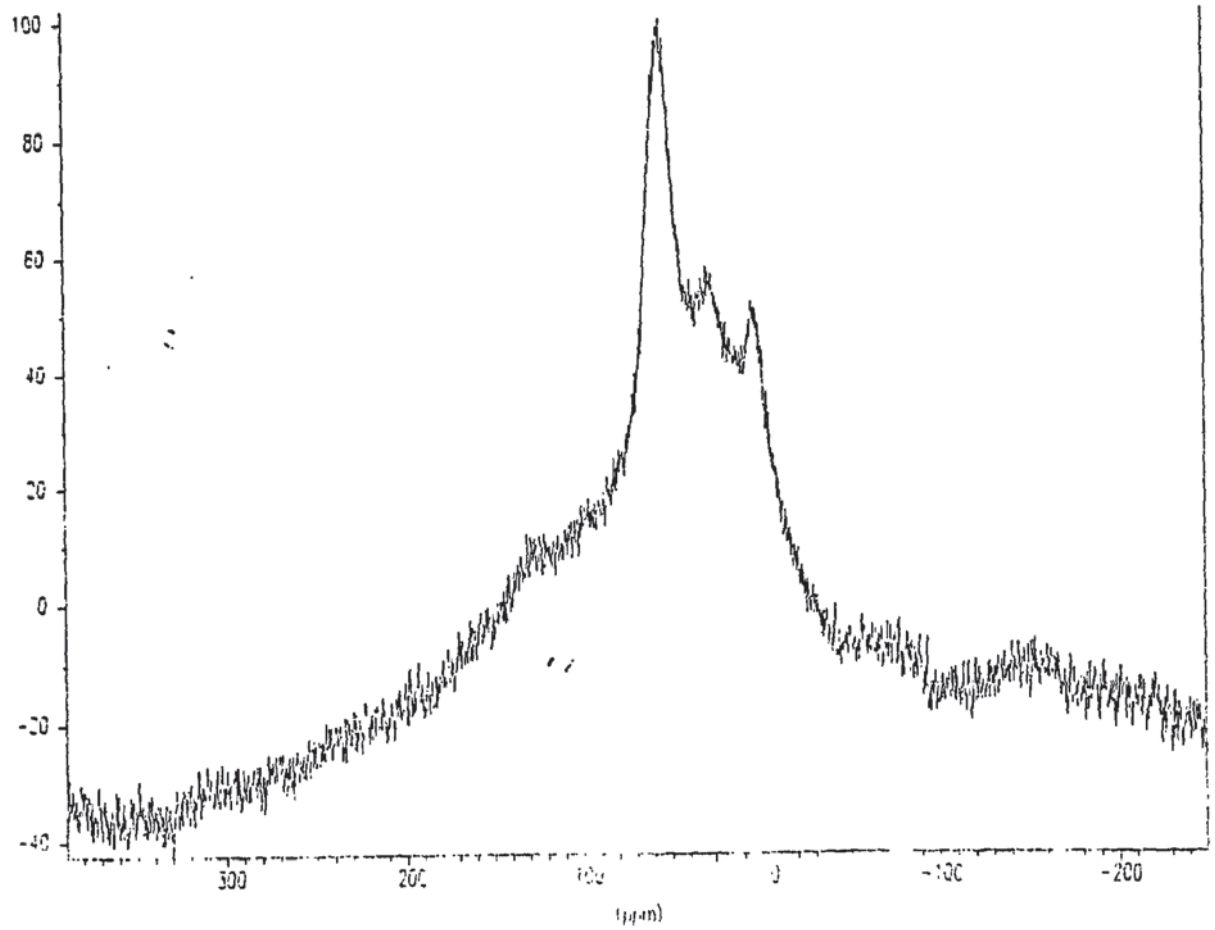

Figure 5.3.3 ^{27}Al MASNMR Spectrum of C800-silicate Z

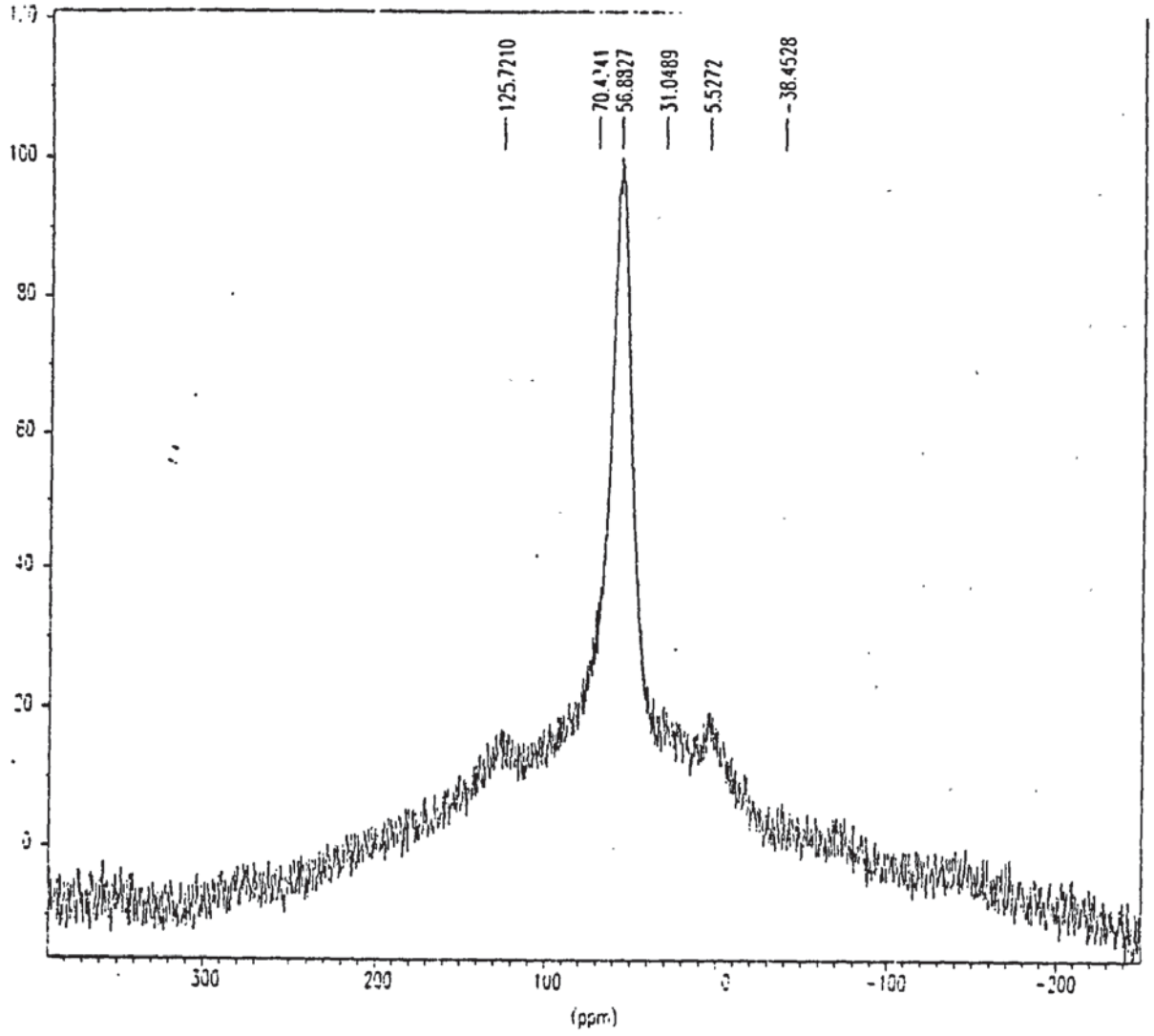

5.3.1 ^{27}Al MASNMR analysis after calcining

Table 5.3.2 ^{27}Al MASNMR results of metakaolin-silicate mixtures before calcining and after calcining at 1000°C for 2 h (w.r.t. $[Al(H_2O)_6]^{3+}$)

Type of Mixture	position of peaks before calcining (ppm)	position of peaks after calcining (ppm)
A800-Y	57.7	58.1
A800-X	57.2,40.8,3	53.4
A800-Z	56.5	59.4
B800-Y	57.1	58
B800-X	57,4.6	53.1
B800-Z	56.2	57.6
C800-Y	58.2	58
C800-X	55.6,27,4.7	52.2
C800-Z	56.9,5.5	57.6

Examination of table 5.3.2 reveals calcining the mixtures produces Al in a tetrahedral coordination in all the samples. This means dramatic changes have taken place on calcining the mixtures, this is especially in samples where all three coordination numbers were seen before calcining. In mixtures where Al existed entirely in tetrahedral coordination before calcining, subtle changes are seen after calcining. Comparing shift values of calcined and uncalcined mixtures we generally see a small shift downfield.

On comparing ^{27}Al NMR chemical shift values of the materials after calcining a pattern is observed. Mixtures of metakaolin with silicates Y or Z yield peaks in a narrow range between 57.6 ppm to 59.4 ppm suggesting very little difference in structure around the Al atoms in these mixtures. However, mixtures containing the silicate X produce differing results. All mixtures containing silicate X yield peaks in

the 52.2 to 53.4 ppm range. Although these shift values are still indicative of a tetrahedral Al environment, the difference in position when compared with the other mixtures points to the presence of subtle differences in structure.

^{29}Si MASNMR analysis of the calcined metakaolin-silicate Y samples produced a resonance at a position similar to that of metakaolin. ^{27}Al NMR analysis of the calcined samples suggests there is no metakaolin in these materials. Therefore the resonance must be due to the formation of a new product on calcining.

^{29}Si MASNMR analysis of the calcined metakaolin-silicate X materials showed these samples to be distinctive, yielding peaks in the regions of the ^{29}Si NMR spectrum not seen for the other samples. This pattern is repeated on ^{27}Al MASNMR analysis, positions of the resonances for metakaolin-silicate X samples differ from the results obtained for the other materials. The lack of initial reactivity in the samples containing silicate X leads to different products being formed after calcining. XRD analysis in section 5.7 reveals the nature of these products.

5.4 Thermogravimetric and Differential Thermal Analysis

Thermogravimetric and differential thermal analysis has been carried out on 2 types of metakaolin-silicate mixtures:

a) Mixtures where the weight ratio of metakaolin to silicate is the same as the weight ratio used in the new refractory

b) Mixtures where the weight ratio of metakaolin to silicate is 1:1

A plot obtained from differential thermal analysis of the samples after heating to a temperature of 1200°C yields two main features:

a) An endothermic peak at approximately 200°C due to the loss in water.

b) An exothermic peak at approximately 1000°C due to the onset of crystallisation.

Table 5.4.1 exhibits the exact temperatures at which the endothermic and exothermic peaks appear and the percentage weight losses incurred for the individual metakaolin-silicate mixtures prepared using the same weight ratios as used in the new refractory.

Table 5.4.1 Percentage weight loss and positions of endo- and exotherms for mixtures prepared using the same weight ratios as used in the new refractory.

Type of Mixture	Weight Loss (%)	Endotherm (°C)	Exotherm (°C)
A800-X	1.3	200	1010
A800-Y	5.2	144	1000
A800-Z	2.4	165	1000
B800-X	3.5	172	1000
B800-Y	5.5	145,210	1015
B800-Z	1.7	200	1010
C800-X	2.3	172	1000
C800-Y	3.8	200	1020
C800-Z	2.1	158	1000

Comparing the data in table 5.4.1 for the mixtures with data for the kaolinites a number of differences are evident:

A) The endotherm appears at approximately 600°C in the kaolinites, whereas in the mixtures it appears at much lower temperatures.

B) There is no change in the temperature at which the exotherm appears but the intensity and sharpness of the exothermic peak is greatly dampened down in the mixtures.

Scrutiny of weight loss data in table 5.4.1 reveals a pattern regarding mixtures containing the silicate Y, these mixtures tend to give the greatest percentage weight loss. This is probably due to greater initial water content or the presence of some volatile impurity in this sample which is being lost on calcination. Weight loss resulting from the loss of silicates through volatilisation at the temperatures used for calcining is not possible therefore the explanation of water loss or impurity loss is the only plausible explanation for the greater weight loss in these materials.

The positions of the endothermic peaks seem to vary randomly, no correlation can be made between peak position and the silicate or metakaolin used.

5.4.1 Study of the exothermic peaks

The most important property of kaolinite as a refractory is the formation of the crystalline phase at temperatures above 1000°C. The temperature at which the exothermic peak appears in the mixtures shows very little change compared with the temperature at which the peak appears in kaolinite. Furthermore, as table 5.4.1 shows, there is also little difference in exothermic peak position amongst the mixtures. However, examination of the plots obtained from differential thermal analysis reveals the nature of the exothermic peaks to be very different from mixture to mixture. Samples containing silicate Y tend to give broad and less intense peaks compared

with other mixtures as shown in figure 5.4.1. Intensity and sharpness of the exothermic peak seen in kaolinites is best maintained in mixtures containing silicates X and Z. Figure 5.4.2 is a differential thermal plot of a metakaolin and silicate X. Figures 5.4.1 and 5.4.2 illustrate the difference in exothermic peak intensity depending on the silicate used in the mixture.

On observation of DTA spectra of a series of mixtures where the silicate remains constant and the metakaolin is changed again a trend can be identified. Mixtures containing the metakaolin A800 generally yield the most intense exothermic peaks. Table 5.4.2 attempts to illustrate these observations by a crude method of measuring exothermic peak heights.

Table 5.4.2 Exothermic peak heights produced by mixtures on DT analysis (cm)

	A800	B800	C800
Silicate X	4.2	1.9	2.0
Silicate Y	1.6	0.7	0.7
Silicate Z	4.5	2.5	3.2

The exothermic peak is due to heat being evolved during rearrangement of the structure to a more crystalline form at high temperatures. If a considerable amount of heat is evolved then we would expect a more intense clearly resolved peak compared with a sample where little heat is evolved and hence very little crystallisation has occurred. Therefore a crude measure of the extent of crystallisation is to compare peak intensities or peak heights as shown in table 5.4.2. Comparison of peak heights amongst mixtures ascertains mixtures containing A800 or silicate Z produce the most intense peaks therefore crystallisation is greater in these samples.

On comparison of these peak heights with the kaolinites pre-mixing, we find, as expected addition of the silicate is detrimental to the formation of a crystalline phase from the kaolinites. This is due to the addition of silicate increasing the proportion of glassy material at high temperature which hinders crystallisation and dissipates the heat evolved.

Figure 5.4.1 Thermogravimetric and DT analysis of C800-silicate Y

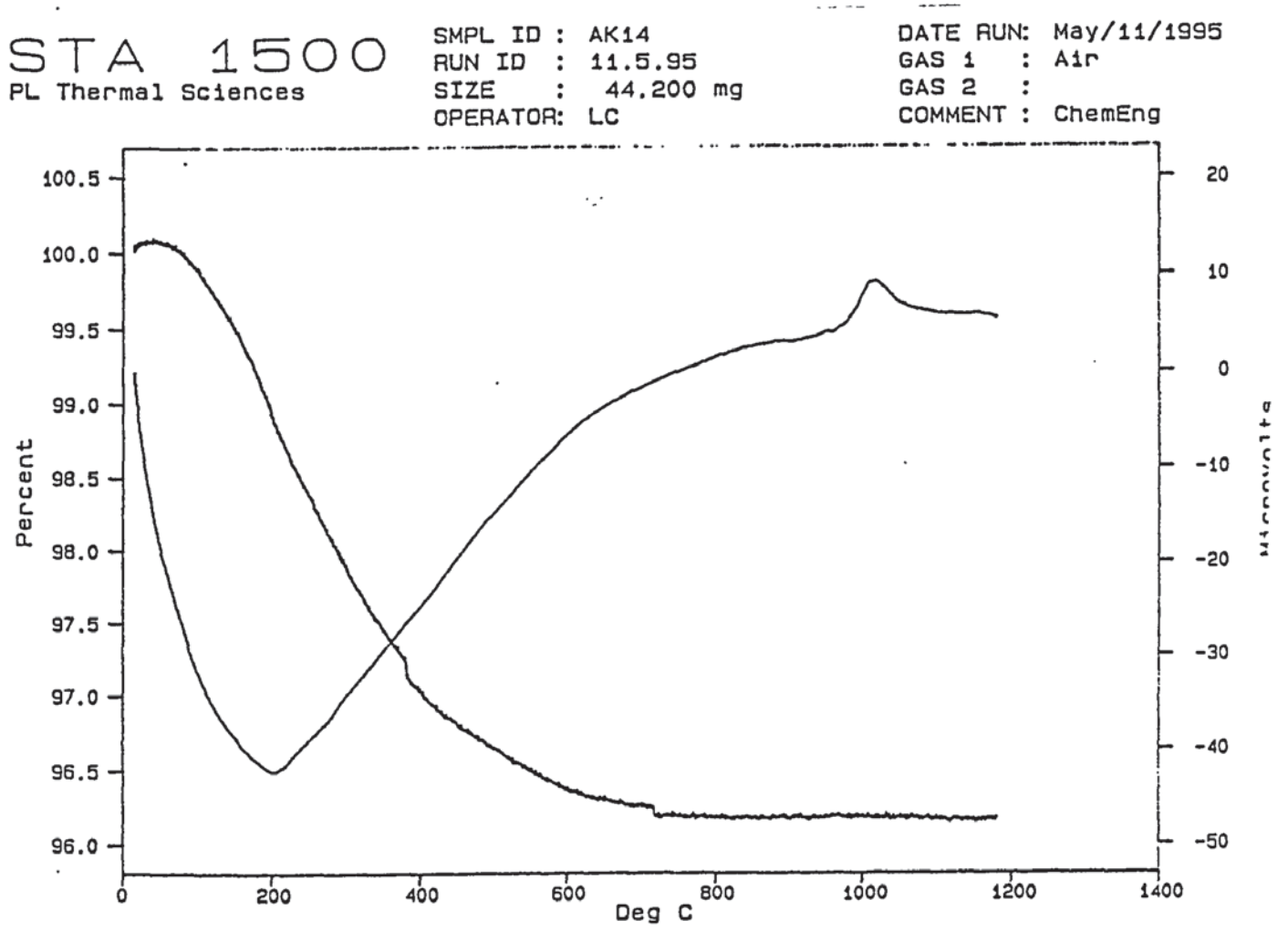

Figure 5.4.2 Thermogravimetric and DT analysis of C800-silicate X

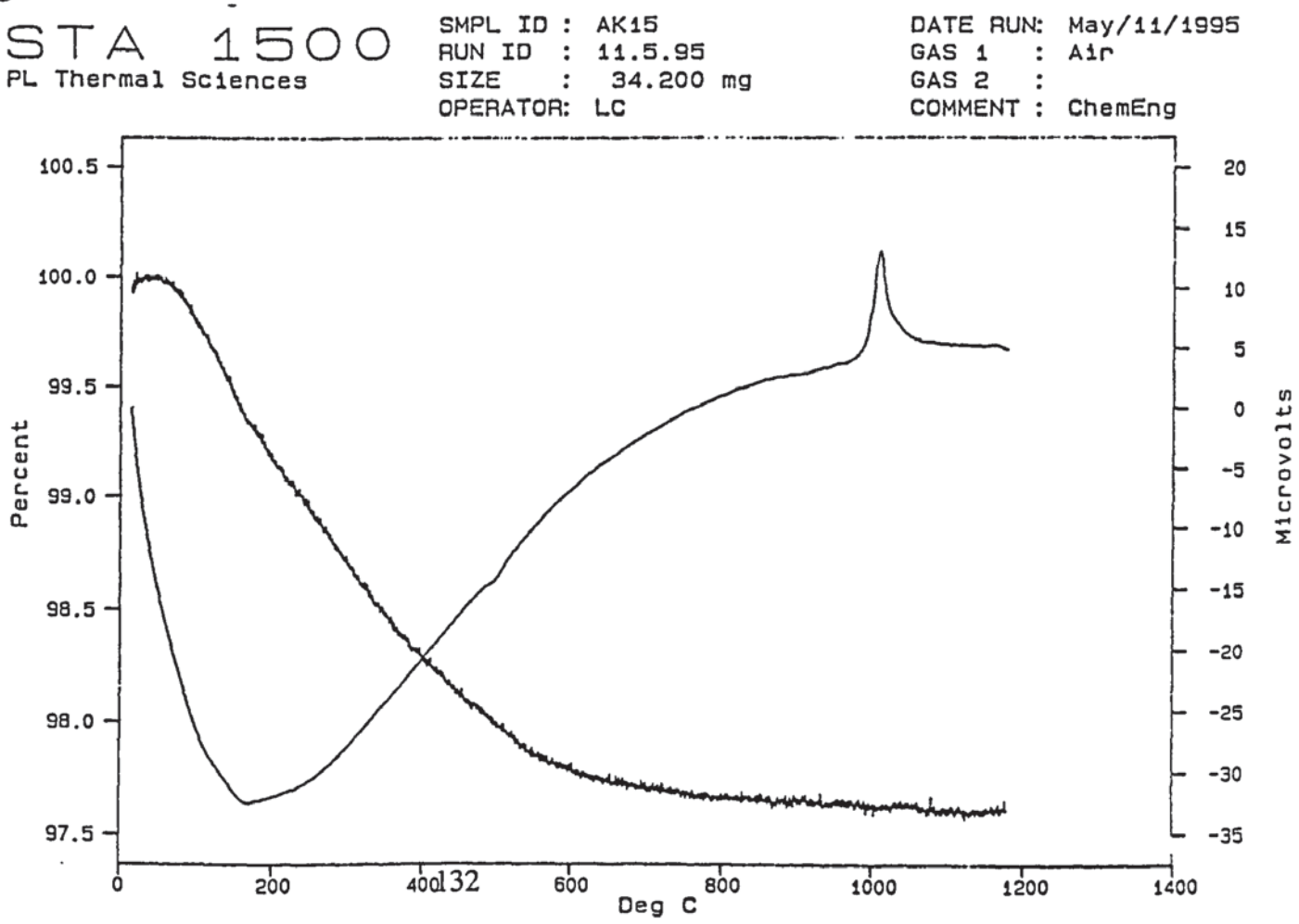

5.4.2 Thermogravimetry and DT analysis of metakaolin-silicate (1:1 weight ratio)

Thermogravimetry and DT analysis was repeated on samples were metakaolin-silicate weight ratio was 1:1 rather than the ratio used in the new refractory. In mixtures of 1:1 weight ratios a greater proportion of silicate is used compared with samples containing weight ratios as used in the new refractory, in that study it was confirmed that addition of silicates was detrimental to the intensity and sharpness of the exothermic peak. In samples where a greater proportion of silicate is used one would expect this effect to be exacerbated.

Table 5.4.3 Percentage weight loss and positions of endo and exotherms for mixtures prepared using 1:1 weight ratios of the component metakaolin and silicate

Type of Mixture	weight loss (%)	Endotherm(s) (°C)	Exotherm(s) (°C)
A800-Y	9	179	1014,1076w
A800-X	4	172	1000w
A800-Z	6	215,476	1000,1076
B800-Y	8.5	186	1151
B800-X	6	200,490	993
B800-C	1.7	200	1068
C800-Y	9	159	1158w
C800-X	4.5	172	1014
C800-Z	6	172,434	1076w

w-weak peak

Table 5.4.3 reveals the exothermic peak has shifted to higher temperatures in these samples compared with samples containing metakaolin-silicate weight ratios as used in the new refractory. This fact is true for all mixtures except for samples containing silicate X where there is little change in the temperature at which the exothermic peak

appears. ^{29}Si MASNMR and ^{27}Al MASNMR analysis indicated a lack of reactivity in samples containing silicate X, differential thermal analysis indicates a lack of reaction between the potassium silicate and metakaolin even on calcining because the temperature at which the exotherm appears is not very different to the temperature at which the exotherm for kaolinite appears. This suggests, in samples containing silicate X, we are simply seeing the exotherm due to the component metakaolin. In samples prepared using the other silicates the temperature at which the exotherm appears is far removed from the temperature at which it appears for the kaolinite. This suggests the exotherm is due to a new product of the silicate - metakaolin reaction in these samples.

The most dramatic change observed is the appearance of a second exothermic peak in A800-Y and A800-Z, this feature is particularly visible in the latter as shown in figure 5.4.3. ^{29}Si NMR analysis revealed the presence of more than one silicon environment in these samples either before calcining or after calcining, possibly indicating the presence of more than one phase in these materials, this manifests itself on DT analysis by the presence of two exotherms in samples A800-Y and A800-Z. However the lack of a second exotherm in other samples that produced similar ^{29}Si MASNMR sheds doubt on this theory.

The second possibility could be explained by the fact that the presence of two exotherms only occurs with metakaolin A800 therefore suggesting product formation is being dictated by the metakaolin used. Metakaolin A800 was identified as the most pure of the three metakaolins studied and seems to distinguish itself again in terms of the interactions taking place with silicates. Appearance of a second exothermic peak demonstrates there are two stages of crystallisation occurring in mixtures containing the metakaolin A800, hence we would expect a greater proportion of crystallinity therefore greater strength in this material.

Figure 5.4.3 Thermogravimetric and DT analysis of A800-silicate Z (1:1 weight ratio)

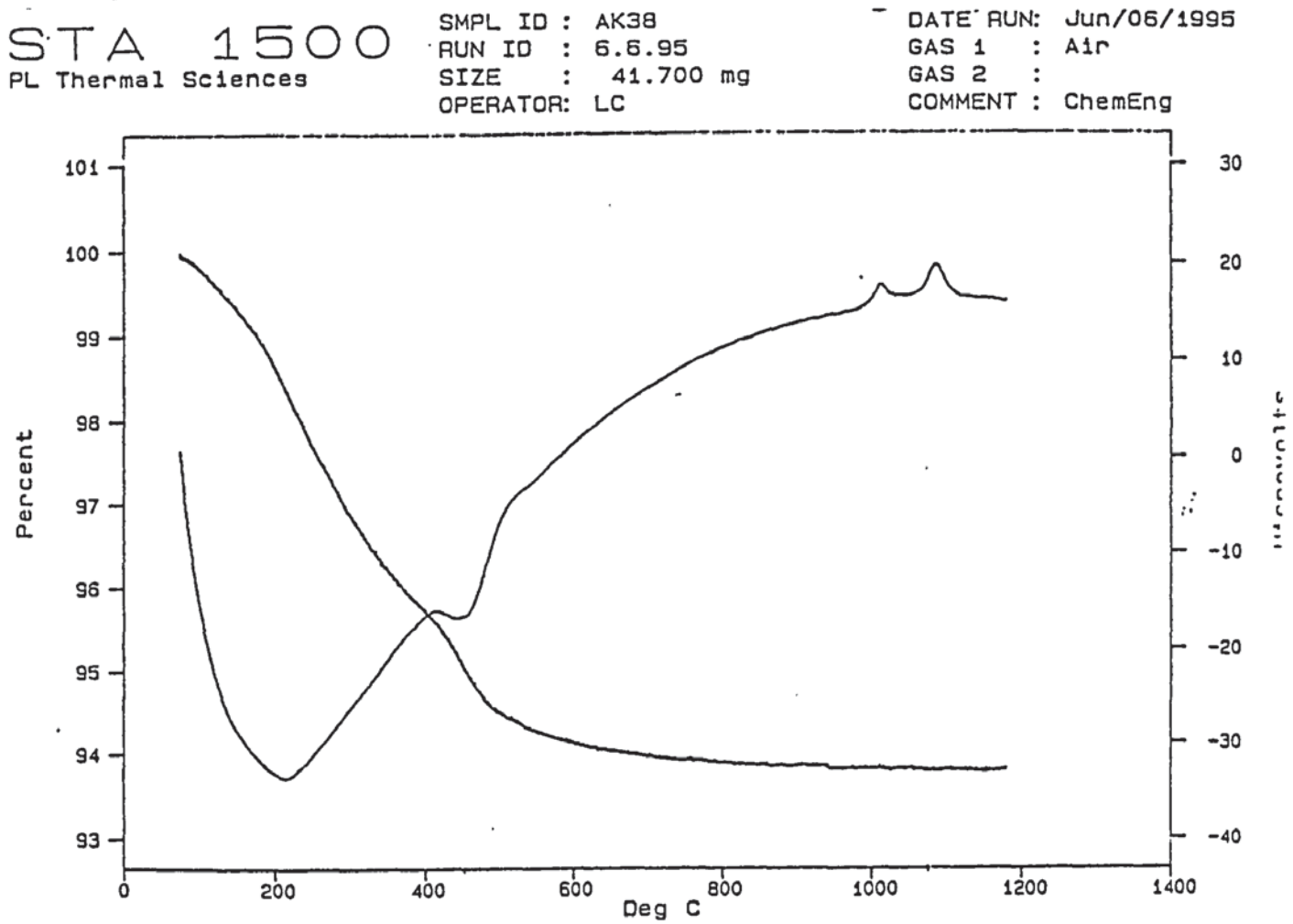

Figure 5.4.4 Thermogravimetric and DT analysis of B800-silicate Y(1:1 weight ratio)

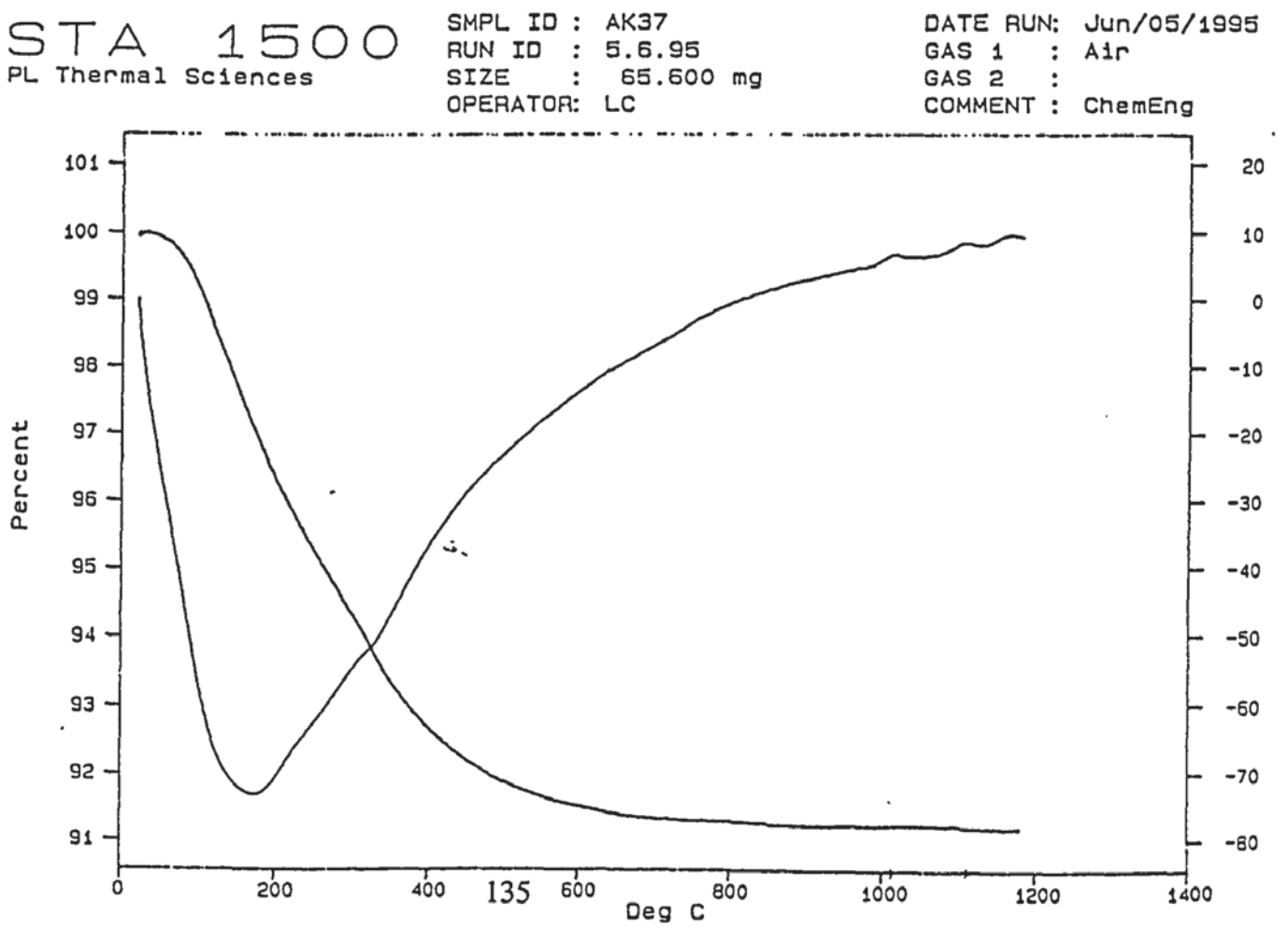

5.4.3 Exothermic peak intensity

On comparing exothermic peak intensities, generally there is a decrease in intensity in all the mixtures when compared with corresponding mixtures prepared using the new refractory formulation as expected. This is illustrated in table 5.4.4 by comparing peak heights.

Table 5.4.4 Exothermic peak heights (cm)

	A800	B800	C800
Sillicate X	1.0	0.5	0.5
Silicate Y	0.1, 0.1	0.1	0.1
Silicate Z	0.2, 0.5	0.5	0.1

Familiar trends can be seen in peak intensity when comparing the different mixtures. Samples containing the metakaolin A800 generally yield greater crystallinity (greatest peak height). When looking at the effect of silicates on intensity of the exothermic peak, mixtures containing silicate X give the most intense peaks. This may be explained by the inactivity of this silicate in the mixture as demonstrated with ^{29}Si MASNMR and ^{27}Al MASNMR, hence we see more of the original kaolinite exothermic peak in these mixtures. Mixtures containing silicate Y show the greatest dampening of the exothermic peak as shown in figure 5.4.4. This clearly demonstrates that the type of silicate used is important in determining the extent of crystallisation on calcining the kaolinite.

5.5 Infrared Analysis

Table 5.5.1 exhibits infrared analysis data for metakaolins and silicates before mixing. Table 5.5.2 exhibits infrared analysis for the metakaolin-silicate mixtures.

Table 5.5.1 Major infrared peaks for metakaolins and silicates (cm^{-1}) before mixing

Silicate A	Silicate C	A800	B800	C800
440,462	471, 490	832	800	800
771	745,7 61	1090	1099	1082
1014,1033	968, 1079			

Table 5.5.2 Major infrared peaks for metakaolin-silicate mixtures (cm^{-1})

	Silicate X	Silicate Y	Silicate Z
A800	467, 803, 1092, 1640	469, 596,717,1017,1656	444, 790, 1064, 1625
B800	469, 579, 791, 1101, 1656	474, 612, 741, 1017, 1420, 1640	466, 769(sh), 1038, 1625
C800	473, 546, 796, 1056, 1653	479, 601, 676, 1017, 1390, 1656	473, 772(sh), 1027, 1625

Inspection of the data for the metakaolin-silicate mixtures shows a general shift in the position of the Si-O peak to lower wavenumbers when compared with position before mixing. This shift is greatest in samples containing silicate Y, the fact that all the silicate Y containing mixtures generate Si-O peaks at 1017 cm^{-1} implies it is the Si-O vibration due to the component silicate rather than a peak produced by reactivity of the silicate with the metakaolin. The positions of the Si-O peaks in mixtures containing silicate X are almost unchanged relative to their situation in the metakaolins, whereas there is a shift to lower wavenumbers in samples containing Silicate Z. This shift is not a simple overlapping of the Si-O peak by portil k as such an occurrence should show a broad Si-O peak which stretches into the 1200 cm^{-1} region as seen in the spectra of Silicate Z. Figures 5.5.1 and 5.5.2 show infrared spectra of the materials before calcining.

Figure 5.5.1 Infrared analysis of A800-silicate Y before calcining

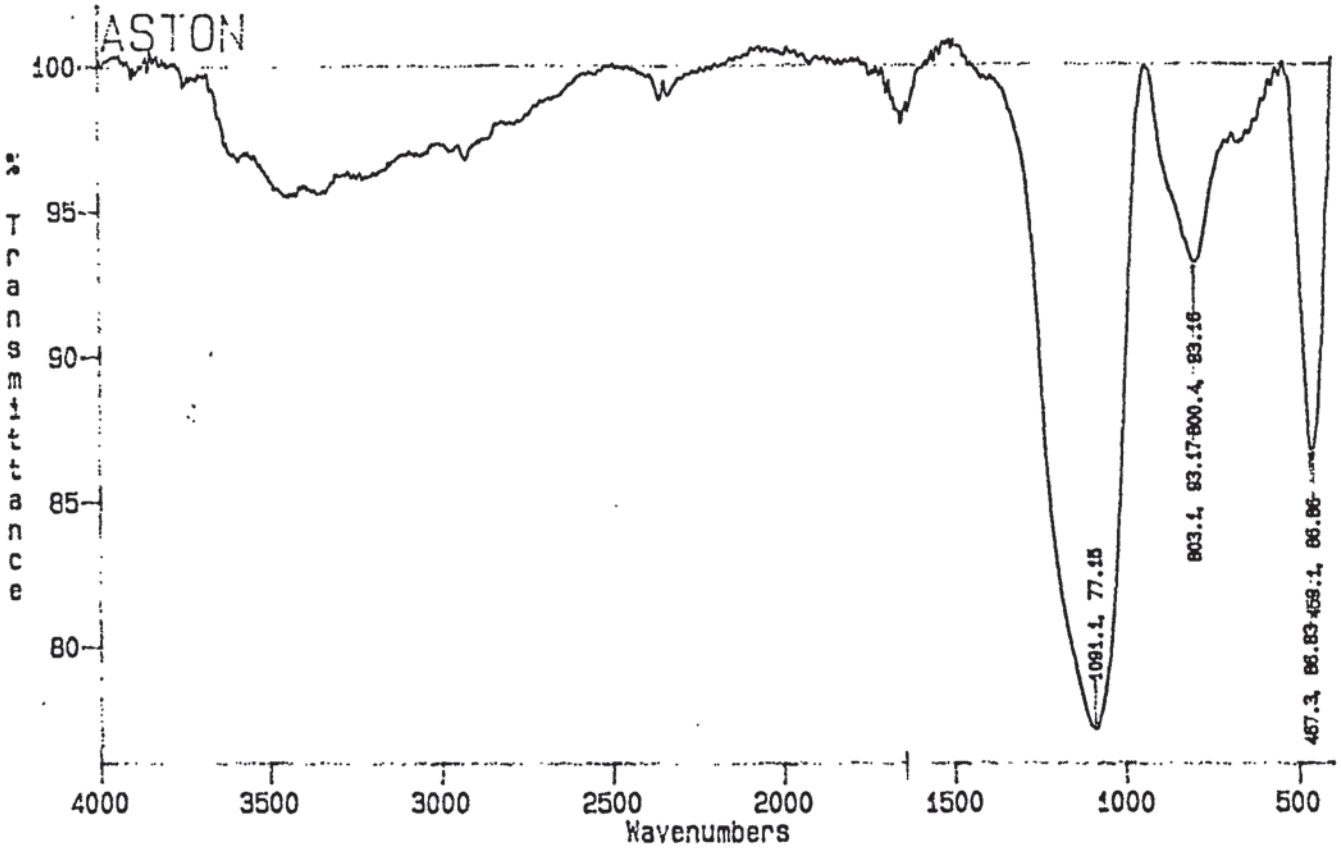

Figure 5.5.2 Infrared analysis of A800-silicate Y before calcining

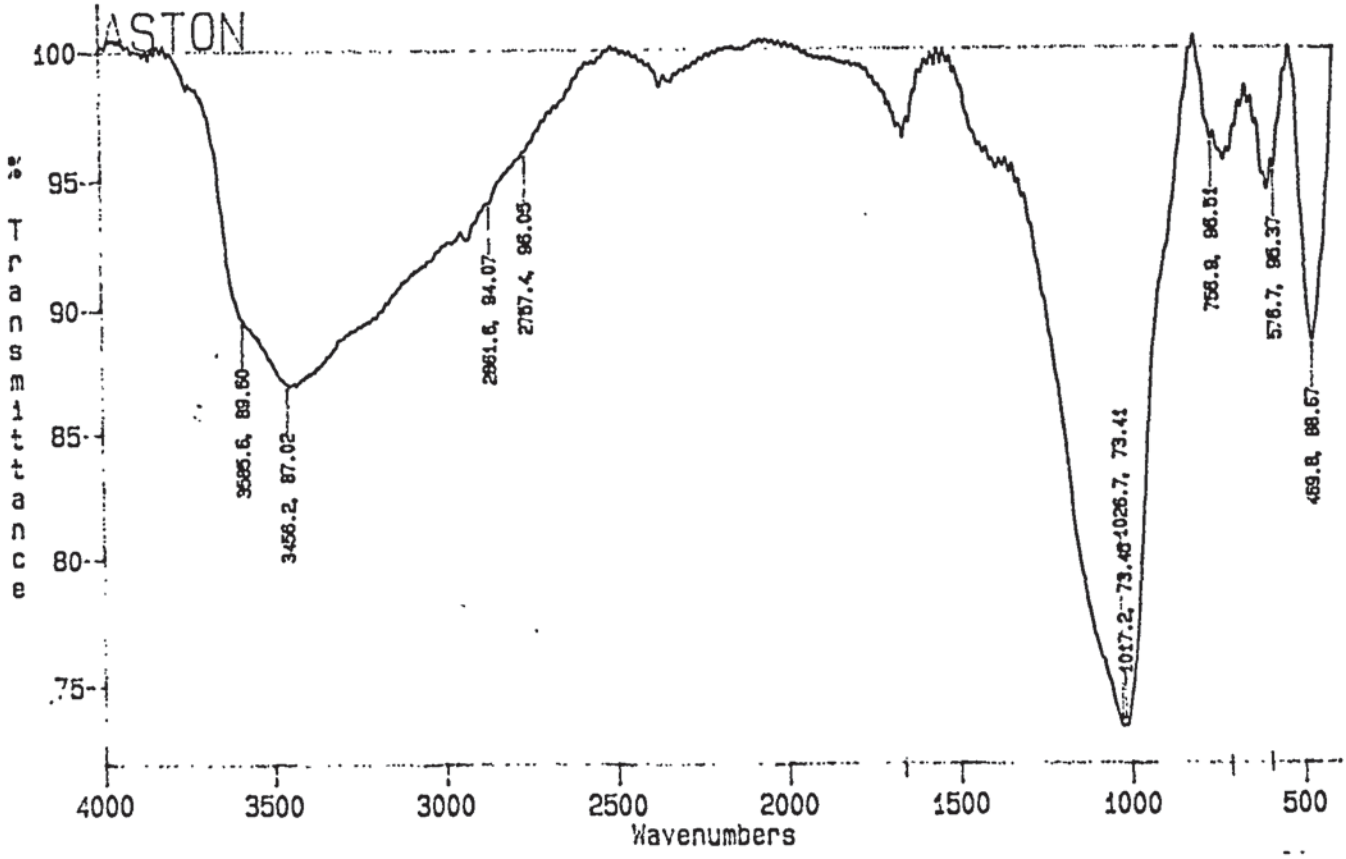

Table 5.5.3.Major Infrared Peaks for calcined and uncalcined metakaolin-Silicate mixtures

Type of mixture	Uncalcined (cm^{-1})	Calcined at 1000°C (cm^{-1})
A800-X	467,803,1091,1640	465,640,790,1049
A800-Y	469,597,757,1017, 1656	465,656,703,765,1032
A800-Z	453,781,1062,1625	466,677,1030
B800-X	469,575,791,1101, 1656	444,547,639,717,767, 1010,1037
B800-Y	474,605,738,1017, 1420,1640	468,531,640,703,1008, 1033
B800-Z	466,769,1046,1625	469,679,687,1036
C800-X	473, 562, 796, 1056, 1416, 1653	466, 734, 796, 1041
C800-Y	479, 601, 759, 1017 1390, 1656	472, 562, 656, 716, 1015, 1015, 1037
C800-Z	473, 772, 1035,1625	465, 671, 765, 1031

When Comparing spectra of the calcined and uncalcined mixtures a general shift to lower wavenumbers for absorption in the Si-O and Si-O-Al regions is observed. This implies an increase in order in the mixture because a shift in absorption to lower wavenumbers suggests appearance of a crystalline phase. On heating we would normally expect a decrease in order and a shift to higher wavenumbers, as seen when calcining kaolinite to form metakaolin, due to an increase in disorder of the structure. Increase in the resolution and appearance of new peaks in the Si-O-Al region on analysis of the calcined samples also indicates a more regular structure. This is consistent with crystallisation occurring at high temperatures as demonstrated by differential thermal analysis.

5.6 Scanning Electron Microscopy

On observation of the scanning electron micrographs of the metakaolin-silicate mixtures it is learnt that there is a marked effect of silicate type controlling microstructure, which is particularly noticeable on calcined samples. Figure 5.6.1 is an example of micrographs obtained from samples containing silicate Y after calcining at 1000°C for 2 h. Figures 5.6.2 and 5.6.3 typify micrographs obtained on analysis of mixtures containing silicate Z and silicate X respectively.

Comparison of the micrographs shows samples containing silicate Y generate many pores and these pores are relatively large (10-150 μm) and independant of the clay source. Pore size and quantity often plays an important role in determining performance of a castable; the greater the number and size of pores the smaller the resistance to spalling. Spalling is the fracture of a refractory caused by thermal, mechanical or structural strain. Samples containing silicate Z generate intermediate sized pores of the magnitude 10-100 μm and some are μm sized. Samples containing silicate X yield very fine, μm sized pores and have the tightest microstructure.

Correlation of weight loss data from thermogravimetric analysis with pore size reveals a pattern. Samples containing silicate Y show greatest weight loss and also have the greatest pore size. This may be due to the pores being created as water is being lost from the material. However, the same correlation cannot be made with silicates X and Z, where weight loss is very similar in both silicate X and silicate Z containing materials but pore size is dependant on the silicate used.

Figure 5.6.1 Scanning electron micrograph of A800-silicate Y after calcining

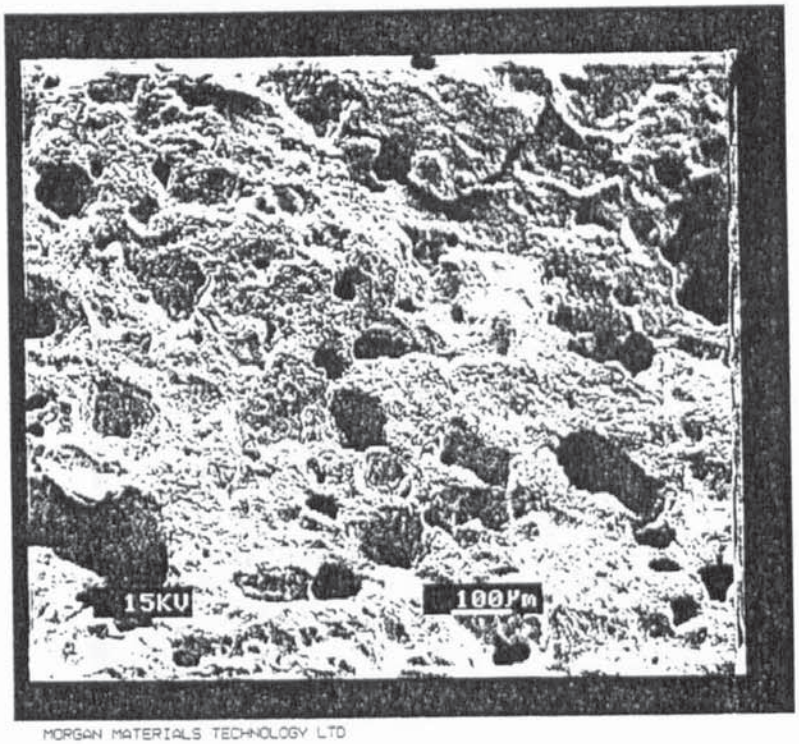

Figure 5.6.2 Scanning electron micrograph of A800-silicate Z after calcining

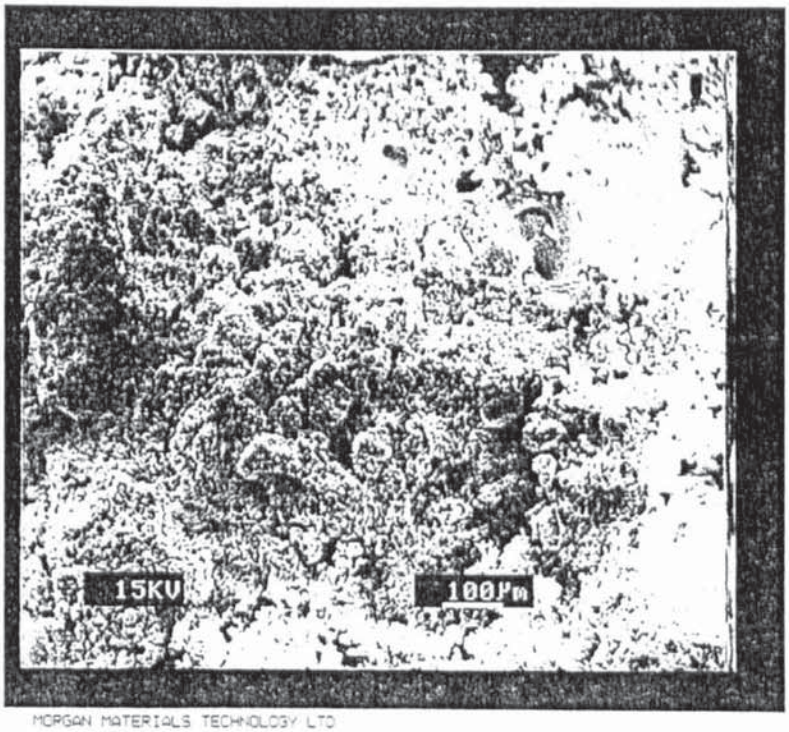

Figure 5.6.3 Scanning electron micrograph of A800-silicate X after calcining

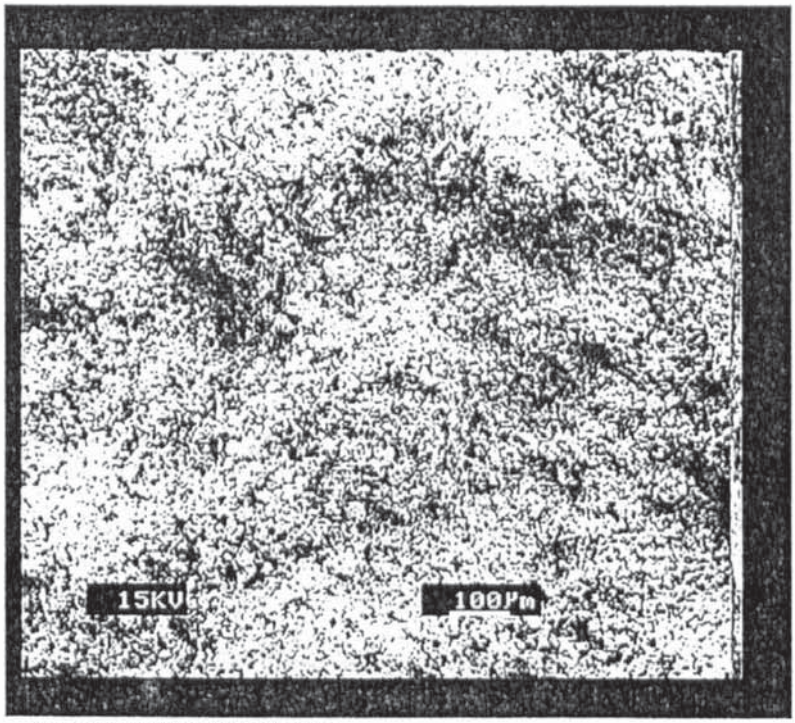

5.6.1 Scanning electron microscopy (uncalcined samples)

Micrographs of uncalcined samples also show microscopic structure is determined by the silicates. Figures 5.6.4, 5.6.5 and 5.6.6 are micrographs typical of samples containing silicates Y, X and Z. Micrographs of samples prepared using silicate Y exhibit large pores but these are larger and less defined compared to the pores seen after calcination due to shrinkage during calcination. Pores are filled with fine crystallites, many fibrous in nature, which disappear on calcination. In terms of pore size and quantity a similar trend to the calcined samples is seen; samples containing silicate Y produce pores of sizes varying in size from 10 μm to 100 μm. Whereas samples prepared with silicate X again give the tightest microstructure. These samples contain pores which are generally smaller than 1 μm.

Another trend is identified when SiO_2:K_2O ratios in the silicates and pore sizes are scrutinized. There is an increase in pore size as the SiO_2:K_2O decreases (i.e K_2O content increases. Table 5.6.1 exhibits this trend.

Table 5.6.1 The relationship between SiO_2:K_2O ratio and pore size

Silicate Type	SiO_2:K_2O(wt%)	Average Pore Size (μm)
silicate Y	1.4	10-150
silicate Z	2.0	10-100
silicate X	2.6	1

Pore size has a significant bearing on the performance of a castable due to spalling effects. Greater pore size confers less resistance to spalling, therefore the performance of a silicate in a castable will decrease with decreasing SiO_2:K_2O ratio.

Figure 5.6.4 Scanning electron micrograph of A800-silicate Y before calcining

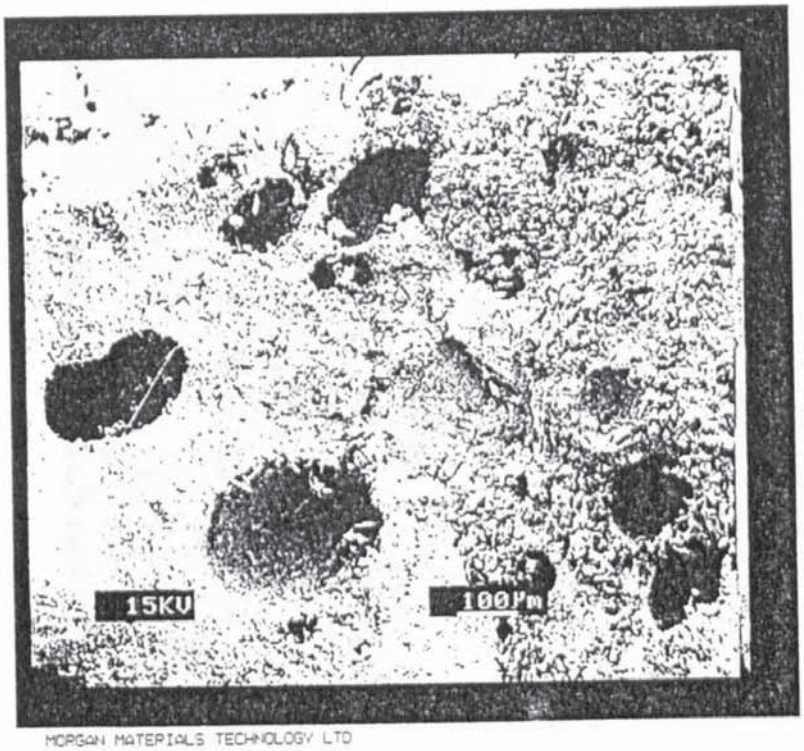

Figure 5.6.5 Scanning electron micrograph of A800-silicate X before calcining

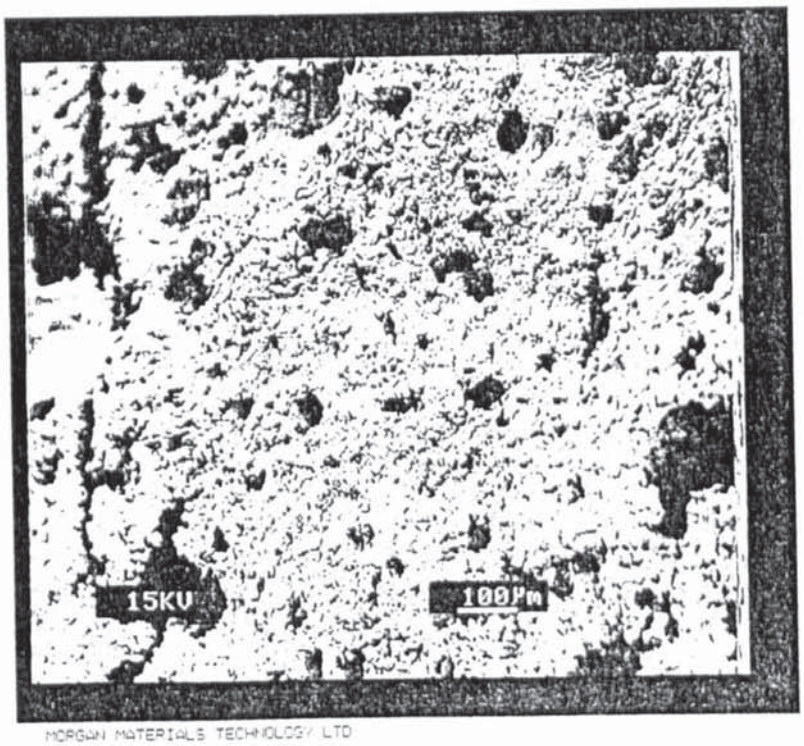

Figure 5.6.6 Scanning electron micrograph of A800-silicate Z before calcining

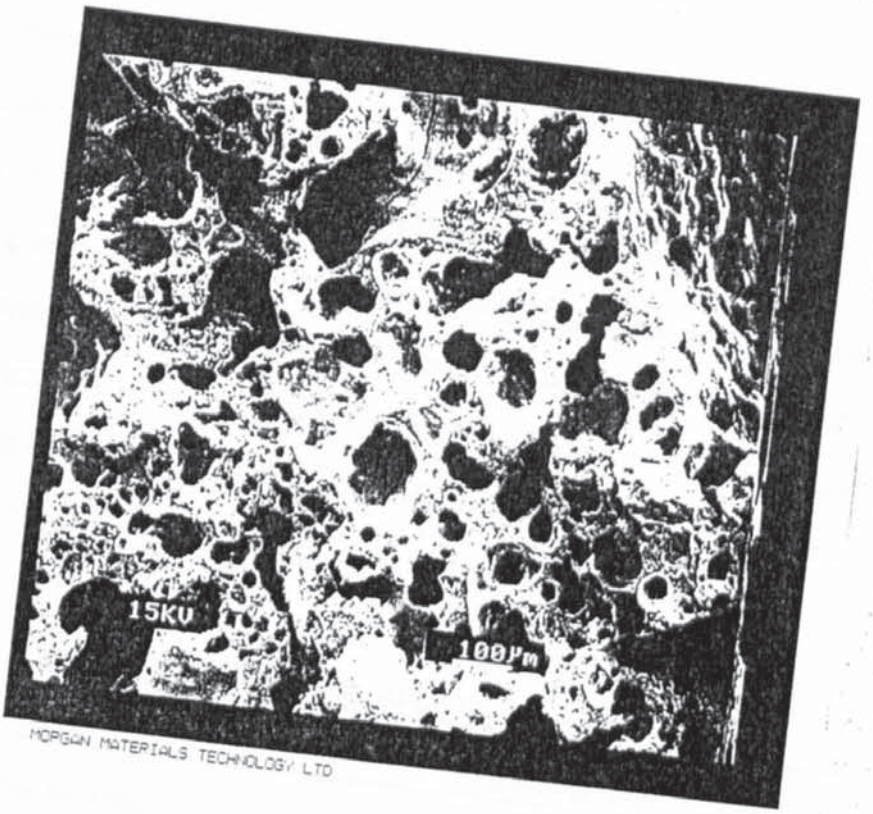

5.7 X-Ray Diffraction

X-Ray diffraction (XRD) patterns were obtained of the calcined metakaolin-silicate samples. These diffraction patterns revealed they were independant of the clay source but very much dependant on the silicate used to produce the sample. XRD patterns for samples containing silicate X were identical regardless of which metakaolin was used for the sample preparation. XRD patterns of samples containing silicate Y were identical to each other, as was the case for samples containing silicate Z. A computer program was used to assist in the identification of the phases present in the samples. Table 5.7.1 exhibits the phases identified in the various materials.

Table 5.7.1 Phases identified in the samples

Sample Identity	Phases Present
Metakaolin-Silicate X	Cristobalite (syn)
	Tridymite-O
Metakaolin-Silicate Y	Leucite (syn)
	Potassium Aluminium Silicate
Metakaolin-Silicate Z	Potassium Aluminium Silicate

Samples containing silicate X were the only ones to produce high temperature phases. However, only polymorphs of silica were seen, no alumina-silica high temperature phase was seen. Calcination of metakaolin-silicate Y samples results in the production of leucite ($K_2O.Al_2O_3.4SiO_2$). Leucite is a well known product of corroding alkali reactions in the reducing environment of a blast furnace. The reaction occurring is as follows:

$$Al_2O_3.2SiO_2 + 2SiO_2 \xrightarrow{+2K,\ +CO} K_2O.Al_2O_3.4SiO_2 + C \qquad (90)$$

Both silicates Y and Z yield potassium aluminium silicate. This is obviously because the metakaolin is reacting with the potassium silicate. This observation lends support to the thermogravimetric and NMR studies which indicated no reactions were taking place between silicate X and metakaolins and that reactions were taking place between metakaolins and silicates Y and Z.

Figures 5.7.1, 5.7.2 and 5.7.3 show the 3 different types of XRD patterns obtained for the 9 samples.

Figure 5.7.1 X Ray diffraction pattern of A800-silicate Z after calcining

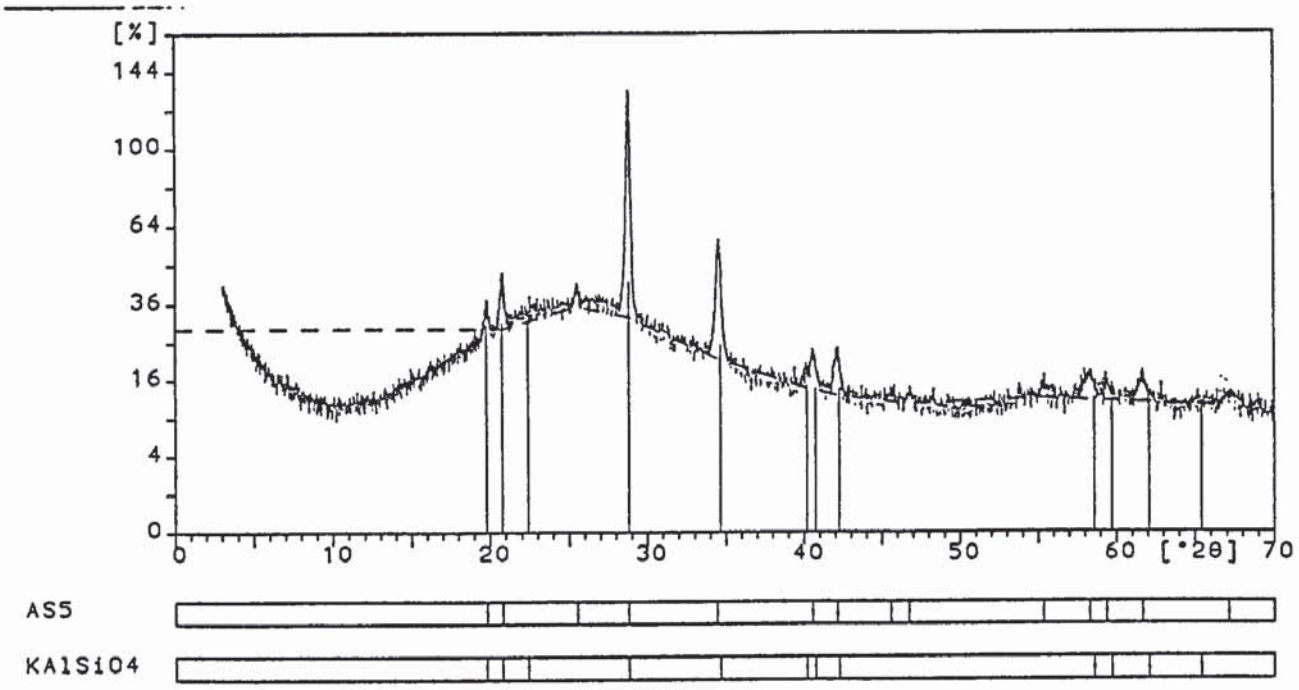

Figure 5.7.2 X Ray diffraction pattern of A800-silicate X after calcining

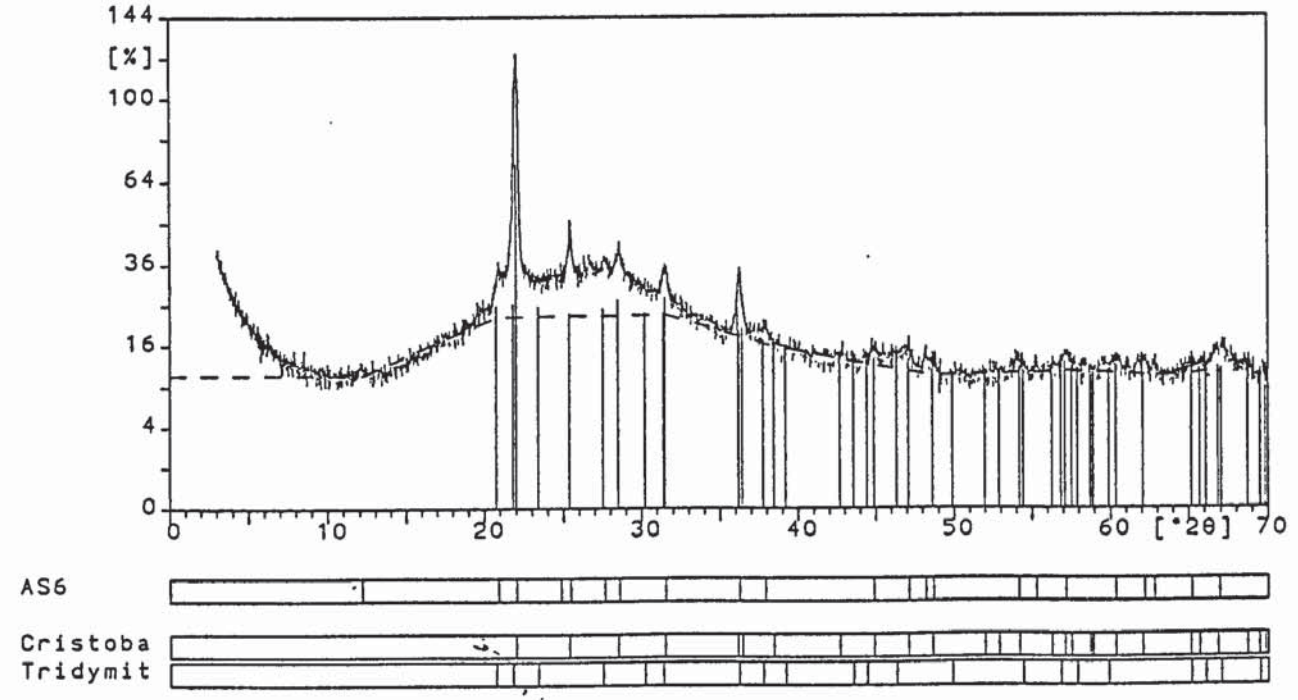

Figure 5.7.3 X Ray diffraction pattern of A800-silicate Y after calcining

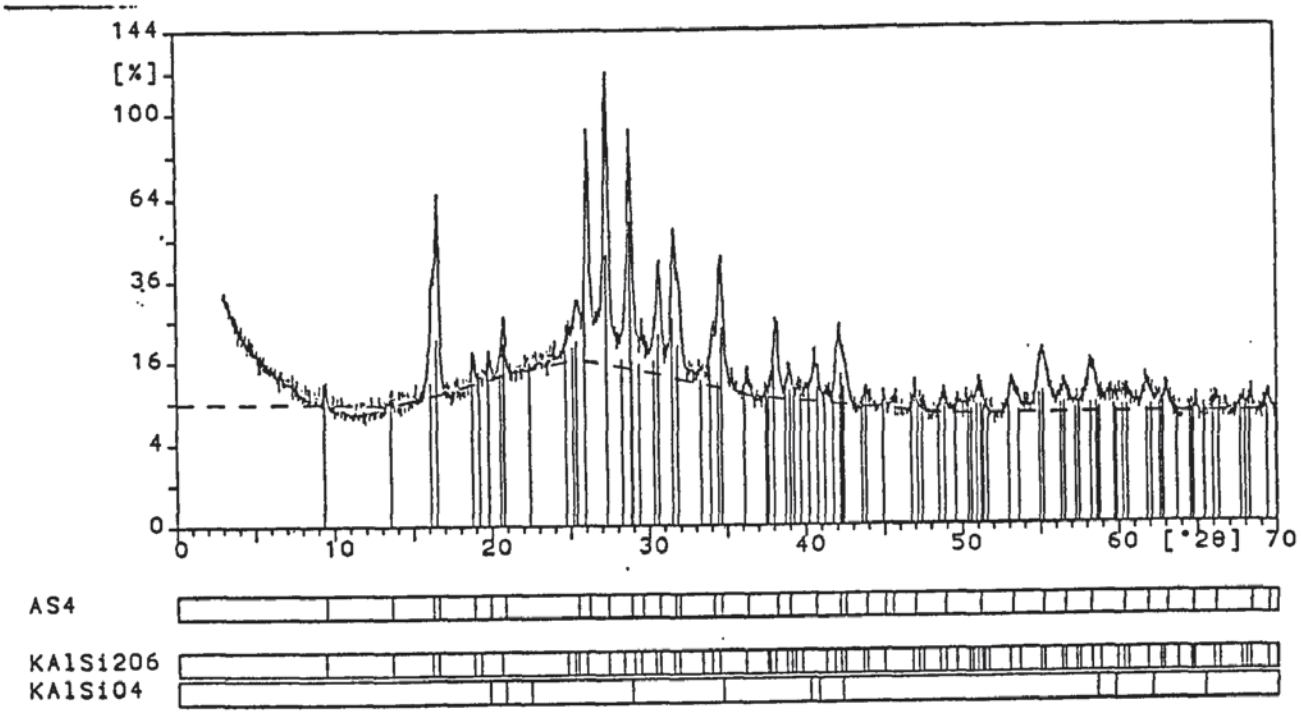

5.8 Summary of results

Metakaolin-silicate X samples show a lack of reactivity, ^{29}Si MASNMR analysis for these samples generally yielded resonances with positions indicative of the component silicate and metakaolin. ^{27}Al MASNMR analysis confirmed the lack of reactivity, spectra generated on the analysis of these samples were generally unchanged when comparing with the ^{27}Al NMR spectrum of the corresponding metakaolin. DT analysis revealed the temperature at which the exotherm appeared was no different to the temperatures at which the exotherms for the kaolinites appear.

After calcining metakaolin-silicate X samples, changes do occur. ^{29}Si MASNMR analysis produces resonances occurring in the free silica region. XRD analysis identifies cristabolite and tridymite, these are polymorphs of silica therefore explain the ^{29}Si MASNMR spectrum obtained for these samples. These results indicate there is a simple breakdown in structure of the metakaolin and silicate after calcining.

Analysis of metakaolin-silicate Y samples show reactions have occurred between the silicate and metakaolin even before calcining. Appearance of Q^3 peaks on ^{29}Si CPMASNMR analysis indicates a depolymerisation reaction has occurred. ^{27}Al MASNMR analysis confirms the ^{29}Si NMR data and also identifies the sites of reactivity to Al atoms in particular the pentacoordinate and octahedral aluminiums. The temperature at which the exotherm appears on DT analysis is sufficiently different from that of the kaolinite exotherm to indicate crystallisation is occurring in a sample other than kaolinite.

Calcination of metakaolin-silicate Y produces two ^{29}Si shift values at around -91ppm and -97 ppm on deconvoluting the ^{29}Si MASNMR spectrum. These are identified by XRD as due to leucite and potassium aluminium silicate respectively. These

assignments can be made because the -97 ppm resonance is seen in metakolin -silicate Z sample and XRD identifies this as due to the potassium aluminium silicate. phase.

Metakaolin-silicate Z samples show the same Q^3 resonance on deconvoluting ^{29}Si MASNMR spectra seen in metakaolin-silicate Y samples but this Q^3 peak is absent on analysis after calcining. In these samples potassium silicate-metakaolin reactions produce only the potassium aluminium silicate phase after calcining as shown by XRD analysis and confirmed by the presence of only one silicon environment on ^{29}Si MASNMR analysis of the calcined material.

The exotherm seen on DT analysis of metakaolin-silicate Y and metakaolin-silicate Z samples at approximately 1070 ^oC is possibly due to potassium aluminium silicate crystallisation as this is the only phase that is present in all the materials that produce the particular exotherm but absent in the samples where no such exotherm is seen.

5.9 Conclusions

There is evidence of silicate X being unreactive in these mixtures from a number of sources:

^{29}Si MASNMR of metakaolin-silicate X mixtures appears to be a sum of the spectra of silicate X and metakaolin because of the broadness of the resonance and position of the resonance. Deconvolution of the spectra yielded two peaks whose positions correspond to unreacted silicate X and the metakaolin confirming the lack of reactivity in these mixtures.

^{27}Al MASNMR spectra of silicate X containing mixtures show no change compared with spectra of the corresponding metakaolin.

DT analysis shows the exothermic peak position to be unaffected in metakaolin-silicate X mixtures.

Infrared analysis shows Si-O position of metakaolin is unaffected with addition of silicate X, this is not the case with other silicates.

XRD studies show silicates Y and Z react with metakaolin to produce potassium aluminium silicate. No such product is formed with silicate X.

Metakaolin A800 is a better performer in terms of crystallisation at high temperatures judging from the exothermic peak intensity on DT analysis and the number of exotherms produced.

Pentacoordinate and octahedral aluminiums in the metakaolin are the reactive centres judging from their disappearance on addition of the silicate to the metakaolin.

The detrimental effect of adding silicate to the appearance of a crystalline phase in kaolinite is especially exaggerated when the silicate is silicate Y. This is illustrated by thermogravimetric analysis where mixtures containing silicate Y exhibit only a weak exothermic peak.

These results show not only is it important to choose the correct kaolinite for refractory development but the particular silicate chosen can also have a significant bearing on the product.

The initial interaction or lack of interaction between the silicate and metakaolin appear to determine the products formed on calcination. Metakolin-silicate X samples show no signs of reaction initially and on calcining a simple breakdown of the metakaolin and silicate seems to occur. Whereas in samples containing silicate Y or silicate Z there is initial reaction between the silicate and metakaolin which continues on calcination and is seen as a product on XRD analysis.

Chapter Six

THREE COMPONENT MIXES

6.1 Introduction

The new refractory is composed of metakaolin, potassium silicate, alumina, silica and a dispersant. The study of metakaolin-silicate interactions demonstated how silicates played an important role in product formation. New mixes were prepared incorporating a third component to see how this effects the metakaolin-silicate interactions or if new interactions are taking place. The third component was either silica or alumina, both of these materials were supplied by Morgan Materials Technology Ltd. Weight ratios were again 1:1:1. Only one type of silica and alumina was used as opposed to the three types of metakaolin and silicate used. Samples of these three component mixtures were prepared as described in section 3.2.2. After sample preparation, setting and drying the material was studied using Infrared, ^{29}Si MASNMR and ^{27}Al MASNMR analyses. Samples were then calcined at 1000° C for 2 h and the analysis repeated.

Infrared analysis, ^{29}Si MASNMR and ^{27}Al MASNMR analyses were carried out for the alumina and silica before their introduction to the mixes so identification of peaks and resonances due to these materials could be made. Figure 6.1.1 displays the ^{27}Al MASNMR spectrum of alumina. The resonance position at 9.6 ppm represents aluminium in an octahedral environment and is charateristic of alumina. Figure 6.1.2 is the ^{29}Si MASNMR spectrum of silica. The resonance position of -111 ppm represents silicon in Q^4 arrangement. Figures 6.1.3 and 6.1.4 are infrared spectra of alumina and silica respectively.

Figure 6.1.1 ^{27}Al MASNMR spectrum of alumina

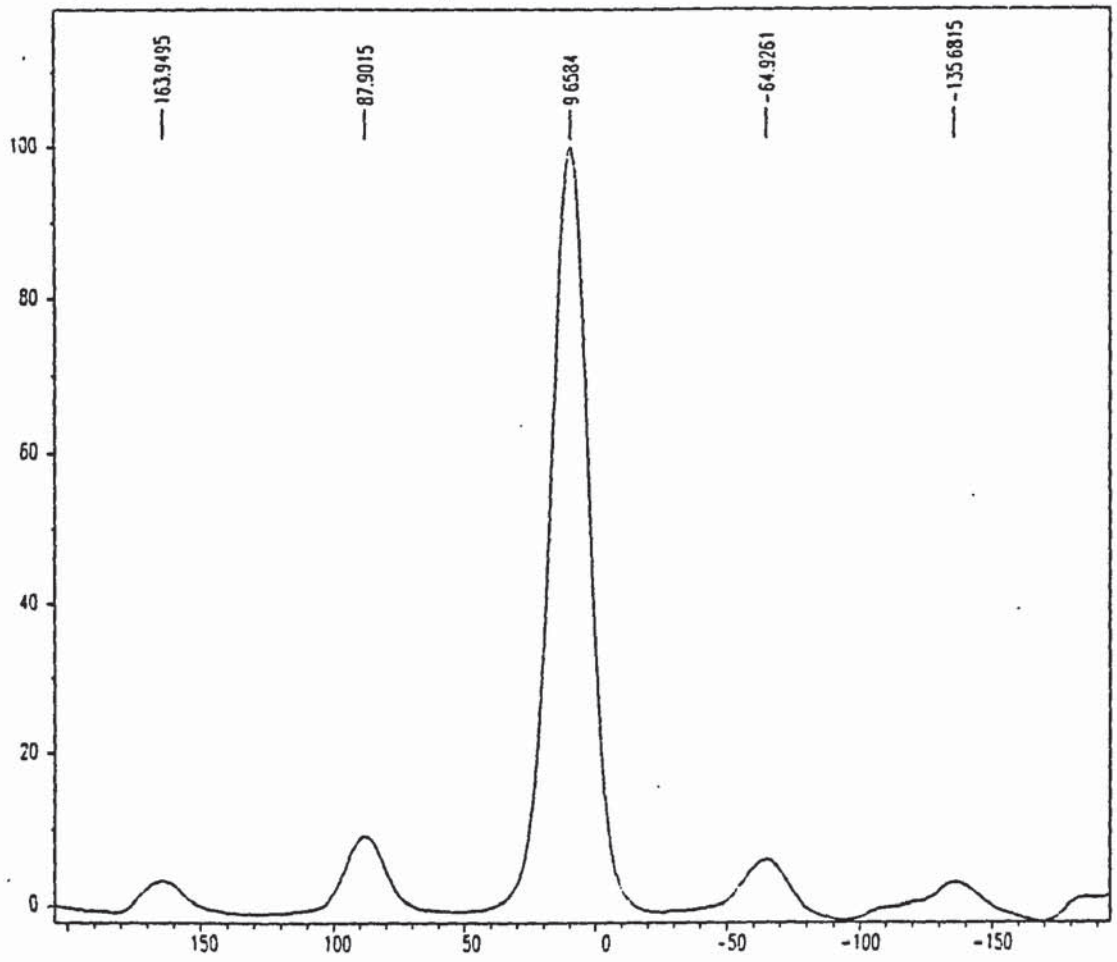

Figure 6.1.2 ^{29}Si MASNMR spectrum of silica

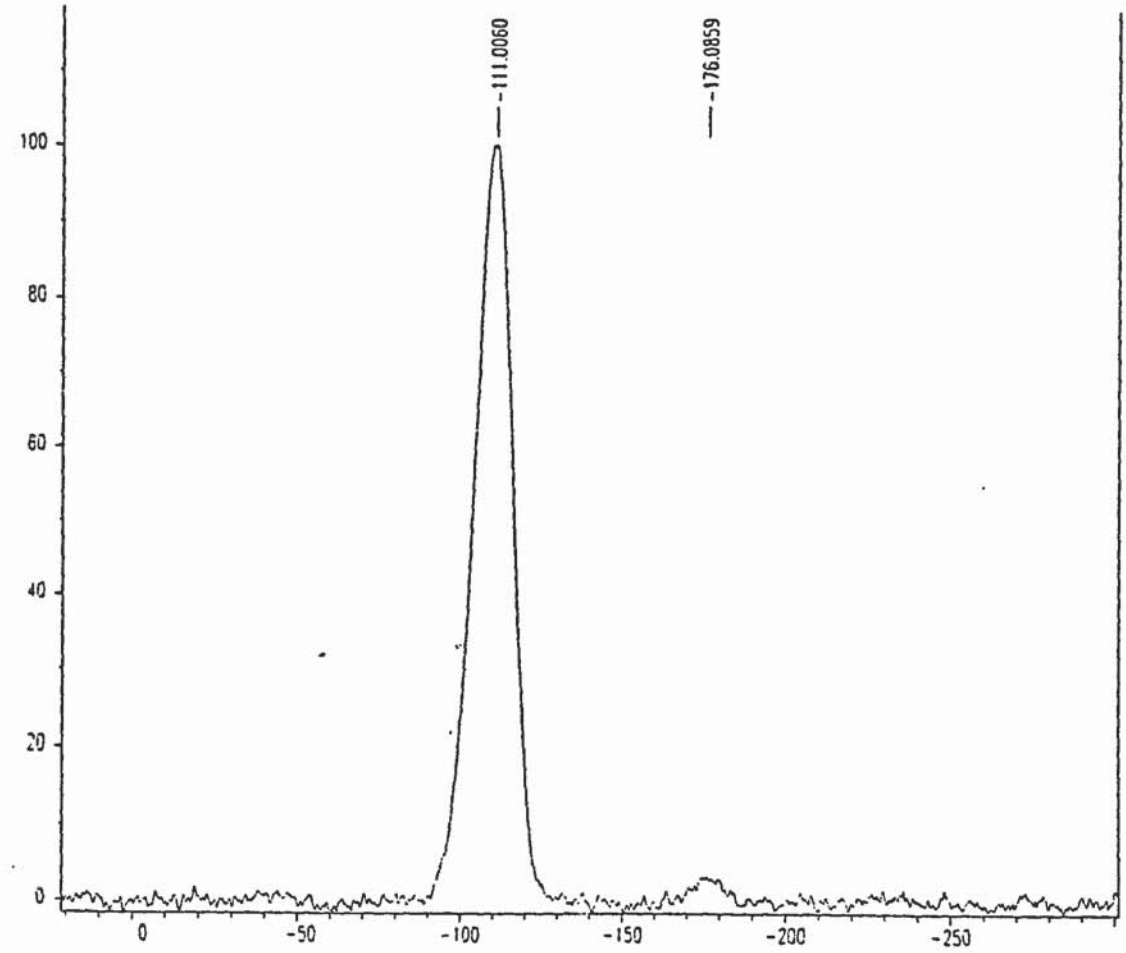

Figure 6.1.3 Infrared spectrum of silica

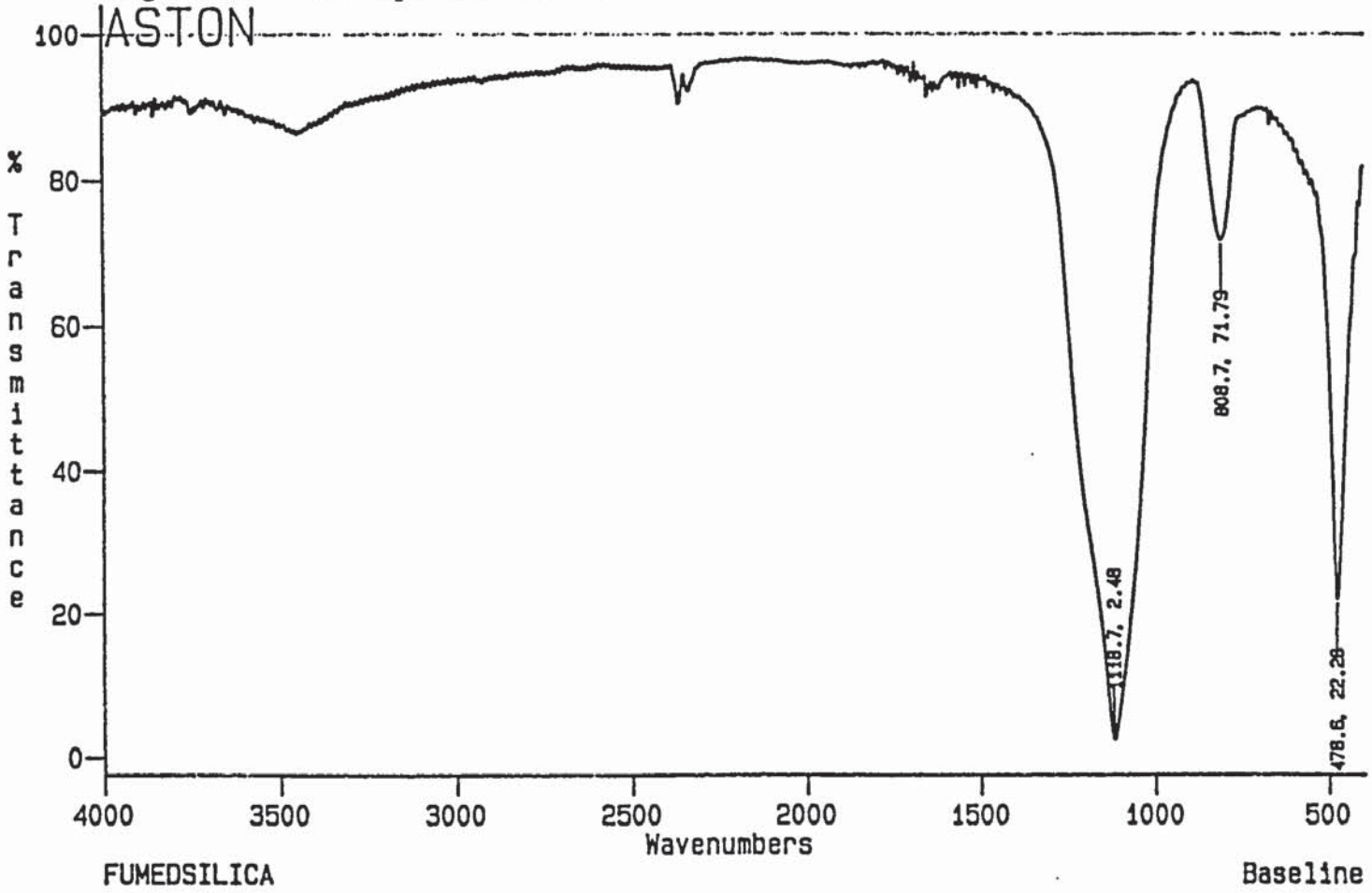

Figure 6.1.4 Infrared spectrum of alumina

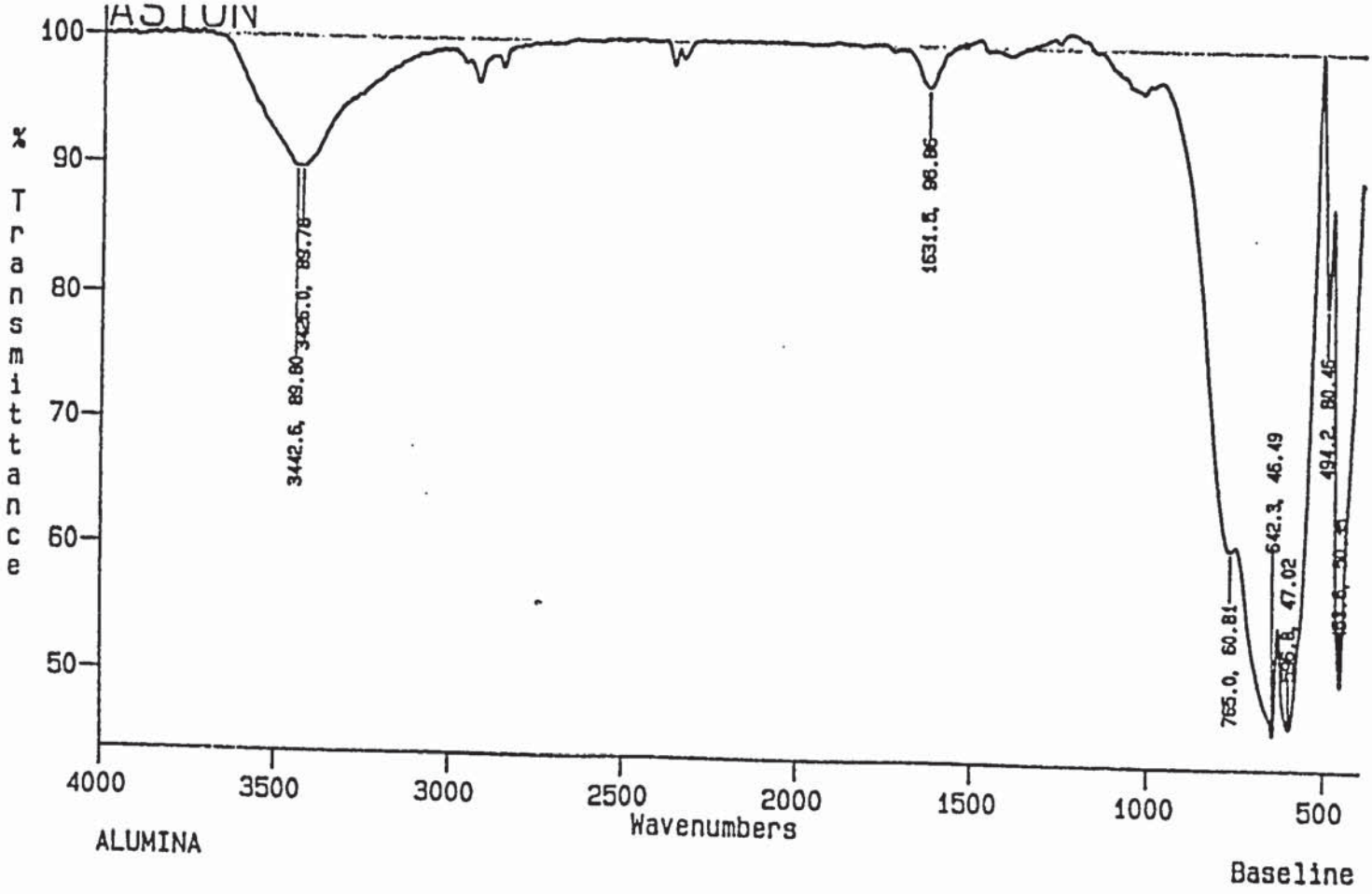

6.2 ^{29}Si MASNMR analysis

Two sets of samples were prepared, one containing silica as the third component and the other containing alumina as the third component. Table 6.2.1 exhibits the results obtained from ^{29}Si MASNMR analysis of the range of samples studied.

Table 6.2.1 ^{29}Si MASNMR shift values of the three component mixes (ppm)

Metakaolin-silicate*	Silica as the third component	Alumina as the third component
A800-X	-104.7	-99.3
A800-Z	-99.6, -106.2	-95
B800-X	-108.1, -97 sh	-94.6
B800-Z	-99.6, -107.8	-97
C800-X	-108.7, -98 sh	-96.6
C800-Z	-98.6, -108 sh	-96.1

key:

sh = shoulder

* – for clarification on the labelling of metakaolin-silicate mixes see chapter 5

^{29}Si MASNMR spectra for the series of samples containing silica as the third component in the mix generally exhibit broad peaks. These broad peaks consist of a single peak and a shoulder to the peak. However, spectra of some of the samples show the broad peak clearly resolved into two peaks. Figure 6.2.1 shows ^{29}Si MASNMR spectrum of C800-Z-silica mix and figure 6.2.2 is the ^{29}Si MASNMR spectrum of sample B800-X-silica. Figure 6.2.2 shows the broad peak is resolved in two component peaks but primarily resonances are broad and unresolved. In order to resolve these broad peaks to achieve a true depiction of the silicon environments a deconvolution technique was applied to the spectra.

Figure 6.2.1 ^{29}Si MASNMR spectrum of sample C800-X-silica

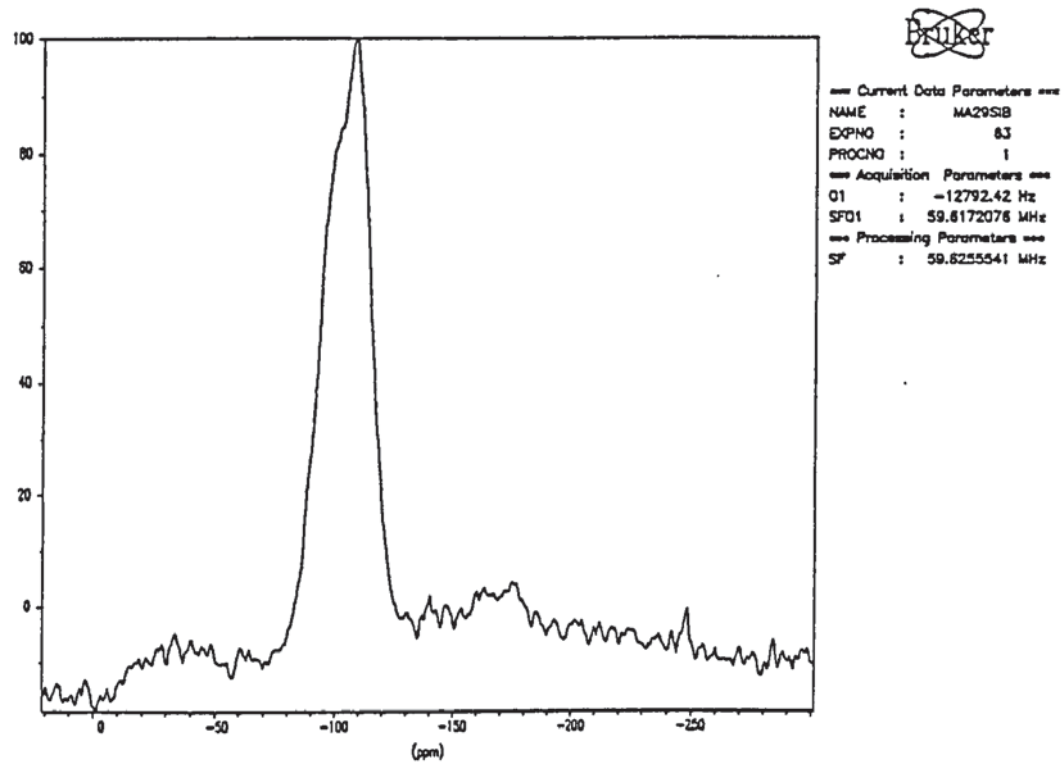

^{29}Si Figure 6.2.2 ^{29}Si MASNMR spectrum of sample B800-Z-silica

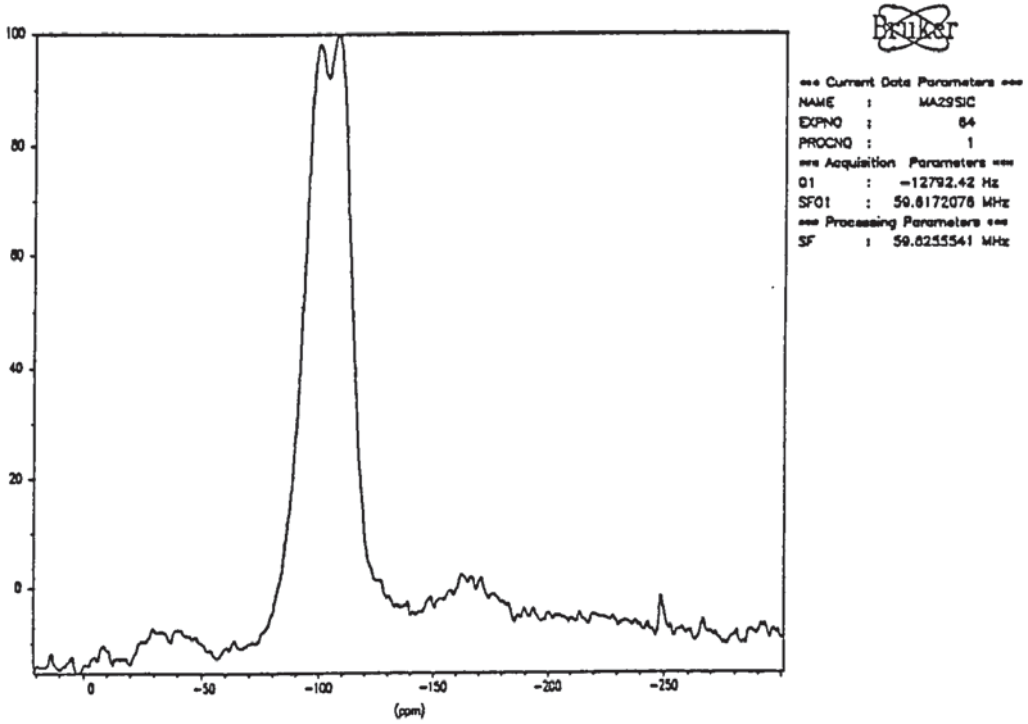

Table 6.2.2 ^{29}Si MASNMR shift values of the three component mixes after deconvolution of the spectra.

Sample type	Resonance position (ppm)
A800-X-silica	-99, -107.6
A800-Z-silica	-100.1 -108.4
B800-X-silica	-98.6, -109
B800-Z-silica	-99.6, -108.6
C800-X-silica	-98, -107.8
C800-Z-slica	-98.8, -107.8

Deconvolution of the ^{29}Si MASNMR spectra for the silica containing three component mixes resolved the broad peaks into two peaks, the positions of these resonances are similar for each sample as is evident from table 6.2.2. The position of the resonance at -108 +/- 1 ppm correlates with the resonance for silica. The resonance at -99 +/- 1 ppm correlates with the resonance seen on ^{29}Si MASNMR analysis of the metakaolin-silicate samples. Therefore the ^{29}Si MASNMR data of the three component samples indicate that there is little interaction taking place, the spectra of the three component samples merely being a sum of the spectra of the corresponding metakolin-silicate and silica spectra. The only difference being the lack of appearance of the Q^3 resonance seen in metakaolin-silicate samples, this could be due to a simple dilution effect, the broad resonance of the added silica dominating the observed spectrum.

Observations of the ^{29}Si MASNMR spectra and the data in table 6.1.1 for the alumina containing samples show only single peaks and no clearly detectable shoulders. The peaks are chiefly broad resonances, as is apparent from figure 6.2.3, and their positions correlate with the positions of the resonances after ^{29}Si NMR analysis of the metakaolin-silicate samples. Deconvolution of the spectra for the three component samples did not give the resolution obtained for the metakolin-silicate only samples.

Figure 6.2.3 ^{29}Si MASNMR spectrum of sample A800-Z-silica

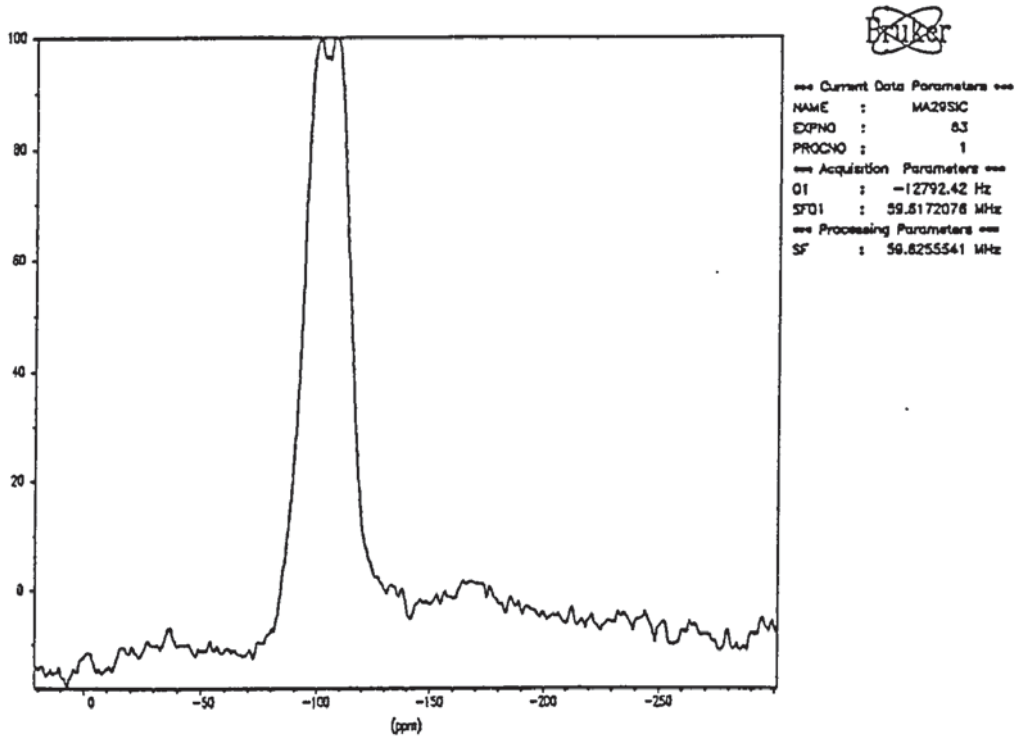

Figure 6.2.4 Deconvoluted ^{29}Si MAS NMR spectrum of sample A800-X-silica

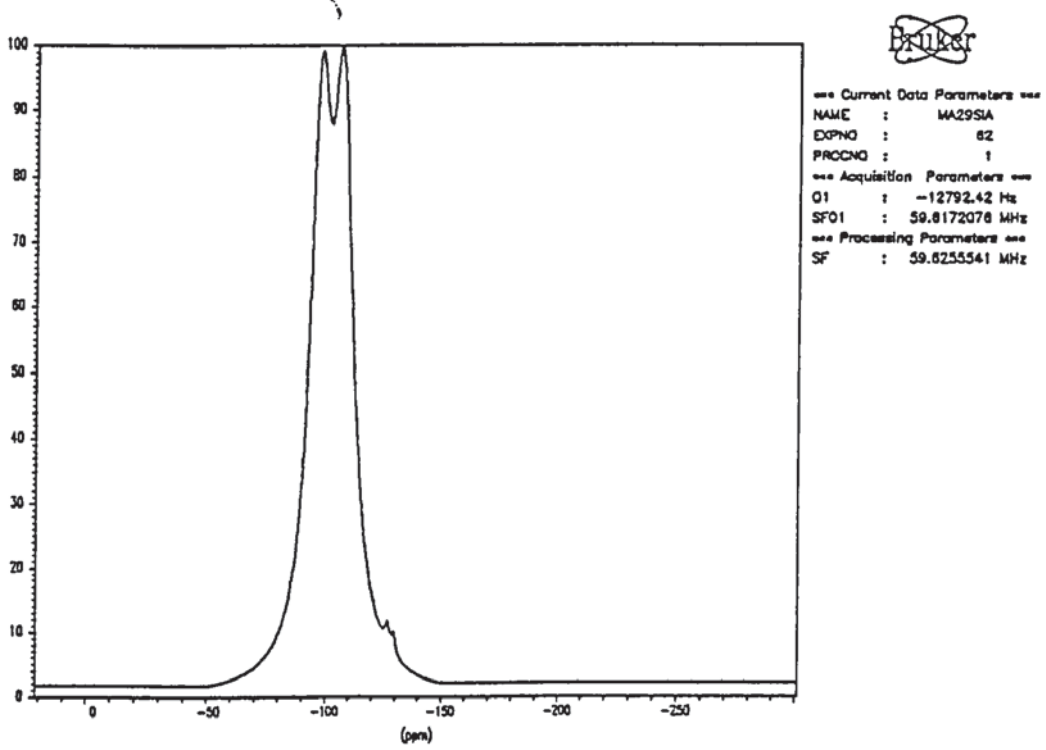

The exception to this is sample A800-X-alumina, figure 6.2.4 is the deconvoluted ^{29}Si MASNMR spectrum of A800-X-alumina. The positions of the two peaks into which the broad peak is resolved are similar to the positions of the resonances seen in the deconvoluted ^{29}Si MASNMR spectrum of A800-X. This again indicates a slowing down of the reactions between the silicate and metakaolin on the introduction of the third component of alumina.

Inspection of ^{29}Si MASNMR data for the metakaolin-silicate samples in section 5.2 revealed two features; Q^3 resonances are present on deconvolution of the ^{29}Si MASNMR spectrum of samples in which the silicate component was silicate Z and Q^4 resonances were seen on deconvolution of ^{29}Si MASNMR spectrum of samples where silicate X is used to prepare the mix. The lack of appearance of these resonances after deconvolution of the ^{29}Si MASNMR spectra of the three component mixes signify that a change has taken place. Although it can be argued that the large peak width at half height and the position of the resonance is sufficient to cause an overlapping of Q^3 and Q^4 resonances that could be present in the material, but as Q^3 resonances were not seen even on ^{29}Si CPMASNMR analysis of the materials we can conclude no such resonances are present. Therefore the rate of the depolymerisation reaction seen on mixing silicates with metakaolins, as described on section 5.2, is reduced on the addition of the third component of silica or alumina.

6.2.1 ^{29}Si MASNMR analysis after calcining

The three component mixes were calcined at 1000°C for two hours and ^{29}Si MASNMR analysis repeated. Table 6.2.3 collects the results obtained.

Table 6.2.3 ^{29}Si MASNMR analysis of the three component samples after calcining at 1000°C, shift values are given in ppm.

Metakaolin-silicate	Silica as the third component	Alumina as the third component
A800-X	-104.2, -110.3	-101.6
A800-Z	-102, -110.7	-101
B800-X	-109.6	-100
B800-Z	-101.9, 111.1	-97.2
C800-X	-104.9	-102
C800-Z	-101, -110.5	-99.5

Overall, in the above results, calcining produces a narrowing in the ^{29}Si NMR resonances. This trend is contradictory to the one seen for the two component samples where a broadening in the resonances was noted after calcining. Explanation for this narrowing can be gained from studying the nature of the broadening on calcining seen in the two component metakaolin-silicate samples. The broadening in these samples is due to a shift to more negative values caused by the change in the silicon environment to Q^4 geometry. This shift to more negative shift values is also seen in the three component mixes on calcining but because there is already a resonance due to silica in this region, the resonance appears as very narrow. However because peak narrowing is also obsserved for samples were alumina is the third component, although to a smaller degree, the above explanation discloses only one of the reasons for the peak narrowing. Another possible explanation is the interaction of the components to produce a more uniform silicon environment. Figure 6.2.5 is a ^{29}Si MASNMR

spectrum of sample C800-X-silica before calcining and figure 6.2.6 is the ^{29}Si MASNMR spectrum of the same sample after calcining. The figures serve to illustrate the narrowing of the resonance observed on calcining. A second possible reason for the peak narrowing is the calcining process may be inducing crystallisation and these crystalline products generate much sharper resonances.

The calcined samples where silica is the third component generally yield two resonances, one due to the silica and the other due to the metakaolin-silicate. As can be seen from table 6.2.3 there are two exceptions, both of these samples contain silicate X. Deconvolution of the the spectra was not able to resolve the peaks. This can be explained by inspection of the data for the metakaolin-silicates. Samples containing silicate X showed the greatest shift of resonances to more negative values on calcining, in fact the values are close to the values obtained for the ^{29}Si MASNMR resonance for silica. This similarity in the position of the metakaolin-silicate resonance and the silica resonance results in the deconvolution technique unable to resolve the peaks. This is further evidence for one of the explanations given for peak narrowing on calcining being due to the shift of the metakaolin-silicate resonances into the silica region leading to overlap of resonances and hence a reduction in peak width at half height.

The data in table 6.2.3 for the samples where alumina is the third component show a significant change in that only one resonance is seen for these samples on ^{29}Si MASNMR analysis. This is even true for samples where the corresponding two component material gave rise to two or more resonances corresponding to silicon in a Q^3 and Q^4 environment. In samples where the third component is silica it is difficult to ascertain the presence or absence of the Q^3 and Q^4 peaks because of the broad peaks generated and as the materials have been calcined ^{29}Si CPMASNMR analysis is not appropriate to identify the Q^3 resonance. These arguments cannot be applied for the three component samples where alumina is the third component. In this case the

Figure 6.2.5 ^{29}Si MASNMR spectrum of sample C800-X-silica before calcining

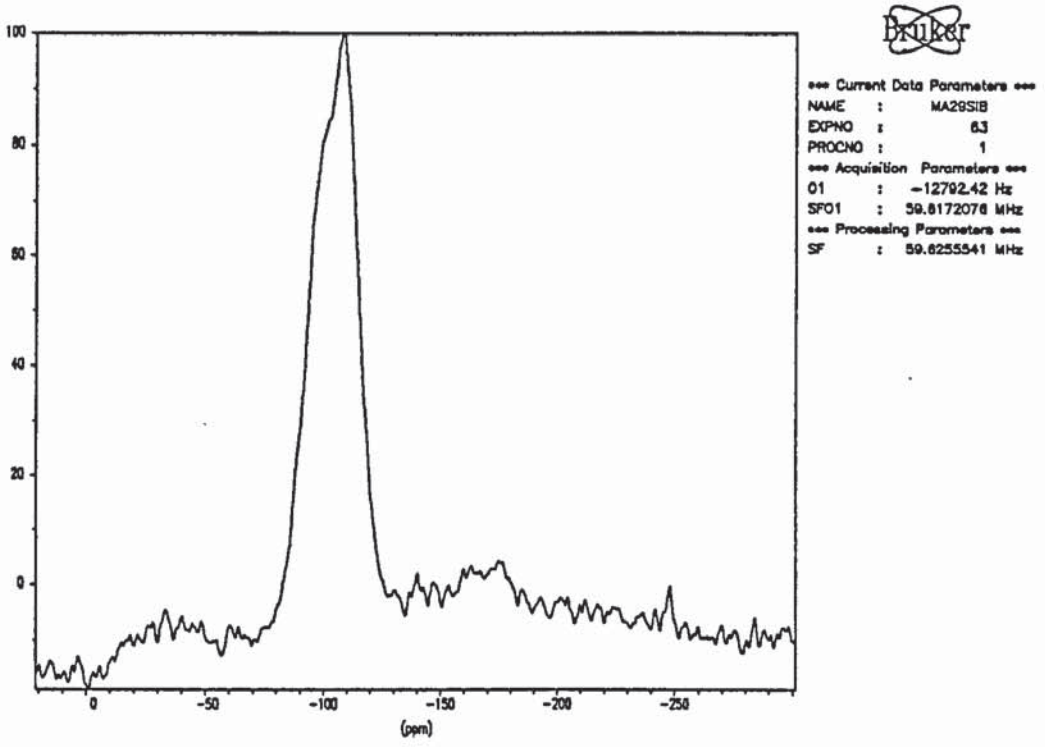

Figure 6.2.6 ^{29}Si MASNMR spectrum of sample C800-X-silica after calcining

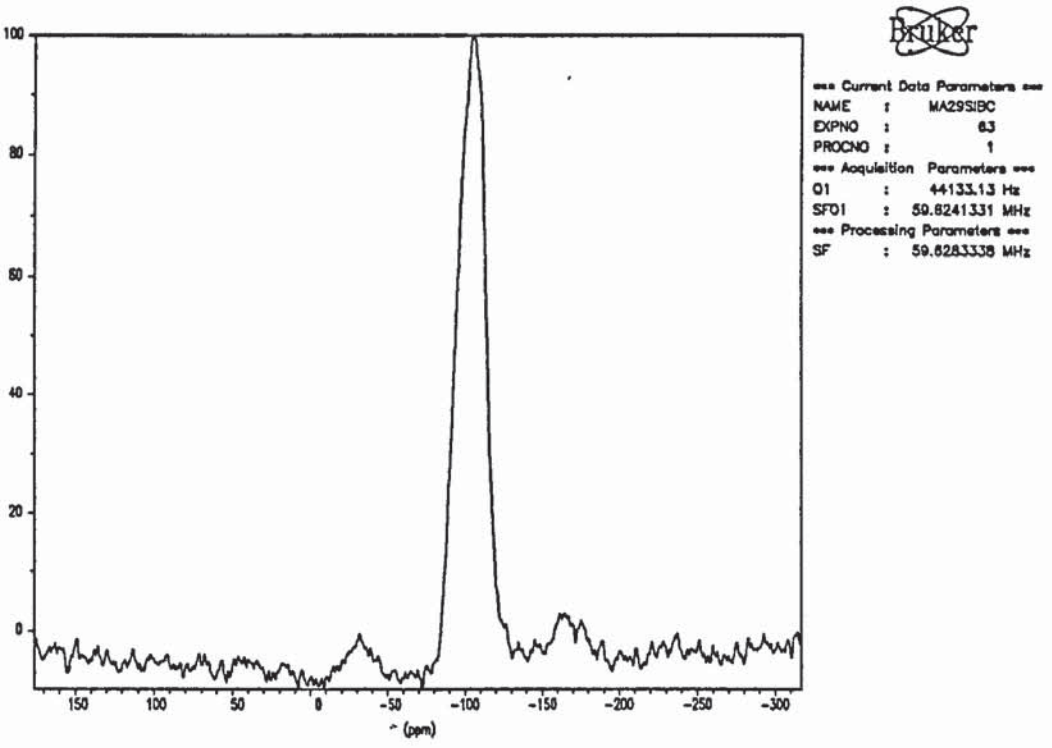

absence of Q^3 resonances in the ^{29}Si MASNMR spectrum of these samples can be interpreted as being due to a lack of silicons in a Q^3 environment. Even after deconvolution resolution of the peaks was unattainable. This suggests we have a unifom silicon environment and the reactions that occurred in order to generate Q^3 and Q^4 resonances in the two component metakaolin-silicate samples are possibly prevented or more probably delayed on the addition of alumina. This is possibly due to the alumina acting as a diluant.

6.3.1 ^{27}Al MASNMR analysis

^{27}Al MASNMR analysis of the two component mixes was useful in identifying changes occurring around the aluminium centre. This method was also applied to the three component mixes. Table 6.3.1 exhibits the results obtained on ^{27}Al MASNMR analysis of the series of samples studied.

Table 6.3.1 ^{27}Al MASNMR shift values of the three component mixes (ppm).

Metakaolin-silicate	Silica as the third component	Alumina as the third component
A800-X	4.1, 52	8.9
A800-Z	6.1, 51.6	8.7, 53 w
B800-X	4.2, 52.9	9.1, 39.7 w
B800-Z	3.5, 52.2	9.4, 56 vw
C800-X	3.5, 53.7	9.4
C800-Z	3.2, 52.6	8.9, 38.5w

w = weak, vw = very weak

6.3.1.1 Silica as the third component

Observation of the ^{27}Al NMR data or the spectra of the samples where silica is the third component in the mix show great similarity from sample to sample. All the materials show two resonances, one in the octahedral aluminium region and the other in the tetrahedral region. The resonance for the tetrahedral aluminium being more intense in all cases. Figure 6.3.1 is the ^{27}Al MASNMR spectrum of sample B800-X-silica and is representative of the spectra obtained for all the samples where silica is used as the third component.

Comparison of the data obtained on ^{27}Al MASNMR analysis of the three component samples where silica is the third component with results obtained for the corresponding metakaolin-silicate samples (see table 5.3.1) reveals interesting features. Samples A800-silicate Z and B800-silicate Z produced no resonance corresponding to octahedral aluminium, as the original metakaolin contained octahedral aluminium, its disappearance after introducing the silicate was deemed to be due to the metakaolin reacting with the silicate. The presence of an octaheral aluminum resonance in the three component samples but not in the corresponding metakaolin-silicate sample reaffirms the ^{29}Si NMR data which indicated a reduction in the reactivity between the silicate and metakaolin on the introduction of the third component of either silica or alumina. ^{27}Al MASNMR indicates not only a lack of reactivity but also a reduction in the interaction seen between the metakaolin and silicate. This is probably due to addition of the silica acting as diluant preventing silicate and metakaolin interactions.

The lack of a resonance corresponding to five coordinate aluminium in the spectra of any of the samples indicates the diluant effect of the silica is mainly reducing the rate of reactions rather than preventing them. The fact that octahedral resonances are present but not pentacoordinate resonances suggests pentacoordinate aluminium reacts preferentially. This further vindicates the observation made after the study of the two component metakaolin-silicate systems that pentacoordinate aluminium is the more reactive species.

6.3.1.2 alumina as the third component

Inspection of the ^{27}Al NMR spectra and data for the three component mixes where alumina is the third component generally reveals an intense, sharp resonance in the octahedral region of the spectrum. This is to be expected considering the large amount of octahedral aluminium in the form of alumina introduced to the mixture. In addition to the octahedral resonance some samples gave a weak pentacoordinate or tetrahedral resonance. There are a number of potential sources for these resonances in the pentacoordinate and tetrahedral region. Firstly spinning side bands could be generated in this region, but spinning side bands as a source of pentacoordinate and tetrahedral resonances can be dismissed as these are observed as symmetrical peaks on either side of the major resonance, but the pentacoordinate and tetrahedral resonances appear as single peaks with no corresponding symmetrical peak.

A second source of the pentacoordinate and tetrahedral resonances could be due to the metakaolin as metakolin-silicate samples produced these peaks on ^{27}Al NMR analysis. After comparisons are made between ^{27}Al NMR data of the three component systems and the corresponding two component systems by reverting to table 5.3.1 it is noticed that two component systems that contained pentacoordinate aluminium are not the ones where pentacoordinate aluminium is seen on the introduction of alumina. For example, analysis of sample C800-Z-alumina produced a spectrum indicating the presence of pentacoordinate aluminium but the analysis of the corresponding two component system indicated an absence of pentacoordinate aluminium. Generally spectra of the two component systems are very different to the spectra of the three component samples in which alumina is the third component. This does not preclude metakaolin as the source of tetrahedral and pentacoordinate aluminium but it does reveal the alumina to be affecting the reactions taking place. Figure 6.3.2 is the ^{27}Al MASNMR spectrum of sample C800-Z-alumina.

Figure 6.3.1 ^{27}Al MASNMR spectrum of sample B800-X-silica

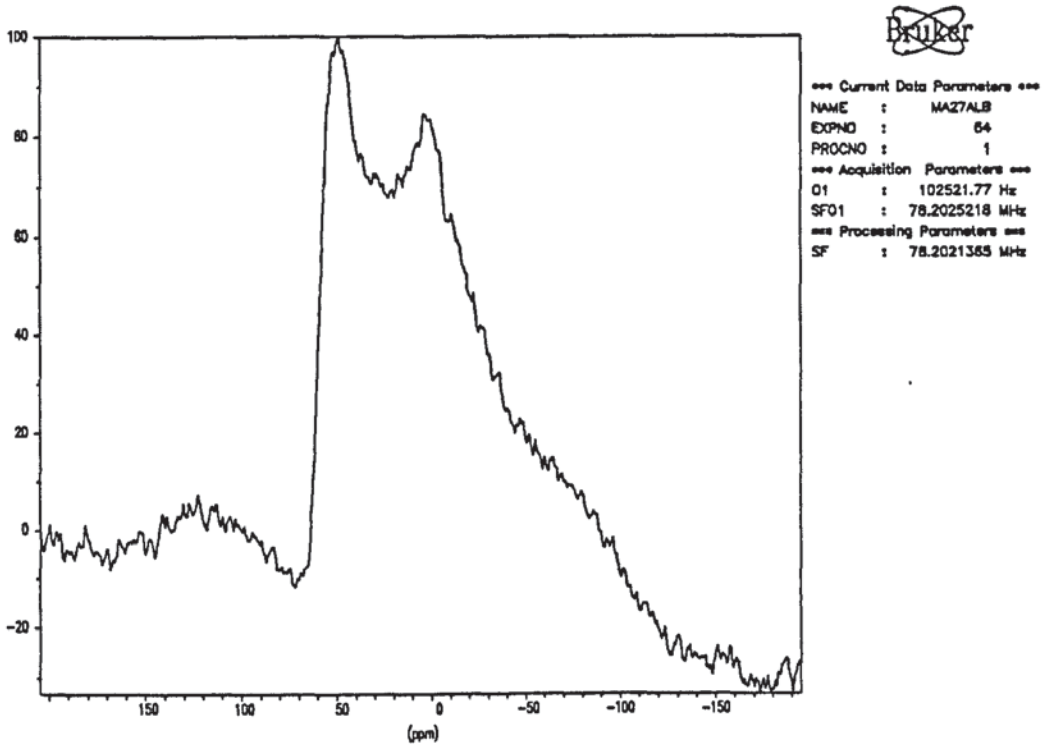

Figure 6.3.2 ^{27}Al MASNMR spectrum of sample C800-Z-alumina

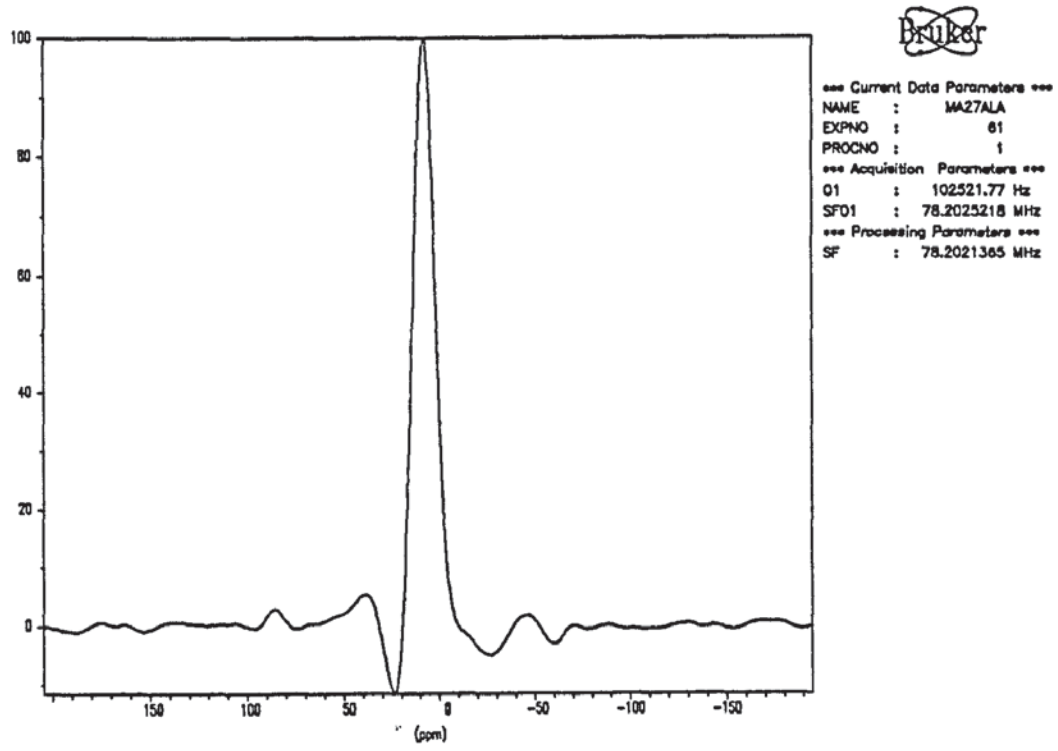

^{27}Al MASNMR spectra of all the metakaolin-silicate samples showed the presence of tetrahedral aluminium, the presence of octahedral aluminum was interpreted as a low rate of reactivity between the metakaolin and silicate, since octahedral aluminium corresponds to the metakaolin remaining unchanged. Whereas presence of a single tetrahedral aluminium after mixing the metakaolin with the silicate indicated a transformation of the metakaolin aluminium environments and thus corresponded to reactions occurring. All the Two component samples prepared using silicate X contained octahedral aluminium and therefore silicate X was deemed to be the most unreactive silicate, the absence of tetrahedral or pentacoordinate aluminium in two of these samples on the introduction of alumina indicates a further reduction in reactivity.

These results suggest that alumina not only acts as a diluant but also appears to influence the reactions taking place.

6.3.2 ^{27}Al MASNMR analysis after calcining

The three component samples were calcined at 1000 °C for two hours and ^{27}Al MASNMR analysis repeated. Table 6.3.2 exhibits the results obtained.

Table 6.3.2 ^{27}Al MASNMR shift values of the three component mixes after calcining at 1000° C, values are in ppm.

Metakaolin-silicate	Silica as the third component	Alumina as the third component
A800-X	54.7	8.9, 52.2
A800-Z	57.6	9.9, 55
B800-X	56.1	9.1, 57.5
B800-Z	55.8	9.4, 53.7
C800-X	52.3	9.5, 51.2
C800-Z	56.7	9.1, 56.1

6.3.2.1 Silica as the third component

Calcination of the samples where the third component is silica produced a similar change as seen in the two component samples, there is a shift to tetrahedral coordination. No residual octahedral or pentacoordiante aluminium is detected after calcination and as is evident from table 6.3.2 this is true for all the samples. Figure 6.3.3 is the ^{27}Al MASNMR spectrum of sample A800-Z-silica after calcining.

Observation of the ^{27}Al NMR data in table 6.3.1 of the three component samples where silica is the third component showed presence of octahedral aluminium in all the samples, for the corresponding metakaolin-silicate samples octahedral aluminium was seen only in the samples where the unreactive silicate X was used and sample C800-silicate Z. This suggests addition of the silica to the two component metakaolin-

silicate mix is preventing reactions taking place. However, inspection of the ^{27}Al NMR data in table 6.3.2 after calcining the samples and comparing this with corresponding data for the metakaolin-silicate samples shows there is very little difference between them. This indicates that the calcining process produces similar products for both the two component and three component systems, hence addition of silica has the effect of slowing the rate of reactions but does not prevent the reactions from taking place.

6.3.2.2 Alumina as the third component

The data for the samples where the third component is alumina show calcination produces a second peak in the tetrahedral region of the spectrum for all the samples and the pentacoordinate peak seen in some of the samples is no longer detected The source of the tetrahedral aluminium is probably alumina as well as the metakaolin since ^{27}Al NMR spectra of samples before calcining where alumina is the third component are different to the corresponding two component systems indicating the involvement of alumina in reactions. Figure 6.3.4 is the ^{27}Al MASNMR spectrum of sample B800-X-alumina after calcining.

Disappearance of the pentacoordinate resonance on calcining suggests five coordinate aluminium exists only as an intermediate. The reaction pathway involves a change from octahedral aluminum to tetrahedral via pentacoordinate aluminium. Since no pentacoordinate aluminium is present after calcination, this is proof that reactions have gone to completion.

Figure 6.3.3 ^{27}Al MASNMR spectrum of sample A800-Z-silica after calcining

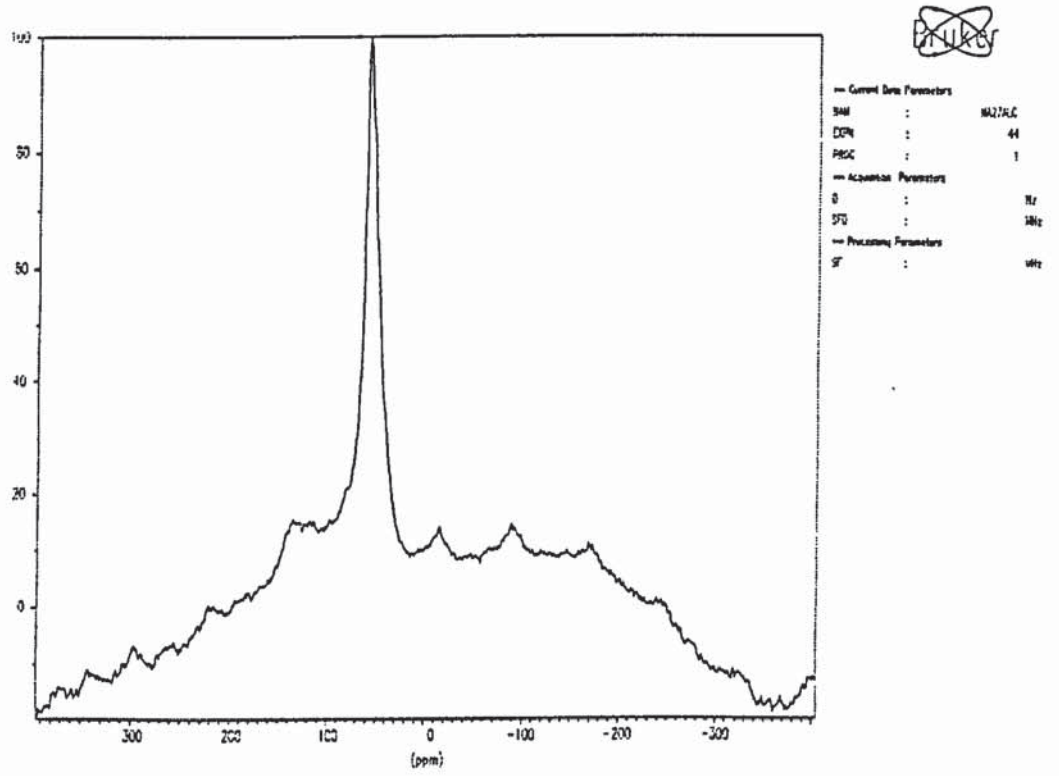

Figure 6.3.4 ^{27}Al MASNMR spectrum of sample B800-X-alumina

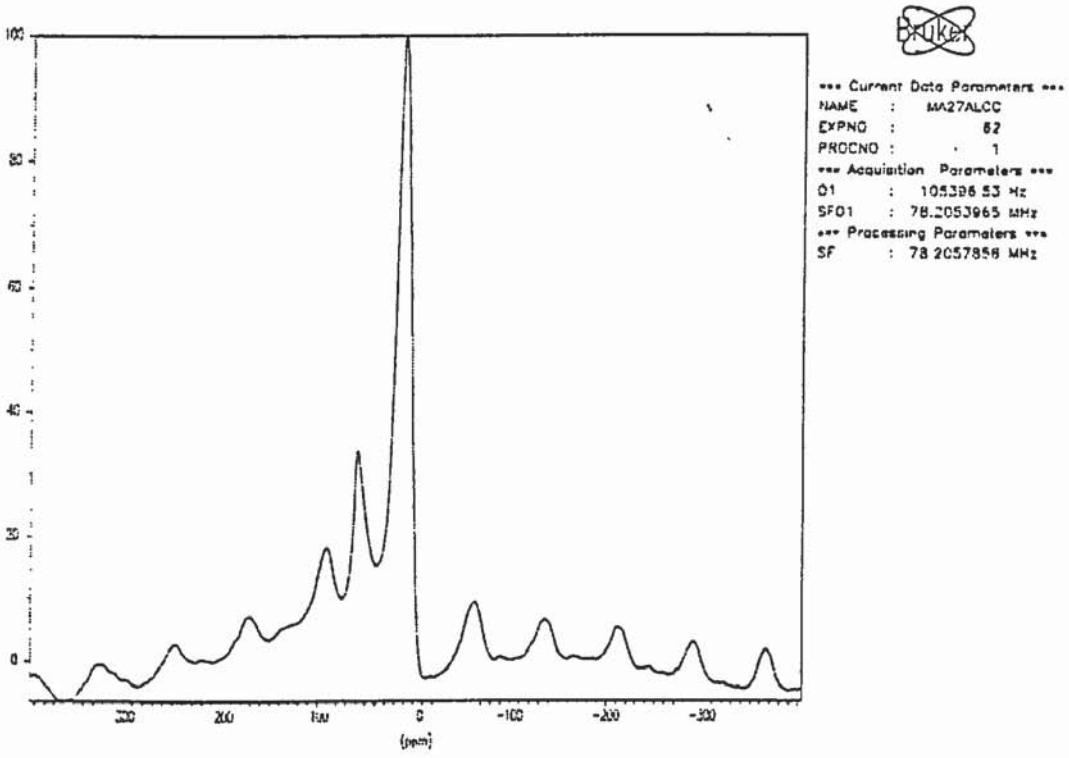

6.4 Infrared analysis

Infrared analysis of the samples was carried out both before and after calcination. Interesting changes were observed on calcination, for example, samples containing silica as third component show a weak peak in the 780-800 cm^{-1} which is identified as due to Si-O-Al vibrations[48]. On calcination the intensity of this peak is greatly increased demonstrating a greater content of Si-O-Al relative to the pre-calcined material. This could only have been achieved by the Al-O content of the metakaolin reacting with the silicate or the silica, as this increase in intensity of the Si-O-Al peak is seen in the two component metakaolin-silicate system it can be concluded the silicate is the reacting material. Figure 6 4.1 is an infrared spectrum of sample B800-Z-silica and figure 6.4.2 is the infrared spectrum of the sample after calcining, these spectra demonstrate the increase in intensity of the Si-O-Al peak intensity seen in all samples on calcination.

Observation of the infrared spectra of the calcined and uncalcined samples where alumina is the third component reveal a pattern. Calcining causes a decrease in the intensity of the peaks in the 600-700 cm^{-1} region . These peaks are due to alumina and a decrease in their intensity indicates a reduction in the amount of alumina present, this correlates with the ^{27}Al NMR data which suggests alumina is taking part in the reaction sequence. Figures 6.4.3 and 6.4.4 are infrared spectra of samples A800-Z-alumina before and after calcining and illustrate the decrease in the intensity of the alumina peaks seen in all samples after calcining.

Figure 6.4.1 Infrared spectrum of sample B800-Z-silica before calcining

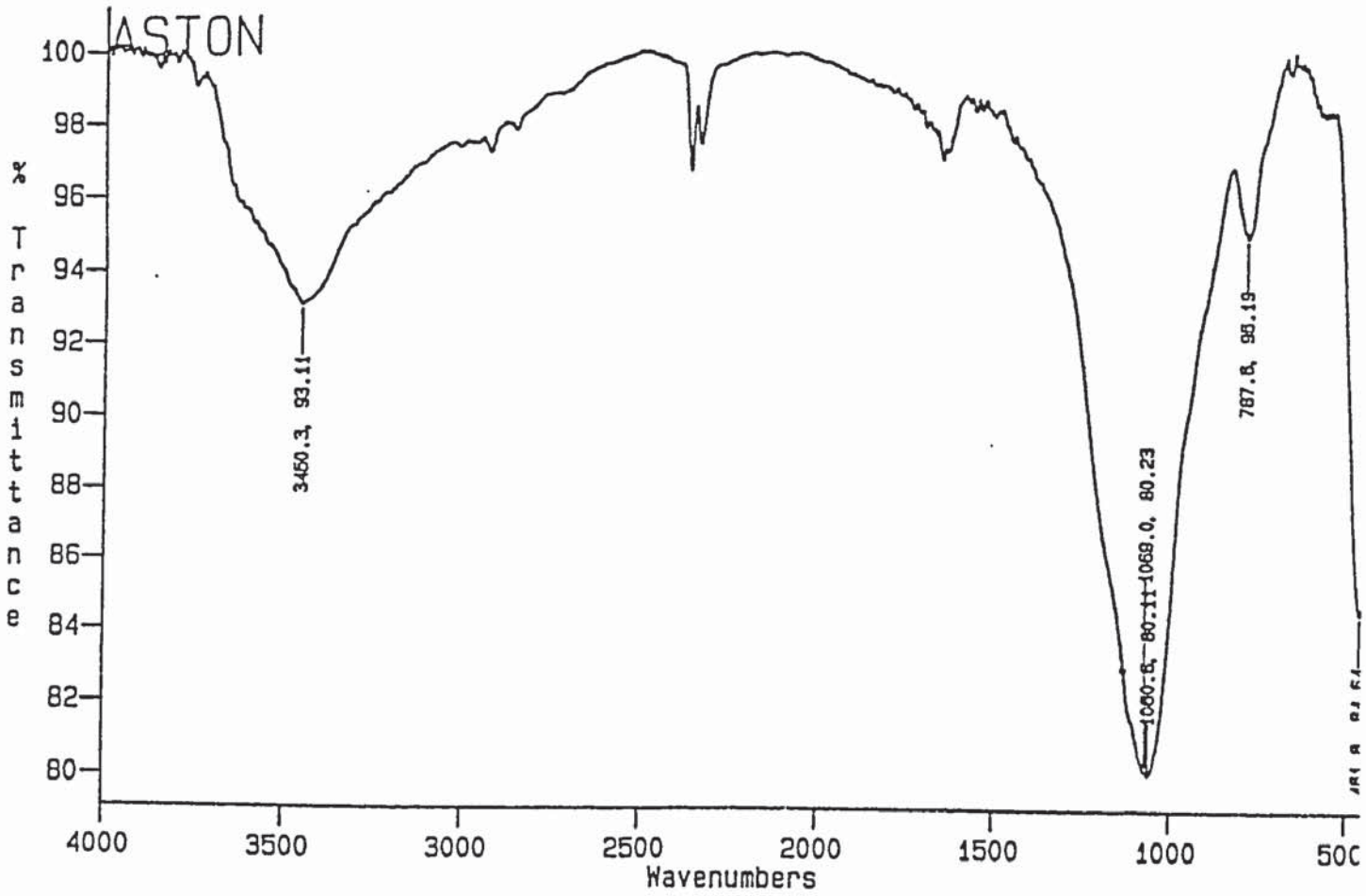

Figure 6.4.2 Infrared spectrum of sample B800-Z-silica after calcining

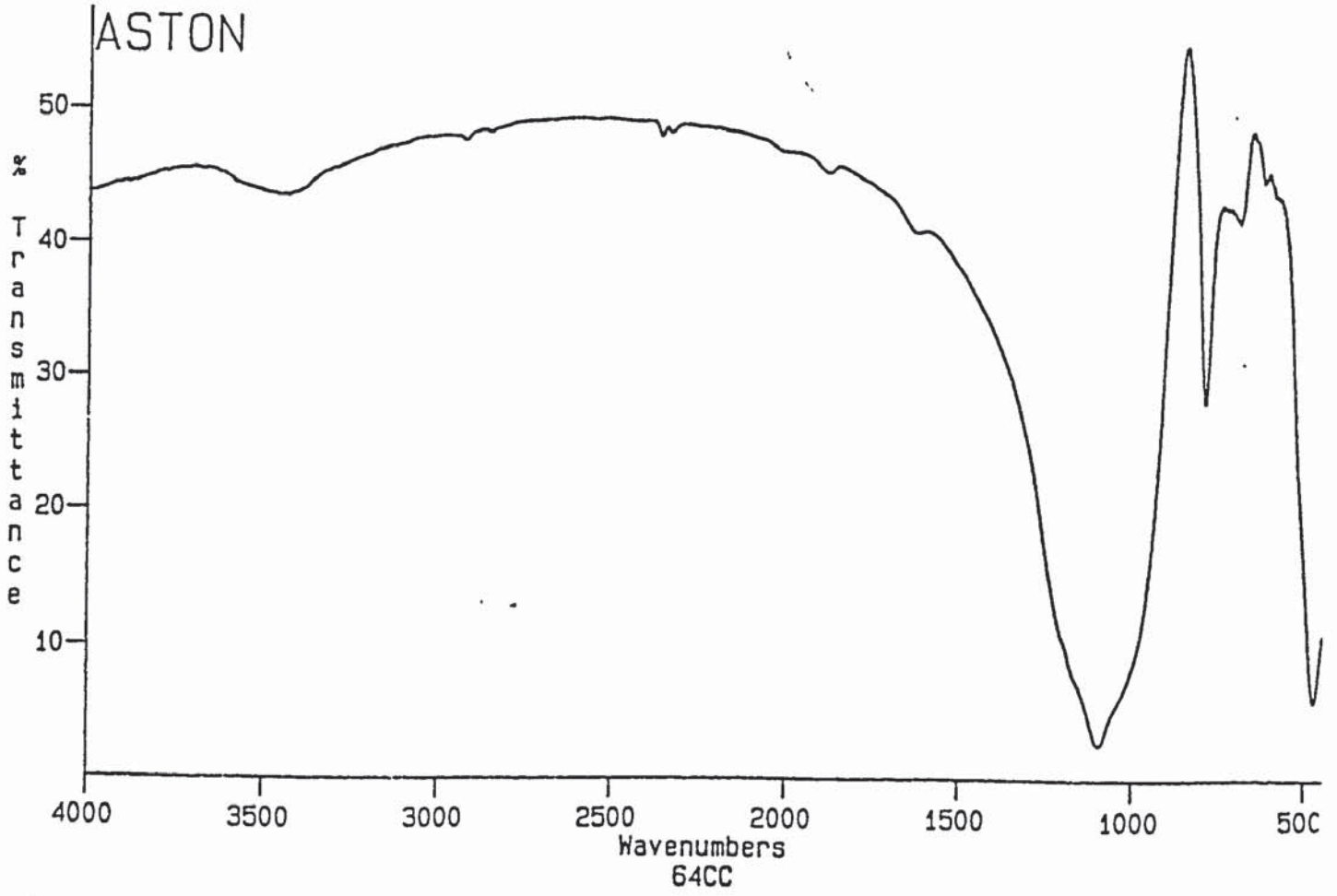

Figure 6.4.3 Infrared spectrum of sample A800-Z-alumina before calcining

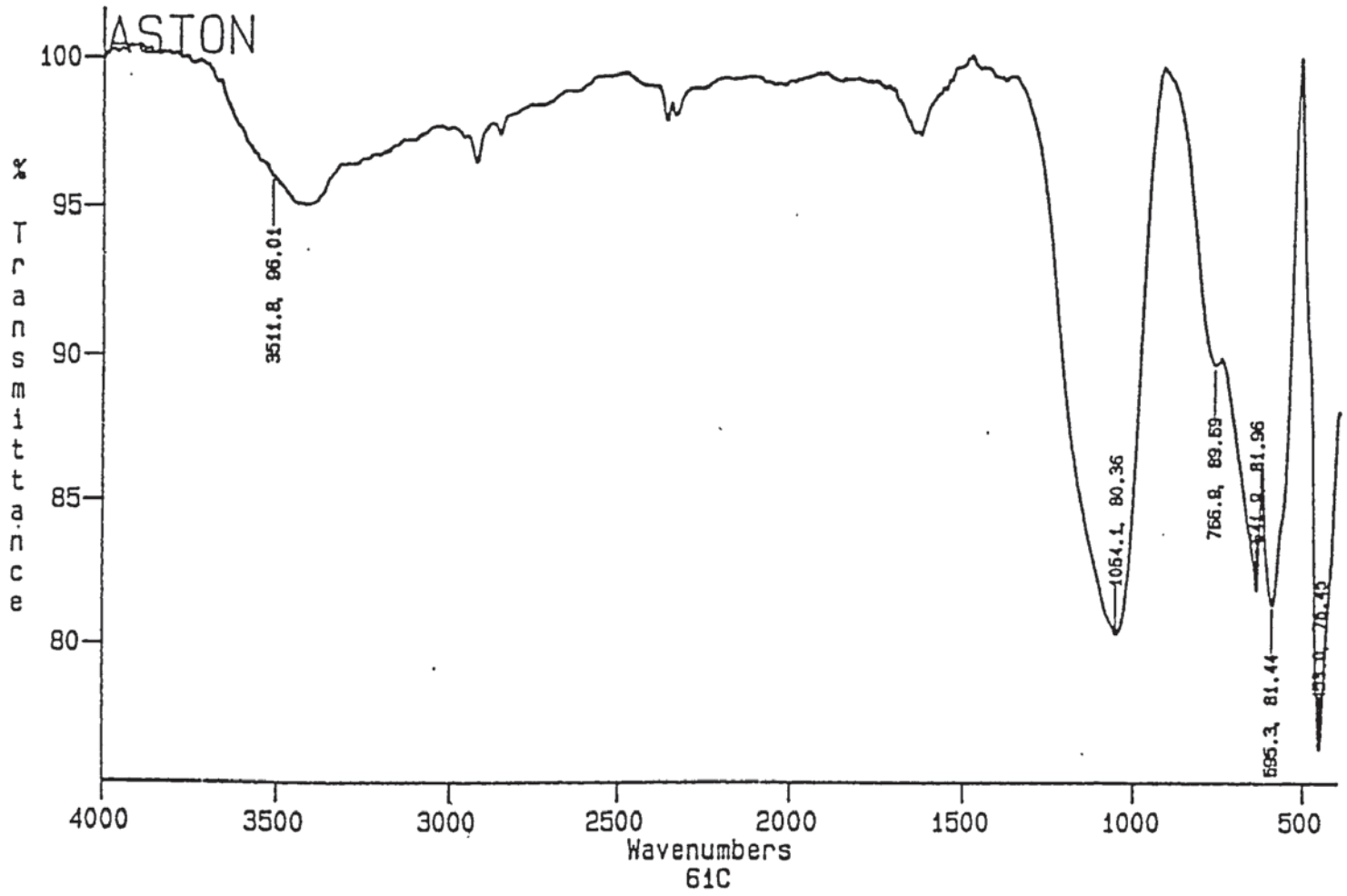

Figure 6.4.4 Infrared spectrum of sample A800-Z-alumina after calcining

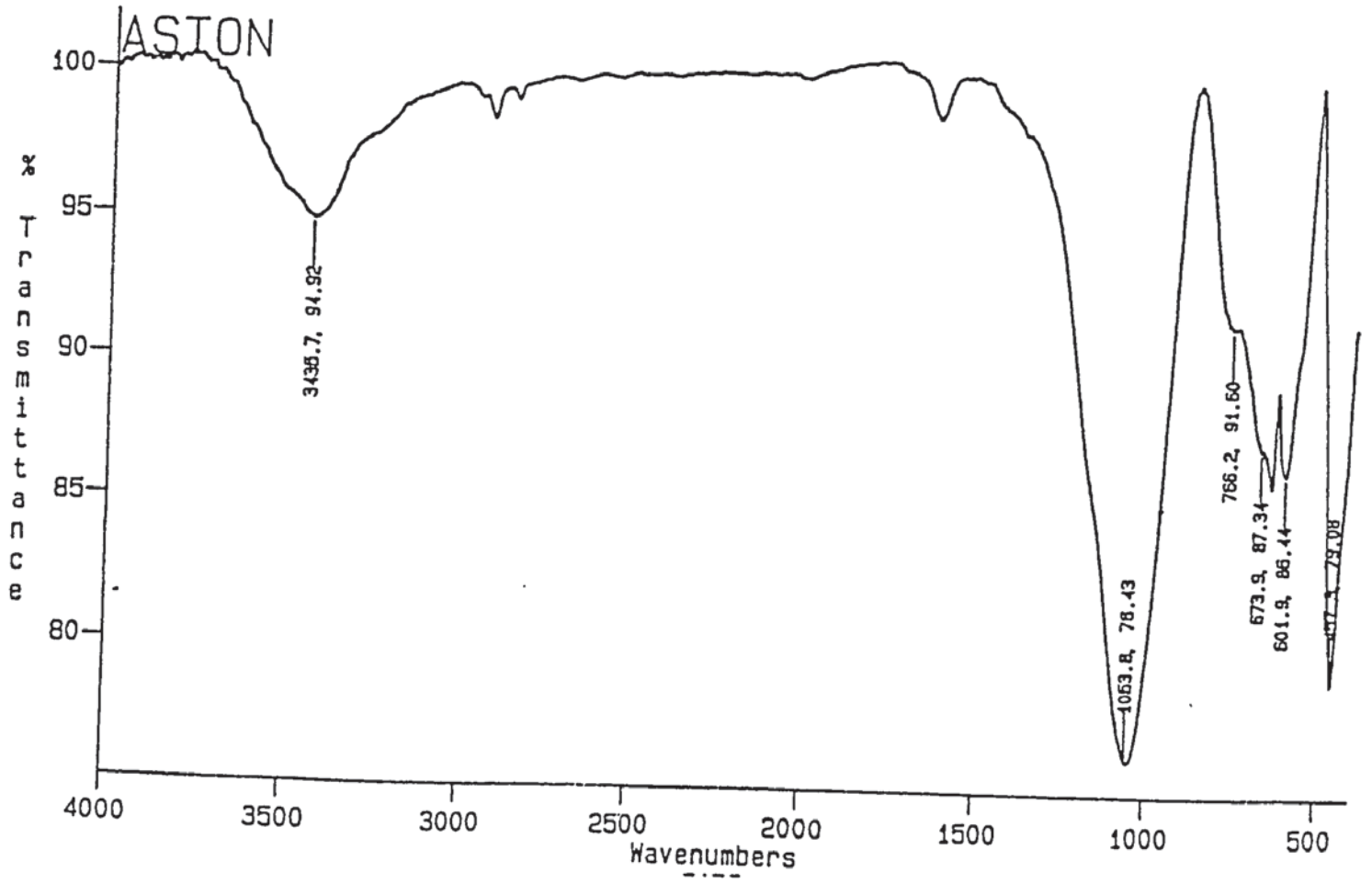

6.5 Summary of results

6.5.1 Silica as the third component

^{29}Si MASNMR analysis of the samples where the third component is silica produced very little evidence of structural change. Resonance positions were unchanged from the positions expected for silica and metakaolin-silicate. Calcining induces a shift to Q^4 position and a narrowing of the resonance indicating a change to more crystalline form.

^{27}Al MASNMR analysis of the unclacined samples appears to indicate that the introduction of silica prevents the reactions of the metakolin and the silicate because residual octahedral aluminium peaks are seen in ^{29}Si NMR spectra of all the samples. whereas the corresponding metakaolin-silicate samples showed no such peaks except in samples containing the relatively unreactive silicate X. However, after calcining there is little to distinguish between the ^{27}Al NMR spectra of the two component samples and the three component samples. This indicates that silica is merely acting to reduce the rate of the reactions rather than preventing them.

The pattern of intial reactivity or the lack of it, is similar in nature to the two component system. For example, two component samples composed of a metakaolin and silicate X generally yielded little evidence of reactivity, this is also true for the three component samples. In the two component samples where there is evidence of reactions occurring, there is also evidence of reactivity in the corresponding three component samples.

The evidence of reactivity obtained on ^{29}Si NMR and ^{27}Al NMR analysis is supported by infrared analysis. Infrared analysis shows little reactivity before calcining but on calcining an increase in the resolution and intensity of the Si-O-Al peak is seen due to reactivity of the Al-O content of the metakaolin with the silicate.

6.5.2 Alumina as the third component.

Study of the samples where alumina is the third component by ^{29}Si MASNMR indicated addition of the alumina is interfering with the metakaolin-silicate reactions as Q^3 resonances present in the spectra of the corresponding metakaolin-silicate were not seen. The absence of a Q^3 peak in these 3 comonent samples suggests alumina is impeding the depolymerisation reactions of the metakaolin and silicate (Q^3 resonance on ^{29}Si MASNMR analysis of the metakaolin-silicate mixes was identified as being caused by a depolymerisation reaction).

^{27}Al MASNMR reveals weak resonances corresponding to tetrahedral or pentacoordinate aluminium reflecting a decrease in reactivity between the silicate and metakaolin as metakaolin-silicate samples gave spectra with intense resonances in the tetrahedral aluminium region. However, after calcining relatively intense tetrahedral peaks were obtained for all the samples again suggesting, as with the addition of silica, the addition of alumina has the effect of reducing rate of the reactions taking place.

After ^{29}Si MASNMR and ^{27}Al MASNMR the source of the tetrahedral aluminium was speculated to be partly due to alumina, Infrared analysis verifies this by the decrease in intensity of the alumina peaks observed after calcining.

6.6 Conclusions

Addition of silica seems to slow some of the reactions seen for the metakaolin and silicate. For example the absence of the Q^3 resonance at -91 +/-1 ppm due to leucite in three component samples indicates leucite is not formed in these samples. Another example is the presence of octahedral aluminim in all the three component mixes where silica is the third component, corresponding metakaolin-silicate samples gave octahedral aluminium resonances only in the samples that contained silicate X. However on analysis of samples where silica is the third component it is discovered data are very similar in nature to the two component systems. This indicates the addition of the third component of silica is not preventing reactions but merely slowing down the rate of the reactions by acting as a diluant.

On anlaysis of samples where alumina is the third component there is evidence of alumina influencing the reactions taking place. For example, ^{27}Al MASNMR anlaysis of the uncalcined samples generate spectra very different to the corresponding two component samples. This fact combined with the observation of a decrease in intensity of the alumina peaks on infrared analysis confirms the involvement of alumina in the reaction process.

The observation that no tetrahedral or pentacoordinate resonances are detected for samples A800-X-alumina and C800-X-alumina is evidence of reactivity in the other samples. Since samples A800-X and C800-X have been shown to contain all three types of aluminium environments as the silicate X is generally unreactive, therefore the ^{27}Al NMR spectra of the two componet mixes is unchanged from the spectrum of the corresponding metakaolin. The fact that no resonances equating to 4 and 5 coordinate aluminium are observed in these two samples, suggest there is an insufficient amount of 4 and 5 coordinate aluminium in the metakaolin to be detectable on ^{27}Al NMR analysis when a large quantity of octahedral aluminium in

the form of alumina is also present in the sample. Therefore we can conclude if 4 and 5 coordinate aluminium resonances are seen then these have been generated by reactions taking place and are not merely due to the metakaolin component of the mix.

The narrowing witnessed for peak widths at half height upon ^{29}Si MASNMR analysis after calcining is an indication of crystallisation taking place in the samples. This is opposite to the effect observed for the two component mixes where a broadening in peak widths at half height was seen on calcining.

The presence of pentacoordinate aluminium in the uncalcined materials and its absence after calcining, together with the presence of a relatively intense tetrahedral resonance after calcining suggests that the reaction process which was identified as Si-O-Al formation involves a change from octahedral to tetrahedral coordination via pentacoordinate aluminium.

Chapter Seven

CONCLUSIONS

7.0 CONCLUSIONS

Study of the individual kaolins identified differences in the level of impurities present in each material. Kaolin A consists of mainly kaolinite and halloysite only whereas kaolins B and C contained a number of other phases.

There is a contrast in the Al:Si ratio in the kaolins, varying from 0.92 to 0.75. The order is:

kaolin A > kaolin C > kaolin B

^{29}Si MASNMR and ^{27}Al MASNMR analysis of the uncalcined kaolins indicated identical bulk silicon and aluminium environments in all the minerals.

In terms of changes on thermal treatment, these are greatest in kaolin A. For example the extent of dehydroxylation and hence the rate of dehydroxylation was greatest in mineral A at any given temperature.

Pentacoordinate aluminium is generated in preference to tetrahedral aluminium on calcination of kaolin A. Metakaolin A contains very little tetrahedral aluminium, whereas metakaolin C contains an equal proportion of tetra-, penta- and octahedral aluminium, metakaolin B contains mainly tetrahedral aluminium.

Potassium silicates showed contrasting SiO_2:K_2O (%) ratios. Silicate X gives a ratio of 2.65, silicate Y and Z give a ratio of 1.43 and 2 respectively.

Table 7.1 shows the general effects of adding the silicate to the metakaolins. There seems to be a strong correlation between the SiO_2:K_2O ratio and the products formed. A low ratio, as in silicate X, generates little interaction between metakaolin and silicate. An intermediate SiO_2:K_2O ratio yielded potassium aluminium silicate phase and no leucite, suggesting potassium aluminium phase is generated preferentially.

Table 7.1 Summary of the metakaolin-silicate interactions

sample	before calcining	after calcining
metakaolin-silicate X	little evidence of reactivity, temperature at which crystallisation occurs is unaffected	minimal pore size in structure, Crystobalite and tridymite formed
Metakaolin-silicate Y	Depolymerisation reaction occurs, increase in the temperature at which crystallisation occurs, very weak exotherm generated,	large pores, Leucite and potassium aluminium silicate formed
Metakaolin-silicate Z	Depolymerisation reaction occurs, increase in the temperature at which crystallisation occurs	pores of intermediate size, potassium aluminium silicate formed

Table 7.1 reveals the importance of the silicates in determining the reactions taking place and the products formed. For example only samples containing silicate Y formed leucite and samples containing silicate X produced little evidence of reactivity.

Table 7.2 summarises the effect addition of silica or alumina has on the metakaolin-silicate interactions. Generally silica slows reactions by having a diluant effect, alumina also has a diluant effect but in some cases it reacts to form tetrahedral aluminium. There is also evidence that addition of alumina modifies the reaction process, since Q^3 resonances seen on ^{29}Si MASNMR analysis of the metakaolin-silicate Z samples are not seen when alumina is added to the mix.

Table 7.2 effect of silica and alumina on metakaolin silicate interactions

sample	silica as the third component	alumina as the third component
Metakaolin A-silicate X	acts as a diluant, slows reaction	acts as diluant, slows reaction
Metakaolin A-silicate Z	acts as a diluant, slows reaction	acts as diluant, slows reaction but also reacts to give 4 coordinate Al, modifies reaction process
Metakaolin B-silicate X	acts as a diluant, slows reaction	acts as diluant, slows reaction but also reacts to give 4 coordinate Al
Metakaolin B-silicate Z	acts as a diluant, slows reaction	acts as diluant, slows reaction but also reacts to give 4 coordinate Al, modifies reaction process
Metakaolin C-silicate X	acts as a diluant, slows reaction	acts as a diluant, slows reaction
Metakaolin C-silicate Z	acts as a diluant, slows reaction	acts as diluant, slows reaction but also reacts to give 4 coordinate Al, modifies reaction process

Chapter Eight

ADSORPTION OF PHENOLS BY MODIFIED MONTMORILLONITES

8.1 General introduction

Montmorillonite was a clay which was evaluated as a component for the new refractory instead of the kaolinite. The main reason the montmorillonite was chosen as the clay substitute was because of the ease of availability, also it was a material frequently used by the other members of the research group. However on using calcined montmorillonite (calcined at 800°C for 2h) rather than the calcined kaolinite as the clay component, problems of mixing and setting were encountered. The refractory when left to set in the form of a brickette consisted of two layers. The montmorillonite did not mix well with the other components of the refractory. After drying, we were left with very lose aggregates rather than a compact brickette as in the case when calcined kaolinite was used as the clay component of the refractory. The application of montmorillonite as a refractory component was abandoned but in the interest of diversifing work and gaining experience in synthetic techniques and analytical techniques other than the ones already used, work was undertaken to evaluate montmorillonite after modification, as an adsorbent for phenolic pollutants.

8.1.1 Adsorption of pollutants by modified clays.

Modified Montmorillonites have been extensively used as adsorbents for oils and greases. Other major applications of montmorillonite include using it as an adsorbent for pet litter. Research into using modified clays as adsorbents for pollutants is a rapidly expanding field. Quartenary ammonium exchanged clays with cement have been effectively used to prevent leaching of pollutants from landfills[91].

The adsorption of organic molecules from aqueous solution by modified clays was first reported by Cowan and White in 1962[92]. McBride et al.[93] were able to modify clays to enhance the adsorption of organics from water supplies, they also showed different clay organic-complexes have widely varying adsorption properties for

benzene, phenol and chlorobenzenes. Mortland showed phenols could be adsorbed from industrial waste streams by quartenary ammonium clays[94].

Studies by Stul et al.[95,96] showed alcohols can be adsorbed from dilute solutions by primary quartenary ammonium cation exchanged clays. Phenolic acids, which are plant growth inhibitors, have been been successfully adsorbed by vermiculites from solution[97]. Mortland et al.[98] showed clays could be tailored for adsorption of specific molecules. Pollutant organometallic compounds can also be adsorbed by modified clays, for example tin compounds can be readily adsorbed by quartenary ammonium exchanged montmorillonites[86].

8.1.2 Phenols in waste

Phenol and substituted phenolic materials arise in nature due to both natural processes and man's activities in the form of industrial waste discharge. They are known to sorb on to clays and the resultant phenolic-clay complexes are known to have an effect on plant growth when present in soils[99]. Another problem is that phenols even when present in very small concentrations may be detected orally when present in drinking water. Chlorophenols, for example can be tasted at a concentration of 0.001mg/litre. Many of these taste and odour producing compounds have the ability to taint fish. Thus, a very small quantity of phenol in the water may completely eliminate the use of fish for food because of the bad taste imparted by the chemical. Furthermore if phenols are present in higher concentration they are toxic as well as powerful irritants. In acute phenol poisoning, the main effect is on the central nervous system, through damage to the kidneys, liver, pancreas, spleen, and oedema of the lungs may result. Consequently contamination of water by phenol or cholorphenols, even in low concentrations, is to be avoided. Thus the removal of phenols and related compounds from waste is desirable. A study has been made to identify the suitability of metal complex exchanged montmorillonite to adsorb phenols and chlorinated phenols.

Montmorillonite was chosen as the adsorbent because of its availability, high surface area, facile cation exchange, high adsorption capabilities and high selectivity when modified, as well as the low cost of Wyoming bentonite which is the source of montmorillonite.

8.1.3 Definitions

Adsorption is the accumulation of one or more components in the interfacial layer. An example of adsorption is condensation of a gas, or the adsorption of a solute, onto a free surface. Examples are carbon dioxide condensed into charcoal layers, or a solution of benzene adsorbed onto a clay mineral. The term used is different from that of absorption which suggests penetration into the mass of the lattice. The counterpart of adsorption is desorption which describes the loss of components from the interfacial layer.

The solid is termed the adsorbant, and the gas or solute the adsorptive. On accumulation at the interfacial layer the adsorptive is termed the adsorbate.

The term sorption will be used to embrace both adsorption and absorption.

Many adsorbents of high surface area are porous and with such materials it is often useful to distinguish between the external and internal surface. The external surface and internal surfaces are difficult to define . For the purpose of studies of clay adsorption the external surface will be defined as the area surrounding the agglomerates or particles and the internal surfaces as the interlayer regions of the clay.

Adsorption may occur such that all adsorbate molecules are in contact with the adsorbent surfaces, such adsorption is termed monolayer adsorption. When only a fraction of the adsorbate molecules are in contact with the adsorbent surfaces, multilayer adsorption is said to have occurred.

The relation, at constant temperature, between the amount adsorbed and the equilibrium concentration of the solute is known as the adsorption isotherm.

8.2 Introduction

Metal complex-exchanged montmorillonites were tested for their ability to adsorb phenol, chloropenol and 2,4,6-trichlorophenol from aqueous solutions of various concentration. Adsorption isotherms were plotted of the results obtained.

Montmorillonite was obtained by purifing Wyoming bentonite, the method of purification is described in section 3.5.1. Metal complexes were intercalated onto the montmorillonite. The metal complexes used were: *tris*-2,2-bipyridyliron(II) perchlorate ($[Fe(bipy)_3](ClO_4)_2$), *bis*-tri-(2-pyridyl)amineiron(II) perchlorate or $[Fe(tripyam)_2](ClO_4)_2$ and *bis*-(hydrotris-(1-pyrazolyl)borato)iron(II) or ($Fe[HB(pz)_3]_2$). These metal complexes were synthesised as described in sections 3.5.2.2, 3.5.2.3 and 3.5.2.4. In the case of the metal complex bis-tri-(2-pyridyl)amine iron(II) perchlorate the ligand tri-(2-pyridyl)amine had to be synthesised from 2,2-bipyridylamine, as described in section 3.5.2.1, to use in the synthesis of the complex. Figures 8.0a and 8.0b are structures of the ligands 2,2-bipyridyl and tri-(2-pyridyl)amine respectively. Figure 8.0c is the structure of the precursor used in the synthesis of the bis-(hydrotris-(1-pyrazolyl)borato)-iron(II) complex.

(a) (b)

Figure 8.0 The structure of (a) 2,2-bipyridyl and (b) *tri*-(2-pyridyl)amine

Figure 8.0(c) The Structure of sodium hydrotris-(1-pyrazolyl)borate

8.2.1 Characterisation of the complexes

The synthesised complexes (methods of synthesis are described in the experimental section) were of distinctive colours as is characteristic of transition metal complexes. Table 8.1 exhibits the colours of these complexes.

Table 8.1 Colours of synthesised complexes and ligands

Complex or ligand	Colour
Tri-(2-pyridyl)amine	white
Tris-2,2-bipyridyl iron(II) perchlorate	red/maroon
Bis-tri-(2-pyridyl)amineiron(II) perchlorate	orange
Bis-(hydrotris-(1-pyrazolyl)borato)iron(II)	mauve

FTIR analysis of the ligands and complexes was also carried. All complexes containing perchlorate show a characteristic perchlorate ion peak at 1100cm^{-1}. Figures 8.1 and 8.2 are infrared spectra of *tris*-2,2-bipyridyl iron(II) perchlorate and *bis*-tri-(2-pyridyl)amineiron(II) perchlorate.

Figure 8.1 Infrared spectrum of *tris*-2,2-bipyridyliron(II) perchlorate

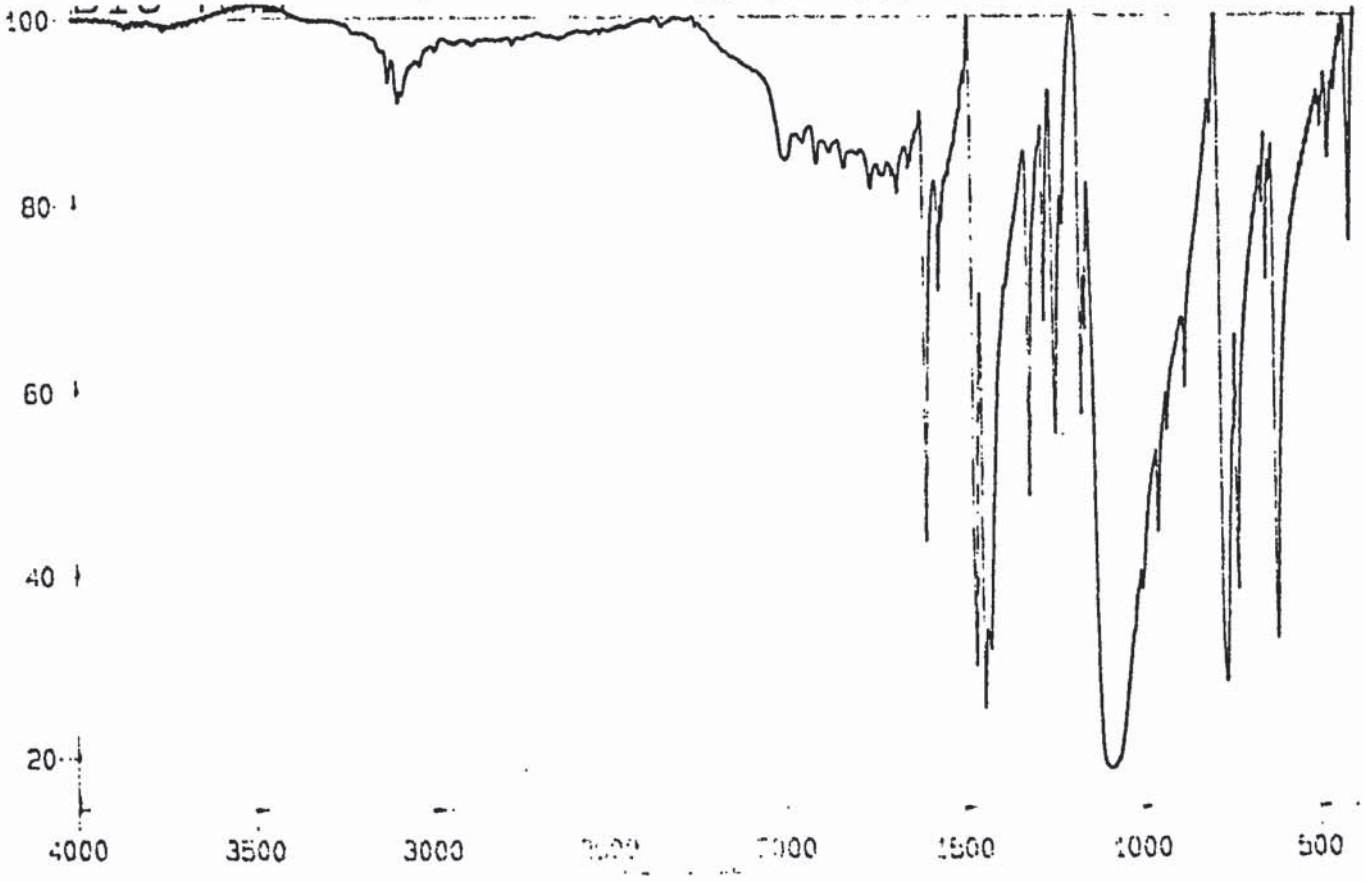

Figure 8.2 Infrared spectrum of *bis*-tri-(2-pyridyl)amineiron(II) perchlorate

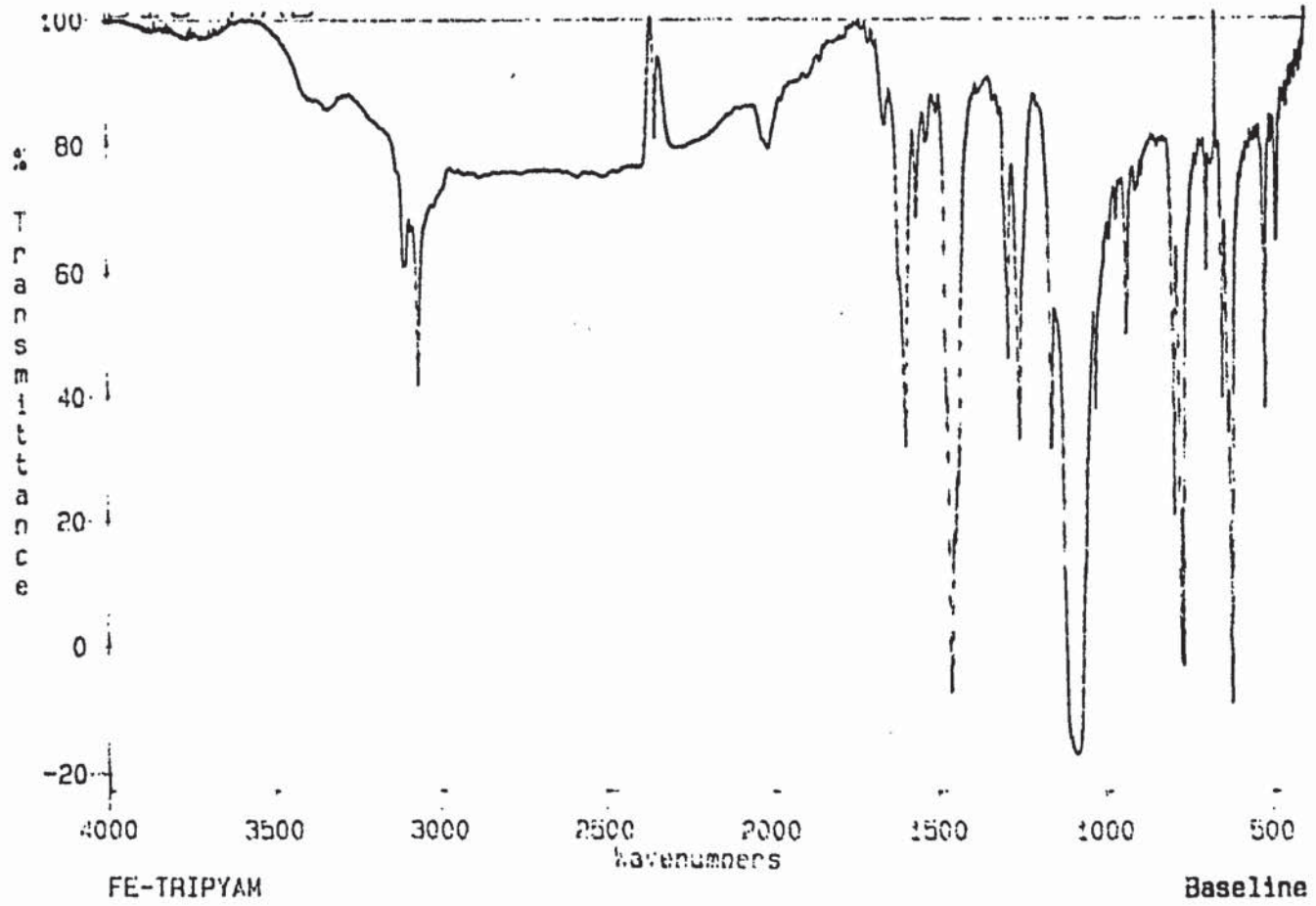

8.3 Swelling property of montmorillonite

The purification process described in section 3.5.1 gives essentially pure montmorillonite with Na, Ca and Mg present as exchangeable ions. Addition of a calculated amount of metal complex allows the exchange of the metal complex for the alkali metal ions . The larger size of the metal complex and the weak forces holding the silicate layers together combine to allow swelling of the montmorillonite by an expansion of the interlayer spacing. Figure 8.3 is a schematic representation of the reaction between montmorillonite and the metal complexes.

Figure 8.3 A schematic representation of the reaction between monmorillonite and the metal complexes.

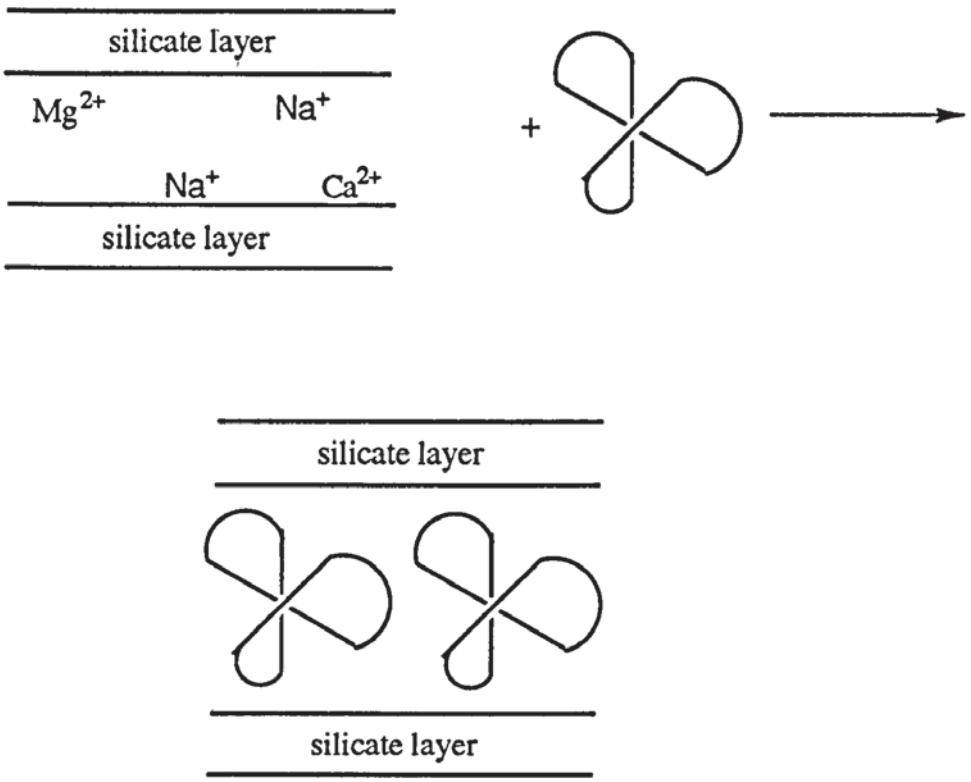

The visible spectra of the transition metal exchanged clays or intercalated clays as in the case of *bis*-(hydrotris-(1-pyrazolyl)borato)iron(II) complex, were the same as the

complex precursors. This indicated that the bonding of the transition metal complexes does not change on exchange with the alkali metal cations in the montmorillonite.

The introduction of various organic groups via the metal complexes between the silicate layers allows the clay to have organophilic properties. The complexes also serve as pillars to prop open the silicate layers ensuring easy access of foreign material to the interlamellar region. Hence their use as adsorbants for organic pollutants such as phenol and chlorophenols.

8.4 Characterisation of the metal exchanged or intercalated montmorillonites

Infrared analysis, ^{27}Al MASNMR and ^{29}Si MASNMR was carried out of the individual metal complexes and montmorillonite before treatment with the complex. Figure 8.4 is the infrared spectrum of montmorillonite. Table 8.2 assigns the absorptions seen on infrared analysis of the montmorillonite to particular modes of vibration.

Table 8.2 Assignments of absorption maxima in IR spectra of montmorillonites[92].

Band position wave number cm^{-1}	Assignment
3634	O-H streching, (Mg, Al)-OH
3433	H-O-H hydrogen bonded water
1635	H-O-H deformation
1115	Si-O stretching in-plane
1040	Si-O-Si stretching
918	Deformation of OH linked to $2Al^{3+}$
888	Deformation of OH linked to Fe^{3+} and Al^{3+}
847	Deformation of OH linked to Al^{3+} and Mg^{2+}
778	Si-O deformation perpendicular to optical axis
671	Si-O deformation parallel to the optical axis

After familiarity with the infrared spectra of the metal complexes and montmorillonite was achieved infrared analysis of samples of montmorillonite after treatment with the metal complexes was carried out to identify whether exchange had taken place. Figures 8.5 and 8.6 are infrared spectra of *bis*-tri-(2-pyridyl)amineiron(II) perchlorate exchanged montmorillonite and *bis*-(hydrotris-(1-pyrazolyl)borato)iron(II) complex intercalated montmorillonite. Observation of the spectrum of the former reveals an

absorption at 1651 cm^{-1}, this absorption is not seen in the infrared spectrum of montmorillonite or *bis-tri*-(2-pyridyl)amineiron(II) perchlorate. The origin of this absorption is probably as result of the shift in one of the *bis*-tri-(2-pyridyl)amine-iron(II) perchlorate peaks. These shifts in bands are often seen on adsorption of a species onto a clay. For example it has been shown when aromatics are adsorbed onto montmorillonite there is a significant shift in the out-of-plane C-H deformations arising from a perturbation of the π electrons in the adsorbed state[93,94], and in cases where benzene forms a complex with a cation present in the montmorillonite interlamellar region, then infrared spectra can be very different to the spectrum of the clay or the liquid benzene[95].

Figure 8.4 Infrared spectrum of montmorillonite

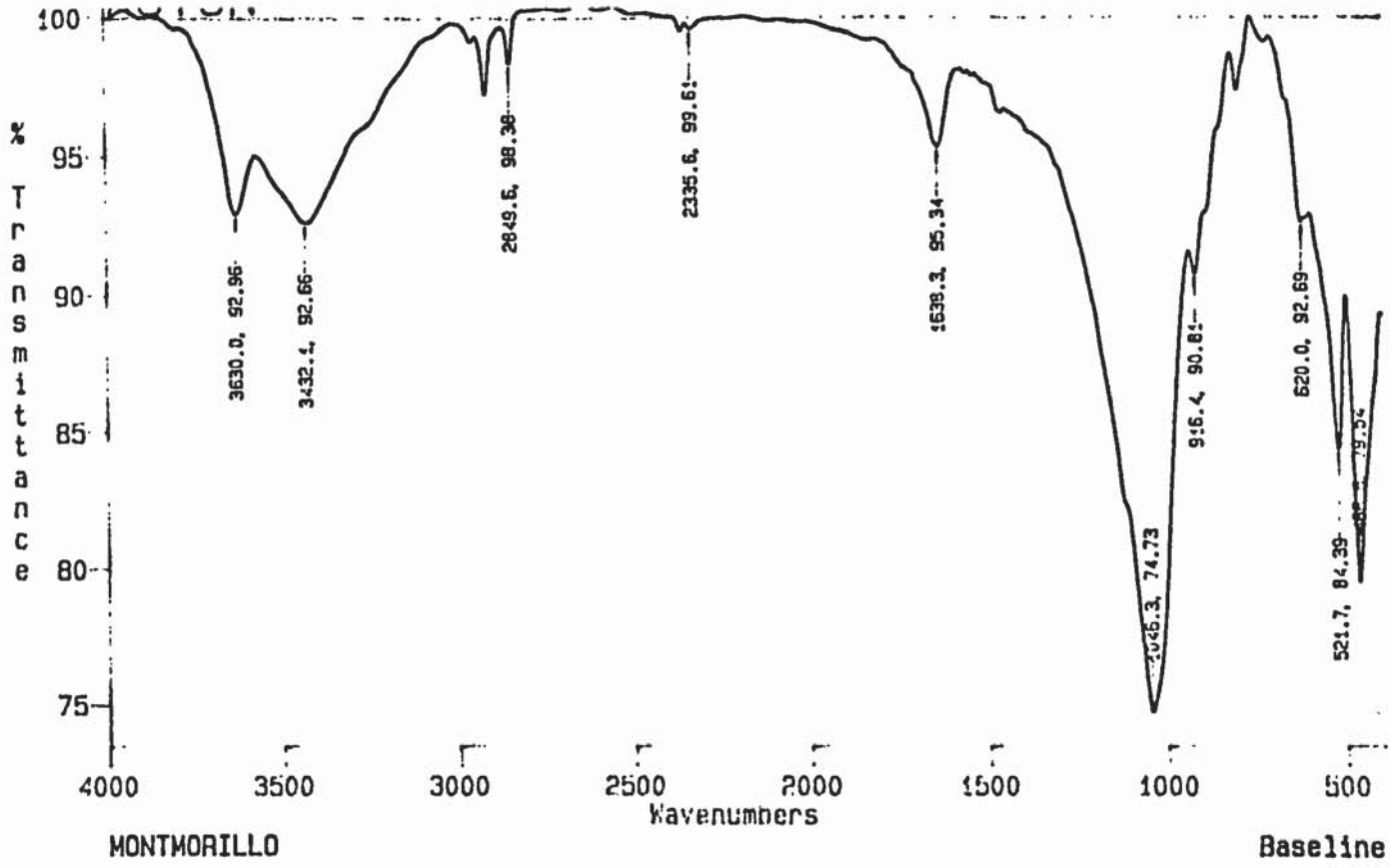

Figure 8.5 Infrared spectrum of *bis*-tri-(2-pyridyl)amineiron(II) exchanged montmorillonite

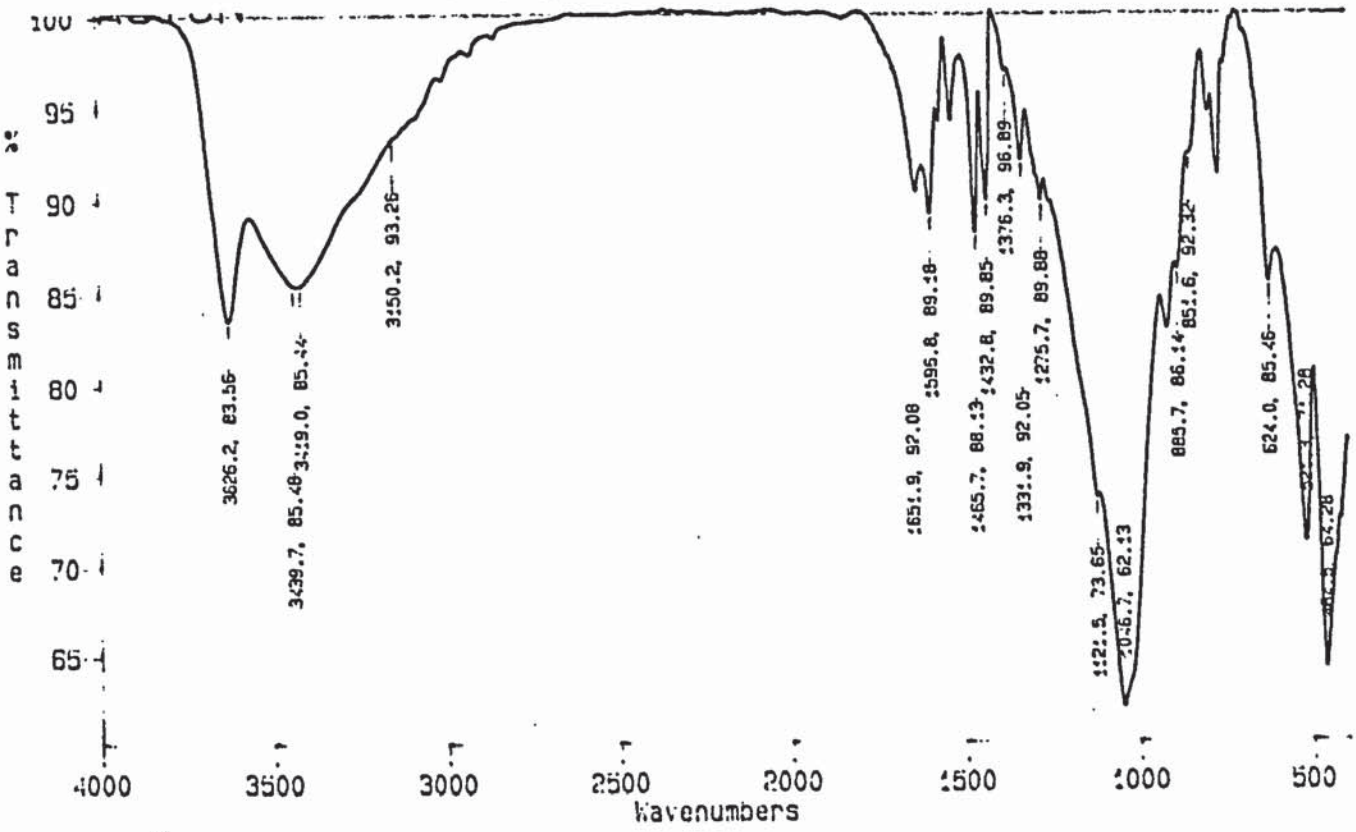

Figure 8.6 Infrared spectrum of *bis*-(hydrotris-(1-pyrazolyl)borato)iron(II) complex intercalated montmorillonite

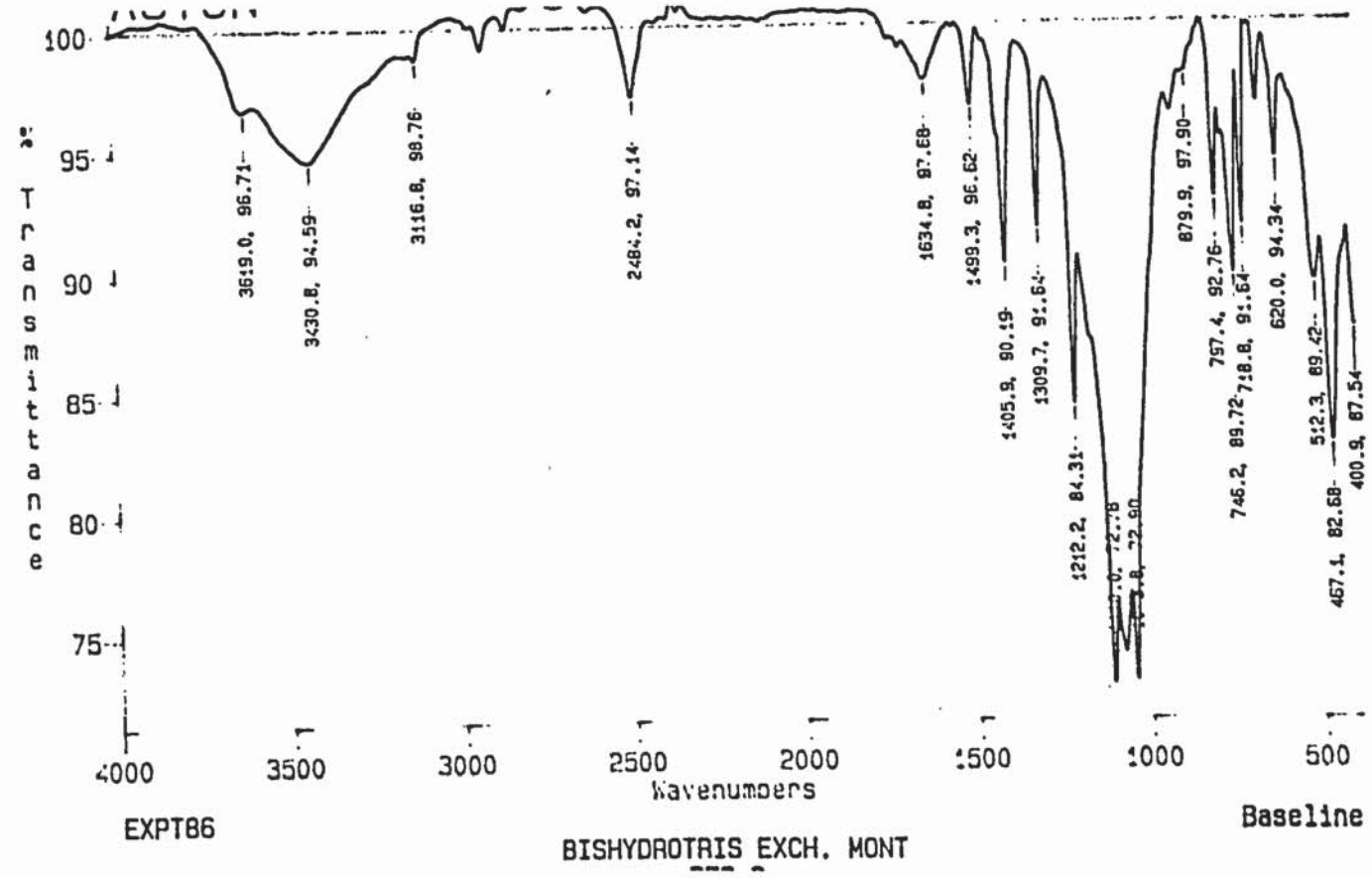

8.4.1 Characterisation by NMR

^{27}Al MASNMR and ^{29}Si MASNMR analysis was carried out on the montmorillonite before the treatment with complexes and after treatment to identify if changes had taken place in terms of silicon and aluminium shift values. The ^{27}Al MASNMR spectrum of montmorillonite consists of two characteristic peaks. The furthest upfield being termed Q^4 and that downfield, Q^3. The Q^4 peak results from the presence of an SiO_2 in the clay, where the silicon shares oxygens with four other silicon atoms. When silicon shares oxygens with three other silicon atoms, as found in the silicate layer of montmorillonite, a Q^3 peak is observed in the spectra. The Q^4 and Q^3 resonances are typically found at -107.5 ppm and -92.9 ppm when tetramethylsilane is used as the standard. Table 8.3 shows the positions of the Q^3 and Q^4 resonances after exchanging or intercalating the three complexes onto the montmorillonite.

Table 8.3 Positions of the Q^3 and Q^4 resonances of montmorillonite and metal complex exchanged montmorillonite

Name	Q^3 (ppm)	Q^4 (ppm)
Montmorillonite	-92.9	-107.5
Tris-2,2-bipyridyl iron(II) perchlorate	-93.9	-107.7
Bis-tri-(2-pyridyl)amineiron(II) perchlorate	-94.1	-107.7
Bis-(hydrotris-(1-pyrazolyl)borato)-iron(II)	-93.7	-107.8

Scrutiny of the data in table 8.3 reveals the Q^4 resonance to be unaffected by the exchange reaction, as expected. The Q^3 peak, however, is seen to shift upfield after exchange has taken place and this is true on exchange of any one of the complexes. This shift in resonance upfield is a consequence of the sodium cation present in montmorillonite deshielding the silicon atom to a greater extent than the exchanged

metal complex. Thus the Q^3 resonance is sensitive to the exchange reaction and confirms the infrared data which show that an exchange reaction has occurred. Figure 8.7 and 8.8 are ^{29}Si MASNMR spectra of *bis*-tri-(2-pyridyl)amineiron(II) exchanged montmorillonite and *bis*-(hydrotris-(1-pyrazolyl)borato)iron(II) intercalated montmorillonite.

^{27}Al MASNMR analysis of montmorillonite show the presence of mainly octahedral alumininium but a weak resonance in the tetrahedral region is also observed. ^{27}Al MASNMR spectra of the iron complex exchanged montmorillonites are similar to the montmrillonite spectra pre-exchanging, in that a major octahedral aluminium peak and a less intense tetrahedral aluminium peak are seen. There are subtle differences in the exact positions of these peaks between the different samples but quadrupolar broadening and the noise observed for these spectra mean these differences cannot be related to differences in structure.

Figure 8.7 ^{29}Si MASNMR spectrum of *bis*-tri-(2-pyridyl)amineiron(II) exchanged montmorillonite

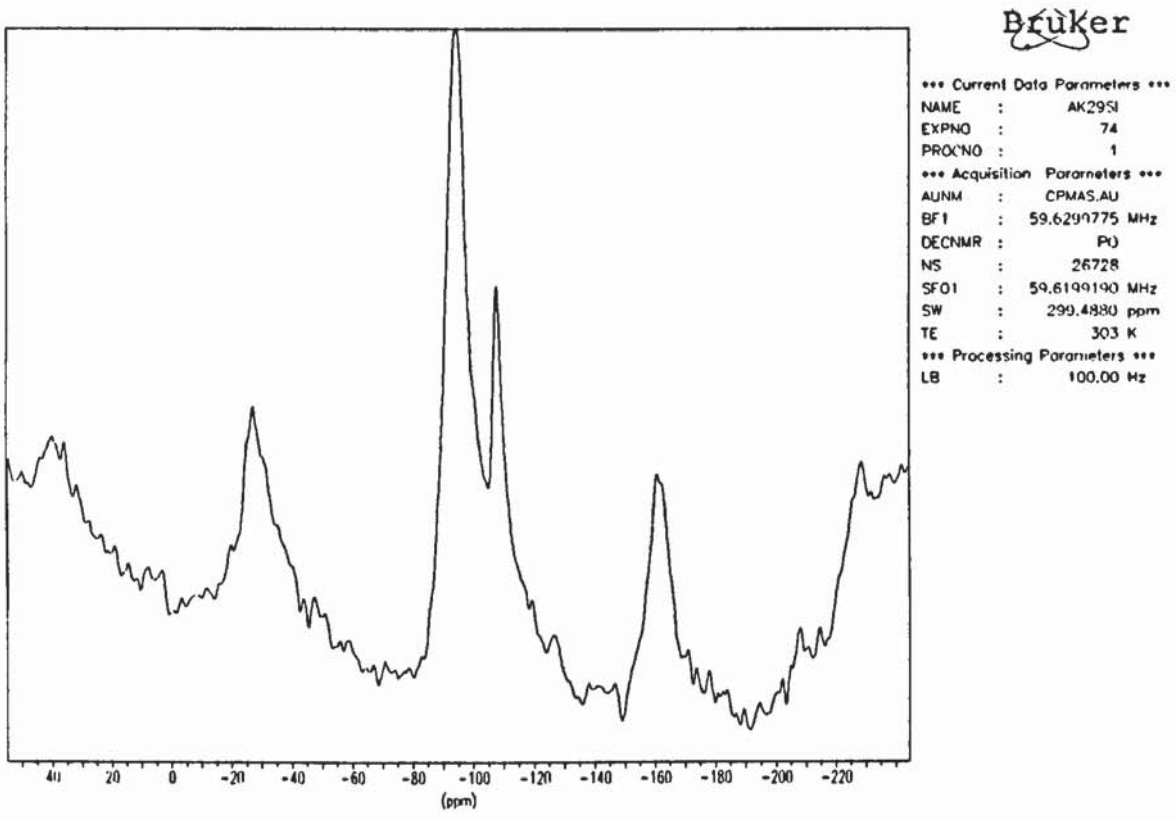

Figure 8.8 ^{29}Si MASNMR spectrum of *Bis*-(hydrotris-(1-pyrazolyl)borato)iron(II) intercalated montmorillonite

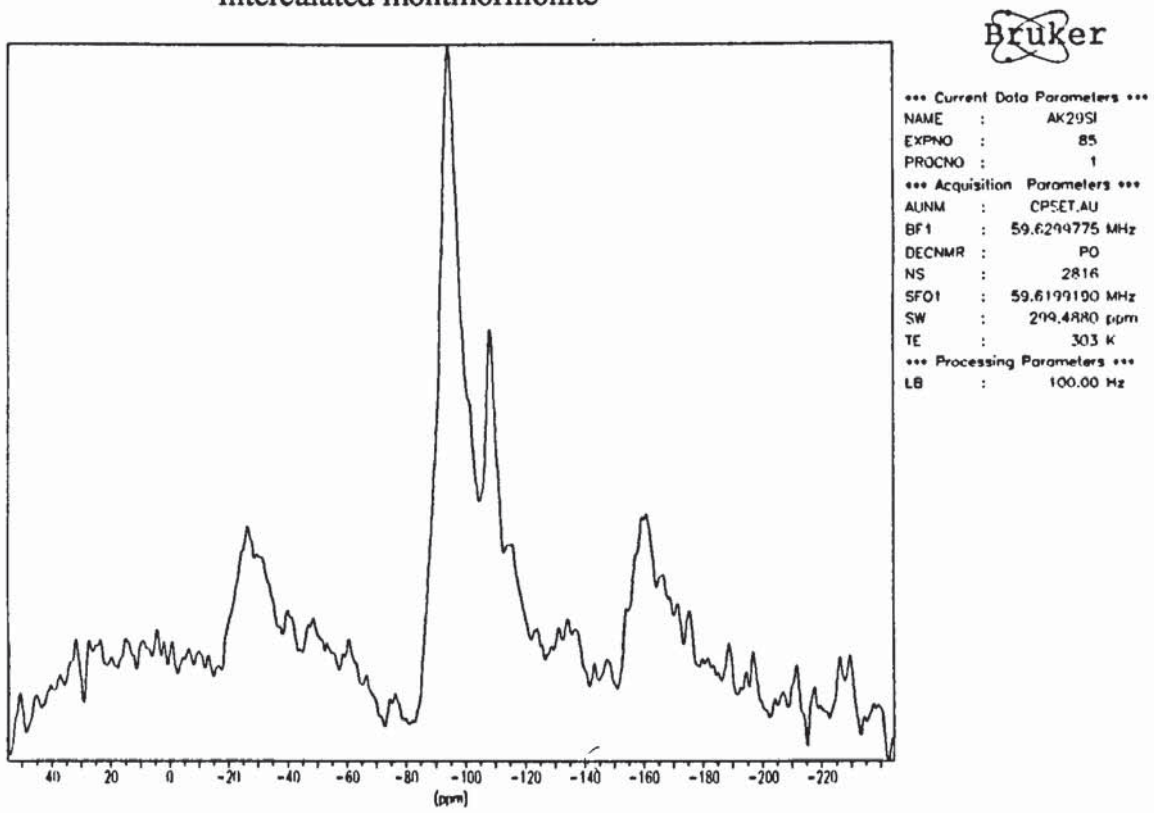

8.5 Adsorption of phenols by the modified montmorillonites

100 mg of montmorillonite exchanged with one of the synthesised complexes was added to a variety of concentrations of trichlorophenol (1.0, 0.8, 0.6, 0.5, 0.4, 0.2, 0.1 mmole/g) in distilled water. The total volume of the solution was 100 cm^3 in each case. The flasks were shaken over two nights in a temperature controlled water bath at 20°C, filtered and the solution analysis carried out by UV spectroscopy. This was repeated using 2-chlorophenol and phenol. Adsorption isotherms were plotted using absorptions at 293 nm for trichlorophenol and at 274 nm for the chlorophenol and phenol in the UV spectrum. These particular wavelengths were used as it was found that Beer-Lambert law is obeyed at these wavelengths in the concentration ranges used.[86]

UV analysis allows the measurement of changes in phenol concentration in solution. Infrared analysis can be employed to identify if phenol has been adsorbed onto the modified montmorillonite. The presence of hydroxyl groups at 3200 cm^{-1} indicate that phenol has been adsorbed by the complex exchanged montmorillonite. This hydroxyl band is easily distinguished from the OH group of montmorillonite which occurs at 3600 cm^{-1}. However infrared analysis does not give the quantitative information required for this study.

8.5.1 Calculation of phenol and chlorophenol concentrations

The adsorption isotherms were plotted by calculating the concentration of the phenol or chlorophenol remainining in solution. This was achieved by obtaining a UV spectrum of the solution after the adsorption process and using the peak height at 293 nm or 274 nm depending on the type of phenol being studied. Since the Beer-Lambert law is obeyed the value obtained for the peak height can be incorporprated into the equation:

$$A = \varepsilon cl$$

where,

A = Absorbance

ε = molecular absoptivity, a constant characteristic of the particular compound at the wavelength l

c = sample concentration, mol/L

l = length of the sample path, cm

The use of the Beer-Lambert equation and the peak height allow the calculation of the concentration of the phenol or chlorophenol and hence the amount adsorbed by the modified montmorillonite. Figure 8.9 and 8.10 are UV spectra obtained after adsorption experiments concerning phenol and *bis-tri*-(2-pyridyl)amineiron(II) exchanged montmorillonite and chlorophenol and *bis-tri*-(2-pyridyl)amineiron(II) exchanged montmorillonite.

Figure 8.9 UV spectrum obtained for a phenol solution

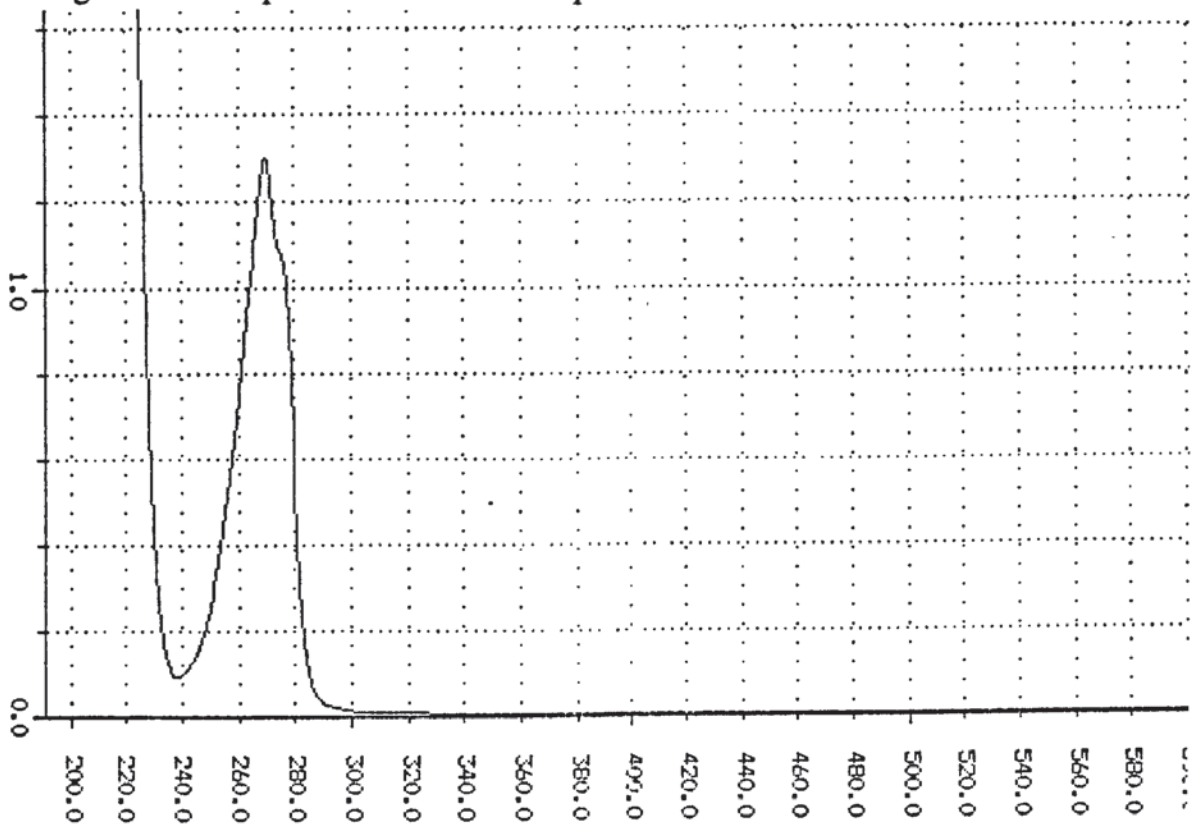

Figure 8.10 UV spectrum obtained for a solution of 2-chlorophenol

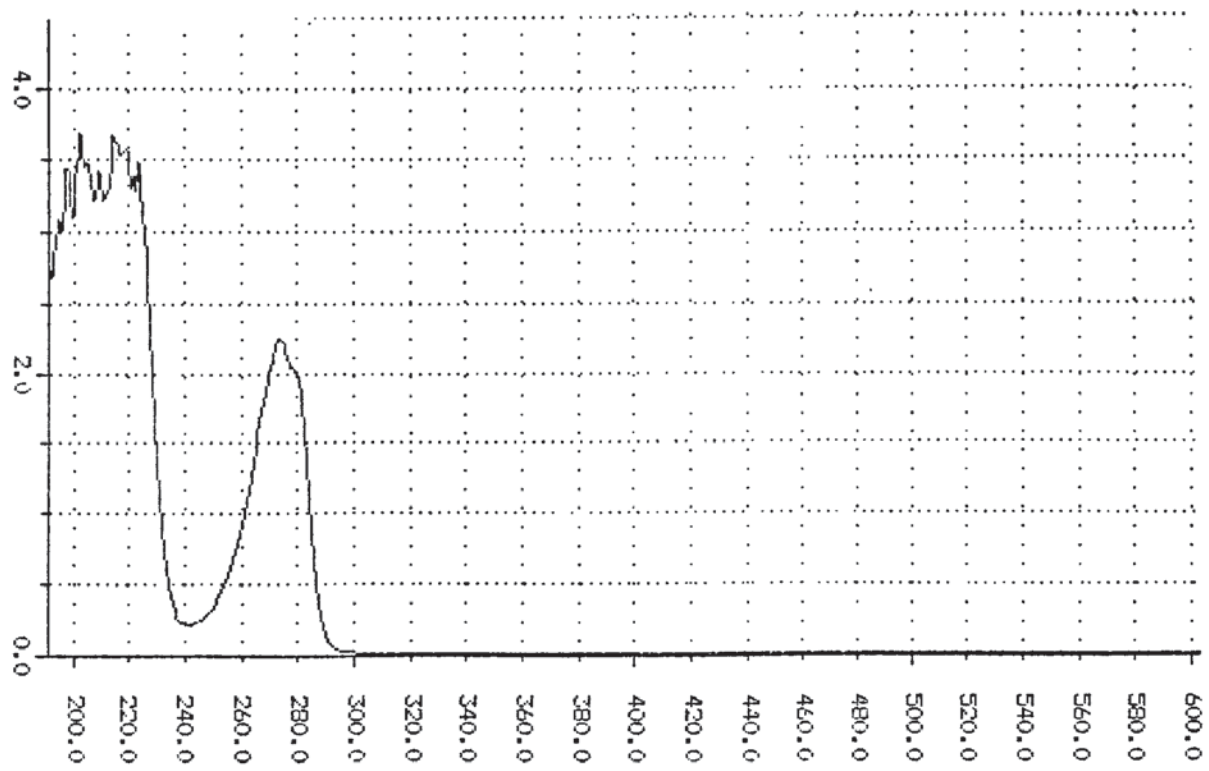

8.5.2 Calculations to find the amount of phenol adsorbed by a modified montmorillonite

Initially the extinction coefficient for phenol was calculated at wavelength 268.8 nm. This was accomplished by gaining UV spectra of a number of phenol solutions of known concentration and calculating the extinction coefficient using the Beer-Lambert equation. The average of the e values was calculated and used in all the calculations concerning phenol. The extinction coefficient for phenol was calculated to be $1.547*10^3$ mol/dm^3. Similarly extinction coefficients were calculated for 2-chlorophenol and 2,4,6-trichlorophenol. These were then used to calculate the amount of phenol, 2-chlorophenol or 2,4,6-trichlorophenol adsorbed by the modified montmorillonites.

8.6 Adsorption of phenol and chlorophenols by iron complex exchanged or intercalated montmorillonite

After calculating the amount of phenol, 2-chlorophenol or 2,4,6-trichlorophenol adsorbed by each of the modified montmorillonites adsorption isotherms were plotted of the results obtained.

8.6.1 Adsorption of phenols and chlorophenols by *tris*-2,2-bipyridyl iron(II) exchanged montmorillonite

(In all cases 2-chlorophenol and 2,4,6-trichlorophenol were used)

Figure 8.11 Adsorption of phenols and chlorophenols by *tris*-2,2-bipyridyl iron(II) exchanged montmorillonite

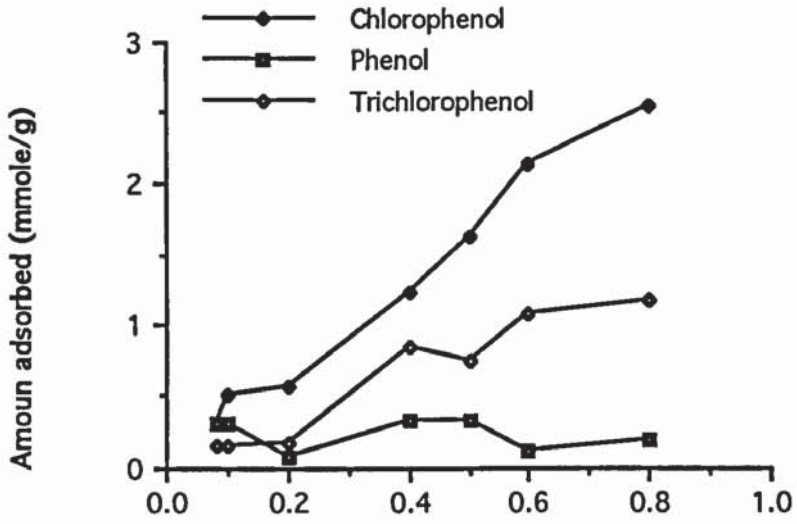

The *tris* 2,2-bipyridyliron(II) complex exchanged montmorillonites adsorb phenol and derivatives of phenol but to varying degrees. The greatest affinity of the metal complex exchanged montmorillonites seems to be for chlorophenol and the least for phenol as demonstrated by the results displayed in figure 8.11. The low affinity for phenol may be explained by solvent-adsorbate interactions being greater for phenol, phenol is more soluble in water than the chlorinated phenols. These solvent-adsorbate interactions are it seems enough to overcome the affinity of tris 2,2-bipyridyl iron(II) complex exchanged montmorillonite for the phenol. On this basis 2,4,6-trichloro-phenol would be expected to be more greatly adsorbed than 2-chlorophenol as it is less soluble in water therefore the influence of adsorbate-solvent interactions would be diminished but in this case the bulkiness of the trichlorophenol relative to cholorophenol probably impedes its adsorption.

8.6.2 Adsorption of phenol and chlorophenols by bis-tri-(2-pyridyl)amineiron(II) exchanged montmorillonite

Figure 8.12 Adsorption of phenol and chlorophenols by bis-tri-(2-pyridyl)-amineiron(II) perchlorate exchanged montmorillonite

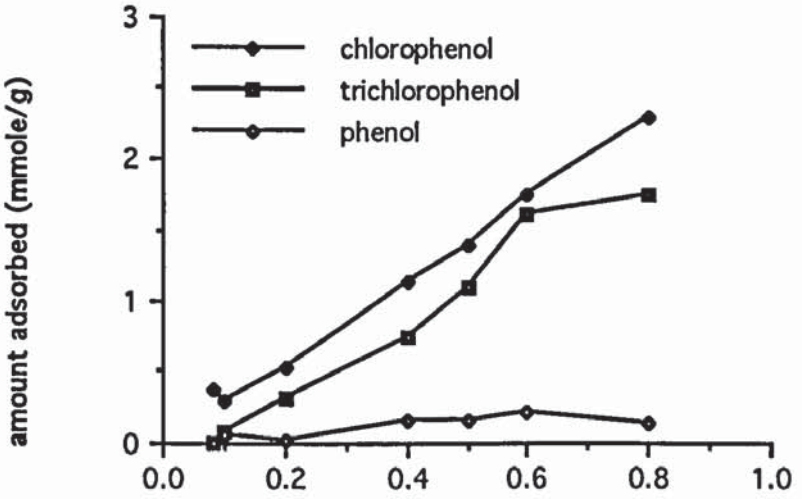

Bis-tri-(2-pyridyl)amineiron(II) perchlorate exchanged montmorillonite shows the greatest capacity of adsorption for chlorophenol, followed by trichlorophenol and then phenol as illustrated by figure 8.12. This pattern of adsorption is similar to the *tris* 2,2-bipyridyliron(II) complex exchanged montmorillonites. However, whereas for the tris 2,2-bipyridyliron(II) complex exchanged montmorillonites adsorption of chlorophenol is much greater at high equilibrium concentrations compared with 2,4,6-trichlorophenol, for the *bis*-tri-(2-pyridyl)amineiron(II) perchlorate exchanged montmorillonite the difference in adsorptions of the two compounds is not as pronounced. The greater adsorption capacity for trichlorophenol in the latter maybe due to a number of reasons. The larger size of the *bis*-tri-(2-pyridyl)amineiron(II) perchlorate complex has an effect of opening the layers further allowing access for the bulky trichlorophenol. Another factor maybe orientation of the pyridine rings in the *bis*-tri-(2-pyridyl)amineiron(II) perchlorate complex maybe more favourable for π-π interactions with the benzene ring of the trichlorophenol.

8.6.3 Adsorption of phenol and chlorophenols by bis-(hydrotris-(1-pyrazolyl)borato)-iron(II) intercalated montmorillonite

Figure 8.13 Adsorption of phenol and cholorphenols by bis-(hydrotris-(1-pyrazolyl)borato)iron(II) complex intercalated montmorillonite

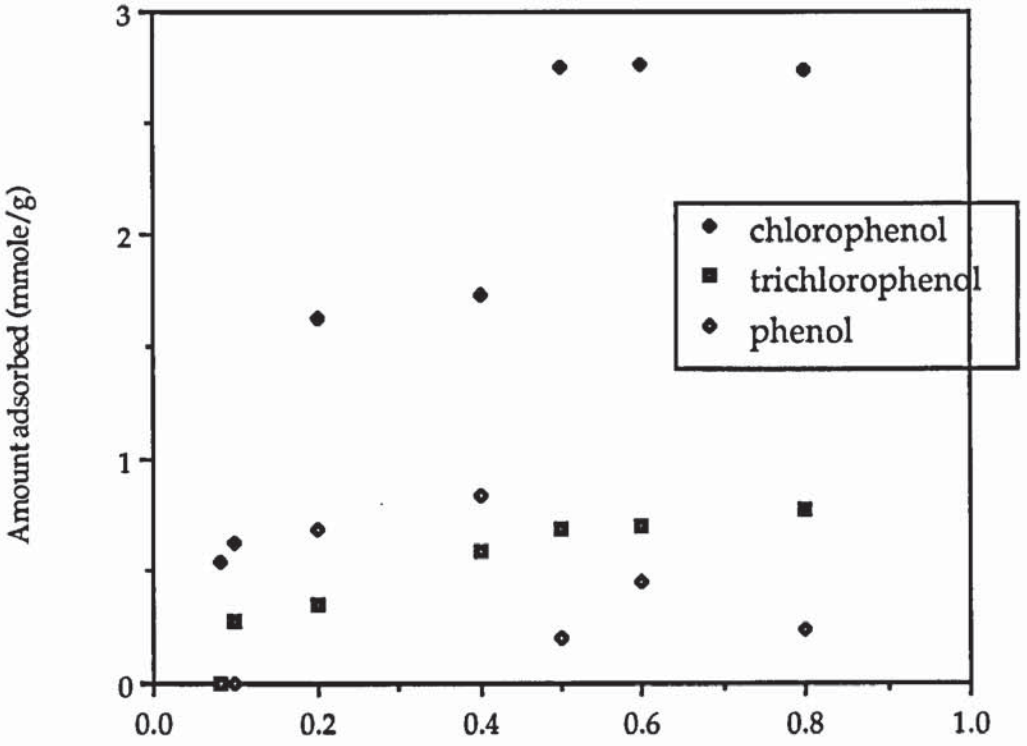

Bis-(hydrotris-(1-pyrazolyl)borato)iron(II) intercalated montmorillonite appears to be effective only in the adsorption of chlorophenol. As can be seen from figure 8.13 very little adsorption of phenol and trichlorophenol takes place, whereas in the case of *tris* 2,2-bipyridyliron(II) cation exchanged montmorillonite and *bis*-tri-(2-pyridyl)amineiron(II) cation exchanged montmorillonite it was obvious that phenol was the least well adsorbed species, it is less apparent for *bis*-(hydrotris-(1-pyrazolyl)borato)iron(II) intercalated montmorillonite. The lack of adsorption for

phenol as explained earlier is due to the greater adsorbant-solvent interaction. The lack of adsorption of trichlorophenol when *bis*-(hydrotris-(1-pyrazolyl)borato)iron(II) complex is intercalated onto montmorillonite is probably due to the size of the complex playing a part. The small *bis*-(hydrotris-(1-pyrazolyl)borato)iron(II) complex probably means steric factors are preventing the approach of trichlorophenol. This would be particulary important at higher concentrations when the adsorbant molecules try to reorient so that their surfaces are perpendicular to the surface of the silicate sheets as opposed to parallel to it at low concentrations[104]. Another factor for the lack of adsorption could be the orientation of the ligand not being suitable to achieve optimum interaction between the aromatic groups, since the aromatic groups can pack in the interlayer region so that the plane of the molecule is parallel to the clay layers or perpendicular to the clay layers.

8.7 Adsorption isotherm type

The adsorption isotherms can be classified according to there shapes. The shape of the isotherm is determined by the method of adsorption taking place. There are many variations on classification of adsorption isotherms but in this case the classification described by Giles et al. is adopted[105].

The type I isotherms show an initial rapid adsorption. The isotherm comprises of a steep slope . The steep slope of the isotherm results from the solute having such an affinity for the adsorbing species that it is very quickly completely or almost completely adsorbed.

The type II isotherms consist of an initial steep slope which becomes flatter (almost linear) and then becomes steep again. This is because as more solute is taken up, there is progressively less chance that a bombarding solute molecule will find a suitable site on which it can be adsorbed. This represents the linear portion of the isotherm. The

linear portion is followed by more rapid adsorption as monolayer coverage is complete and multilayer adsorption begins.

The type III isotherms consist of a slope which increases in gradient exponentially. The initial part of the curve results from a mechanism opposite to that described for type II isotherms. The more solute there is already adsorbed, the easier it is for additional amounts to become adsorbed via van der Waals interactions.

The type IV This is similar to type II isotherms but the form of the curve is more exaggerated to give an 'S' shape curve. In type IV isotherms a plateau is seen after the rapid increase in adsorption.

The type V isotherm is uncommon, normally it is seen when the adsorbate-adsorbent interaction is weak.

The type VI isotherm consists of steps the nature of which are dependant on the system and the temperature. The steps represent successive layer adsorption on a uniform region, the step heights represent the monolayer capacity for each adsorbed layer.

Type C - partitioning - The availability of adsorption sites remains constant at all concentrations up to saturation, thus the shape of the isotherm is linear. The constant partitioning of solute between solution and substrate right up to the maximum adsorption characterises partitioning . Conditions favouring partitioning include the solute having a higher affinity for the adsorbent than for the solvent. The linearity suggests that the number of sites for adsorption remains constant. Thus as more solute is adsorbed more sites must be created. This could arise when the solute has a higher attraction for the adsorbent than the solvent itself has and the solute may be able to

penetrate into the structure of the adsorbent in regions not already penetrated by the solvent

Besides these seven isotherms there are borderline cases which may be difficult to assign to one type. Thus one isotherm may have characteristics of more than one type of isotherm class or may be difficult to fit in any of the types. In the case of monolayer coverage of solute, it is not necessarily the case that the solute molecules are close packed or that the monolayer is entirely solute molecules, there may be solvent also present. The monolayer may well consist of clusters of solute molecules adsorbed on the most active sites.

8.7.1 Classification of the adsorption isotherms obtained in the study

Table 8.4 Classification of the adsorption isotherms

	Adsorption isotherm type		
	phenol	chlorophenol	trichlorophenol
$[Fe(bipy)_3]^{2+}$-montmorillonite	IV	IV	unassignable
$[Fe(tripyam)_2]^{2+}$-montmorillonite	unassignable	C	V
$Fe[HB(pz)_3]_2$-montmorillonite	unassignable	IV	C

Generally in cases where a reasonable amount of adsorption had taken place isotherms could be assigned to one of the seven varieties, although in some cases the closest match was used to classify the isotherm. As can be seen from table 8.4 adsorptions of these solutes mostly generates type IV isotherms.

8.8 Conclusions

The adsorption capacities of the three different types of modified montmorillonites, namely *tris*-2,2-bipyridyliron(II) exchanged montmorillonite, *bis*-tri-(2-pyridyl)-amineiron(II) exchanged montmorillonite and *bis*-(hydrotris-(1-pyrazolyl)borato)-iron(II) exchanged montmorillonite are comparable for the different phenols. The only observed difference is *bis*-(hydrotris-(1-pyrazolyl)borato)iron(II) intercalated montmorillonite appears to have a lower capacity for the adsorption of trichlorophenol compared to the other modified montmorillonites.

Generally there appears to be an order in susceptibility of the phenols to adsorption by the modified montmorillonites. Chlorophenol is adsorbed more effectively than trichlorophenol, which in turn is more effectively than phenol. M.A. M. Lawrence[86] postulated the distinction in adsorption efficiencies of the phenol and 2,4,6 trichlorophenol for all adsorbents could be due to the ability for the 2,4,6 trichlorophenol to interact with ligands to a greater degree than the phenol due to the ligands being relatively electron rich and the 2,4,6 trichlorophenol being relatively electron deficient. This combined with the low 2,4,6 trichlorophenol-water (adsorbate-solvent) interaction may explain the increased interaction with the adsorbent. Figure 8.14 is a schematic representation of the interactions between 2,4,6 trichlorophenol and the 2,2'-bipyridyl iron(II) complex.

Figure 8.14 A schematic representation of the interactions between 2,4,6-trichlorophenol and the 2,2'-bipyridyliron (II) complex

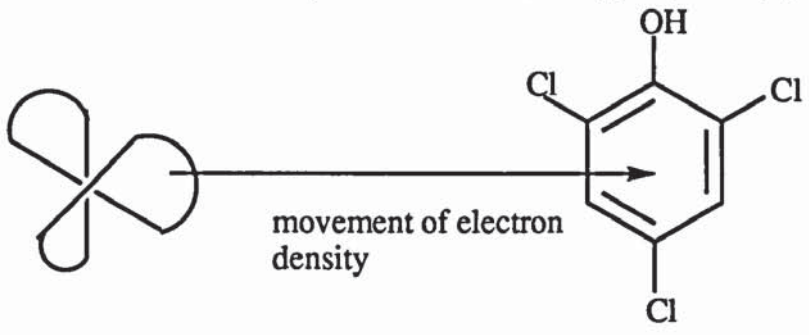

However, 2-chlorophenol is adsorbed more effectively than 2,4,6-trichlorophenol, this may be explained by the bulkiness of 2,4,6 trichlorophenol ensuring it cannot be packed as efficiently as the 2-chlorophenol in the interlamellar layers.

8.8.1 Comparing results on adsorption with previous work.

The values for the absorptions appear to be relatively high when compared with previous work. Huang[99] reported adsorptions of phenolic acids in solutions containing 0.1μmole/ml phenolic acid of 19.5μmol/g and 17.3μmol/g of clay by Na-vermiculite and K-vermiculite respectively. Work done by Kelly[104] on adsorption of pyridine by Na-montmorillonite showed maximum sorption of less than 3meq/g clay. Lagaly[65] attempted to optimise adsorption by working at different pH values but even he could only manage a maximum adsorption of oxalic acid by sodium montmorillonite of 0.8mg/g which converts to less than 0.01mmol/g.

More recent work by Lawrence[86] concerning the adsorption of phenols and chloro-phenols by tetramethyphosphonium montmorillonite and tetramethylammonium montmorillonite reported results more comparable to our results but again maximum adsorptions reported by Lawrence were lower when compared with our data. However the order we found when comparing the extent of adsorption of the phenol compounds is also observed in Lawrence's work.

REFERENCES

1 Low Temperature Synthesis of Kaolin Minerals, C. DeKimpe, M. C. Gastuche, The American Mineraologist, (1964), 49(1), 1-16

2 Structure and Properties of Amorphous Silicoaluminas, A. Leonard, Sho SuZuki, J. J. Fripiat, C. DeKimpe, J. Phys. Chem., 68(9), 2608-2617

3 Effects of the Structure of Silica -Alumina gel on the Hydrothermal synthesis of Kaolinite, S. Satokawa, Y. Osaki, S. Samejima, R. Miyawaki, S. Tomura, Y. Shibasaki, Y. Sugahara, Clays and clay minerals, (1994), 42(3), 288-297

4 Hydrothermal Synthesis of Kaolinite, Dickite, Beidellite. and NontroniteR. H. Ewell, H. Insley. , J. of Research of the National Bureau of Standards, (1935) 15, 172-179,

5 Thermal Shock and Size Effects in Castable refractories, B. Cotterell, Sze Woo Ong, and Caidong Qin, J. Am. Ceram. Soc. (1995), 78(8), 2056,-2059

6 Technology of Monolithic Refractories, Akira Nishikawa, Plibrico Company, (1984), 24, Chicago.

7 Comparison of Hot Strength of Bauxite-based New Bond Castable with Analogous Bauxite-based Low Cement Castable, A. Wynn, Confidential Report, (1994), Morgan Materials Tech. Ltd.

8 Kaolin Clays and their Industrial Uses, J. M. Huber, J. M. Huber Corporation, (1955), New York.

9 R. E. Grim, Clay mineralogy. Mcgraw Hill, (1953), New York.

10 The Chemistry of Clay Minerals, C. E. Weaver, L. D. Pollard, Mineralogical Society, Longman Scientific an Technical, (1973), Bath, G. B.

11 A. J. Leonard, J. Amer. Ceramic Society, 1977, 60, 37.

12 Refractories Manual, J. Zotos, A. Ayrazian, American Foundrymen's Society, (1963), Des Plaines, Illonois

13 Structural Analysis of the Transition Phases in the Kaolinite-Mullite Thermal Sequence, A. J. Leonard, J. Am. Ceram. Soc., (1977), 1-2, 37-43

14 Resolution of thermal peaks of kaolinite in thermomechanical analysis and differential thermal analysis studies, Akshoy K. Chakraborty, J. Am. Ceram. Soc., (1992), 75(7), 2013-2016.

15 The Mechanism of kaolinite dehydroxylation followed by High Resolution ^{27}Al and ^{29}Si NMR, R. C. T. Slade, T. W. Davies, Colloids and Surfaces, (1989), 36, 119-125,

16 Mechanism for the Dehydroxylation of Kaolinite, Dickite from Room Temperature to 455°C, P. R. Suitch, J. Am. Ceram. (1986), 69(1), 61-65,

17 Outstanding Problems in the Kaolinite-Mullite Reaction Sequence Investigated by ^{29}Si and ^{27}Al Solid State Nuclear Magnetic Resonance: I, Metakaolinite, K. J. D. MacKenzie, I. W. M. Brown , R. H. Meinhold, M. E. Bowden, J. Am. Ceram. Soc. (1985), 68(6), 293-297

18 Reexamination of the Kaolinite-Mullite Reaction series, A. K. Chakraborty, D. K. Gosh, J. Am. Ceram., (1978), 61(3-4), 170-173

19 The "Kaolinite-Mullite Reaction Series: III, The High Temperature Phases", G. W. Brindley , M. Nakahira, J. Am. Ceram. Soc, (1959), 42(7), 319-324

20 Characterisation of the Spinel Phase Formed in the Kaolin-Mullite Thermal Sequence, K Okada, N. Otsuka, J. Ossaka. J. Am. Ceram. Soc., (1986), 69(10), C251-C253

21 Structural Characterisation of the Spinel Phase in the Kaolin-Mullite Reaction Series Through Lattice Energ, S. Mazumdar, B. Mukherjee, J. Am. Ceram. Soc. (1983), 66(9), 610-612

22 Mullite Development from Fibrous Kaolin Mineral, T. W. Campos, H. De Souza Santos, P. De Souza Santos, J Am. Ceram. Soc. (1976), 59(7-8), 357-360

23 Role of Impurities on Formation of Mullite from Kaolinite and Al_2O_3-SiO_2 Mixtures, S. M. Johnson, J. A. Pask. Ceramic Bulletin, (1982), 61(8), 838-842

24 The Effect of Impurities on the Formation of Mullite from Kaolin type minerals, K. J. D. Mackenzie, Dept. Of Ceram. and Refractory Tech., Univ. of Sheffield, (1968), 97-109

25 Flash Calcines of Kaolinites: Effect of Process Variables on Physical Characteristics, R. C. T. Slade, T. W. Davies, H. Atakul, R. M. Hooper, J. Materials Science, (1992), 27, 2490-2500

26 Evolution of Structural Changes during Flash Calcination of Kaolinite, R. C. T. Slade, T. W. Davies, J. Mater. Chem. (1991) 1(3), 361-364

27 Flash Calcines of Kaolinites: Kinetics of Isothermal Dehydroxylation of Partially Dehydroxylated Flash Calcines and of Flash Calcination Itself, R. H. Meinhold, H. Atakul, T. W. Davies, R. C. T. Slade, J. Mater. Chem., (1992), 2(9), 913-921

28 Flash Calcination of Kaolinite: Mechanistic Information from Thermogravimetry, R. C. T. Slade, T. W. Davies, H. Atakul, J. Mater. Chem., (1991), 1(5), 751-756

29 E. Lippma, M. Magi, A. Samoson, G. Engelhardt, A. R. Grimmer, Structural Studies of Silicates by Solid State High Resolution ^{29}Si NMR, J. Am. Ceram. Soc., 1980, 102, 4889-4893

30 K. A. Smith, R. J. Kirkpatrick, E. Oldfield, D. M. Henderson, High-resolution Silicon-29 Nuclear Magnetic Resonance Spectroscopic Study of Rock-Forming Silicates, American Mineralogist, 68, 1206-1215, 1983

31 Solid State 27Al and 29Si Magic Angle Spinning NMR of Aluminosilicate gels, S. Komarneni, R. Roy, C. A. Fyfe, G. J. Kennedy, and H. Strobl, Communications of the Am. Ceram Soc., J. Am. Ceram. Soc., (1986). 69(3), C42-C44.

32 J. Am. Chem. Soc, (1981), 103(17), 4994

33 P. F. Barron, R. L. Frost, J. O. Skjemstad, A. J. Koppi, Detection of Two Silicon Environments in Kaolins by Solid-state ^{29}Si NMR, Nature, 302, 49-50, 1983

34 Thermal Reactions of Kaolinite Studied by Solid State 27-Al and 29-Si NMR, R. H. Meinhold, K. J. D. MacKenzie, I. W. M. Brown, J. Materials Science Letters, (1985), 4, 163-166

35 Outstanding Problems in the Kaolinite-Mullite Reaction Sequence Investigated by ^{29}Si and ^{27}Al Solid State Nuclear Magnetic Resonance: II, High Temperature Transformations of Metakaolinite, I. W. M. Brown , K. J. D. MacKenzie, M. E. Bowden, R. H. Meinhold, J. Am. Ceram. Soc. (1985), 68(6), 298-301

36 Aluminium-27 and Silicon-29 Magic angle spinning Nuclear magnetic Resonance Study of the Kaolinite-Mullite Transformation, J. Sanz, A. Madani, J. M. Serratosa, J. S. Moya, S. Aza, J. Amer. Ceram. Soc., (1988), 71(10), C418-C421

37 D. Mueller, W. Gessner, H. J. Behrens, G. Scheller, Chem. Phys. Lett. (1981), 79, 59

38 D. Mueller, D. Hoebbel, W. Gessner, Chem. Phys. Lett. (1981), 84, 25

39 Nuclear Magnetic Resonace (NMR) - A Powerful Tool in Cement and Concrete Research, H. Justnes, I. Meland, J. O. Bjoergum, J. Krane, T. Skjetne, Advances in Cement Research, (1990), 3(11), 105-110,

40 Thermal Reactions of Pyrophyllite Studied by High Resolution Solid State 27Al and 29Si Nuclear Magnetic Resonance Spectroscopy, K. J. D. MacKenzie, I. W. M. Brown, R. H. Meinhold, M. E. Bowden, J. Am. Ceram. Soc. (1985), 68(5), 266-272

41 Charaterisation of Synthetic and Naturally Occurring Clays by ^{27}Al and ^{29}Si Magic Angle Spinning NMR Spectroscopy, S. Komarneni, C. A. Fyfe, G. J. Kennedy, and H. Strobl, Communications of the Am. Ceram Soc., J. Am. Ceram. Soc., (1986). 69(3), C45-C47.

42 Literature Highlights, I Siberian, Reactivity of Solids, News Brief, 1989, 6(4), 374-375

43 Solid State MAS-NMR as a Tool to Study the reaction Mechanism in Blended Cement , Blast-Furnace Slag Cement and Cement-Like Binders, H. S. Pietersen, A. Kentgens, G. Nachtegaal, W. S. Veeman, J. M. J. M. Bijen, Delft Technical University, Materials Science Dept, Netherlands, (1991), 1-4

44 Characterisation of Ceramic Reactions by Solid State NMR, J. Drennan, G. Neal, M. B. Trigg, M. E. Smith, 371-376

45 The Infrared Spectra of Layer Silicates, V. C. Farmer, J. D. Russell, Spectrochimica Acta, (1964), 20, 1149-1173

46 Replacement of OH by OD in Layer Silicates and Identification of the Vibrations of these groups in Inrfared Spectra, J. D. Russell, V. C. Farmer, B. Velde, Mineralogical Magazine, (1970), 37, 869-879

47 FTIR of Deuterated Smectites, Bukka, Miller, Shabtai, Clays and Clay Minerals, 1992, 40(1), 96-97

48 Isomorphous Substitution and Infrared Spectra of the layer lattice silicates, V. Stubican, R. Roy, Amer. Mineralologist, (1961), 46, 32-51

49 Infrared Spectra of Layer-Structure Silicates, V. Stubican, R. Roy, J. Amer. Ceram. Soc., 44(12), 625-627

50 Infrared Spectroscopy study of Tetrahedral and Octahedral Substitutions in an Interstratified Illite-Smectite Clay, Clays and Clay Minerals, E. Srasra, F. Bergaya, J. J. Fripiat, 1994, 42(3), 237-241

51 Infrared Spectra of clay minerals, J. M. Hunt, M. P. Wisherd, L. C. Bonham, Anal. Chem.,1950, 22(12), 1488-1491

52 Infrared Determination of the Kaolin Group Minerals, Nature, (1960), 185, 835-837

53 The use of Diffuse Reflectance FT-IR Spectroscopy for the Quantitative Analysis of a Number of Silanised Kaolin Clays, T. J. Porro, S. C. Pattacini, Applied Spectroscopy, (1990), 44(7), 1170-1175

54 Applied Spectroscopy, (1987), 41(3), 472-475

55 The use of Far Infrared Interferometric Spectroscopy for Mineral Identification, S. J. Larson, G. W. F. Pardoe, H. A. Gebbie, Amer. Mineralogist, 1972, 57, 998-1002

56 An Infrared Spectroscopic study of the Isothermal Dehydroxylation of Kaolinite at 470°C, J. G. Miller, J. Phys. Chem., (1961), 65, 800-804

57 Far Infrared Spectra of Montmorillonite, Kaolinite and Illite, E. E. Angino, Nature, 1964, 185, 569-571

58 Quantitative analysis of Corroded Glass using Infrared Frequency Shifts, D. E. Clark, E. C. Etheridge, M. F. Dilmore, L. L. Hench, Glass Technology, (1977), 18(4), 121-123

59 Interpretation of the Kaolinite-Mullite Reaction Sequence from Infrared Absorption Spectra, H. J. Percival, J. F. Duncan, P. K. Foster, J. Amer. Ceram. Soc., (1974), 57(2), 57-61

60 Clay Minerals: Their structure Behaviour and Use, G. Brown, The Royal Society, (1984), London

61 Smectite Clay Minerals: Properties and uses, I. E. Odom, Phil. Trans. R. Soc. London, (1984), 391-409

62 Formation of Copper (II) Arene Complexes on the Interlamellar Surfaces of Montmorillonite, M. M. Mortland, T. J. Pinnavia, Nature Physical Science, (1971), 229, 75-77

63 B. K. G. Theng, Fomation and Properties of Clay-Polymer complexes, Developments in Soil Science, 9, 1979, 11.

64 Clay-Organic Interactions: Problem and Recent Results, G. Lagaly, The Clay Minerals Society, (1987), 343-351

65 The Properties and Uses of Clays which Swell in Organic Solvents, T. R. Jones, Clay Minerals, (1983), 18, 399-410

66 Thermodynamics of the Exchange of n-Alkylammonium Ions on Na-Montmorillonite, E. F. Vansant, J. B. Uytterhoeven, Clays and clay minerals, (1972), 20, 47-54

67 Orientation of Trimethylphenylammonium (TMPA) on Wyoming Montmorillonite: Implications for Sorption of Aromatic Compounds, J. J. Stevens, S. H. Anderson, Calys and Clay Minerals, (1996), 44(1), 132-141

68 Hectorite Complexes with Cu (II) and Fe (II)-1,10-Phenanthroline chelates, V. E. Berkheiser, M. M. Mortland, Clays and Clay minerals, (1977), 25, 105-112

69 Co-ordination Compounds on the surface of laponite: Tri-2-pyridylamine Complexes, S. P. Bond, C .E. Hall, C. J. McNerlin, W. R. McWhinnie, D. J. Walton, J. Mater. Chem., (1992), 2(1), 37-41

70 Ion Exchange and Intersalation Reactions of Hectorite with Tris-Bipyridyl Metal Complexes, S. M. F. Traynor, M. M. Mortland, T. J. Pinnavaia, Clays and Clay Minerals, (1978), 26(5), 318-326

71 Clay Supported Catalysts: an Extension of Phase Transfer Catalysis, Inorganica Chimica Acta, P. Monsef-mirzai, W. R. McWhinnie, (1981), 52, 211-214

72 Chemical and Structural Properties of Clay Minerals Modified by Inorganic and organic material, T. J. Bandosz, J. Jagiello, K. A. G. Amankwah, J. A. Schwarz, Clay Minerals, (1992), 27, 435-444

73 Applications of Microwave Dielectric Heating Effects to Synthetic Problems in Chemistry, D. Michael, P. Mingos, D. R. Baghurst, Chem. Soc. Rev., (1991), 20, 1-47

74 The Rapid Synthesis of Organic Compounds in Microwave Ovens, R. N. Geyde, F. E. Smith, K. C. Westaway, Can. J. Chem., (1987), 66, 1988, 17-26

75 Application of Commercial Microwave ovens to Organic Synthesis, R. J. Giguere, T. L. Bray, S. M. Duncan, Tetrahedron Letters, (1986), 27((41), 4945-4948

76 Application of Microwave Heating Techniques for the Synthesisof Solid State Inorganic Compounds, D. R. Baghurst, D. Michael, P. Mingos, J. Chem. Soc., Chem. Commun., (1988), 829-830

77 Rapid Synthesis of Magnesium Aluminophosphate-5 by Microwave Dielectric Heating, S. L. Cresswell, J. R. Parsonage, P. G. Riby, M. J. K. Thomas, J. Chem. Soc. Dalton Trans., (1995), 17, 2315-2316

78 S. P Bond, A. Gelder, J. Homer, W. R. McWhinnie, M. C. Perry, J. Mater. Chem., (1991), 1, 327

79 Microwave Drying of Boehmite Sol Intercalated Smectites, K. G. K. Warrier, P. Mukundan, S. K. Ghosh, S. Sivakumar, A. D. Damodaran, J. Materials Science, (1994), 29, 3415-3418

80 Synthesis of Tri-(2-pyridyl)amine, J. P. Wibaut. G. L. C. La Bastide, Res. Trav. Chem., (1933), 52, 493

81 Studies in Coordination Chemistry. Part XIII. Magnetic Moments and Bond Types of Transition-Metal Complexes, F. H. Burstall, R. S. Nyholm, J. Chem. Soc., (1952), 3570-3579

82 Complexes of Tri-(2-pyridyl)amine. Part I. Complexes with Cobalt (II) Nickel (II), and Copper (II) perchlorates, G. C. Kulasingam, W. R. McWhinnie, J. C. Draper, J. Chem. Soc., (1966), 1199-1203

83 Complexes of Tri-(2-pyridyl)amine. Part II. Some Complexes with Metal Halides. The Ligand Field Strength of terdentate Tri-(2-pyridyl)-amine, G. C. Kulasingam, W. R. McWhinnie, J. Chem. Soc., (1967), A, 1253-1255

84 Boron-Pyrazole Chemistry. II. Poly(1-pyrazolyl)borates, S. Trofimenko, J. Am. Chem. Soc., (1967), 89(13), 3170-3177

85 Some Hydridotris(3,5-dimethylpyrazolyl)borate complexes of Zinc, Cadmium and Mercury-Synthetic, Structural, and NMR invetigations, W. R. McWhinnie, Z. Monsef-Mirzai, M. C. Perry, N. Shaikh, Polyhedron, (1993), 12(10), 1193-1199

86 The Adsorption of Phenolic and Organotin Compounds by Clays and Cation Exchanged Clays, M. A. M. Lawrence, Ph.D. Thesis, (1996)

87 The Near Infrared Combination Band Frquencies of Dioctahedral Smectites, Micas, and Illites, J. L. Post, P. N. Noble, Clays and Clay minerals, 1993, 41(6), 639.

88 J. A. Gadsden, "Infrared spectra of minerals and related compounds", 1976, 85.

89 Kinetics of dehydroxylation of kaolinite and halloysite, G. W. Brindley, M. Nakahira, J. Am Ceram. Soc. 1957, 40(10), 346

90 Technology of monolithic refractories, Plibrico Company, 1984, Chicago, 227-228

91 Optimisation of cement-based stabilisation/solidification of organic containing industrial wastes using organophilic clays, D. M. Montgomery., C. J. Sollars and R. Perry , Waste Management and Research, 1991, 9, 21-34.

92 Adsorption by organo-clay complexes, C. T. Cowan, D. White, Clays and Clay Minerals, 1962, 11, 459-467.

93 Adsorption of organic molecules by clays in aqueous suspension, M. B. McBride, T. J. Pinnavia, M. M. Mortland, Advanced Environmental Science Technology, (1977), 8, 145-154.

94 Priority pollutants I - A perspective view , ES and T special report, Environmental Science and Technology, 1979, 13 (4), 416-423.

95 The adsorption of of n-aliphatic alcohols from dilute solutions on RNH_3-montmorillonites. Part I- Distribution at infinite dilution, M. S. Stul, A. Maes, J. B. Uyttterhoeven, Clays and Clay Minerals, (1978), 26(5), 309-317.

96 The adsorption of of n-aliphatic alcohols from dilute solutions on RNH3-montmorillonites. Part I- Distribution at infinite dilution, M. S. Stul, A. Maes, J. B. Uyttterhoeven, Clays and Clay Minerals, (1979), 27(5), 377-386.

97 Clay-organic complexes as adsorbents for phenols and chlorophenols, M. M. Mortland , Clays and Clay Minerals, (1986), 34, 581-585.

98 Retention of phenolic acids by noncrystalline hydroxy- aluminium and -iron compounds and clay minerals of soils, P. M. Huang, T. S. C. Huang, M. K. Wang, M. H. Wu, N. W. Hsu, Soil Science, 1977, 123, 213-219

99 Studies in adsorption, Giles C. H., MacEwan T.H., Nakhwa S. N., Smith D., J. Chem. Soc, 1960, Pt 3, 3973-93.

100 FTIR study of deuterated montmorillonites: structural features relevant to pillared clay stability, K. Bukka, J. D. Miller, J. Shabtai, Clays and Clay Minerals, 1992, 40(1), 92-102

101 Formation of copper (II) arene complexes on the interlamellar surfaces of the montmorillonite, M. M. Mortland, T. J. Pinnavaia, Nature physical science, 1971, 229, 75-77.

102 Infrared spectra and energy of adsorption of aromatic compounds on silica, G. A. Galkin, A. V. Kiselev, V. L. Lygin, Trans. Faraday Soc., 1964, 60, 431-439

103 Benzene complexes with Copper(II)montmorillonite, H. E. Doner, M. M. Mortland, Science, 1969, 166, 1406-1407

104 Sorption of aromatic organic compounds by montmorillonite, part 1- orientation studies, R. Green e-Kelly, Trans. Faraday soc.1955, 51, 412-424

105 Studies in adsorption, Giles C. H., MacEwan T.H., Nakhwa S. N., Smith D., J. Chem. Soc, 1960, Pt 3, 3973-93.

APPENDIX

Figure A1- XRD trace of kaolin c

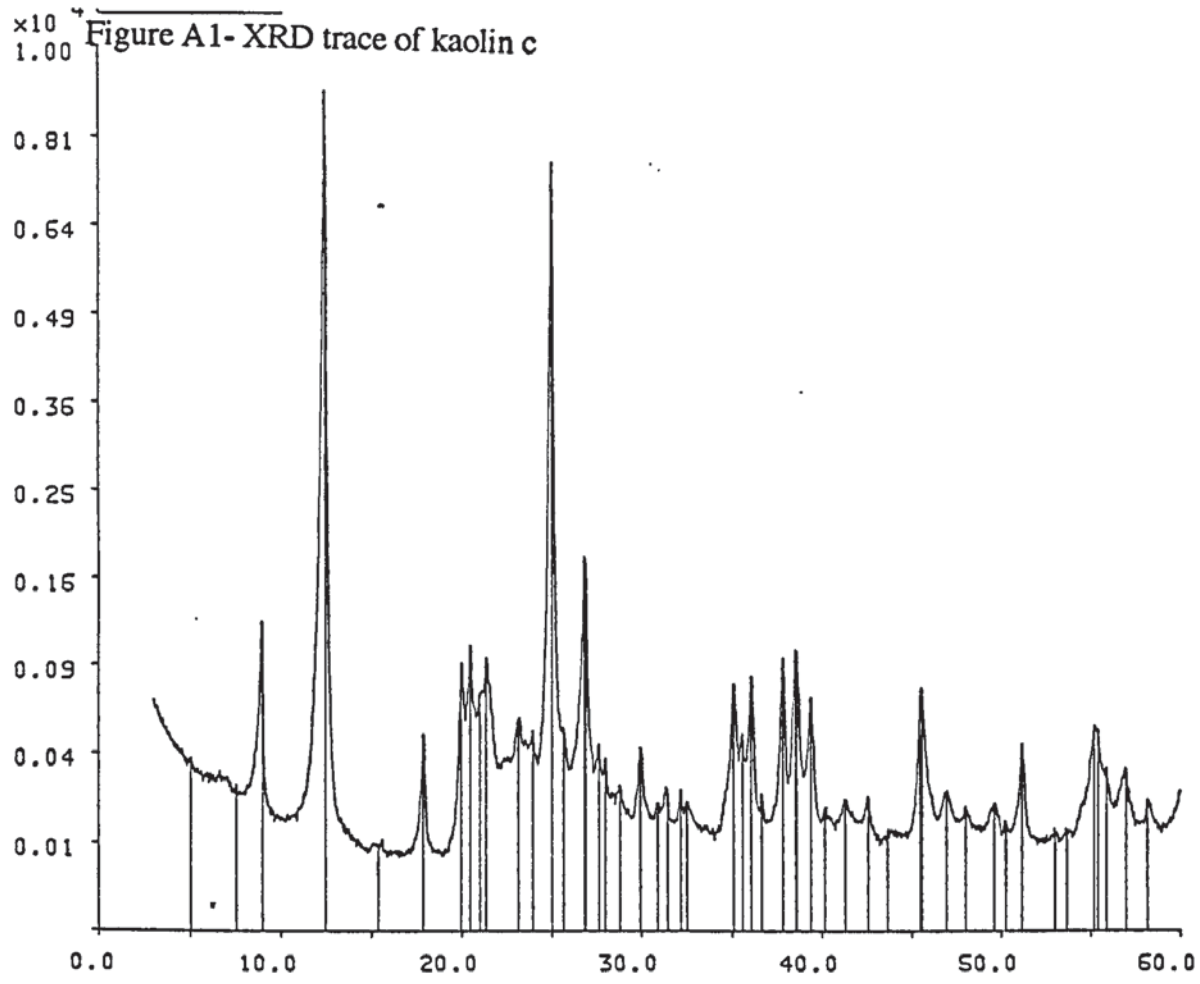

Figure A2- XRD trace of kaolin A

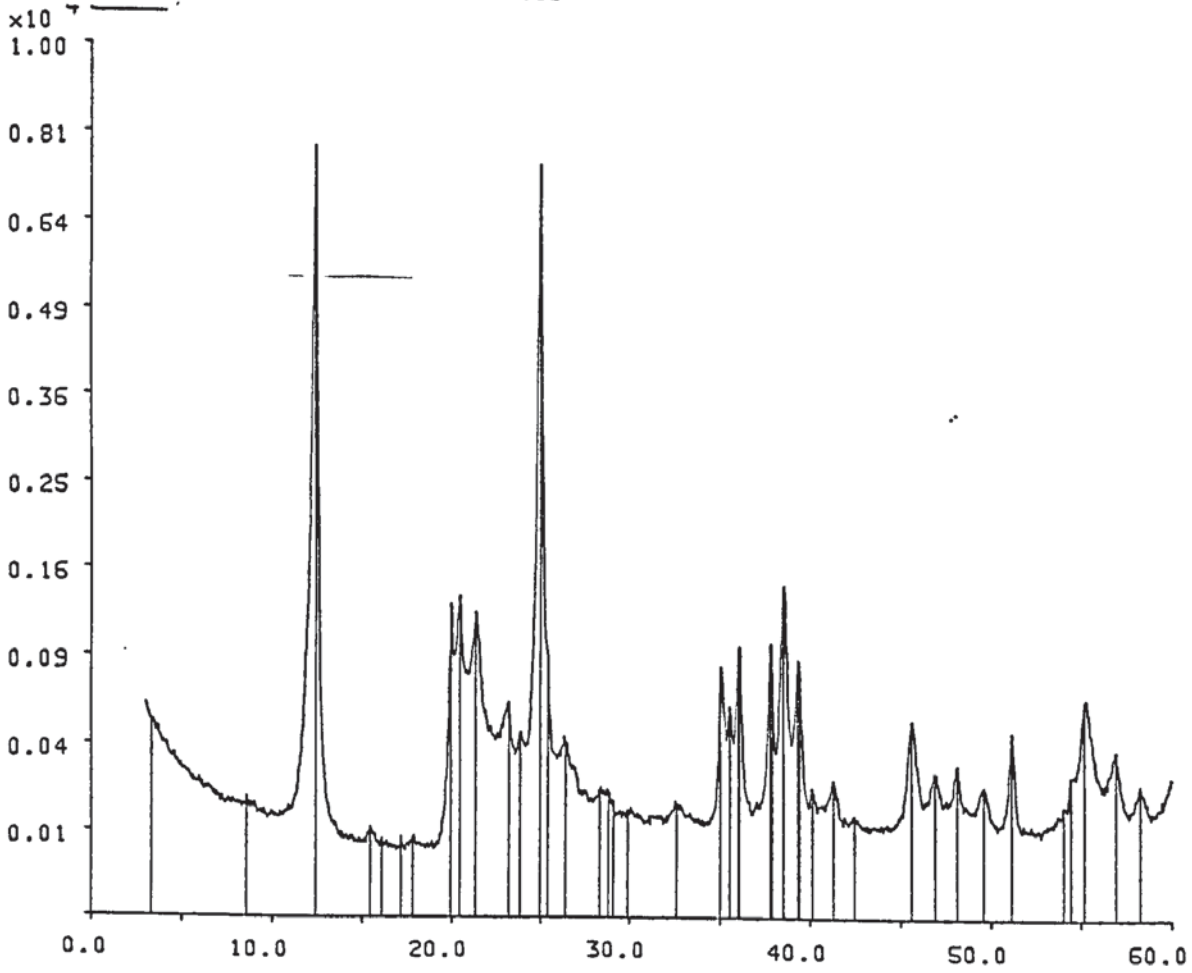

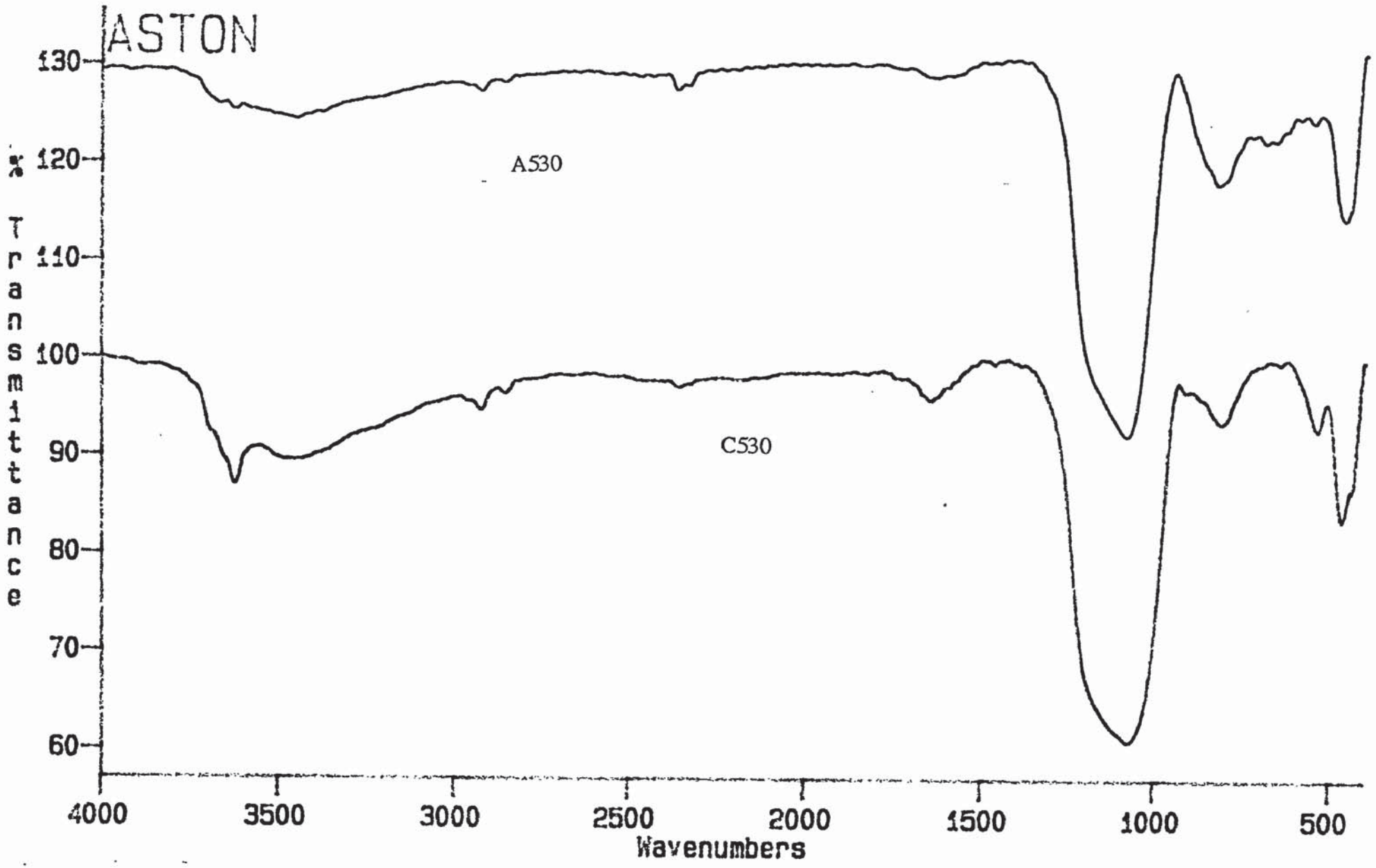

Figure A3- Infrared spectrum of kaolins A and C after calcining at 530°C